

Table of contents

1	Introduction	6
1.1	Poly(lactic acid) (PLA)	6
1.1.1	General features of PLA	6
1.1.2	Stability and biodegradation of PLA	8
1.1.3	Optical properties of PLA in the UV-Vis range	10
1.1.4	Lactic acid production	11
1.1.5	Ring opening polymerization of lactide	12
1.1.5.1	Lactide synthesis	15
1.1.5.2	Cationic polymerization	16
1.1.5.3	Anionic polymerization	17
1.1.5.4	Coordination-insertion polymerization	18
1.1.5.5	Carbene catalyzed polymerization	21
1.1.6	Synthesis of cyclic PLA	23
1.1.7	Typical applications of PLA	24
1.1.7.1	Commercial applications	24
1.1.7.2	PLA stereocomplex	25
1.1.7.3	PLA blends and composites	26
1.1.7.4	Copolymers and modified PLA	26
1.2	Poly(ϵ -caprolactone) (PCL)	26
1.2.1	General features of PCL	26
1.2.2	Synthesis and physicochemical properties of PCL	27
1.2.3	Biodegradability and biocompatibility of PCL	28
1.3	Poly(ethylene glycol) (PEG)	30
1.3.1	General properties of PEG	30
1.3.2	Melting, solidification and crystallinity of PEGs	31
1.3.3	PEG in biomedical applications	33
1.3.4	PEG Biocompatibility and toxicity	35
1.3.5	The use of PEG as a reaction medium	36
1.3.5.1	Examples of Cu-catalyzed reactions in PEG	37
1.3.5.2	Examples of Pd-catalyzed reactions in PEG	39

1.4	Metal-polymer macrocomplexes	42
1.4.1	Structure of different macrocomplexes	43
1.4.2	Main examples of macrocomplexes	45
1.4.3	Applications and research outlook	48
1.5	Pd- and Cu-based catalysis of some organic reactions	49
1.5.1	Pd-catalyzed aerobic oxidation of alcohols to carbonyl compounds	49
1.5.1.1	The Pd(OAc) ₂ / pyridine catalytic system	50
1.5.1.2	Other homogeneous Pd-based catalytic systems	51
1.5.1.3	Catalytic systems based on Pd nanoparticles	52
1.5.2	Pd- and Cu-catalyzed cyanation of aryl halides	57
1.6	Ultrasounds in green reaction media	58
1.6.1	Acoustics in liquid media	58
1.6.2	Cavitation and sonochemistry	59
1.6.3	Devices for ultrasounds generation	62
1.6.4	Sonochemistry in aqueous solvent	63
1.6.4.1	Organic reactions in water phase and emulsions	64
1.6.4.2	Sonochemical polymerization reactions in aqueous solvent	66
1.6.4.3	Synthesis of inorganic nanoparticles and nanomaterials	69
1.6.5	Sonochemistry in ionic liquids	72
1.6.5.1	Ionic liquid-catalyzed organic reactions	72
1.6.5.2	Organic reactions requiring the addition of a catalysts	74
1.6.5.3	Synthesis of nanoparticles and nanostructures in ionic liquids	75
1.6.5.4	Coordination chemistry in ionic liquids	77
1.6.6	Sonochemistry in other green solvents	77
1.6.7	Solvent-free sonochemical reactions	79
1.6.7.1	Solvent-free organic reactions	79
1.6.7.2	Bulk polymerization reactions	81
2	Experimental	85
2.1	Reagents and solvents	85
2.2	Synthetic procedures	85
2.2.1	P(L)LA-Py (L1) and P(LD)LA-Py (L2) macroligands	85
2.2.2	PCL-Py (L3) macroligand	86
2.2.3	MeO-PEG-Py (L4) macroligand	86
2.2.4	(MeO-PEG-PyH ⁺)OTs ⁻ ((HL4)(OTs)) macroligand	86
2.2.5	MeO-PEG-Bn (L5) macroligand	87

2.2.6	P(L)LA- <i>b</i> -P(LD)LA-Py (L6, L8) and P(D)LA- <i>b</i> -P(LD)LA-Py (L7, L9) macroligands	87
2.2.7	Py-P(L)LA-Py (L10) bifunctional macroligand.....	87
2.2.8	MeO-PEG-P(<i>o</i> -anisyl) ₂ (L11) macroligand	88
2.2.9	<i>trans</i> -[PdCl ₂ (L1) ₂] (1) and <i>trans</i> -[PdCl ₂ (L2) ₂] (2) macrocomplexes.....	88
2.2.10	PdCl(η^3 -allyl)(L1) (3) macrocomplex	88
2.2.11	<i>cis</i> -[Pd(η^3 -allyl)(L1) ₂]BAr' ₄ (4) and <i>cis</i> -[Pd(η^3 -allyl)(L1)(L2)]BAr' ₄ (5) macrocomplexes	89
2.2.12	[Pd(L1) ₄](SbF ₆) ₂ (6); [Pd(L2) ₄](SbF ₆) ₂ (7) and [Pd(L1) ₂ (L2) ₂](SbF ₆) ₂ (8) macrocomplexes	89
2.2.13	[Pd(L1) ₂ (L2) ₂](OTs) ₂ (9) macrocomplex	89
2.2.14	<i>trans</i> -[PdCl ₂ (4-EtPy) ₂] (4-EtPy = 4-ethylpyridine) (10) complex	90
2.2.15	<i>trans</i> -[PdCl ₂ (L3) ₂] (11) macrocomplex.....	90
2.2.16	[Pd(L3) ₄](SbF ₆) ₂ (12) macrocomplex.....	90
2.2.17	[Pd(L1) ₂ (L3) ₂](SbF ₆) ₂ (13) macrocomplex	90
2.2.18	[Pd(L3) ₄](OTs) ₂ (14) macrocomplex	91
2.2.19	[Pd(L1) ₂ (L3) ₂](OTs) ₂ (15) macrocomplex	91
2.2.20	[Pd(L1) ₄](OTs) ₂ (16) macrocomplex	91
2.2.21	<i>trans</i> -[Pd(OAc) ₂ (L1) ₂] (17) and <i>trans</i> -[Pd(OAc) ₂ (L3) ₂] (18) macrocomplexes	91
2.2.22	<i>trans</i> -[Pd(OAc) ₂ (4-EtPy) ₂] (19) complex.....	92
2.2.23	<i>trans</i> -[Pd(OAc) ₂ (L4) ₂] (20) macrocomplex	92
2.2.24	[Pd(L4) ₄](OTs) ₂ (21) macrocomplex	92
2.2.25	Pd(0)@[2(HL4)(OAc)] (22) and Pd(0)@[2L4 + 2(HL4) (OTs)] (23) stabilized Pd-nanoparticles	92
2.2.26	Pd(0)@[2L4 + 2(HL4) (OAc)] (24) stabilized Pd-nanoparticles	93
2.2.27	Pd(0)@4L5 (25) stabilized Pd-nanoparticles	93
2.2.28	Mesylation of poly(ethylene glycol) monomethyl ether	93
2.3	Instruments and characterization	94
2.3.1	¹ H, ¹³ C{ ¹ H} and ³¹ P{ ¹ H} NMR spectroscopy	94
2.3.1.1	NMR spectroscopic data for L1	94
2.3.1.2	NMR spectroscopic data for L2	94
2.3.1.3	NMR spectroscopic data for L3	94
2.3.1.4	NMR spectroscopic data for L4	95
2.3.1.5	NMR spectroscopic data for (HL4)(OTs)	95
2.3.1.6	NMR spectroscopic data for L5	95

2.3.1.7	NMR spectroscopic data for L6	96
2.3.1.8	NMR spectroscopic data for L7	96
2.3.1.9	NMR spectroscopic data for L8	96
2.3.1.10	NMR spectroscopic data for L9	97
2.3.1.11	NMR spectroscopic data for L10	97
2.3.1.12	NMR spectroscopic data for L11	97
2.3.1.13	NMR spectroscopic data for 1 and 2	97
2.3.1.14	NMR spectroscopic data for 3	97
2.3.1.15	NMR spectroscopic data for 4	98
2.3.1.16	NMR spectroscopic data for 5	98
2.3.1.17	NMR spectroscopic data for 6 – 8	99
2.3.1.18	NMR spectroscopic data for 9	99
2.3.1.19	NMR spectroscopic data for 10	99
2.3.1.20	NMR spectroscopic data for 11	99
2.3.1.21	NMR spectroscopic data for 12	100
2.3.1.22	NMR spectroscopic data for 13	100
2.3.1.23	NMR spectroscopic data for 14	101
2.3.1.24	NMR spectroscopic data for 15	101
2.3.1.25	NMR spectroscopic data for 16	102
2.3.1.26	NMR spectroscopic data for 17	102
2.3.1.27	NMR spectroscopic data for 18	103
2.3.1.28	NMR spectroscopic data for 20	103
2.3.1.29	NMR spectroscopic data for 21	103
2.3.1.30	¹ H NMR data for cyanation products	104
2.3.2	HPLC-UV	105
2.3.2.1	UV spectra of HPLC peaks of cyanation products	105
2.3.3	Gel Permeation Chromatography (GPC)	110
2.3.4	UV-Vis spectroscopy	110
2.3.5	Differential Scanning Calorimetry (DSC)	110
2.3.6	Thermo-Gravimetric Analysis (TGA)	111
2.3.7	X-Ray Powder Diffraction (XRPD)	111
2.3.8	X-Ray Photoelectron Spectroscopy (XPS)	111
2.3.9	Gas Chromatography (GC-FID / GC-MS)	111
2.3.10	Transmission Electron Microscopy (TEM)	112
2.3.11	Inductively Coupled Plasma (ICP)	112

2.3.12	X-ray crystallographic study of complex 10	112
2.3.13	NMR experiments of stepwise macroligand dissociation from macrocomplexes 4 and 6.....	114
2.3.14	Centrifugation experiments with water solutions of 23 and 25.....	114
2.4	Catalysis.....	114
2.4.1	Aerobic oxidations in toluene catalyzed by 17 – 19	114
2.4.2	Stability test of L1 and L3 carried out under aerobic oxidation conditions	115
2.4.3	Recycling experiments with 17+2L1 and benzyl alcohol	115
2.4.4	Aerobic oxidations in water catalyzed by 20 – 25	115
2.4.5	Stability test of L4 performed under basic aerobic oxidation conditions ...	116
2.4.6	Recycling experiments with 23 and cinnamyl alcohol	116
2.4.7	Cu-catalyzed cyanation of aryl halides under sonochemical conditions	116
3	Results and discussion.....	118
3.1	Synthesis of PLA- and PCL-based Pd macrocomplexes	118
3.1.1	Macrocomplexes combining P(L)LA- and P(LD)LA-based macroligands	118
3.1.2	Macrocomplexes combining P(L)LA- and PCL-based macroligands	128
3.2	Aerobic oxidation of alcohols catalyzed by PLA-based Pd macrocomplexes	135
3.3	Water phase aerobic oxidation of alcohols catalyzed by PEG-stabilized Pd nanoparticles	148
3.4	PEG as solvent for the Cu-catalyzed cyanation of aryl halides under sonochemical conditions.....	161
3.5	Synthesis of PLA- and PEG-based macroligands for future developments ...	174
3.5.1	Synthesis of PLA-based stereoblock copolymers	175
3.5.2	Synthesis of Py-P(L)LA-Py difunctional macroligand	176
3.5.3	Synthesis of phosphine end-capped PEG methyl ether (L11)	178
4	Conclusions	180
5	References	183

1 Introduction

1.1 Poly(lactic acid) (PLA)

1.1.1 General features of PLA

PLA is an aliphatic, semi-crystalline polyester with interesting properties of biodegradability and biocompatibility which can be produced from renewable resources. Most commonly, the “L” enantiomer of lactic acid (LA) is employed as the starting monomer on account of its wide natural availability and low cost (L-LA is the product of the bacterial fermentation of many polysaccharides). The resulting isotactic, semi-crystalline P(L)LA is indeed the only PLA with competitive properties from a commercial point of view. Since D-LA can be obtained from fermentative processes only at very high costs, P(D)LA from D-LA is markedly more expensive and generally produced from oil based feedstocks.

High molecular weight (MW) PLA is a white to transparent rigid polymer with physico-chemical properties between those of polystyrene and poly(ethylene terephthalate).¹ Similarly to other polyesters, PLA is a thermoplastic polymer with a relatively high glass-transition temperature (T_g) (up to 60 °C), maximum melting temperature (T_m) of c.a. 180 °C, high gas permeability, good mechanical and chemical resistance as well as a high stability towards thermal degradation (decomposition takes place at temperatures as high as 180 – 200 °C)² (Figure 1.1).

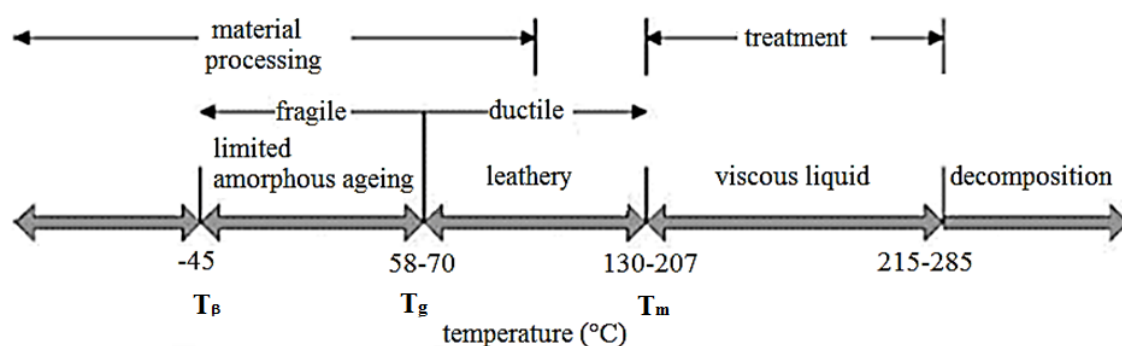


Figure 1.1 – Metastable states of semi-crystalline, high MW PLA³

Both pure P(D)LA and pure P(L)LA are semi-crystalline materials in which limited amounts of amorphous regions are formed due to some stereo-irregularities in the polymer chains; these may stem from stereo-errors during polymerization as well as from enantiomeric impurities contained in the starting monomer.

Inside the crystalline domains, the PLA chain can show two different morphological structures: type “ α ” (10_3 -helical conformation; 2 helices in each pseudo-orthorhombic unit cell) or type “ β ” (3_1 -helical conformation; 6 helices in each orthorhombic unit cell). Conversion between the two types is possible only at high temperatures or under harsh mechanical stress.⁴

The highest grade of crystallinity can be attained in two ways, which are (i) by addition of nucleating agents in proper solvents followed by thermal annealing (slow process, seldom utilized); (ii) by rapid application of a mechanical stress (more commonly utilized).

Highly crystalline PLA is soluble in few halogenated organic solvents and in THF⁵ and, compared to the amorphous counterpart, shows higher stiffness (*i.e.* increased Young’s modulus) as well as impact, penetration and flexion resistance. As the amorphous regions grow, the polymer becomes easily soluble in many common organic solvents. In order to obtain totally amorphous PLA (*i.e.* P(LD)LA), the less abundant enantiomer of LA must be present during polymerization in a quantity of at least 15%, nonetheless, crystallinity can also be lowered by introducing stereo-errors during the chain growth. The grade of crystallinity has a strong influence on the physico-mechanical properties of the material, as shown in Table 1.1. On the other hand, while the T_g varies slightly (in the 50 – 60 °C interval), a decrease in crystallinity markedly lowers the T_m of PLA allowing its industrial processability at a temperature sufficiently far from thermal degradation. Hence, a compromise between mechanical performances and processability can be sought case by case depending on the requirements of the final application. Moreover, if required by polymer processing, it is possible to increase the PLA melt elasticity by the addition of moderate quantities of cross-linkers (*e.g.* peroxides) or natural oils to increase the MW or branching of the polymer chains. In order to obtain commercially competitive properties for the most part of its applications, PLA should have a MW of at least 55000 g/mol. PLA is a biocompatible material; LA is indeed a non-toxic intermediate of human and animal metabolic cycles.

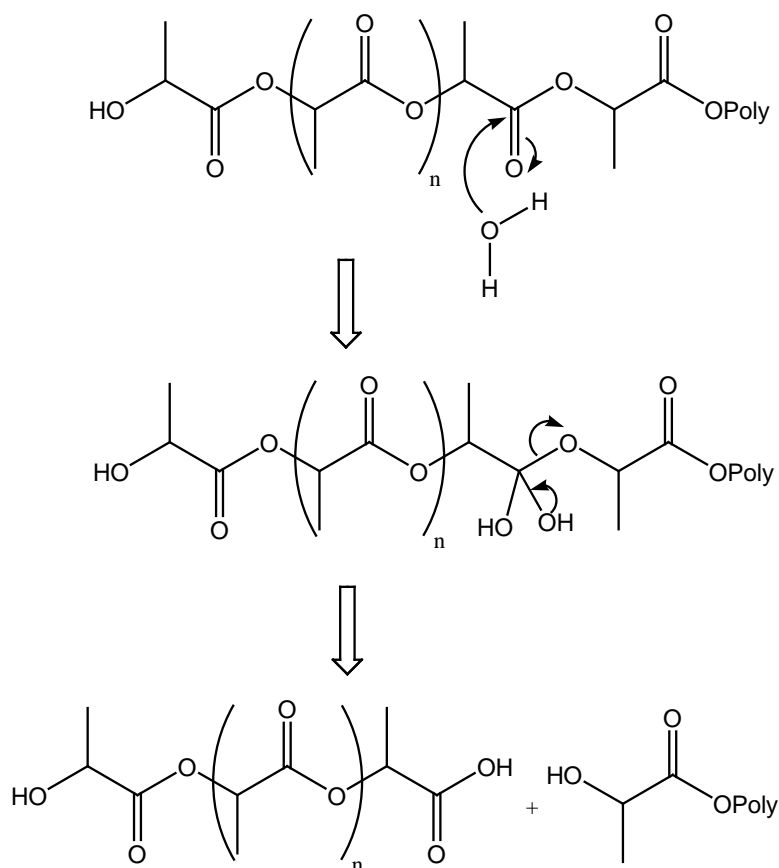
Property	P(L)LA	P(L)LA (annealing)	P(LD)LA
Traction resistance (MPa)	59	66	44
Elongation at break (%)	7.0	4.0	5.4
Modulus of elasticity (MPa)	3750	4150	3900

Yield strength	70	70	53
Flexural strength (MPa)	106	119	88
Izod Test (unnotched) (J/m)	195	350	150
Test di Izod (notched) (J/m)	26	66	18
Temperature of deflexion under load (°C)	55	61	50
Rockwell hardness	88	88	76
Vicat softening temperature (°C)	59	165	52

Table 1.1 – Influence of crystallinity on physical and mechanical properties of PLA⁶

1.1.2 Stability and biodegradation of PLA

PLA can be degraded either via a hydrolytic / enzymatic pathway (Figure 1.2) or via a thermo-oxidative process. The mechanism of biodegradation needs an initial, abiotic, step of ester hydrolysis to lower the MW of the polymer to a degree which is acceptable to become a substrate of the enzymes that are responsible for the second phase of the chain degradation (Scheme 1.1). The rate of the hydrolysis depends on many factors, including pH, environmental humidity or polymer crystallinity; the global rate of biodegradation can also be enhanced by the presence of enzymes like esterases or lactate dehydrogenases and can be lowered by their inhibitors.



Scheme 1.1 – Ester hydrolysis of PLA and lowering of its MW

The rate of the enzymatic phase is notably lowered by crystallinity on account of the reduced accessibility of the tightly packed domains, while it can be enhanced by the presence of residual quantities of monomer or other impurities that perturb the order of chain packing. As expected, the addition of stabilizers or the chemical functionalization of PLA may play a major role too.

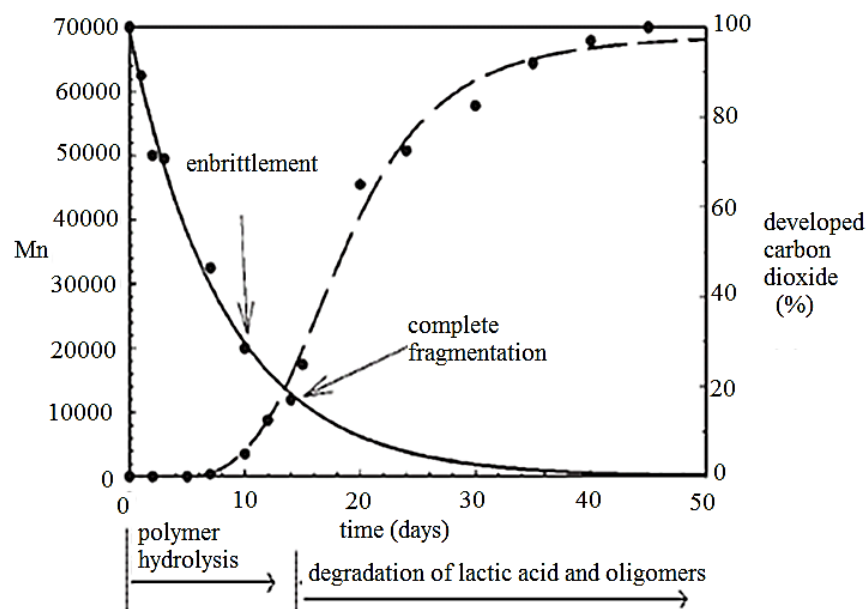


Figure 1.2 – PLA degradation times⁷

At temperatures higher than 180 - 200 °C PLA degrades due to the following processes:

- Hydrolysis catalyzed by traces of water and residual monomer (acidic environment).
- Depolymerization by residual amounts of catalyst.
- Random chain scissions.
- Intermolecular transesterification between monomers and oligomers followed by formation of cyclic structures.

It is possible to enhance PLA thermal stability by eliminating monomer and catalyst impurities (peroxides are effective deactivators for commonly used Sn-based catalysts) as well as by end-capping of the oxydryl groups which are responsible for uncontrollable transesterification reactions. Among the conventional purification techniques, polymer dissolution and reprecipitation is probably the most frequently exploited.

1.1.3 Optical properties of PLA in the UV-Vis range

UV radiation (400 – 100 nm) is commonly subdivided into three intervals. The UV-A region is the less energetic (400 – 315 nm) and includes the most part of the light intensity that reaches the earth surface; the UV-B region (315 – 280 nm), although partially shielded by the ozone layer of the atmosphere, is responsible for a number of photochemical polymer degradation processes. The UV-C region (280 – 100 nm) is

completely shielded by the atmosphere and can have practical importance only if generated artificially. The UV barrier properties of PLA were compared to those of several common traditional properties⁸ finding that, while PET absorbs any radiation with wavelength inferior to c.a. 310 nm, PLA transmits 85% of the intensity still at 250 nm and absorbs significantly only below 225 nm (Figure 1.3).

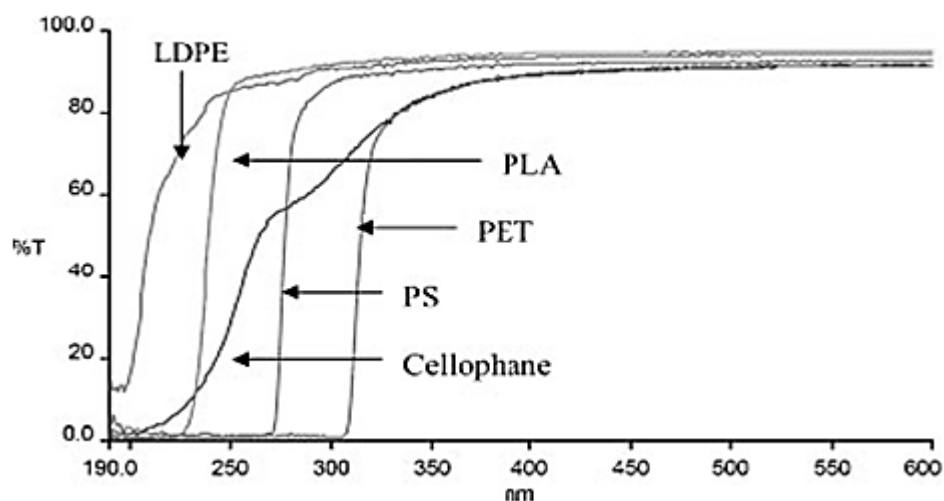


Figure 1.3 – Transmittance of PLA (98% L-lactide; Cargill Dow LLC) and several common commercial polymers

Hence, PLA for packaging, fabrics or coating applications often needs optically active additives or chemical modifications to cope with specific requirements.

Optical properties in the visible range are also of pivotal importance for many polymeric materials since many application fields require a neutral transparent look with minimum absorption and which, even more importantly, should not be spoiled by any color dominant. On the other hand, there is often the need to produce colored items with different hues and intensities and, hence, to develop properly compatible pigments and dyes as well as to directly functionalize the polymer chain with chromophores. Tests conducted on commercial PLA samples showed color properties quite close to those of traditional packaging polymers with a very slight tendency towards cold tones, good luminosity and a very low yellowing index (which are generally positive assets for the aesthetics of this class of materials).²

1.1.4 Lactic acid production

There are two main procedures to obtain LA in industrially relevant quantities, which are (i) a petrochemical synthesis that accounts for only a minor percentage of volumes but constitute the most important way of producing racemic LA, and, after purification,

D-LA; (ii) a fermentative process that transforms a number of possibly renewable sugar sources into exclusively L-LA by means of the so called “LAB” (*i.e.* Lactic Acid Bacteria) and is utilized in the vast majority of industrial plants.

Some commonly utilized LABs are *Carnobacterium*, *Enterococcus*, *Lactococcus*, *Lactobacillus*, *Leuconostoc*, *Oenococcus*, *Pediococcus*, *Streptococcus*, *Tetragenococcus*, *Vagococcus*.⁹ With the exception of streptococci, which are pathogenic and hence excluded from large scale productions, these bacteria are catalogued as GRAS (Generally Regarded As Safe). Homofermentative bacteria produce exclusively LA while heterofermentative bacteria yield a mixture of LA, ethanol, acetate, formate and carbon dioxide. LABs require the addition of several nutritive substances to the regular feed of sugar since they are not able to produce ATP, B vitamin and several amino acids. In order to optimize productivity, these bacteria are kept at a constant pH during fermentation by the addition of NaOH; this compensates for the production of acid, which would otherwise inhibit bacterial growth and activity. Moreover, the quantity of oxygen is controlled and the temperature is set to c.a. 40 °C. Under these ideal conditions, some LABs reach very high levels of LA yield (around 90% of acid from glucose). NaOH is also useful to recover the product as sodium lactate after fermentation, which is achieved by means of a liquid-liquid extraction with alcohols with low solubility in water and a high partition coefficient for the product. The whole fermentative process is 3 – 6 days long while important research efforts are made to improve the overall performance from an economical and environmental point of view.

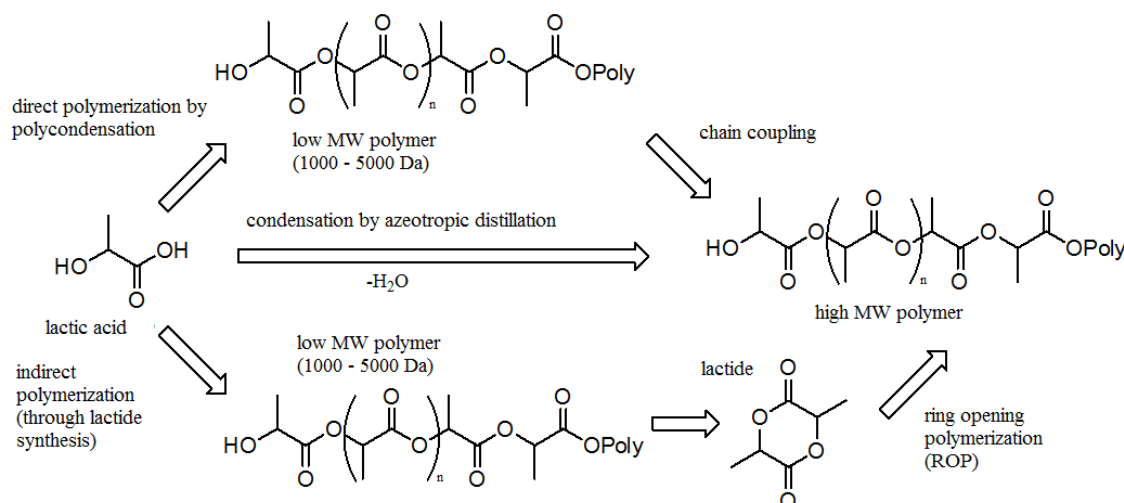
LA can also be obtained from different feedstocks at experimental level; as an example, high yield hydrothermal processes were developed to convert glycerol into sodium lactate in the presence of NaOH with the aim of exploiting this abundant byproduct of biodiesel production. The main side products of this procedure are sodium acrylate, oxalate, formate and carbonate.¹⁰

Raw LA is efficiently purified through a reduced pressure distillation of the acid followed by crystallization, affording LA with 99% chemical purity and 98.6% enantiomeric excess.¹¹

1.1.5 Ring opening polymerization of lactide

Several procedures afford high MW PLA and are based on three main processes (Scheme 1.2), which are (i) dehydro-polycondensation of LA, (ii) coupling reactions between oligomers and (iii) ring opening polymerization (ROP) of *3,6-dimethyl-1,4-dioxandione*, or “lactide” (*i.e.* the cyclic dilactone of LA).¹ The latter is undoubtedly the

most widespread and industrially relevant and was utilized throughout this work.



Scheme 1.2 – Main processes for the synthesis of high MW PLA¹

A notable advantage of ROP is the absence of byproduct (and particularly water) release during polymerization which avoids unwanted hydrolysis reverse-reactions and improves the MW control.

Table 1.2 lists some important thermodynamic parameters related to the ROP of many 5- and 6-membered cyclic monomers; the fundamental requirement for a favored polymerization is a negative free Gibbs enthalpy of the ring opening. According to Flory's assumption the reactivity of an active center is independent of the polymerization grade and expressed as

$$\Delta G_p = \Delta H_p^\circ - T(\Delta S_p^\circ + R \ln[M])$$

In which $[M]$ is the equilibrium monomer concentration. The polymerization is complete when the thermodynamic equilibrium is reached ($\Delta G_p = 0$); at this stage the concentration of residual monomer is given by the standard parameters according to the following relation

$$[M]_{eq} = \exp(\Delta H_p^\circ/RT - \Delta S_p^\circ/R)$$

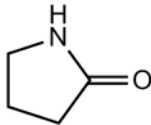
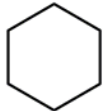
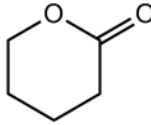
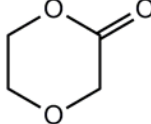
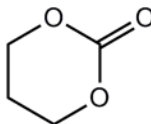
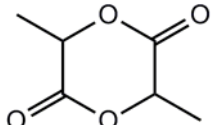
Monomer	Ring size	Monomer/Polymer state	ΔH_p° (kJ/mol)	ΔS_p° (J/mol K)	$[M]_{eq}$ (mol/L)
γ -Butyrolactame 	5	liquid/crystalline	0.4	-30.1	5.1×10^2
Cyclohexane 	6	liquid/crystalline	2.9	-1.05	1.36×10^2
δ -Valerolactone 	6	liquid/crystalline	-27.4	-65.0	3.9×10^{-1}
1,4-Dioxane-2-dione 	6	liquid/solution	-13.8	-45	2.5
Trimethylene carbonate 	6	solution/solution	-26.4	-44.8	5.1×10^{-3}
L,L-Lactide 	6	solution/solution	-22.9	-41.1	1.2×10^{-2}

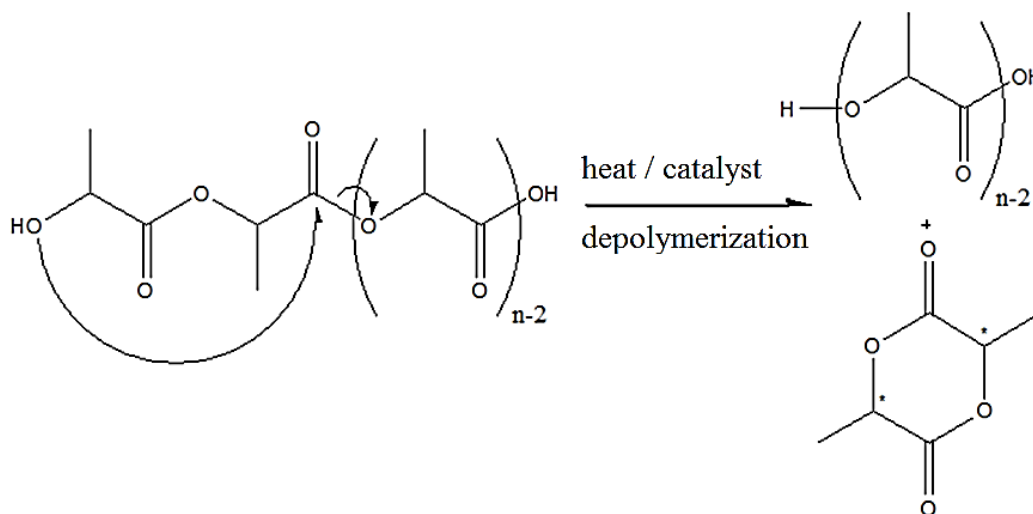
Table 1.2 – Standard parameters of polymerization of some cyclic monomers¹²

The polymerization kinetic is typically first order, with a rate which depends strongly on the steric hindrance of the residues attached to the ring.¹³

Even starting from enantiomerically pure lactide, the risk of racemization during the ring opening reaction needs to be taken into account; in order to avoid negative effects on the polymer tacticity and, hence, crystallinity the polymerization temperature should be kept under rigorous control. The catalyst/monomer system can be optimally designed to yield isotactic, syndiotactic, partially atactic or heterotactic polymer chains.

1.1.5.1 Lactide synthesis

Both at a laboratory and industrial scale, lactide is synthesized by a back-biting depolymerization reaction (reduced pressure, $T = 240\text{ }^{\circ}\text{C}$) of a PLA oligomer obtained by direct polycondensation of LA ($\text{MW} = 1000 - 5000\text{ g/mol}$) (Scheme 1.3).



Scheme 1.3 – Back-biting depolymerization of PLA oligomer to synthesize lactide

U.S. based *Cargill* developed a continuous industrial process for the synthesis of lactide and purification of its vapors by a reverse-flow distillation at reduced pressure.¹⁴ Lactide carries two chiral centers, therefore three isomers are possible, namely two enantiomers (DD- and LL-) and the “meso” form LD-lactide (Figure 1.4). Which of the three is obtained by the back-biting reaction mainly depends on the characteristics of the oligomer and, hence, on the optical purity of the starting LA. The MW of the oligomer utilized as prepolymer is kept low by conducting the polycondensation step in the absence of any catalyst. This reduced pressure polycondensation, carried out at around $150\text{ }^{\circ}\text{C}$, retains almost quantitatively the configuration of the converted LA, on the other hand, stereo-conservation during depolymerization step is less straightforward and depends chiefly on the chosen temperature and the nature of the employed catalyst.

While the “meso” form has a lower T_m compared to the two enantiomers and can easily be separated by crystallization, DD- and LL- forms are characterized by the same physical properties and form a thermodynamically favored stereocomplex if present in equal molar amounts. The latter complex show a higher T_m compared to any single isomer (precisely $126 - 127\text{ }^{\circ}\text{C}$ vs $97\text{ }^{\circ}\text{C}$) and, interestingly, an analogous phenomenon is observed for the stereocomplex formed by the relative polymer chains (*i.e.* L-PLA and D-PLA).

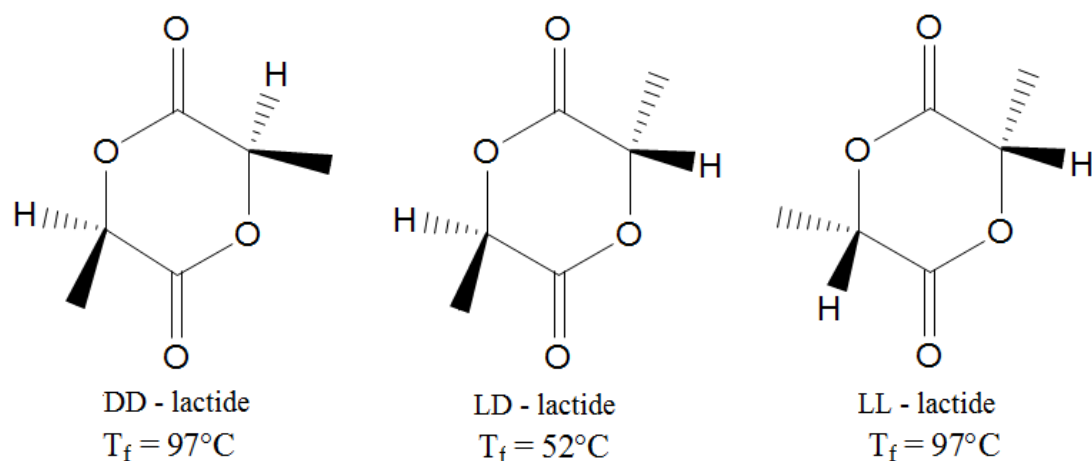
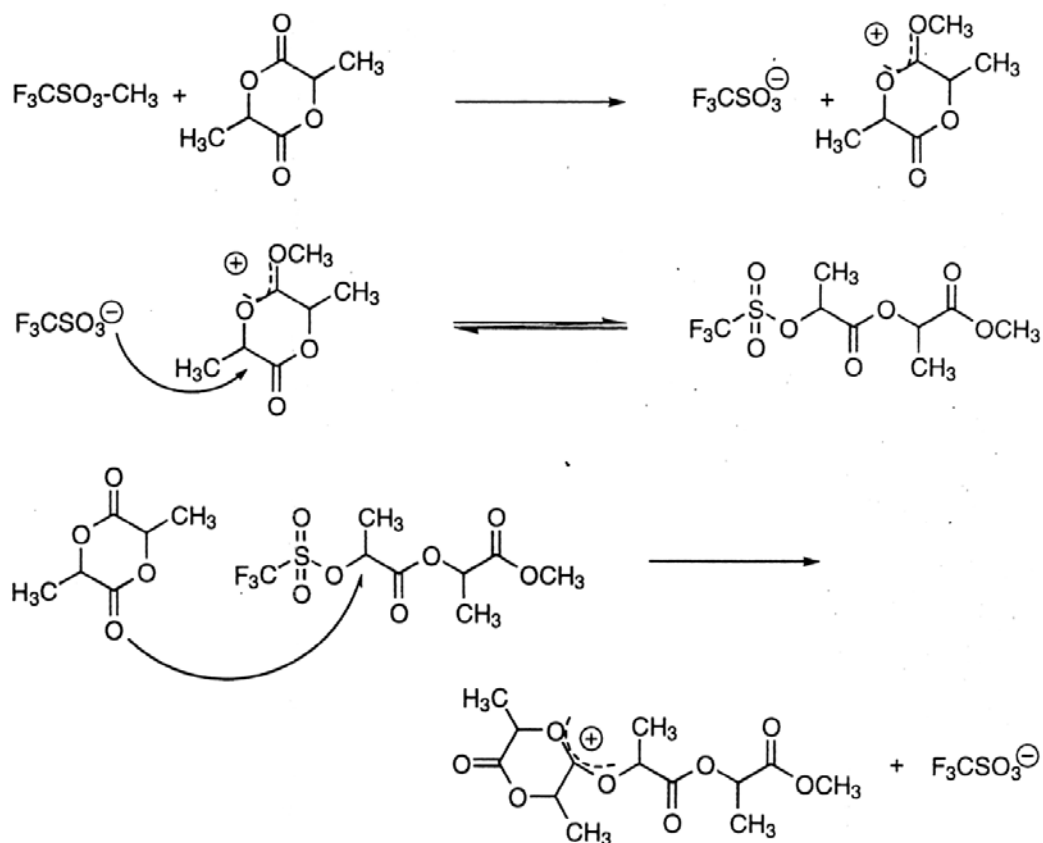


Figure 1.4 – Lactide isomers and respective melting temperatures

The back-biting reaction yields a crude lactide containing impurities like LA oligomers and unwanted lactide isomers, therefore a fractionate crystallization in toluene or a sublimation is usually carried out to obtain a satisfactory purity grade and, hence, to run a proper ROP. The enantiomeric excess can be easily assessed by measuring the melting point or the optical rotation of the dimer.

1.1.5.2 Cationic polymerization

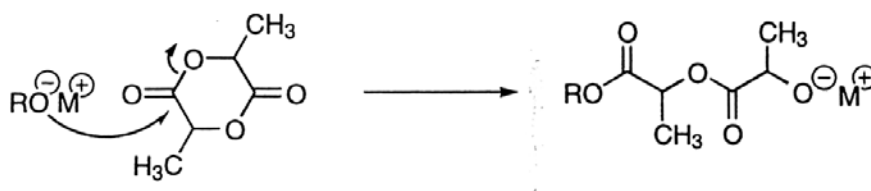
Three main groups of compounds are able to promote the ring opening through a cationic mechanism, which are (i) protic acids like HBr or HCl, (ii) Lewis acids like ZnCl_2 or AlCl_3 and (iii) acylating agents like Et_3O^+ or BF_4^- . Good results were described by Kricheldorf utilizing trifluoromethane sulfonic acid (or “triflic” acid) (Scheme 1.4) or methyldifluoromethane sulfonic acid (or “methyl-triflic” acid). Optically active, high MW PLA is obtained at a temperature below 100°C under these conditions. Moreover, racemization is avoided on account of the $\text{S}_{\text{N}}2$ character of the initiator attack on the protonated or methylated lactide.¹⁵



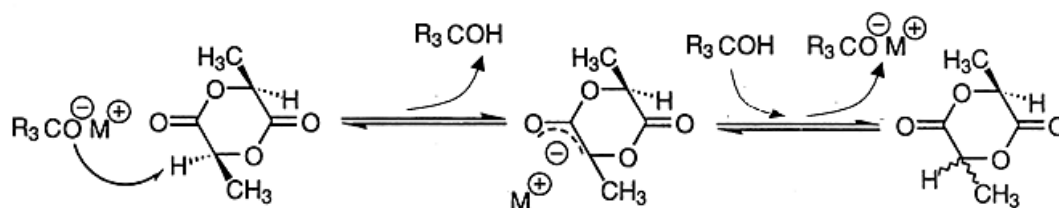
Scheme 1.4 – Mechanism of the cationic ROP of lactide

1.1.5.3 Anionic polymerization

In this polymerization the opening of the cyclic structure is due to the reaction of an anion like potassium methoxide with the carboxylic group of lactide with formation of alkoxide terminations capable of reacting with further lactide molecules (Scheme 1.5). Anionic polymerization of lactide allows for an exceptional control over MW and, especially, over polydispersity index (PDI), yielding polymers very close to the ideal PDI of 1. Nonetheless, racemization is fairly probable if the temperature is not kept close to 0°C (with obvious detrimental effects on polymerization rate) due to deprotonation / random protonation equilibria involving lactide and the ROM^+ initiator (Scheme 1.6).¹⁶



Scheme 1.5 – Mechanism of the anionic ROP of lactide



Scheme 1.6 – Deprotonation / random protonation mechanism responsible for racemization of lactide

1.1.5.4 Coordination-insertion polymerization

Differently from the above mechanisms, coordination-insertion ROP allow to obtain PLA from bulk lactide, with huge cost and environmental benefits. Moreover, the utilized catalysts are less toxic, more tolerant to impurities and required in smaller quantities, adding appeal to this procedure, which is capable of producing biocompatible, high MW, optically active PLA with negligible probability of racemization. It is possible to use zero-valent metals, although the most efficient catalysts are organic salts of Sn(II) and Zn(II), Al alkoxides and compounds of rare earths or group IV metals.^{17,18} The role of the catalyst is enhanced by the covalent bond between the “p” and “d” empty orbitals of the non-bonding doublets of oxygen and the metal.

Among Sn-based compounds, Sn(II)-bis-2-ethylhexanoate (Sn(Oct)₂ or tin “octoate”) (Figure 1.5) deserves to be mentioned on account of its relatively low cost, high activity (yields over 90%) and low racemization (below 1% in moles of lactide). Tin octoate is soluble in melted lactide, enabling bulk polymerization and is catalogued as GRAS (Generally Regarded As Safe) by the FDA, assuring biocompatibility even in the presence of residual traces in the polymer. The presence of free carboxylic groups has no effect on the final MW although the polymerization rate is lowered due to complexation of the Sn(II) ion. On the other hand, free hydroxyl groups influence directly the MW of PLA by acting as chain initiators and, hence, functionalizing groups (Scheme 1.7).¹⁹

In the present work, Sn(Oct)₂ was constantly utilized as ROP catalyst and OH-containing initiators were used to functionalize the polymer and to control its MW.

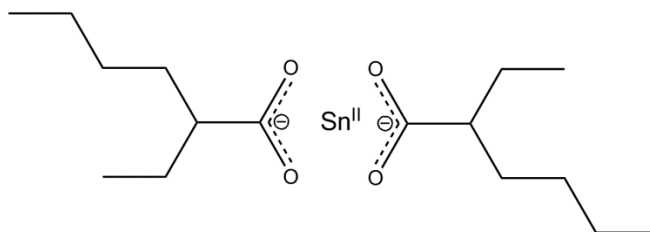
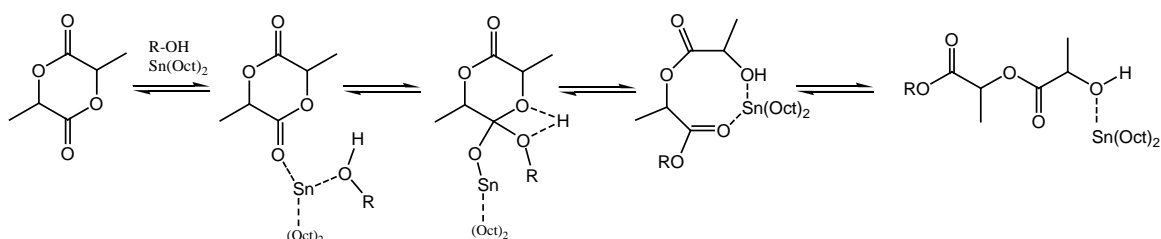
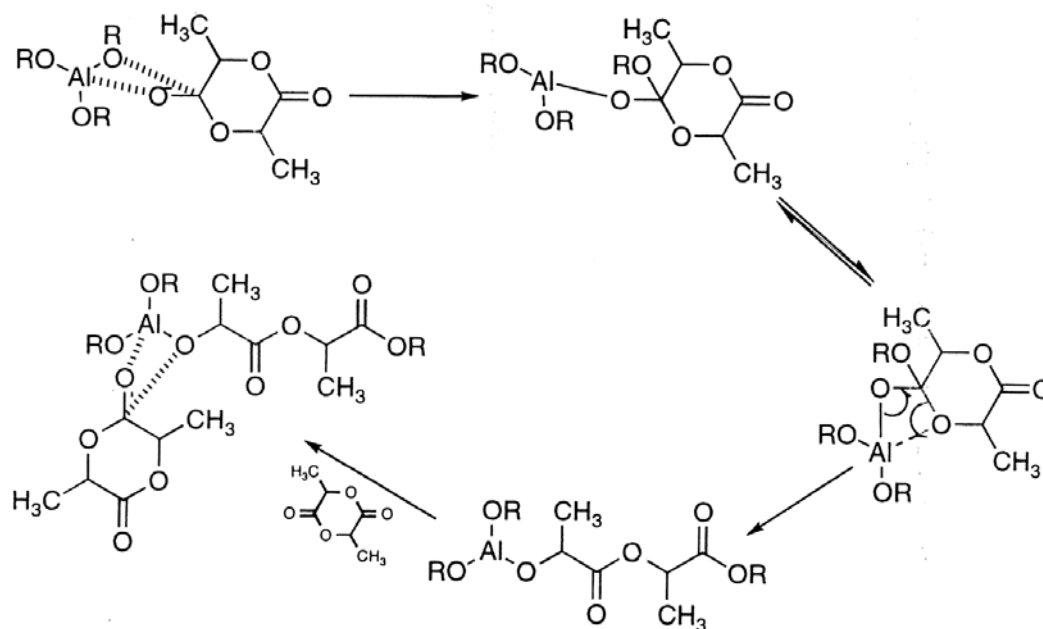


Figure 1.5 – Structure of $\text{Sn}(\text{Oct})_2$



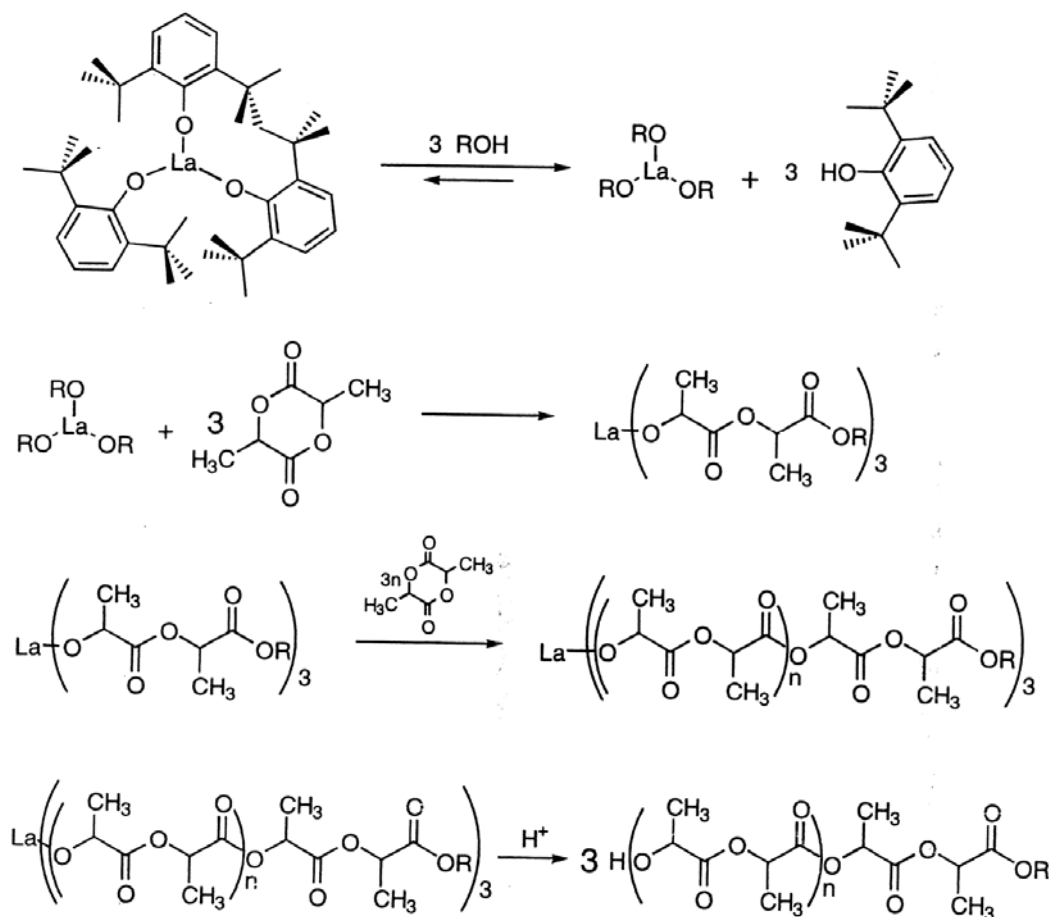
Scheme 1.7 – Mechanism of the $\text{Sn}(\text{Oct})_2$ catalyzed ROP of lactide in the presence of an R-OH initiator

Al alkoxides yield a polymer with relatively low PDI and a high MW. The coordination mechanism is different from that of Sn compounds, nevertheless the role of a RO^- group inserted on one end of the growing chain is still analogous (Scheme 1.8), as demonstrated by Kricheldorf with NMR analyses,²⁰ and the possibility of end-functionalization is maintained.²¹ Y and La organic compounds were studied and showed impressive results in terms of polymerization rate, MW and PDI even at room temperature, low catalyst loading and mild conditions.



Scheme 1.8 – Hypothesis on the catalytic mechanism of the Al alkoxide catalyzed ROP of lactide

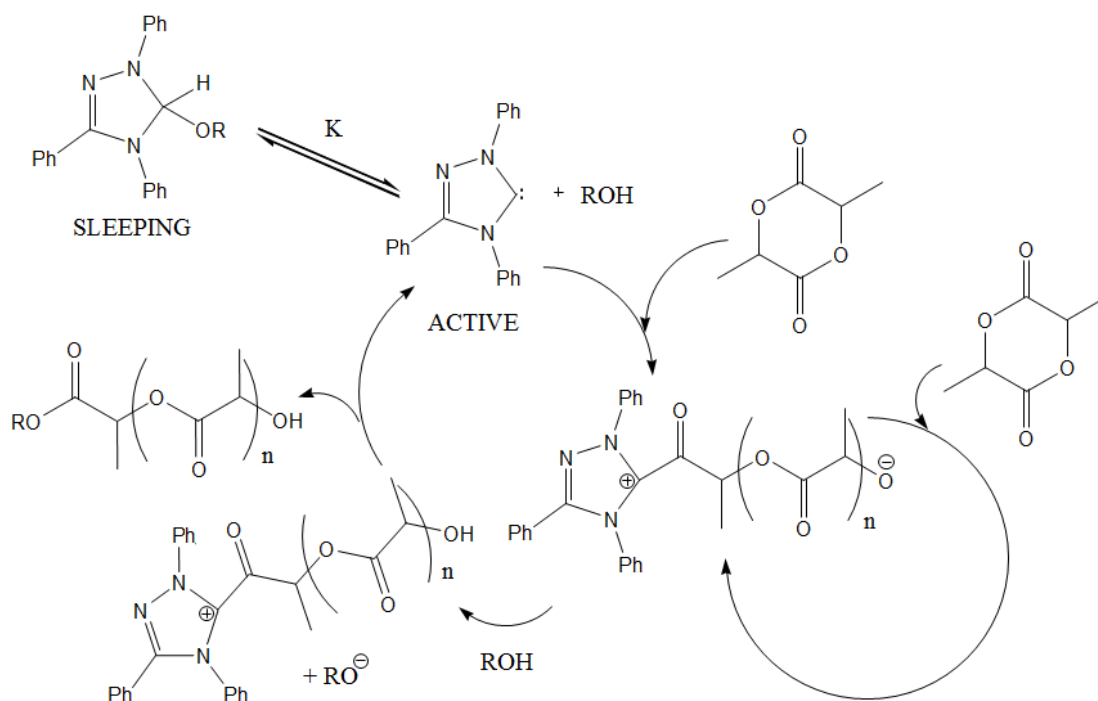
The mechanism relies on catalyst activation by OH groups with formation of $\text{La}(\text{OR})_3$ followed by substitution of OR groups with lactide molecules and rapid polymerization²² (Scheme 1.9).



Scheme 1.9 – Mechanism of the La-alkoxide catalyzed ROP of lactide in the presence of an R-OH initiator

1.1.5.5 Carbene catalyzed polymerization

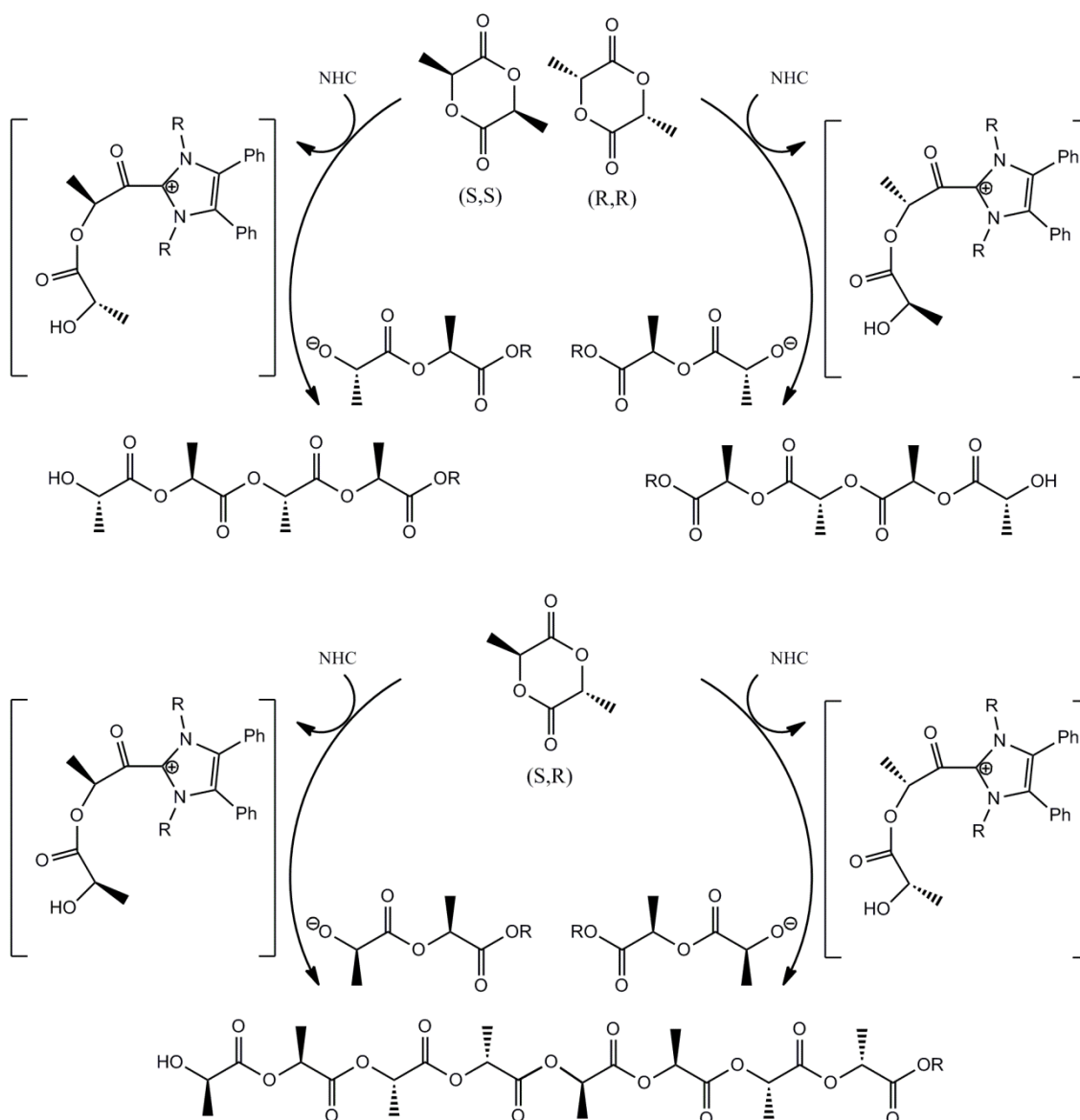
Carbene catalyzed polymerization is a particular case of ROP, also called “Zwitterionic Ring Opening Polymerization”, characterized by the replacement of metal-based catalysts with N-heterocyclic carbenes (NHCs).²³ This technique is called “zwitterionic” because such is the polymer chain during its growth, bearing a positive charge on the heterocycle and a negative charge on the terminal oxygen at the same time (Scheme 1.10). These organic catalysts are highly instable, hence the carbene functionality is formed *in situ* by the addition of a strong base capable of deprotonating the relatively acidic organic carbon. The so obtained catalyst is extremely reactive and immediately initiates the polymerization process to give high MW and low PDI PLA. Again, in the presence of oxydrylic compounds the polymerization rate is high and the control over MW is good, while in the absence of OH groups specific carbenes promote the formation of cyclic PLA. The chemistry, and hence the activity of the heterocycle can be finely tuned by functionalization of the ring and modification of its electronic or steric properties.



Scheme 1.10 – Mechanism of the carbene catalyzed ROP of lactide in the presence of an *R-OH* initiator²⁴

Sterically hindered NHCs induce a very high stereoselectivity and yield stereoregular PLA (Scheme 1.11); precisely, isotactic polymer is obtained from pure LL- or DD-lactide while a heterotactic polymer is favored if the meso-form of lactide is the starting monomer. This is due to the chain-end control mechanism during the macromolecule growth, in which an L-termination tends to react favorably with an L-centre on the lactide molecule.

In order to functionalize the resulting polymer, the heterocycle can be modified by addition of an -OR group which is released as the carbene is formed and initiates the ROP as seen in the aforementioned examples.



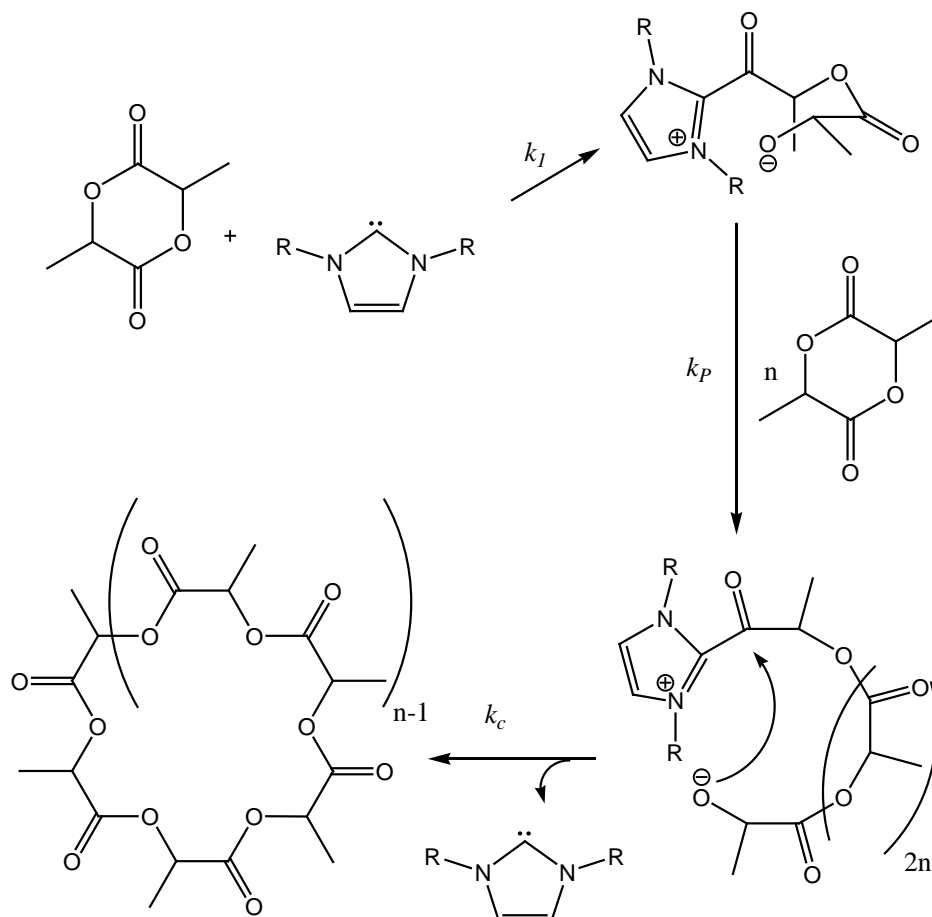
Scheme 1.11 – Mechanism of the chain-end controlled growth of PLA catalyzed by NHCs; isotactic PLA from *L,L-* (*S,S-*) or *D,D-* (*R,R-*) lactide (top) and heterotactic PLA from *meso-* (*SR-*) lactide (bottom)²⁵

1.1.6 Synthesis of cyclic PLA

It is generally difficult to synthesize high MW macrocycles due to both enthalpic and entropic reasons. Some methods utilize a polymeric support to chemically bind the growing chain with the aim of releasing a low MW cyclic PLA at each step by intramolecular reactions. Kricheldorf²⁶ developed a method to expand the size of a ring in a kinetically controlled fashion by means of cyclic Sn-alkoxides initiators. Intensive research was carried out in order to minimize the quantity of residual tin impurities contained in the high MW polymer.

A different approach relies on the carbene catalyzed “Zwitterionic Ring Opening Polymerization” of lactide in the absence of oxydrylic initiators (as mentioned above).

This method affords cyclic PLA with a MW ranging from 7000 to 26000 g/mol under mild conditions (room temperature) and within short reaction times of few tenths of minutes (Scheme 1.12).



Scheme 1.12 – Mechanism of the carbene catalyzed ROP of lactide to cyclic PLA

1.1.7 Typical applications of PLA

1.1.7.1 Commercial applications

PLA can be employed in a number of different applications on account of its good physical and chemical properties; since its T_g and T_m values resemble those of some common commercial polymers (like polystyrene) the required modification of industrial techniques and machinery is minimal. PLA is a suitable polymer for packaging²⁷ and, showing a relatively high permeability to water vapor, it favors the preservation of fresh foods like fruit or vegetables and enhance their shelf life; furthermore, its biodegradability is a strong benefit in terms of waste disposal issues.

As a coating material, PLA is often applied on paper to increase its barrier properties²⁸ although thin films of the polymer alone can also be produced with good mechanical

performances for wrapping applications. In order to optimize this latter use, a number of plasticizers can be added, such as LA oligomers, PEG-bound stearic acid, PPG benzoate and others. A PLA textile fibre is already produced by the U.S. based *Nature Works* with the *Ingeo* trademark²⁹ and can be used without modification as well as easily combined with other common fibres like cotton. Electro-spinning techniques allow to obtain fibres with impressive length and very small diameter showing a particularly high mechanical performance (Figure 1.6).

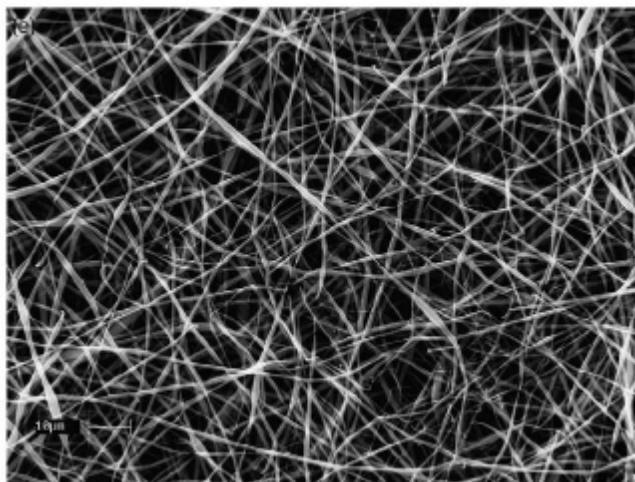


Figure 1.6 – SEM image of PLA nanofibres produced by electro-spinning³⁰

PLA films are utilized for mulching in agriculture because they biodegrade within about one year if exposed to normal atmospheric conditions, without the need of additional removal work and, on account of its biocompatibility, without releasing pollutants to the soil.³¹

1.1.7.2 PLA stereocomplex

The blending of equal amounts of P(L)LA and P(D)LA yields a stereocomplex with different properties compared to each pure polymer.³² This phenomenon is due to the H-bond interactions between groups of the two complementary chains and shifts the T_m of the material from 180 °C of P(L)LA to an impressive 230 °C. Stereocomplexes between star-shaped macromolecules show a further increase in stability due to a higher number of links between different arms.

PLA stereocomplexes can be obtained by means of two procedures, which are (i) solubilizing a 1:1 blend of P(L)LA and P(D)LA;³³ (ii) the *in situ* polymerization of a 1:1 blend of L-LA and D-LA utilizing specific chiral catalysts.³⁴

1.1.7.3 PLA blends and composites

PLA is often blended with PEG with the aim of lowering its T_m and crystallinity; the modification of these physical properties, as well as of the biodegradation rate, is proportional to the amount of PEG and inversely proportional to its MW. The most common blends are PLA / PEG mixtures: in these materials T_m and crystallinity are lower than those of pure PLA and the resulting biodegradation rates are consequently altered.³⁵

The combination of PLA with some inorganic fillers like calcium hydroxyapatites yields biodegradable and biocompatible composite materials with interesting properties of porosity to be exploited for the production of bone prostheses.³⁶ By tuning the blending temperature it is possible to optimize the interaction of the material with the desired biological tissue or system. Composites of P(LD)LA with hydroxyapatite grains showed promising performances as shape-memory materials responsive to pH, temperature or electromagnetic field variations with potential biomedical applications.³⁷

1.1.7.4 Copolymers and modified PLA

PLA alcoholic and carboxylic end-groups can usefully react with different monomers or with the terminal groups of different polymers to give a wide range of block copolymers. These have, generally, lower T_g and T_m values than pure PLA, although copolymers containing salicylic acid lactone or morpholinedione are notable exceptions; the latter can be synthesized from glycolic acid and α -aminoacids.³⁸ Hence, after protection of their functional groups it is possible to insert on the PLA chain some side groups capable of interacting with polypeptidic sequences.³⁹

1.2 Poly(ϵ -caprolactone) (PCL)

1.2.1 General features of PCL

Poly(ϵ -caprolactone) (PCL) was one of the earliest polymers synthesized by the Carothers group in the early 1930s⁴⁰ and became commercially available following efforts to identify synthetic polymers that could be degraded by microorganisms.⁴¹ PCL can be prepared by either ring opening polymerization of ϵ -caprolactone (CL) using a variety of anionic, cationic and coordination catalysts or via free radical ring-opening polymerization of 2-methylene-1-3-dioxepane.⁴²

PCL is a hydrophobic, semi-crystalline polymer; its crystallinity tends to decrease with the increase of molecular weight. The good solubility of PCL, its low melting point ($T_m = 59\text{--}64\text{ }^\circ\text{C}$) and exceptional blend compatibility has stimulated extensive research into

its potential application in the biomedical field.⁴³⁻⁴⁵ Among the numerous advantages over other biopolymers, PCL is characterized by tailorable degradation kinetics and mechanical properties as well as ease of shaping and manufacturing, which enables to obtain appropriate pore sizes and to control the delivery of drugs contained within its matrix. Functional groups could also be added to render the polymer more hydrophilic, adhesive, or biocompatible which enabled favourable cell responses. PCL degrades at a slower rate than polyglycolide (PGA), P(LD)LA and the respective copolymers and was therefore originally used in drug-delivery devices that had to remain active for over 1 year and in slowly degrading suture materials. During the last decades the interest on PCL derived mainly from the field of tissue engineering research on account of its peculiar rheological and viscoelastic properties, which renders it easy to manufacture and manipulate into a large range of structures and scaffolds (Figure 1.7).⁴⁶⁻⁵⁰

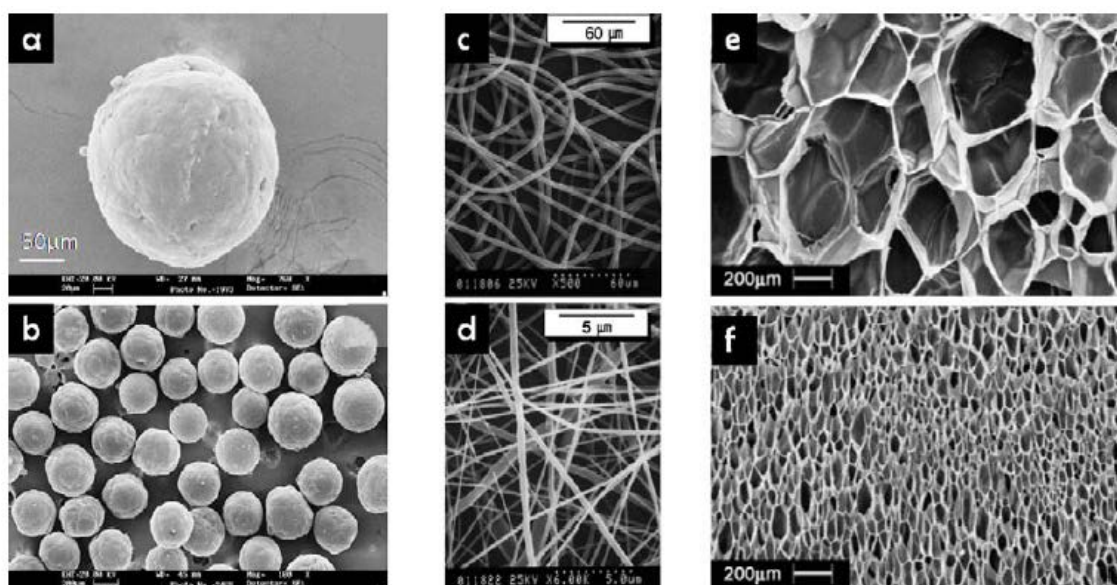


Figure 1.7 – Micrographs of PCL nanospheres (a, b), nanofibers (c, d,) and foams (e, f)

The relatively inexpensive production routes for PCL, compared with other aliphatic polyesters, are very advantageous; furthermore, the fact that a number of PCL containing drug-delivery devices already have FDA approval and CE Mark registration enhances commercialization. Interestingly, in spite of their clear advantages, PCLs have not been widely translated to the clinic use.

1.2.2 Synthesis and physicochemical properties of PCL

Similarly to PLA, PCL is prepared by the ROP of its cyclic monomer, CL, with catalysts such as $\text{Sn}(\text{Oct})_2$ and in the presence of low molecular weight alcoholic initiators to control the molecular weight of the polymer.^{43,51} There are several other processes

which can be exploited for the polymerization of PCL, including anionic, cationic, coordination/insertion ROPs, and analogous characteristics can be highlighted with respect to PLA (see above paragraphs) and other lactones. The number-average molecular weight (M_n) of PCL samples may generally be in the range from 3000 to 80,000 g/mol⁵² although each polymerization method affects the resulting MW, PDI and end group composition.⁴³

PCL is a semi-crystalline polymer having a T_g of -60 °C and melting point ranging between 59 and 64 °C, which enables easy formability of the polymer at relatively low temperatures. PCL is soluble in chloroform, dichloromethane, carbon tetrachloride, benzene, toluene, cyclohexanone and 2-nitropropane at room temperature. It shows low solubility in acetone, 2-butanone, ethyl acetate, dimethylformamide and acetonitrile and is insoluble in ethanol, petroleum ether and diethyl ether⁵³. PCL can be blended with other polymers to improve stress-crack resistance, dyeability and adhesion; moreover, blending is often used to have better control over the permeability of materials. PCL was used in combination with polymers such as cellulose propionate, cellulose acetate butyrate, PLA and PLA / PGA copolymers with the aim of tuning the rate of drug release from microstructure.⁴⁵ Polymer blends based on PCL were categorized with three types of compatibility, which are (i) exhibiting only a single T_g ; (ii) mechanically compatible, showing the T_g values of each component but with superior mechanical properties; (iii) incompatible, exhibiting the enhanced properties of phase-separated materials.⁵⁴ Compatibility of PCL with other polymers depends on the ratios between the components.

Copolymers (block and random) of PCL can be obtained using many monomers and prepolymers; examples include ethylene oxide, poly(vinyl chloride), chloroprene, poly(ethylene glycol), polystyrene, diisocyanates (urethanes), tetrahydrofuran, glycolide, lactide, δ -valerolactone, substituted caprolactones, 4-vinyl anisole, styrene, methyl methacrylate and vinyl acetate.⁴³

1.2.3 Biodegradability and biocompatibility of PCL

PCLs can be biodegraded by outdoor living organisms (bacteria and fungi), but they are not biodegradable in animal and human bodies because of the lack of suitable enzymes.⁵⁵ Hence, although the polymer is bioresorbable, the process takes a relatively long time and initially propagates via hydrolytic degradation. The PCL homopolymer shows a total degradation time of 2–4 years (depending on the starting molecular weight),⁵⁶⁻⁵⁸ nonetheless, the rate of hydrolysis can be altered by copolymerization with

other lactones or glycolides / lactides.⁴²

As previously described for PLA, PCL undergoes a two-stage degradation process comprising: (i) the non-enzymatic hydrolytic cleavage of ester groups; (ii) an intracellular degradation which takes place when the polymer is more highly crystalline and of low MW (*i.e.* lower than 3000 g/mol). In the first stage, the degradation rate of PCL is essentially identical to the *in vitro* hydrolysis at 40 °C and obeys the first order kinetics. It was hypothesized that the HO• radical was likely to be a significant cause of PCL degradation in implantable devices.⁵⁹ Chen et al. studied the *in vitro* degradation behavior of PCL microparticles and compared it to that of PCL film (PBS buffer at 37±1 °C; pH = 7.4). The physical shape of the PCL specimen had no obvious effect on its degradation rate, suggesting that homogeneous degradation dominates the process. Accelerated degradation models for PCL have been investigated by several groups, primarily utilizing thermal methods.⁵⁹ Persenaire et al. proposed a two-stage thermal degradation mechanism of PCL⁶⁰ and found that in the first stage there was a statistical rupture of the polyester chains via ester pyrolysis reactions. The second stage led to the formation of CL as the result of an unzipping depolymerization process.

Pitt et al. showed that the mechanism of *in vivo* degradation of PCL, PLA and their random copolymers was qualitatively the same. The degradation rate of random copolymers was much higher than those of the homopolymers under the same conditions.⁶¹ On the other hand, the degradation rate of PCL / PLA block copolymers was found to be intermediate between PCL and PLA homopolymers and increased with PLA content in the 0 – 40% range.⁶² However when the PLA content was greater than 40%, the degradation was found to exceed that of the homopolymers.⁶³

Degradation kinetics are highly dependent upon the molecular weight of the polymer(s). High molecular weight molecules take a much longer time to degrade, necessitating a greater number of ester bonds to be cleaved in order to generate water-soluble monomers/oligomers and, hence to allow erosion to proceed.

For the study of intracellular degradation, low molecular weight ($M_n = 3000$ g/mol) PCL powders were used, reporting that the powdered polymer was rapidly degraded and absorbed within 13 days inside the phagosomes of macrophages and giant cells, and that the sole metabolite was 6-hydroxyl caproic acid. Figure 1.8 illustrates the mechanism of hydrolytic PCL degradation. 6-Hydroxyl caproic acid and acetyl coenzyme A are formed as hydrolysis intermediates, which in turn enter the citric acid cycle and are eliminated from the body.⁶⁴

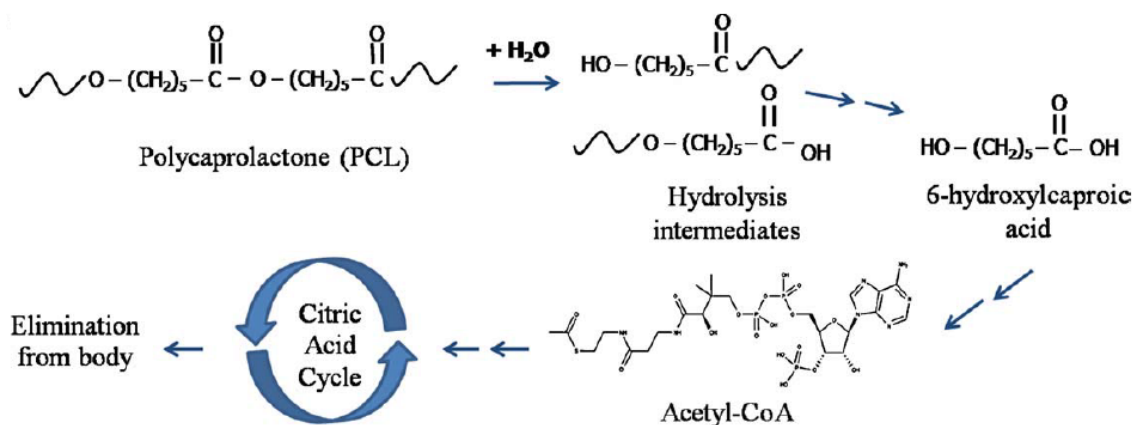


Figure 1.8 – Intracellular degradation process of PCL via its hydrolysis intermediates

In general, bioresorbable polymers and devices are well tolerated by living tissues;⁶⁵ nonetheless, the release of acidic degradation products from bioresorbable polymers and implants may contribute to some secondary inflammatory reactions. The determination of both the degradation rate of PCL and the local tissue clearance are crucial in predicting the concentration of byproducts present in the tissue and the resultant host response. The inflammatory response due to PCL / PLA copolymers after implantation in male wistar rats was studied in detail by Pitt and co-workers.⁶⁶ The injection of microspheres into the body resulted in the activation of neutrophils and caused mild localized inflammation. Inflammatory reactions in bones were less pronounced than in muscles.

1.3 Poly(ethylene glycol) (PEG)

1.3.1 General properties of PEG

Poly(ethylene glycol)s are employed in a number of widespread applications since they present low toxicity⁶⁷ and are approved for food⁶⁷ and biomedical use.^{68,69} They are especially utilized in the field of drug discovery⁷⁰ on account of their hydrophilicity, decreased interaction with blood and high bio-compatibility. PEGs are also used as soluble polymeric supports for catalysts in organic synthesis⁷¹ and as eco-friendly alternatives to substitute volatile or halogenated organic solvents. PEGs are not flammable or corrosive as well as readily commercially available at low cost, being formed from ethylene oxide by simple epoxide ring opening.

PEG is an amphiphilic polymer with a high solubility in water and in many organic solvents including toluene, dichloromethane, ethanol, and acetone. It is insoluble in less polar solvents such as hexane, cyclohexane or diethyl ether,⁷² and in scCO_2 .⁷³ It is able

to dissolve many common organic solids, some coordination compounds (such as metal phosphine complexes) and it presents some interesting characteristics including high polarity, high boiling point and expandability with CO₂.⁷³ Moreover, PEG is stable to acidic or basic, oxidative or reductive conditions and at high temperatures (up to 150 – 250 °C).⁷⁴ On account of a relatively large heat of fusion, PEG is among the most promising candidates as a safe and cost-effective energy-storage material to replace conventional phase-change compounds like inorganic salt hydrates and their mixtures.⁷⁵ Being (much cheaper) acyclic analogues of crown ethers, special properties arise from their cation complexation ability:⁷⁶ the same PEG can coordinate metal cations of different sizes, due to a flexible helical conformation generating cavities with variable sizes. However, the salt complexation ability depends on the nature of the metal cation and of the anion as well as on the MW of PEG.

1.3.2 Melting, solidification and crystallinity of PEG

Depending on its MW, the T_m of PEG may vary in the range of 1 – 66 °C while the heat of fusion lies in the range of 165.0 – 189.7 J/g (Figure 1.9).⁷⁵ PEGs with low molecular weight (less than 800 g/mol) are viscous liquid at room temperature; those having a molecular weight above 900 g/mol are waxy solids, but they melt at a moderate temperature (45–55 °C) and can therefore be used as viscous liquid solvents. MW also influences the degree of crystallinity of the polymer in the range of 83.8 – 96.4%; the increased tendency of high MW polymers toward the formation of a crystalline phase is related to their lower segmental mobility and more convenient geometrical alignment. It was observed that the T_m of a blend of PEGs lies between the values relative to the pure components; hence, an advantage of using blends as a replacement for pure PEGs is the possibility of fine-tuning the physico-chemical properties of the resulting material.

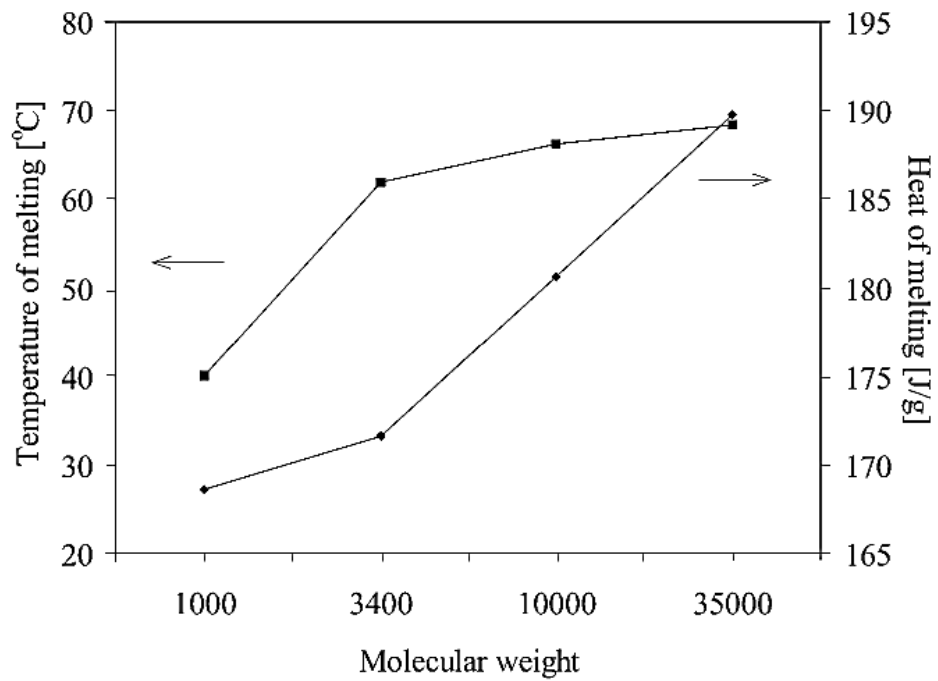


Figure 1.9 – Melting temperature and heat of melting of PEGs with different MW

An increase in MW causes also the increase in the solidification temperature; during solidification numerous small spherical structures join together and impinge on their neighbours forming a multi-layered lamellar texture (Figure 1.10). The kinetics of this process (namely, the spherulite growth rate) proved to be stable with time until the impingement with other spherulites occurs.

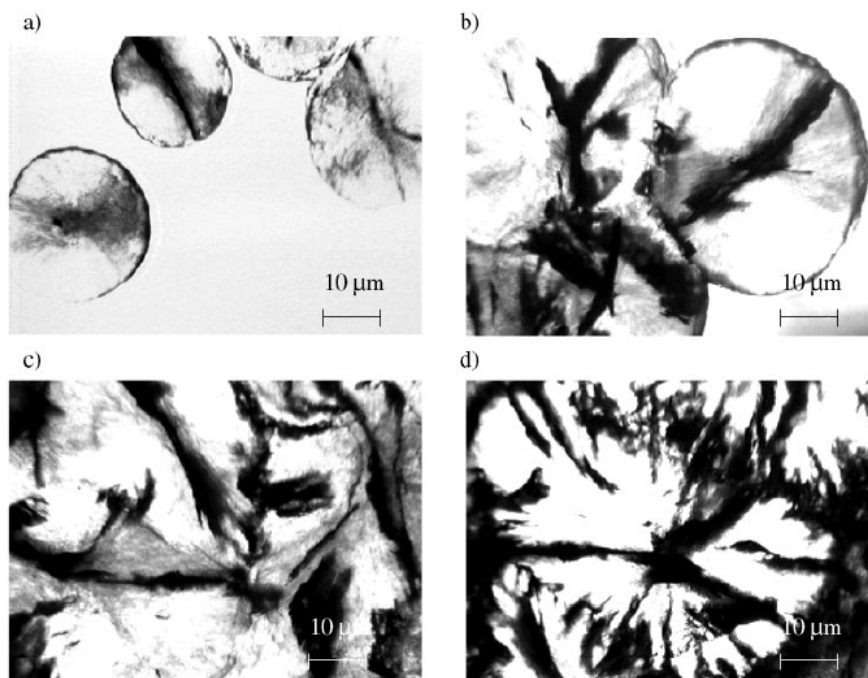


Figure 1.10 – Optical micrographs of PEG-10000 solidification steps (a to d)

It is worth noting that the polyether structure is an easy target for thermal oxidative degradation in the presence of an oxygen atmosphere. At elevated temperature (over 70 °C) PEG peroxides are formed, leading to a random chain-scission process with the formation of complex mixtures of oxygenated, low molecular weight PEGs.⁷⁴

1.3.3 PEG in biomedical applications

The ability of PEG to influence the pharmacokinetic properties of drugs and drug carriers is currently utilized in a wide variety of established and emerging pharmaceutical applications (Figure 1.11). The change in the pharmacokinetics of administered drugs upon shielding by or binding to PEG results in prolonged blood circulation times. This, consequently, increases the probability that the drug reaches its site of action before being recognized as foreign and cleared from the body. Therefore, the majority of conjugated drugs as well as liposomal and micellar formulations on the market or in advanced clinical trials are PEG-containing products.⁷⁷ In fact, all polymer-based stealth drug-delivery systems that have been brought to the market up to now contain PEG-functionalized (PEGylated) products, and no other synthetic polymer has yet reached this status.^{78,79,77}

It is currently the most used polymer in the biomedical field of drug delivery and the only polymeric therapeutic that has market approval for different drugs. The success of PEG is based on its hydrophilicity, decreased interaction with blood components, and

high biocompatibility. Not every non-ionic hydrophilic polymer can provide stealth behavior since a number of structural parameters influence the biological and stabilizing effects and have to be carefully taken into consideration.⁸⁰ The molecular weight as well as the polydispersity index of the polymer has been shown in many applications to be important in this respect. The molecular weight of PEG commonly used in pharmaceutical and medical applications ranges from 400 to about 50000 g/mol. PEG with a MW in the range of 20000 – 50000 g/mol is mostly used for the conjugation of low molecular weight drugs such as small molecules, oligonucleotides, and siRNA with the aim of increasing the size of these conjugates above the renal clearance threshold. PEGs with lower MW (in the range of 1000 – 5000 g/mol) are often used for the conjugation of larger drugs, such as antibodies or nanoparticulate systems. In this way, opsonization and subsequent elimination by the reticuloendothelial system is avoided, enzymatic degradation is reduced, and cationic charges are hidden. PEG of about 3000 g/mol to 4000 g/mol is given orally as a laxative.

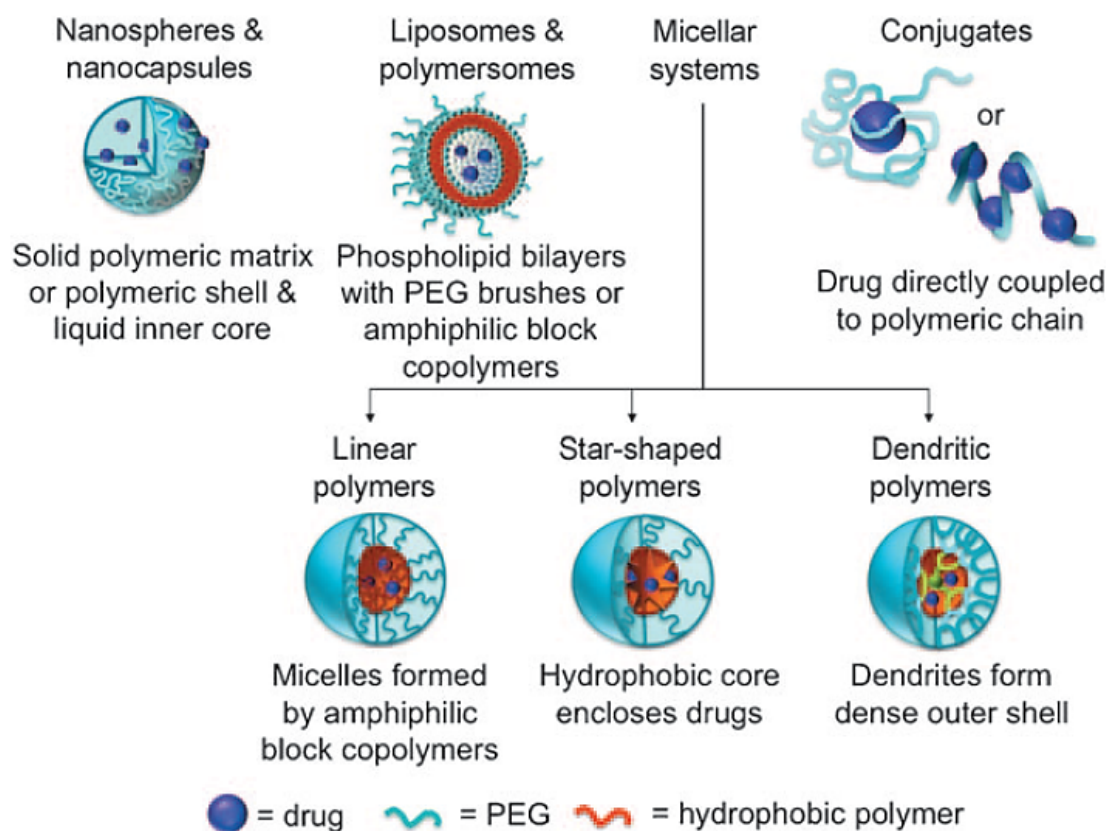


Figure 1.11 – PEG-based carrier systems for drug-delivery

In principle, a biodegradable polymer would be more beneficial in certain biomedical applications, since difficulties in achieving complete excretion would be avoided. However, it should be kept in mind that the excretion of the polymer is not directly

dependent on its molecular weight but rather on the hydrodynamic volume, which is affected by the architecture of the polymer. For example, star-shaped polymers and dendrimers show lower hydrodynamic volumes than linear polymers with similar molecular weight.^{81,82} In general, a polymer with PDI below 1.1 provides an acceptable homogeneity to ensure reproducibility in terms of body-residence time and immunogenicity of the carrier system.^{83,77} This demand is fulfilled by PEG, since very well defined polymers with PDIs around 1.01 are readily accessible by the anionic polymerization of ethylene oxide.

When attached to hydrophobic drugs or carriers, the hydrophilicity of PEG increases their solubility in aqueous media and provides them with a greater physical and thermal stability; at the same time, it prevents or reduces aggregation of these drugs *in vivo*, as well as during storage. This properties result from the steric hindrance and / or masking of charges through the formation of a “conformational cloud” generated by the highly flexible polymer chains, which have a large number of possible conformations. The higher the rate of transition from one conformation to another, the more the polymer exists, statistically, as a cloud which prevents interactions with blood components as well as protein (*e.g.* enzymatic degradation or opsonization followed by uptake by the reticuloendothelial system).⁸⁴ The formation of an efficient sterically hindering cloud on the surface of particles is also influenced by factors such as the molecular weight, the surface density, and the way PEG is attached to the surface (*e.g.* mushroom-like or brush-like PEGylation, Figure 1.12).^{85,86}

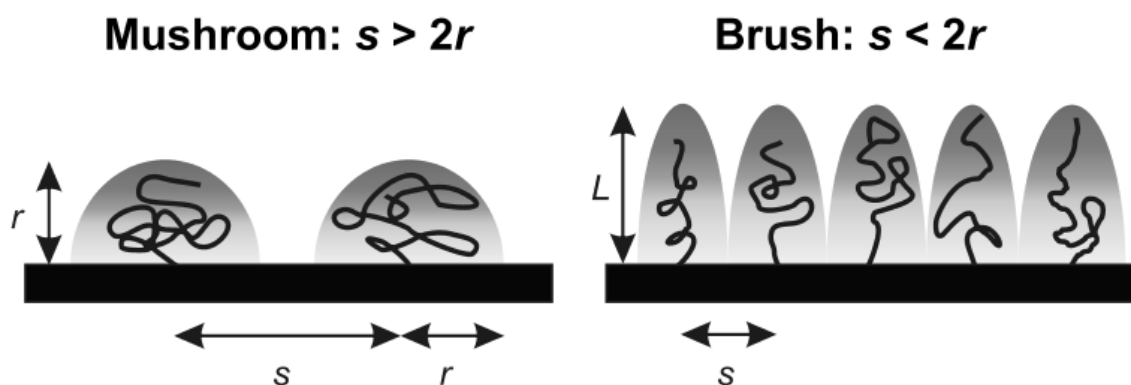


Figure 1.12 – Mushroom-like and brush-like surface PEGylation

1.3.4 PEG biocompatibility and toxicity

Since PEG is a non-biodegradable polymer, the use of low MW PEGs would be preferable for applications in which excretion from the body is needed. However, oligomers with a molecular weight below 400 g/mol were found to be toxic in humans

as a result of sequential oxidation into diacid and hydroxy acid metabolites by alcohol and aldehyde dehydrogenases. The oxidative degradation significantly decreases with increasing MW and, therefore, a polymer well above 400 g/mol should be used to avoid toxicity.^{87,88} On the other hand, the molecular weight should not exceed the renal clearance threshold to allow complete excretion of the polymer (a MW limit of 20000 – 60000 g/mol is reported for non-degradable polymers, corresponding to the albumin excretion limit and a hydrodynamic radius of approximately 3.5 nm).^{89-91,83,77}

The most prominent side product formed during the synthesis of PEG is 1,4-dioxane (*i.e.* the cyclic dimer of ethylene oxide). Currently, 1,4-dioxane is stripped off from the product under reduced pressure. Dioxane is classified by the International Agency for Research on Cancer (IARC) in group 2b (*i.e.* possibly carcinogenic in humans with sufficient evidence from animal experiments). Therefore, the European Pharmacopoeia (Ph. Eur.) limits the dioxane content to 10 ppm for pharmaceutical applications. Nonetheless, an evaluation of dioxane by the US Department for Health and Human Services revealed that rats exposed over two years to 111 ppm of 1,4-dioxane in air did not show any evidence of dioxane-caused cancer or any other health effects.

PEG can also contain residual ethylene oxide from the polymerization process that is classified by IARC in group 1 (carcinogenic in humans), as well as formaldehyde, which is in the same group. As a consequence, the Ph. Eur. limits the content of ethylene oxide to 1 ppm and the amount of formaldehyde to 30 ppm in PEG for pharmaceutical applications. The toxicity of these contaminants clearly demonstrates the necessity of using pharmaceutical grade PEG for biomedical applications.

1.3.5 The use of PEG as a reaction medium

PEG finds application as the reaction medium in substitution, oxidation, reduction and organometallic transformations;⁹² moreover, the intrinsic characteristics displayed by PEG allowed the development of synthetic methods for the generation of metal nanoparticles (NPs) according to the principles of the polyol method.⁹³⁻⁹⁶ The process was first introduced to produce submicron-sized metal powders of uniform shape and narrow size distribution at low temperature under closed-system conditions. The metal species is reduced in solution at a temperature usually below that used either by solid-state methods or under reducing conditions in the presence of hydrogen. The redox^{97,98} process involves the simultaneous reduction of the metal precursor, suspended in a liquid polyol (usually ethylene glycol), and oxidation of the polyol solvent. The polyol acts not only as the reaction solvent but also as a reducing agent and stabilizer, limiting

particles growth and preventing their agglomeration and sintering. However, optimization of the experimental parameters is necessary depending on the utilized metal compound. The main parameters driving the size, morphology and size distribution of the NPs are the reaction temperature and time, together with the MW of PEG.^{99,100} In addition, the combination of the advantages of sonication or microwave irradiation together with the intrinsic characteristics of PEG (high viscosity, low volatility, high permanent dipole) can provide powerful tools to generate NPs. Also the mode and order of reagent additions, the use of additives (nucleating and protective agents) and the substrate concentration are important factors to take into accounts in the optimization of reaction conditions.

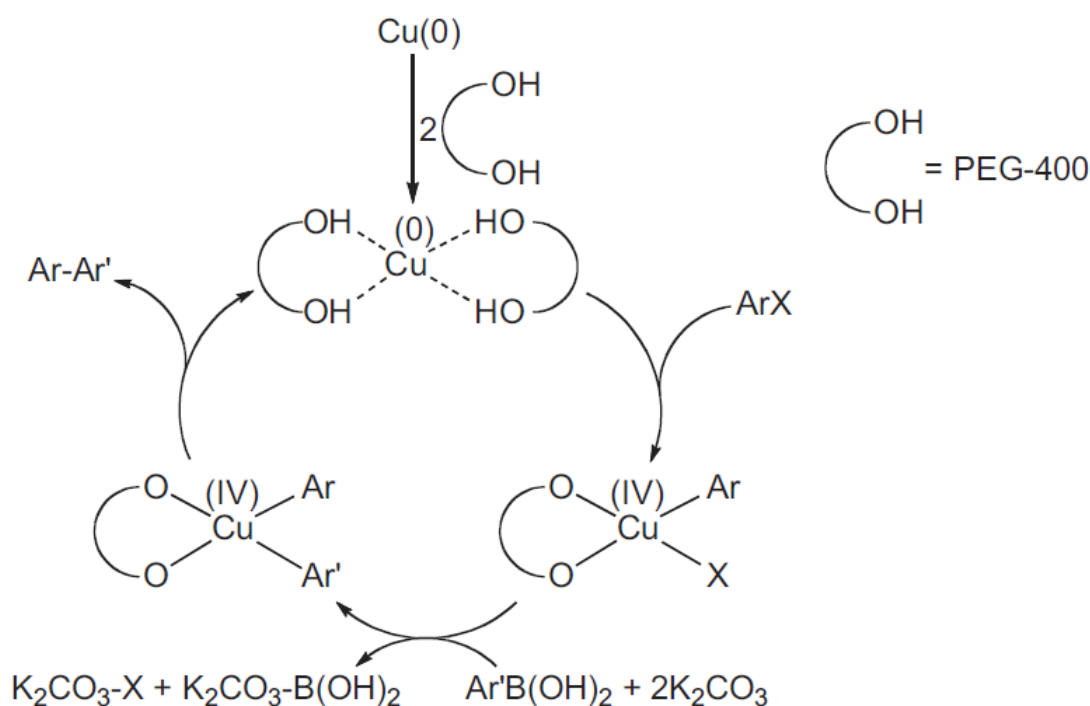
The use of PEG as the reaction solvent for metal-catalyzed organic reactions allows for an easy recovery of the products and the possibility to recycle the PEG-metal catalytic system. Mainly, two protocols can be used, depending on the physical state of the PEG used in the experiment. (i) In the case of liquid PEGs (MW lower than 800 g/mol) hexane, cyclohexane or diethyl ether are added to the crude mixture: the reaction product is usually recovered in the organic phase, while the metal catalyst remains in the PEG phase and can be reused for further cycles by adding new substrates. In some cases it could be necessary to add some water during the extraction, in order to reduce the viscosity of the PEG medium and to allow an easier recovery of the product. In order to avoid the leaching of metal catalyst into the organic phase, it is also possible to freeze the biphasic system organic solvent / PEG before proceeding with the separation. (ii) In the case of solid PEGs (MW above 1000 g/mol), the reaction product and the PEG-metal catalytic system can be separated by a simple and convenient experimental work-up procedure based on a precipitation / filtration step. The crude of the reaction is usually dissolved in a small amount of CH_2Cl_2 , and precipitated by pouring into diethyl ether (or tert-butyl methyl ether), a solvent in which the polymer is completely insoluble. The solid catalytic system comprising PEG and metal is recovered as a precipitate, while the organic product is recovered in the filtrate and isolated by simple evaporation of diethyl ether. The use of solid PEGs also allows to recycle the catalytic system; the catalyst containing precipitate obtained from the first experiment can be fed again with the substrates and the reaction can be carried out for further cycles.

1.3.5.1 Examples of Cu-catalyzed reactions in PEG

The ligand-free Cu-catalyzed Suzuki-Miyaura cross-coupling reaction between iodobenzene and 4-methylphenylboronic acid (K_2CO_3 , 110 °C, 8 h) gave a higher yield

when PEG was used as solvent (84%) in the place of DMF (72%).¹⁰¹ Carrying out the same reaction for 12 h in PEG-400 or PEG-200 resulted in a 99% product yield. A useful synthetic procedure was developed using copper powder as the catalyst precursor and high to excellent product yields were observed with good tolerance to various functional groups. In addition to aryl iodides, it was possible to convert aryl bromides and activated aryl chlorides under these conditions.

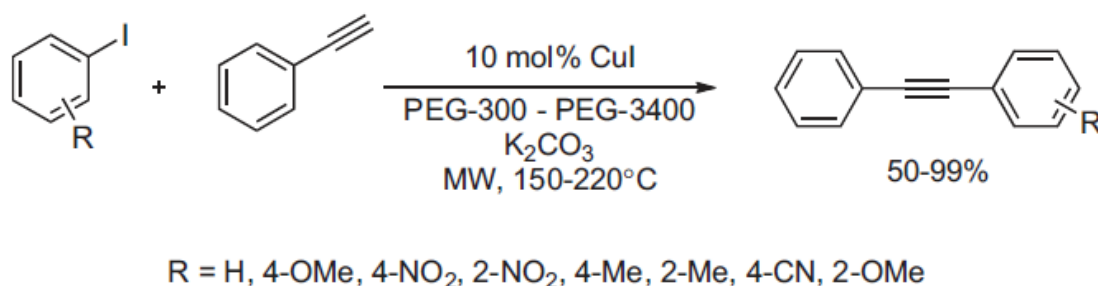
Recycling of the catalyst showed a yield decrease from 99% in the first run to 66% in the sixth run. The proposed reaction mechanism assumed a classical oxidative addition, transmetalation and reductive elimination cycle with the PEG acting not only as a recycled medium, but also as a ligand (Scheme 1.13).



Scheme 1.13 – Mechanism of Cu-catalyzed Suzuki-Miyaura coupling in PEG-400

A simple catalytic system was developed to perform Cu-catalyzed Sonogashira reaction in PEG (Scheme 1.14).¹⁰² Copper(I) iodide (10 mol%) and potassium carbonate were used in a various PEGs to afford diphenyl acetylenes in good to high yields. The catalytic system utilized an advantage of microwave heating and the efficiency of PEG reaction medium, which was superior to DMF. In the studied system, important advantages of PEG mainly concern the absence of homocoupling products in the studied system and easy recycling by precipitation. High efficiency of PEG as solvent in ligand-free conditions was observed for Sonogashira cross-coupling between phenylacetylene and iodobenzene;¹⁰³ however, the utilized CuBr / BINOL catalytic system was more

efficient in DMF than in PEG-400.



Scheme 1.14 – Sonogashira cross-coupling between phenylacetylene and aryl iodides

Sreedher et al. have developed a Cu(I)-based catalytic system with high efficiency in one-pot synthesis of 1,4-disubstituted 1,2,3-triazoles.¹⁰⁴ The reaction was carried out via nucleophilic displacement and 1,3-dipolar cycloaddition and several solvents were involved in the comparison (THF, CH₃CN, DMSO, *t*-BuOH), resulting in selection of PEG-400 and water as the best options. For a large number of substrates, the reaction in PEG-400 did not require a base, and proceeded in higher yields for a shorter period of time. Catalyst recycling was successfully carried out.

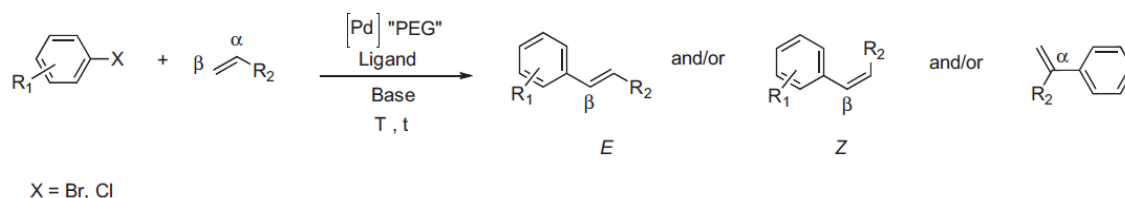
The *in situ* formation of Cu-based nanoparticles was observed in a Cu₂O / Cs₂CO₃ / PEG-3400 system, which allowed the development of a mild, simple and efficient protocol of N-arylation.¹⁰⁵ The reaction was carried out without additional ligands and its practical utilization was enhanced by microwave heating, while the important role of PEG to generate and stabilize nanoparticles was underlined by the authors. The scope of the developed synthetic reaction included cross-coupling of indole and benzimidazole with aryl iodides and bromides.

PEG was employed as the reaction medium in transition metal-mediated living radical polymerizations¹⁰⁶ and, specifically, studies of the Cu-catalyzed polymerization of methyl methacrylate and styrene showed accelerated kinetics in PEG compared to traditional organic solvents. The easy and efficient recovery, an important advantage of PEG system, resulted in polymer product with greatly reduced amount of residual metal. Polymerization of methyl methacrylate in PEG-600 was reported in CuX₂ / TMEDA catalytic system.¹⁰⁷ The process was carried out in a kinetically well-controlled manner and resulted in a product with quite narrow polydispersity.

1.3.5.2 Examples of Pd-catalyzed reactions in PEG

Heck–Mizoroki coupling allows the arylation of a double bond in the presence of a

Pd(0) catalyst (Scheme 1.15). For acyclic electron-poor olefins, the terminal β -arylation product is always obtained as a mixture of *E* (major product) and *Z* (minor product) isomers, while in the presence of electron-rich mono substituted linear olefins, a mixture of α - and/or β -arylated products is obtained. The regioselectivity depends on the mechanism involved (*i.e.* neutral or cationic), and on the nature of both the halide coordinating the metal center in the oxidative addition intermediate and the bidentate ligand.

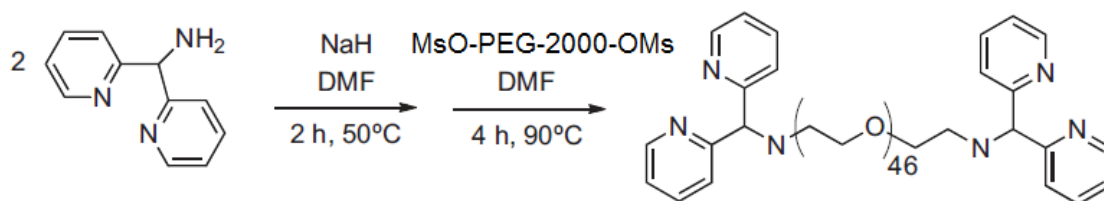


Scheme 1.15 – General scheme for the Heck-Mizoroki arylation reactions in PEG

As reported by Chandrasekar et al.,¹⁰⁸ when PEG-2000 was used as the reaction medium, without additional ligand, a single regioisomer was obtained with a good *E* / *Z* diastereoselection, independently on the electronic nature of the starting olefin. The C-C bond formation was achieved by reacting aryl bromides carrying electron-withdrawing or electron-donating substituents with activated electron-deficient ($R_2 = \text{CO}_2\text{Et}$), neutral ($R_2 = \text{Ph}$) and less reactive electron-rich ($R_2 = n\text{-BuO}$) olefins in the presence of the catalytic system composed of PEG-2000, $\text{Pd}(\text{OAc})_2$ and Et_3N . In all cases, the aryl palladium species attacks the β -carbon of the olefin, which is in sharp contrast with the results obtained either in ionic liquids,¹⁰⁹ leading almost exclusively to the arylation of the α -olefinic carbon of butyl vinyl ether, or in conventional solvents (DMF, DMSO, CH_3CN)^{110,111} where products are obtained with a variable α / β ratio. The method did not seem to be useful for the reaction of aryl chlorides. Recycling was carried out for five runs, with constant yields and 90% of palladium retained in the PEG phase, as determined by residual analysis.

In a Wacker-type oxidation process, alkenes were oxidized to ketones using a PEG-200 / PdCl_2 / $\text{H}_3\text{PV}_2\text{Mo}_{10}\text{O}_{40}$ catalytic system,¹¹² in aerobic conditions. Propene was converted into acetone (89%) in a palladium-catalyzed process leading to Pd(0), which is re-oxidized to Pd(II) by a polyoxometalate affording a V(IV) species; the latter was then converted into the active polyoxometalate in the presence of the molecular oxygen. For higher 1-alkenes, the corresponding 2-ketones were obtained in low yield (20%) with total conversion of the remaining substrate to 2-alkenes via an acid-catalyzed

isomerization. Hou and co-workers¹¹³ described the aerobic oxidation of alcohols using a PEG-2000 / Pd(OAc)₂ catalytic system, in which 2,2-dipyridyl amine end-groups are covalently attached to PEG-2000 (Scheme 1.16) to improve Pd stabilization.

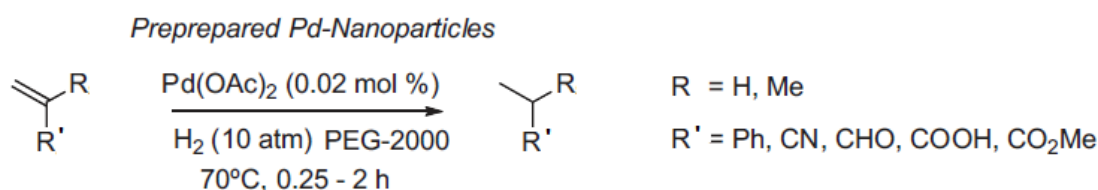


Scheme 1.16 – Functionalization of PEG with 2,2-dipyridyl amine end-groups

Aromatic alcohols, aliphatic secondary and allylic alcohols were converted into the corresponding ketones with good yields (>86%) in the presence of molecular oxygen (1 atm). However, the reaction was not effective if PEG-2000-Pd(OAc)₂ was used as catalytic system due to the formation of a large amount of bulk Pd, as shown by TEM analysis, proving the positive effect of the 2,2-diaminopyridyl ligand, able to keep homogenous the system all along the process and for the four consecutive catalytic cycles. Dominguez and co-workers¹¹⁴ developed a method for the synthesis of aromatic ketones using secondary alcohols, methylene compounds or benzyl substrates, in an aerobic oxidation process using Pd NCN- and CNC-type pincer complexes; these proved very active when PEG-400 was used as the reaction solvent instead of water or DMSO / water mixtures. The target oxidation gave excellent yields (up to 99%) with a relatively low catalyst loading (down to 10⁻⁸ mol%) and for a large variety of substrates, regardless of steric and electronic effects. The final product could be recovered by low-temperature extraction (-78 °C) while the PEG phase, containing the catalytically active species, could be recycled up to six times.

Jiang and co-workers⁹⁹ reported the *ex situ* preparation of nanoparticles from a PEG-2000 / Pd(OAc)₂ system without the use of any ligand. Although a high hydrogen pressure (10 atm) was necessary to achieve full conversion (Scheme 1.17), the catalytic system was effective for the selective hydrogenation of alkenes, especially those bearing electron-withdrawing groups. The catalytic system could be effectively recycled ten times and the products recovered by extraction after each cycle were analyzed by atomic absorption spectroscopy (AAS), showing the absence of palladium leaching. The palladium nanoparticles were prepared in liquid PEG-400, PEG-800, PEG-1000 or solid PEG-2000 and PEG-4000 from Pd(OAc)₂ and their efficiency was tested in the hydrogenation reaction of cyclohexene. Keeping constant the concentration of

$\text{Pd}(\text{OAc})_2$, the best activity and selectivity was obtained in PEG-800, PEG-1000 or solid PEG-2000. Complete conversion of starting materials was possible in 80 – 110 min showing that the activity is not only dependent on nanoparticles size (*i.e.* 3 – 5 nm for PEG-400 and PEG-800; 7 – 9 nm for PEG-2000), but it is also a function of the polymer MW. It was suggested that the mass transfer of organic compounds was more favorable in PEG-2000 than in the case of PEG-800 or PEG-1000 due to the bigger gap between PEG molecules around the palladium particles. In PEG-4000 the catalytic activity was poor with only 6% conversion of cyclohexene after 90 min, which could be due to factors such as larger nanoparticles size (19 – 23 nm), highly viscous medium, poor mass transfer, ineffective stabilization of particles (precipitation of black palladium was observed).



Scheme 1.17 – Synthesis of alkenes by Pd-NPs catalyzed hydrogenation

1.4 Metal-polymer macrocomplexes

This new class of products has recently expanded the application fields of macromolecules, gaining increasing research interest during the last decade, and includes polymers or copolymers functionalized with ligand groups involved in metal coordination bonds. The resulting metal-polymer complexes demonstrate peculiar properties such as tunability of MW, novel optical activity or the capability of the metal centre of catalyzing organic reactions while still anchored to the macromolecular ligand.

It is worth mentioning that the easy end-functionalization of PLA and PCL, which stems from the ROP mechanism in the presence of oxydrylic initiators, favors the use of these polymers for the synthesis of macrocomplexes. The vast range of available initiators allow to optimize the coordination properties of these macromolecular ligands while a proper monomer / initiator ratio gives polymers with a good control over MW. In the case of PLA, the use of different isomers of starting lactide allows to tune the crystallinity and, hence, solubility of the obtained macroligand or macrocomplex. This synthetic versatility is not the only asset of PLA and PCL, since biodegradability and biocompatibility are suitable for its use in drug-delivery systems or biologically active compounds in general. On the other hand, a post-functionalization approach is

commonly adopted in the case of PEG; macroligands can be obtained from commercial non functionalized polymers by activation of the end-group(s) (*e.g.* via mesylation or tosylation of the terminal CH₂OH moiety) followed by reaction with a molecule bearing the ligand group.

1.4.1 Structure of different macrocomplexes

The position of the metal-ligand centre with respect to the polymer chains determines the overall structure of a macrocomplex (Figure 1.13). Starting from an end-monofunctionalized linear polymer “A-[-]” (“[-]” = ligand group) it is possible to obtain, by complexation of a metal ion “M”, A-[M]-A homodimers, which are called “homoleptic” polymers and copolymers, or A-[M]-B heterodimers (or “heteroleptic” polymers and copolymers). In the latter case it is necessary to develop a synthetic strategy which is selective towards the heteroleptic product and avoids the statistical formation of the two homoleptic species A-[M]-A and B-[M]-B. The reversibility of the coordination bond which links the polymer chains appears as a promising feature for several applications. As an example, when A and B are polymers with different affinity towards a certain solvent it is possible to obtain phase separation at a nanoscopic level as long as the complex is preserved and phase separation at a macroscopic level as soon as decomplexation takes place. On the other hand, if the ligand group is placed on the termination of a covalent block copolymer “A-*b*-B-[-]” it is possible to obtain A-*b*-B-[M]-B-*b*-A complexes which retain micro-phase separation regardless of the state of the metal centre. As expectable, placing two ligand groups at the chain ends of polymer “B” it is possible to reversibly synthesize a tri-block A-[M]-B-[M]-A macrocomplex by addition of “A-[-]” macroligands.

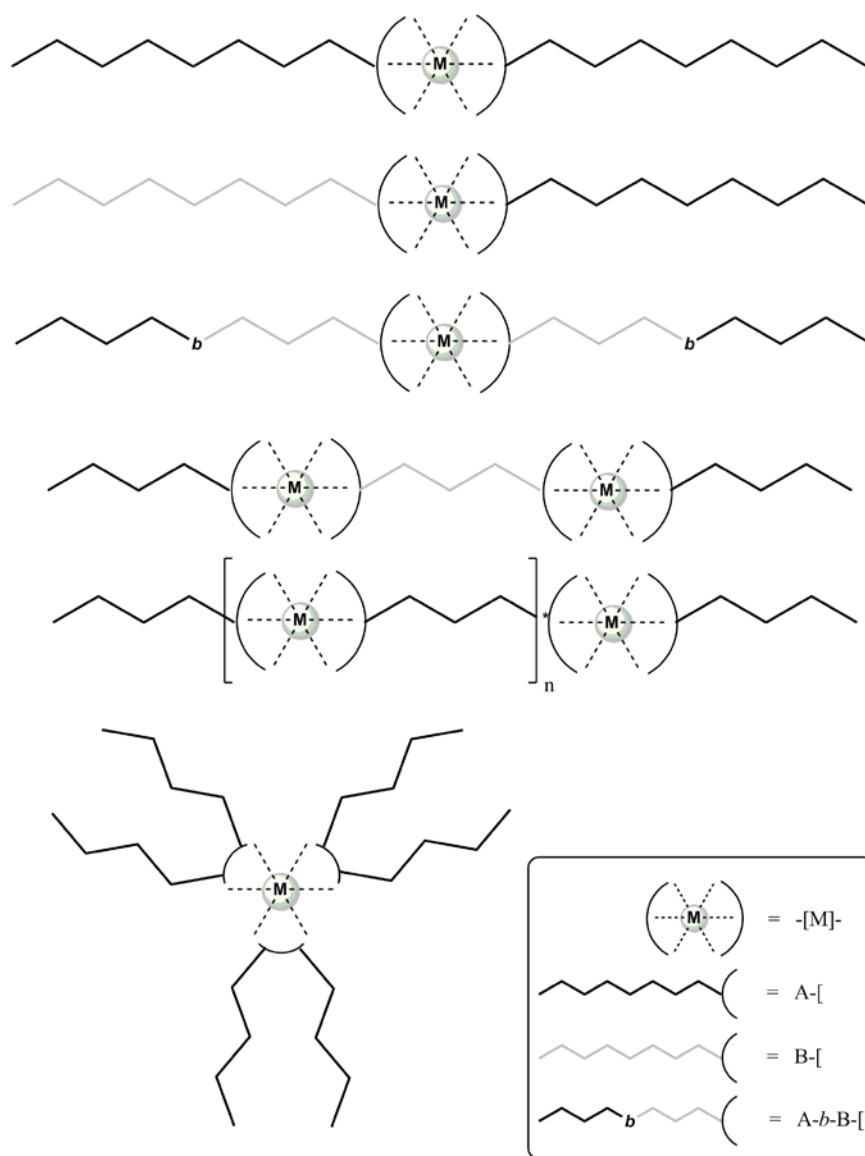


Figure 1.13 – Graphic representation of supramolecular architectures of some metal-polymer macrocomplexes

Designing analogous synthetic pathways, the number of supramolecular combinations rises greatly as well as the physico-chemical properties that can be obtained. A different approach is to functionalize both polymer chain ends and synthesize a long sequence of metal complexes capable of bonding these “macromonomers” in analogy to a polycondensation (the obtained MWs are often quite high in this cases). Importantly, a variety of star-shaped architectures can be obtained by the coordination of monofunctionalized polymers to metal centers that can accommodate more than two ligands, or, alternatively, by the synthesis of multi-arm macroligands. It is worth noting that the charge on the metal complex has a marked influence on the supramolecular aggregation processes and, hence, on the morphology of these species. Moreover, the counter-ion employed to neutralize the charged macrocomplexes (and particularly its

steric hindrance) may play a significant role and disturb the interactions between polymer chains or metal cations.

1.4.2 Main examples of macrocomplexes

The most studied metal-ligand system in the field of linear macrocomplexes is probably the versatile $\text{Ru}[\text{terpy}]_2^{\text{II}}$. Terpyridine-based macroligands were prepared by different procedures, which are (i) functionalization of preformed polymer chains;^{115,116} (ii) by termination of anionic styrene polymerizations with chloroterpyridine¹¹⁷ and (iii) using the ligand as an initiator onto which polymer chains are directly grown.¹¹⁸⁻¹²¹ The latter synthetic method allows, in principle, to obtain a quantitative functionalization although it is viable only with a limited number of polymerization techniques (such as NMRP; RAFT; ROP). Among other transition metal ions, Ru(II) is chosen because, in spite of long complexation times and harsh oxidation conditions, the stability of its complexes with bipyridines and terpyridines is particularly high and the synthesis can be selectively directed towards heteroleptic macrocomplexes (Figure 1.14).

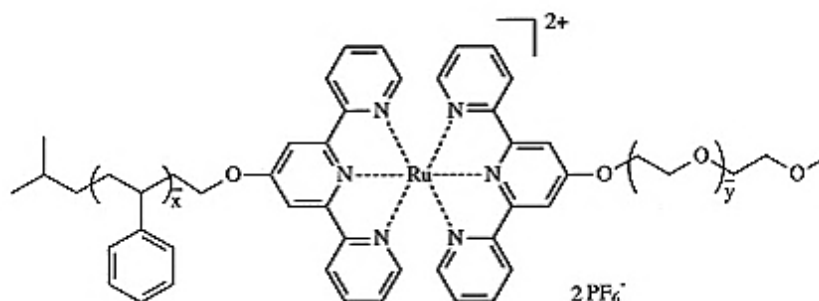


Figure 1.14 – PS-[Ru]-PEO linear heteroleptic macrocomplex¹²²

More precisely, the latter target is achieved by coordination of an “A-[]” type macroligand to a Ru(III) ion (which can accommodate a single terpyridine) followed by the addition of a “B-[]” type species under reducing conditions (since Ru(II) can accommodate two terpyridine ligands).¹²³ This strategy was exploited to synthesize macrocomplexes by combination of hydrophobic PS- and hydrophilic PEG-based macroligands of different MW, with morphologies depending on the MW combination. The difference in morphology, which could be observed and characterized in the melted and solution state, was also rationalized on the basis of the steric hindrance of the employed counter-ion (Figure 1.15). In the presence of a relatively small anion like PF_6^- PS and PEO chains are positioned radially around a core composed by the $\text{Ru}[\text{terpy}]_2^{\text{II}}$ centers and the anions themselves. When a larger anion like BPh_4^- is employed the aggregation follows a lamellar pattern in which the two micro-phases (hydrophilic and

hydrophobic) are in alternation with the charged metal centers and the neutralizing anions.

Totally biocompatible macrocomplexes were prepared in which a Fe(II) ion links together two phenyl-terpyridine functionalized PLA chains; despite iron was used in the place of ruthenium these complexes proved sufficiently stable to resist the shear forces of GPC analyses.¹²⁴

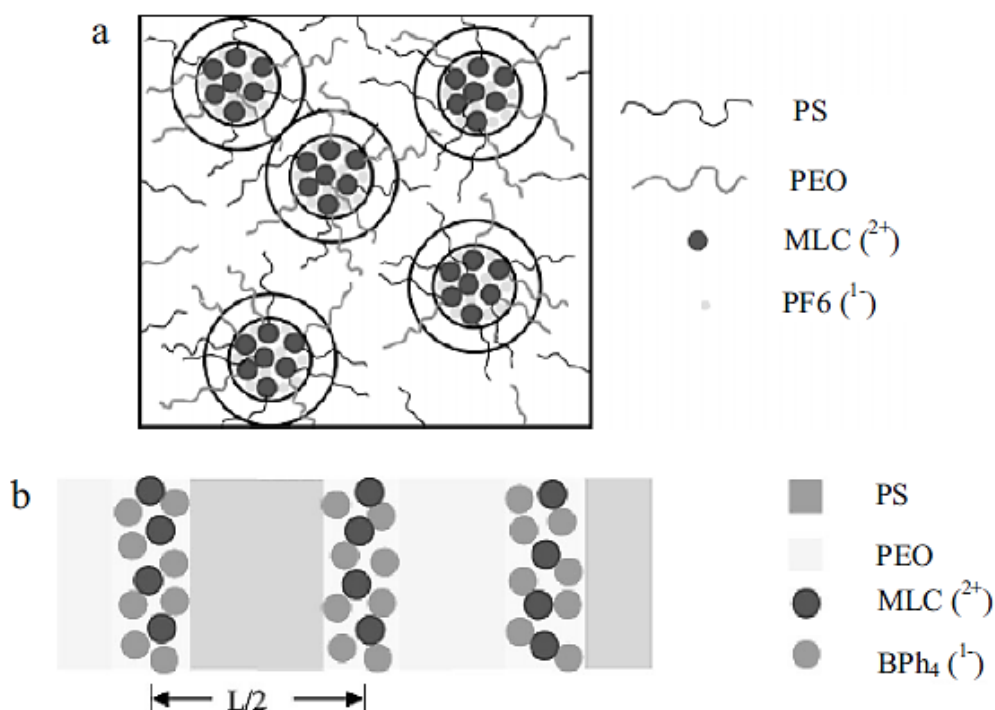
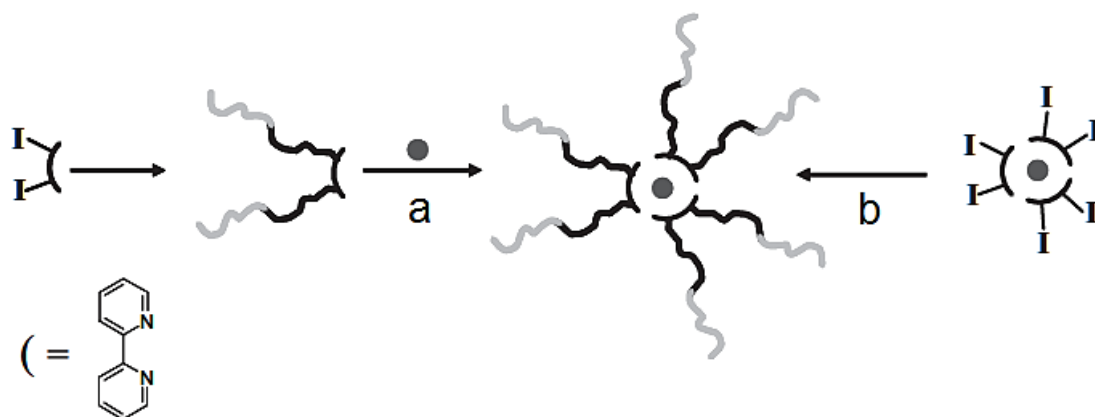


Figure 1.15 – Melt morphology model for the heteroleptic macrocomplex: (a) in the presence of PF_6^- ; (b) in the presence of BPh_4^- .¹²³

Star-shaped macrocomplexes bearing 3 to 6 arms were synthesized by coordination of Ru(II) or Fe(II) ions with three bipyridine-based macroligands consisting of one or two polymer chains. In this particular case, the formation of complexes bearing two different polymer species (“hetero-arm” star copolymers) can follow two pathways, which are (i) the formation of homoleptic complexes between ligands carrying different polymer chains on the same bipyridine or (ii) the formation of heteroleptic complexes.^{125,126} The first option requires an orthogonal synthetic strategy to obtain the macroligand from a bifunctional initiator, nonetheless selectivity is no more an issue during the complexation step and a wide range of metal ions become available, including the less stable but biocompatible Fe(II).¹²⁷ On the other hand, the possibility of inducing macro-phase separation by means of a decomplexation reaction is lost since the link between

the two species of polymers is covalent.

Star-shaped homoleptic complexes were also prepared in which every arm consists in a covalent block copolymer obtained, as an example, by the sequential ROP of lactide and ϵ -caprolactone initiated by bis-hydroxymethylbipyridine.¹²⁸ Other possible strategies to obtain similar effects include the combination of ROP and ATRP yielding PCL or PLA blocks linked to PtBA or PMMA blocks as well as the sequential ATRP of styrene and methyl acrylate¹²⁹ (Scheme 1.18/a).



Scheme 1.18 – Alternative methods for the synthesis of star-shaped macrocomplexes: (a) utilizing macroligands; (b) utilizing a macroinitiator

The same products can be synthesized, alternatively, utilizing a preformed iron or ruthenium complex bearing functionalized bipyridines as a “macroinitiator” for the subsequent polymerization (Scheme 1.18/b).^{130,131} As an example, Fe(II) complexes bearing dibenzoylmethane (Dbm) -PCL, Dbm-PLA and Dbm-PCL-*b*-PLA macroligands^{132,133} could be obtained both by the macroligands based pathway and the macroinitiator based route. It is worth noting that the Fe(Dbm)₃ complex utilized as an initiator for the ROP of lactide gave macrocomplexes with very low PDI in the absence of any added catalyst, hence effectively replacing Sn(Oct)₂.

Four-arm star-shaped PEG macrocomplexes were synthesized by coordination of four Cu(I) ions with four dipyridylpyridazine-based macroligands arranged in a grid-like fashion,¹³⁴ nonetheless, the use of a metal center which is relatively prone to oxidation requires to avoid any aqueous environment and limits the application field.

Pt(II) ions were coordinated by a bipyridinic macroligand bearing two polymer chains of different chemical nature (PEG, PMMA or PCL) and neutralized by chloride or toluene-dithiolate anions. Interestingly, the high activation energy for the formation of a bis-bipyridinic complex (partly due to the steric hindrance of planarly positioned

chelating ligands) hampered the coordination of a second ligand to this metal center.¹³⁵

Conjugated macromonomers of varied chemical nature (among them, fluorene-containing monomers) were polymerized by means of Zn(II) complexation reactions with the terpyridine functionalized terminations.^{136,137} The resulting coordination polymer showed superior photo- and electro-luminescence properties compared to the monomer with the possibility of tuning these parameters by varying lateral substituents. An important class of opto-electronic materials is based on the macrocomplexation of Ir(III) ions by bipyridinic, phenylbipyridinic or β -diketonic ligands; both conducting and non-conducting polymers were bound to the metal center through their end-groups or their side functional residues.^{138,139}

Some novel macrocomplexes were synthesized within this thesis; firstly, PLA-, PCL- and PEG-based macroligands bearing an end-capping pyridine moiety were obtained. Afterwards, these macroligands were coordinated to Pd(II) forming macrocomplexes with (i) neutral linear, (ii) monocationic V-shaped or (iii) bis-cationic star-shaped structures.¹⁴⁰

1.4.3 Applications and research outlook

Metal-polymer macrocomplexes are attracting increasing research interest on account of the possibility that they offer to obtain functionalized “soft-materials” with novel tunable properties, greatly expanding the application field of conventional polymers. Micelles from the assembly of amphiphilic macrocomplexes are particularly studied¹⁴¹ since the reversibility of the coordination bond, and hence of the link between hydrophobic and hydrophilic domains paves the way towards new biomedical nanosystems as well as new strategies for the preparation of water dispersions of hydrophobic polymers.^{142,141}

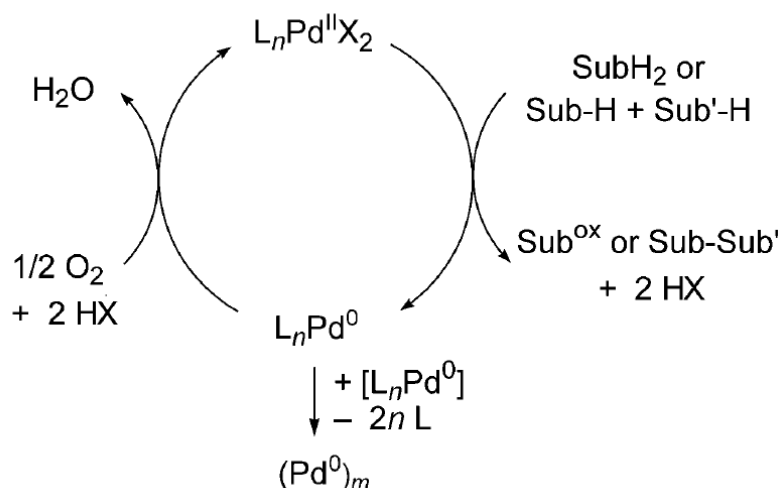
The synthesis of stimuli-responsive biocompatible aggregates at the nanometric scale appears as a promising tool to enhance the potential selectivity and effectiveness of drug-delivery systems. Moreover, with the view of increasing the environmental performance of chemical processes it is chiefly important to be able to synthesize tunable heterogeneous catalysts in which the metal centre is anchored to a (possibly soluble) polymeric support. A number of photo- and electro-luminescent macrocomplexes are showing interesting properties that could be employed to develop novel polymer light emitting diodes (P-LED) or optoelectronic devices in general. Lastly, macrocomplexes based on conducting macroligands may be utilized for the production of new generation photovoltaic cells. Intense research efforts are aimed at

the preparation and characterization of an increasingly wide range of functional polymers and building-blocks to be combined in new supramolecular structures, as well as aimed at the development of more refined theoretical models on which rational synthetic strategies could be based in the future.¹⁴³

1.5 Pd- and Cu-based catalysis of some organic reactions

1.5.1 Pd-catalyzed aerobic oxidation of alcohols to carbonyl compounds

The oxidation of alcohols to carbonyl compounds is a chemical transformation of great interest both from an academic and industrial point of view and has attracted intensive research over the years.¹⁴⁴ Pd-based catalytic systems proved particularly effective for this class of reactions, particularly when air or O₂ were utilized as inexpensive, safe and environmentally friendly oxidants (*i.e.* for aerobic oxidations).¹⁴⁵ When Pd(II) complexes are employed in the presence of molecular oxygen, the overall oxidation reaction conforms to the two-stage “Pd oxidase” cycle depicted in Scheme 1.19.



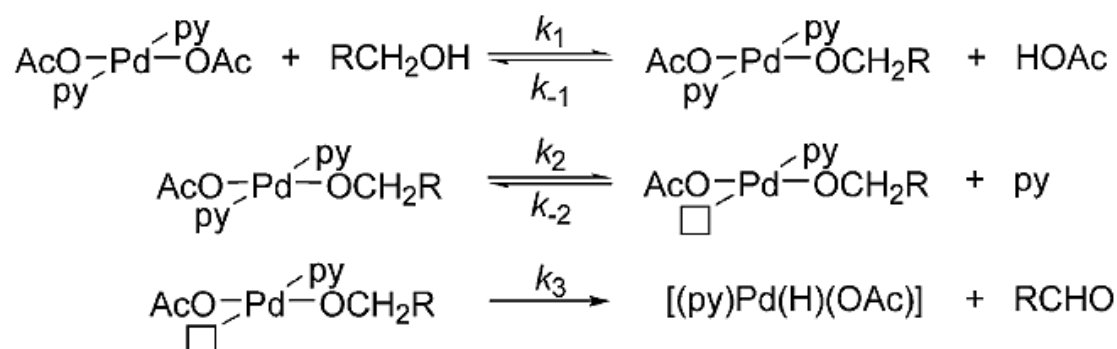
Scheme 1.19 – General two-stage “Pd oxidase” cycle for aerobic oxidation reactions

In 1977, Blackburn and Schwartz reported the first example of palladium-catalyzed alcohol oxidation that underwent dioxygen-coupled turnover in the absence of a cocatalyst.^{146,147} The aerobic oxidation of secondary alcohols proceeded with a PdCl₂ (1%) / NaOAc (5%) catalytic system in ethylene carbonate at ambient temperatures and 1 atm of oxygen pressure. The rate of these relatively slow reactions (1 – 2 turnovers per hour) was independent on oxygen pressure; however, palladium metal precipitation could be avoided if the reaction was conducted at 3 atm of oxygen pressure. Over the following 20 years, relatively little progress in this area was achieved, until a significant

breakthrough was reported by Peterson and Larock, who employed the Pd(OAc)₂ (5%) / DMSO (solvent) catalytic system for the oxidation of a wide range of benzylic and allylic alcohols with molecular oxygen (1 atm) as the only oxidant.¹⁴⁸ The reactions were relatively slow (less than 1 turnover per hour), but the corresponding carbonyl compounds were produced in moderate to excellent yields (42–95%). Other palladium sources (*i.e.* PdCl₂, Pd(O₂CCF₃)₂, [Pd(Dba)₂]) were significantly less effective than Pd(OAc)₂, and different solvents (*i.e.* CH₃CN, DMSO / H₂O mixture) also led to lower yields. Anionic bases such as NaHCO₃ and K₂CO₃ (2 equivalents) significantly enhanced the reaction rate and product yield for secondary alcohol substrates.

1.5.1.1 The Pd(OAc)₂ / pyridine catalytic system

Palladium(II) compounds bearing either mono- or bidentate nitrogen ligands are suitable to catalyse the aerobic oxidation of alcohols to ketones or aldehydes in the homogeneous phase, with water or hydrogen peroxide formed as the only side product.¹⁴⁵ Developed roughly in the same period of the aforementioned Pd(OAc)₂ / DMSO system, Uemura's catalytic system (*i.e.* *trans*-[Pd(OAc)₂(pyridine)₂] (Scheme 1.20) is characterized by its versatility to oxidize structurally different alcohols and has found even wider application.¹⁴⁹ The major concern with this catalytic system refers to the stabilization of palladium in its catalytically active oxidation state (*i.e.* Pd(II)), avoiding thus the formation of Pd(II) aggregates¹⁵⁰ and the successive precipitation of palladium black, which is almost inactive in aerobic oxidations carried out in toluene. Hence aerobic alcohol oxidations were carried out either with a Pd(OAc)₂ : pyridine ratio of 1 : 4 (*i.e.* the “optimized Uemura” catalytic conditions)^{151,149,145} or in the presence of sterically hindered 3-substituted pyridine derivatives.¹⁵²



Scheme 1.20 – Mechanistic sequence for Pd(II)-catalyzed alcohol oxidation in the presence of the *trans*-[Pd(OAc)₂(pyridine)₂] system (Uemura's system)

Recently, Stahl has reported the application of the “optimized Uemura” catalytic system

in a high-pressure continuous-flow tube reactor to convert alcohols into aldehydes or ketones on a kg-scale.¹⁵³ Compared to magnetically stirred autoclaves, the much more efficient contact of the gaseous phase (*i.e.* air) with the solution phase, which contains the homogeneous catalyst, permitted a much more efficient re-oxidation of Pd(0) to Pd(II).

Another important issue concerning the application of the Uemura's catalytic system for a future application in pharmaceutical synthesis,¹⁵³ is related to an efficient anchoring of the catalyst in order to be quantitatively separated from the reaction solution after catalysis. The only attempt in this direction employed hydrotalcite as catalyst support.¹⁵⁴

In order to contribute to this field of research, in this thesis a different approach is presented to recycle the catalytic system, which consists in the coordination of Pd(OAc)₂ by 4-pyridinemethylene-end-capped P(L)LA and PCL macroligands.¹⁵⁵ These polymers are soluble under the applied catalytic conditions (*i.e.* toluene, 70 °C) and easily recoverable by precipitation, combining the advantages of homogeneous and heterogeneous catalysis.^{156,157} In the realm of alcohol oxidation reactions, the concept of soluble polymer-supported catalysts has been mainly applied in 2,2,6,6-tetramethylpiperidine-1-oxyl (TEMPO),¹⁵⁸⁻¹⁶² polyoxometalates^{163,164} and sulfoxide¹⁶⁵ catalyzed reactions.

1.5.1.2 Other homogeneous Pd-based catalytic systems

In 2000, Sheldon and co-workers reported the first example of direct dioxygen-coupled alcohol oxidation in aqueous solution.¹⁶⁶ This advance offers potential advantages with respect to product isolation and should be considerably safer under aerobic reaction conditions. The optimized Pd precatalyst was [(PhenS*)Pd(OAc)₂], which upon dissolution in water forms the dimer depicted in Figure 1.16 (*i.e.* the resting state during catalysis). The described reaction conditions were: catalyst (0.2 – 0.5 mol%), NaOAc (10%), air pressure of 30 bar, 100 °C. The advantages of operating in aqueous solution were partially offset by the requirement for elevated pressures and the limited water solubility of many organic substrates, but, overall, the reactions were remarkably effective. Catalytic rates (up to 100 turnovers per hour) and turnover numbers (200–400) were significantly higher than those reported for previous catalytic systems.

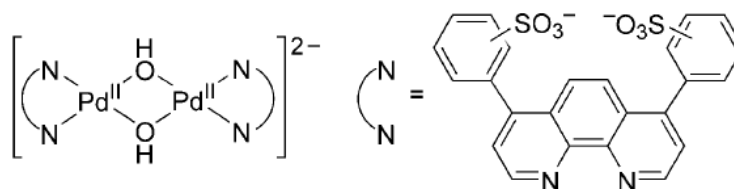
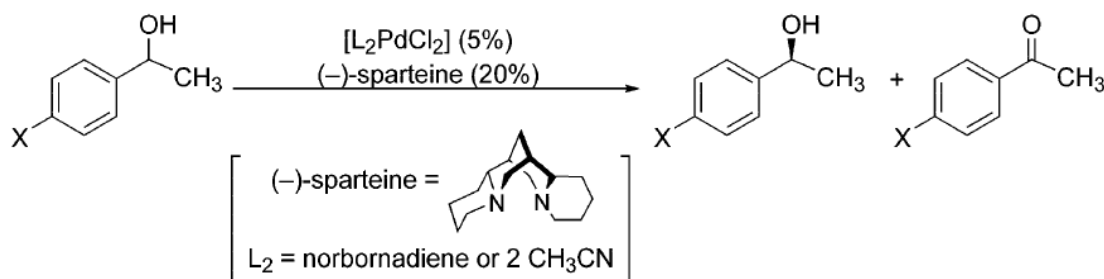


Figure 1.16 – Dimeric complex obtained from the dissolution in water of $[(\text{PhenS}^*)\text{Pd}(\text{OAc})_2]$

In the field of enantioselective oxidations, the development of aerobic oxidative kinetic resolution of secondary alcohols, reported independently by the groups of Sigman and Stoltz, represented a significant advance.^{167,168} The catalyst system consisted of $[(\text{-})\text{-sparteine})\text{PdCl}_2]$ (5%) together with excess $(\text{-})\text{-sparteine}$ (20%), since the chiral palladium complex itself was inactive in the absence of exogenous ligand. This reaction was particularly effective for aryl- and *t*-butyl-substituted ethanol derivatives (Scheme 1.21), while *t*-butanol was a particularly effective solvent or additive.



Scheme 1.21 – Enantioselective oxidation of aryl-substituted ethanol derivatives catalyzed by the $[(\text{-})\text{-sparteine})\text{PdCl}_2] / (\text{-})\text{-sparteine}$ system

Hallman and Moberg demonstrated that a chiral cyclometallated Pd catalyst, in combination with pyridine, catalyzes the oxidation of *sec*-phenethyl alcohol and 1- and 2-octanol in toluene under an air atmosphere,¹⁶⁹ although the oxidation of racemic *sec*-phenethyl alcohol displayed no significant resolution with this catalytic system. Lastly, Sigman and co-workers reported that $\text{Pd}(\text{OAc})_2$ (3%) / triethylamine (6%) is an effective alternative to the $\text{Pd}(\text{OAc})_2$ / pyridine catalyst and allows alcohol oxidations to be run at room temperature¹⁷⁰ and that a catalyst based on N-heterocyclic carbene-coordinated Pd successfully oxidizes alcohols at quite low catalyst loadings (0.1 – 0.5 mol%) in the presence of catalytic quantities of acetic acid (2%).¹⁷¹

1.5.1.3 Catalytic systems based on Pd nanoparticles

Many of the most efficient heterogeneous catalysts employed for the aerobic oxidation of alcohols are based on metal (particularly palladium) nanoparticles. Metal

nanoparticles can be considered as the bridge between classical heterogeneous catalysts, which are stable, recoverable and minimize product contamination, and soluble metal-ligand complexes, which are very selective and generally more active.¹⁷² While heterogeneous catalysts are often synthesized by means of a top-down approach, NPs are normally obtained through bottom-up synthetic procedures from a metal containing molecular precursor. The reduction step from the precursor to the zero valent metal NP is typically performed utilizing a chemical reducing agent^{173,174} (H_2 and NaBH_4 are among the most frequently used) or an electrochemical procedure;¹⁷⁵ moreover, several techniques can be employed to enhance or promote NPs synthesis, including ultrasonication,^{176,177} laser ablation¹⁷⁸ or gas-phase organometallic deposition.¹⁷⁹

It is well known that catalytic performances can be very sensitive to the size of the active phase, and indeed many Pd-NPs-catalyzed organic reactions such as hydrogenations, Heck and Suzuki couplings (Figure 1.17), and vinyl acetate synthesis proved to be structure sensitive.¹⁸⁰⁻¹⁸³ In other words, the conversion rate per surface Pd atom in these reactions changes with the size of Pd particles.

It has been proposed that defects on the Pd-NPs surface are involved in the mechanism of C-C bond formation in the Heck reaction, which implies that the activity should be related to the number of low-coordinate surface atoms.¹⁸⁴⁻¹⁸⁶ It has also been suggested that flat π -adsorption of the aromatic ring of an aryl halide over a “large” Pd-NP is responsible of activation of the C-X bond prior to formation of a σ -aryl-Pd complex at the Pd-NP surface.¹⁸⁷ However, a homogeneous mechanism attributing the catalytic activity to palladium species leaching from the heterogeneous catalyst (Pd/C or Pd/MOx) into the solution is also frequently suggested.¹⁸⁸⁻¹⁹⁰ Furthermore, the finding that unsupported palladium salts are active even under extremely low concentration in the absence of ligands (other than halides or acetate) and that dilution improved the catalysis led Reetz to propose an equilibrium between Pd-NPs and catalytically active palladium fragments.^{191,192}

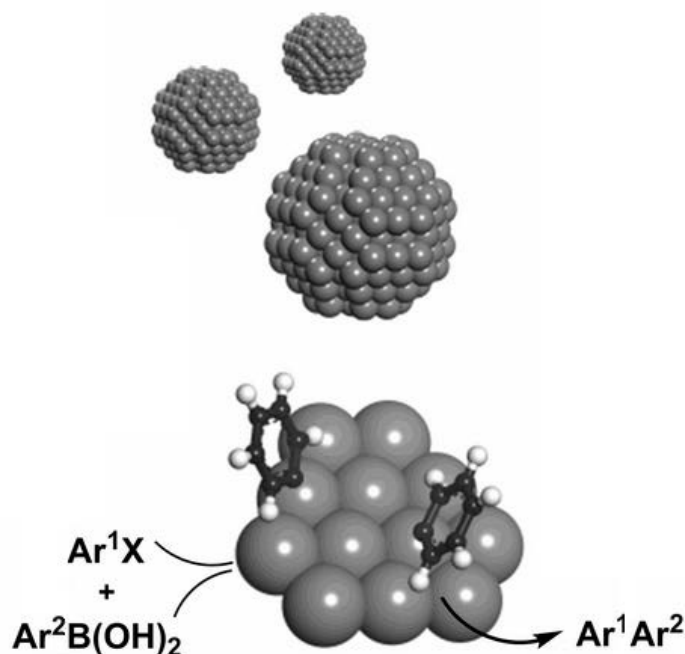


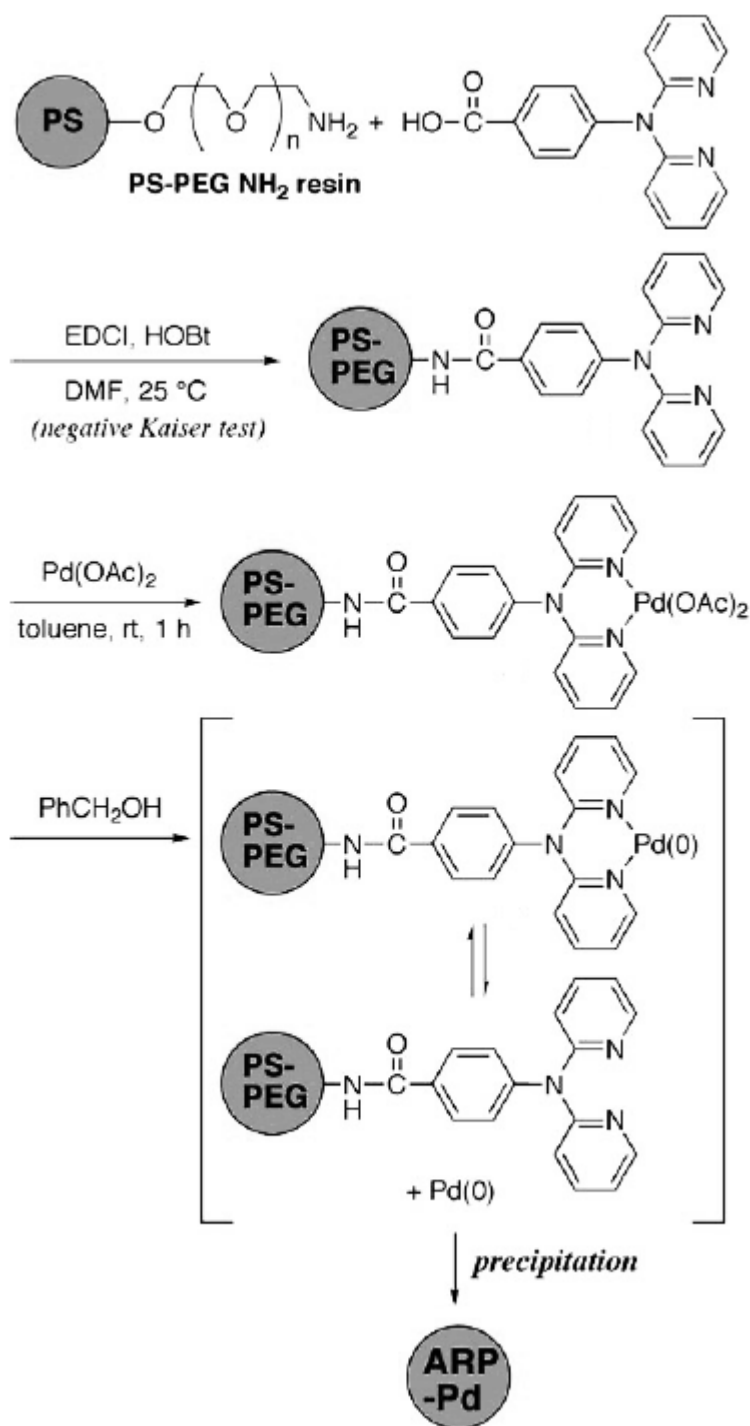
Figure 1.17 – Graphic representation of a Pd-NPs catalyzed Suzuki C-C coupling reaction

Although many papers have been published in the field of Pd-NPs-catalyzed oxidation of alcohols and moderate to excellent turnover numbers or selectivities were reported, studies on the relationships between nanoparticle properties and catalytic performance are not abundant. For better understanding the structure / activity relationship in the Pd-NPs-catalyzed aerobic oxidation of alcohols, further investigations are still required; nevertheless, it is generally agreed that an accurate control of the nanoparticle size is crucial to obtain reproducible and consistent results.¹⁷³

Grunwaldt and co-workers¹⁹³ clarified that metallic Pd is more active for the aerobic oxidation of benzyl alcohol than Pd oxide species using in situ X-ray absorption spectroscopy; nevertheless a few papers report that palladium oxide can act as the active phase for alcohol oxidations.^{194,195} Many recent studies have shown that supported Pd nanoparticles are excellent catalysts for the selective aerobic oxidation of alcohols.¹⁹⁶⁻¹⁹⁹ Mori and his group compared the catalytic activities of two Pd / hydroxyapatite catalysts containing Pd nanoclusters with mean diameters of 3.8 and 7.8 nm for the aerobic oxidation of 1-phenylethanol and benzhydrol and found that the smaller Pd nanoclusters (3.8 nm) gave a higher TOF than the larger Pd nanoclusters.²⁰⁰ Moreover, Chen and co-workers demonstrated that the mean size of particles played a key role in the aerobic oxidation of benzyl alcohol with SiO₂-Al₂O₃-supported Pd-NPs.²⁰¹ Varying the mean size of Pd particles in the range from 2.2 to 10 nm, the intrinsic turnover frequency per surface Pd atom for benzyl alcohol conversion showed a maximum at a medium size of

3.6 – 4.3 nm, revealing that the reaction was structure-sensitive. The existence of an optimum particle size implies that an appropriate ratio of the edge and corner Pd atoms to the terrace Pd atoms is required for the conversion of benzyl alcohol. The authors suggest that not only the β -hydride elimination of the Pd-alcoholate intermediate but also the chemisorption of alcohol on the surface of Pd nanoparticles determines the rate of benzyl alcohol oxidation.

Catalytically active NPs are stabilized or supported by a number of different methods; they can either be incarcerated in organic cross linked polymers,^{202,203} anchored onto carbon,²⁰⁴ alumina²⁰⁵ and hydroxyapatite¹⁹⁶ or stabilized by end-functionalized PEG (Scheme 1.22).^{173,206,207,92} The latter polymer, which is cheap, biocompatible and water soluble, decreases the polarity of the aqueous phase due to hydrogen bond interactions between water molecules and the polymer backbone.¹⁵⁷ As a result, PEG can be considered as a co-solvent in water increasing the solubility of organic compounds which is mandatory for an efficient aqueous phase catalysis.



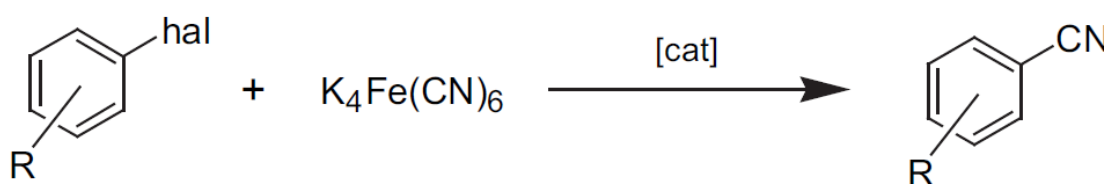
Scheme 1.22 – Example of a PS / PEG-based amphiphilic resin dispersion of Pd-NPs

Within the field of Pd-NPs catalysis, in this thesis we present the synthesis and coordination chemistry of 4-pyridinemethylene end-capped PEGs and the corresponding Pd(II) macrocomplexes, which upon reduction with dihydrogen pressure, gave PEG-stabilized Pd-NPs, characterized by different degrees of NP-aggregation. The Pd(II)- and Pd(0)-based compounds were screened as catalysts for the aerobic oxidation of α,β -unsaturated alcohols in water.²⁰⁸

1.5.2 Pd- and Cu-catalyzed cyanation of aryl halides

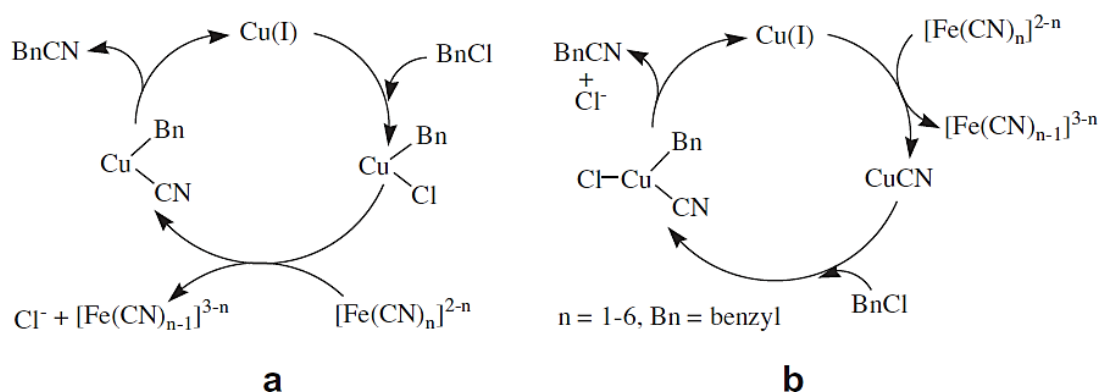
The cyanation of aryl halides is a reaction of great practical importance since aromatic nitriles constitute a class of widespread organic intermediates as well as fine chemicals with applications as pharmaceuticals, perfumes or dyes.^{209,210} Traditionally employed cyanation procedures mostly rely on stoichiometric amounts of extremely toxic metal cyanides.²¹¹

This latter issue was tackled by Beller and co-workers²¹² introducing non-poisonous, inexpensive potassium hexacyanoferrate(II) as the cyanide source (Scheme 1.23) coupled with a phosphine-free Pd catalyst. Since then, intensive research was carried out and further improvements were proposed, including heterogeneous catalysts,^{213,214} large scale experimental setups²¹⁵ or microwave reactors.²¹⁶



Scheme 1.23 – Cyanation of aryl halides using $K_4[Fe(CN)_6]$ as the cyanide source

A major step forward in this field of research was achieved by replacing costly and toxic palladium with copper-based catalytic systems.²¹⁷⁻²²⁰ The hypothesized catalytic cycle²²⁰ starts with the oxidative addition of benzyl chloride (or halide in general) to the catalytically active Cu(I) species. The resulting benzyl copper species, which is possibly a η^1 -benzyl or η^3 -benzyl copper intermediate, undergoes a transmetallation to afford a benzyl copper cyanide adduct, followed by reductive elimination to give the expected nitrile and regenerate the catalytically active Cu(I) species (Scheme 1.24/a). The order of oxidative addition and transmetallation steps in such a catalytic cycle is unknown, so it is possible that the transmetallation step precedes oxidative addition (Scheme 1.24/b).



Scheme 1.24 – Simplified mechanisms for Cu-catalyzed cyanation of aryl halides

More recently, few examples of microwave-accelerated syntheses carried out in environmentally benign solvents such as water or poly(ethylene glycol) emerged.^{221,222} Nonetheless, a troublesome common feature of all the described copper-catalyzed cyanation reactions was the need for a very high catalyst loading, which is in the range of 10 – 30 mol%. Lower Cu-catalyst loading inexorably led to a dramatic drop in nitrile formation.

In order to contribute to this field of research, in this thesis a probe sonicator was coupled with melted PEG as reaction medium and the newly developed cyanation procedure was tested on a range of aryl iodides and bromides. Inexpensive, ligand-free copper catalysts were employed in combination with potassium hexacyanoferrate(II) as the cyanide source.²²³

1.6 Ultrasounds in green reaction media

1.6.1 Acoustics in liquid media

Acoustic waves that fall in the human hearing range (*i.e.* ‘sonic’ waves) have frequencies that cover the 20 Hz - 20 KHz interval; below and above these extremes, ‘infrasounds’ and ‘ultrasounds’ (US) are respectively positioned. The latter constitute the basis for a number of applications in science and technology and are further subdivided into ‘power US’ (20 KHz to 1 MHz) and ‘high frequency US’ (1 MHz upwards) according to their utility as energy source or as therapeutic and diagnostic low intensity waves. Sound waves consist in alternating compression and decompression of a gaseous, liquid or solid medium possessing elastic properties. Waves propagate longitudinally (through any kind of medium) or transversely (through solids only); dealing here with US-enhanced chemical reactivity (*i.e.* sonochemistry), liquids are the only acoustic media of practical concern and transverse waves will not be considered.

Under the effect of a sonic wave the acoustic pressure P_a at a given distance from the source oscillates with time (t) according to²²⁴

$$P_a = P_A \sin 2\pi ft$$

where P_A is the maximum acoustic pressure of the wave and f is the frequency. It is useful to define the intensity of a wave, I , as the energy flowing per unit area and time (usually expressed in W cm^{-2}); intensity is related to the maximum acoustic pressure, P_A , by

$$I = P_A^2 / 2\rho c$$

where ρ is the density of the medium and c is the speed of sound in the medium. As the distance from the acoustic source, l , increases, the intensity of the wave tends to decrease from the initial value, I_0 , on account of absorption phenomena such as viscous or frictional interactions between molecules of the medium. Hence, the absorption coefficient, α , is an important parameter to be introduced:

$$I = I_0 e^{-2\alpha l}$$

α depends on the density (ρ) and viscosity (η) of the medium according to

$$\alpha = \frac{8\eta_s \pi^2 f^2}{3\rho c^3}$$

which can be modified to take into account temperature losses in the medium into

$$\alpha = \frac{2\pi^2 f^2}{\rho c^3} \left[\frac{4\eta_s}{3} + \frac{(\gamma - 1)K}{C_p} \right]$$

where γ is the ratio of heat capacity at constant pressure (C_p) to constant volume (C_v) and K is the thermal conductivity of the medium. The absorption coefficient has a great practical importance since it indicates how efficiently acoustic energy is transferred to the reaction mixture.

1.6.2 Cavitation and sonochemistry

During the decompression phase of a power US wave the molecules of a liquid may experience forces strong enough to outbalance Van Der Waals interactions and, locally,

separate from each other. When it happens, some very small cavities are formed in the bulk that tend to expand until the pressure is low enough to sustain their growth. At this stage any component of the reaction mixture may evaporate into the void and reduce the negative pressure bias between the inside of the cavity and the surrounding liquid. After few compression-decompression cycles, the cavity can either be sustained by vapors and become a bubble with life time long enough to reach macroscopic dimensions, or instead implode violently producing hot-spots with rather extreme temperatures and pressures of around 5000 K and 1000 atm (Figure 1.18).^{225,226} Because of this very peculiar phenomenon, sonication is locally capable of quickly providing the activation energies needed to trigger chemical reactions while maintaining the average conditions of the mixture relatively mild.

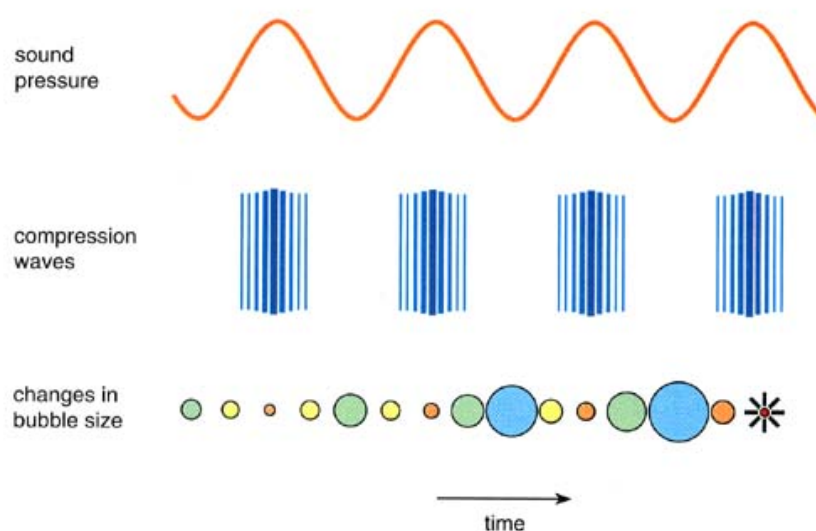


Figure 1.18 – Schematic representation of acoustic compression waves and cavitation

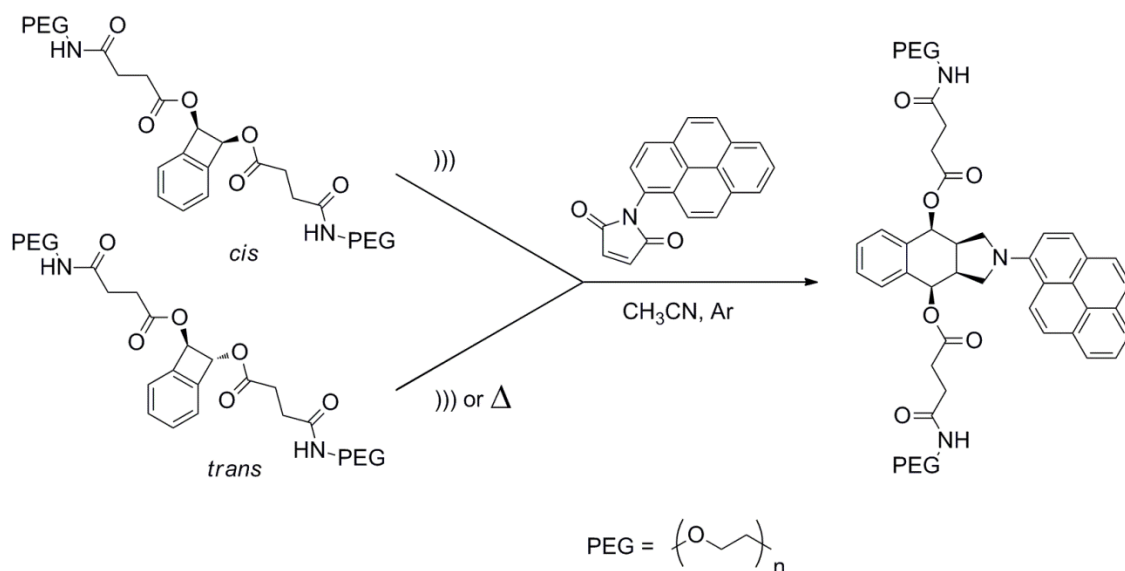
The extent of cavitation strongly depends on the intensity and frequency of ultrasonic waves. A higher intensity facilitates the formation of cavities since molecules in the bulk are subjected to higher pulling and pushing forces; hence not only the generation of void is more likely, but also the implosion tends to be more violent. There is normally an upper limit to the amplitude of waves that is imposed by the resistance of the sonication apparatus. Higher frequencies, on the other hand, harness the process by reducing the lapse of time available for molecules to win interactions and separate before the wave period comes to completion. Keeping other parameters constant, cavitating a liquid with a higher US frequency requires more power from the probe. It is worth noting that the physical properties of the reaction mixture, although of minor relevance in some conventional reaction setups, are extremely important in sonochemistry. Considered the

physics of wave propagation and attenuation as well as the basis of cavitation, it is evident that density, viscosity, vapor pressure, surface tension and heat capacities may all influence the efficacy of an US-promoted process. The presence of microscopic solid impurities in the liquid is also a crucial factor favoring cavitation, since even very small air pockets embedded on the particles surface have a marked nucleating effect for bubbles.

Sonochemistry is often subdivided in two categories of reactions in which the US enhancement is due to different reasons. Nonetheless, these beneficial effects can coexist and cooperate in the same chemical transformation. (i) Homogeneous reactions with radical intermediates may be accelerated by cavitation if sufficiently volatile reactants enter the cavity where the formation of the radical species is favored. Solvent molecules can also undergo bond cleavage and act as indirect source of radicals for less volatile substrates, which in any case experience strong shock waves from nearby imploding cavities. (ii) Heterogeneous reactions or nanoparticle catalysis can benefit from the vigorous and diffuse agitation provided by sound waves, maximizing contact between phases. Even more important, the implosion of cavities in the proximity of a surface produces very intense streams of liquid that impact and ‘clean’ or even disintegrate the outer layers of the solid, constantly increasing the exposed area of the catalyst and hence its activity.

Sonochemical acceleration of homogeneous ionic reactions is rarely described and generally less remarkable from a quantitative point of view, but accurate kinetic analyses suggest that variations in reagents or intermediates solvation may lead to a reduction in activation energy and hence in a rate enhancement.²²⁷

Interestingly, using US as the energy source can not only accelerate a chemical reaction but also alter its selectivity. This phenomenon was firstly observed by Ando and co-workers sonicating benzyl bromide in a toluene suspension of alumina-supported potassium cyanide²²⁸. Benzyl cyanide was obtained in good yield as the result of an aliphatic nucleophilic substitution while under conventional oil-bath heating the product was a mixture of regioisomeric phenyl-tolyl methanes from a Friedel-Crafts reaction. An even more outstanding selectivity switch was reported by Moore and co-workers studying the US-promoted electrocyclic ring cleavage of a benzocyclobutene bearing a poly(ethylene glycol) (PEG) chain at each cyclobutene side (Scheme 1.25).²²⁹



Scheme 1.25 – Electrocyclic ring cleavage of a PEG-tagged benzocyclobutene: selectivity shift under sonication

Both *cis*- and *trans*-cyclobutene derivatives yielded the same (*E,E*) isomeric diene, violating the Woodward-Hoffmann rules on the conservation of orbital symmetry. Provided a molecular weight higher than a threshold value of typically 30-40 KDa, polymers can thus be employed as ‘mecanophores’ to channel acoustic energy towards target bonds and force a reaction toward a normally disfavored pathway or direction, as also observed for retro Diels-Alder,²³⁰ metal-ligand decoordination^{231,232} or 1,2,3-triazole ‘unclicking’.²³³

1.6.3 Devices for ultrasounds generation

The phenomenon of cavitation is not a recent discovery as it had already been detected and described in the late nineteenth century as the origin of erosion damages on boat propellers’ metal surfaces. Nonetheless it was not until the 1980s that modern US equipment became widespread, relatively inexpensive laboratory tools and allowed to perform sonochemistry in an effective and controlled fashion. Generation of ultrasonic waves is achieved by the use of piezoelectric materials subjected to an electrical potential alternating with a frequency at a determined value in the US range. However, the transmission of mechanical oscillations to the reaction mixture can be engineered in two quite different layouts. (i) Sonication probes (*i.e.* direct sonicators) (Figure 1.19) are titanium alloy rods (other materials may be used in case of particular requisites) connected to the generator and directly immersed into the reaction mixture. The probe tip can have different geometries; small diameters (microtips probes) deliver focused, high-intensity sonication where large diameters allow better treatment of large volumes

at the expense of intensity.

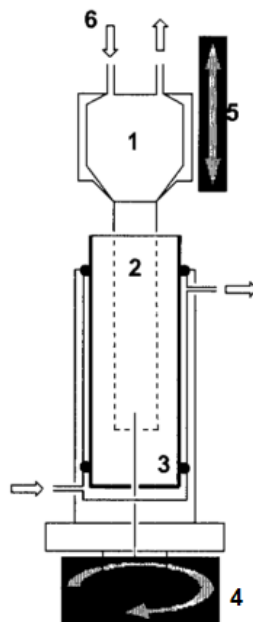


Figure 1.19 – Sonochemical reactor: 1) transducer and booster, 2) horn, 3) thermostated reactor, 4) eccentric rotation, 5) vertical excursion, 6) refrigeration system

(ii) Sonication baths (*i.e.* indirect sonicators) transmit acoustic waves from one or multiple metal horns to a volume of water in which the reaction tube is immersed, avoiding contact between the mixture and any part of the equipment. Although normally a lower US intensity is available, baths are useful when contamination or sample loss must be prevented as well as for the treatment of several samples at the same time. Common US cleaning baths operate at very low acoustic intensities but possess the same construction scheme.

In the following paragraphs a number of significant examples of sonochemical syntheses are subdivided according to the employed solvent and the nature of the reaction.

1.6.4 Sonochemistry in aqueous solvent

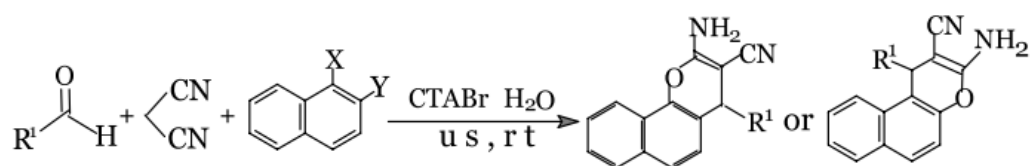
Due to its intrinsic safety and environmental friendliness, water represents the obvious benchmark among green solvents. Sonochemical reactors, in analogy with the ubiquitous sonication cleaning baths, often operate in water or aqueous solutions since cavitation is considerably efficient and negligible costs favor the use of large volumes and, hence, the scalability of the process. It is also worth noting that ultrasounds facilitate to overcome the mayor limitation of reactants water solubility, which is particularly troublesome in organic synthesis, by producing a very efficient agitation

and maximizing the contact between phases.

1.6.4.1 Organic reactions in water phase and emulsions

In one of the first remarkable papers in the field, the group of Cravotto described the use of high-intensity ultrasounds to promote the aldol reaction between acetophenone and non-enolizable aldehydes in catalyst-free, aqueous heterogeneous systems.²³⁴ Good yields of aldol products were obtained in sonication times shorter than 1 h avoiding the elimination reactions to enones which were commonly observed in conventional conditions. Notably, a probe sonicator operating at 20 kHz and 250 W afforded faster and more selective transformations not only with respect to vigorous magnetic stirring but also to a relatively high frequency (35 kHz), low power (140 W) ultrasonic cleaning bath, highlighting the pivotal role played by the acoustic intensity of the experimental setup.

On the other hand, Jin and co-workers demonstrated the efficacy of a 25 kHz, 500 W sonication bath as the energy source for the three-component reaction of aromatic aldehydes, malonitrile and phenols to prepare 2-amino-2-chromenes (Scheme 1.26) in high yields and relatively short times (*i.e.* 2.5 h).²³⁵ The authors point out how the combination of aqueous solvent and 10% cetyltrimethylammonium bromide (CTABr) as a phase-transfer catalyst afforded results that could not be reproduced if water was replaced by ethanol or dichloromethane and attribute this marked solvent effect to the water-induced hydrophobic interactions between substrates and catalyst.



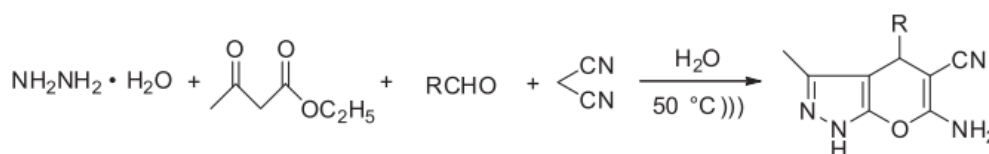
Scheme 1.26 – US-accelerated synthesis of 2-amino-2-chromenes

Neutral aqueous solvent compared favorably with respect to acetonitrile in the US-promoted Michael addition of thiols to 4-hydroxy-2-alkynoates (using a sonication bath at room temperature).²³⁶ The beneficial role of water is suggested to derive from the hydrogen bond interaction with both the carbonyl oxygen and the thiol group; indeed, the reaction in acetonitrile proceeds in similar yields only in the presence of NaHCO_3 as an additional base. When amines are employed as substrates instead of thiols a sequential conjugate addition/lactonization reaction leads to amino-furan-2-ones and, in

these conditions, a test in water without sonication revealed a significant, although not dramatic decrease in reaction rate.

The rate of Pd-catalyzed Heck coupling of aryl iodides with activated olefins in the presence of sodium dodecane-1-sulfonate showed a marked dependence on temperature²³⁷ and a probe sonicator needed to be coupled with oil bath heating to enhance the yield of cinnamamide from 35% (at 40 °C) to 47% (60 °C) to 96% (90 °C). According to the authors, however, the sonochemical enhancement is evident since, employing 5% Pd(OAc)₂ and K₂CO₃ as the auxiliary base, reactions with >99:1 selectivity towards the *E* isomer could be completed in only 20 min.

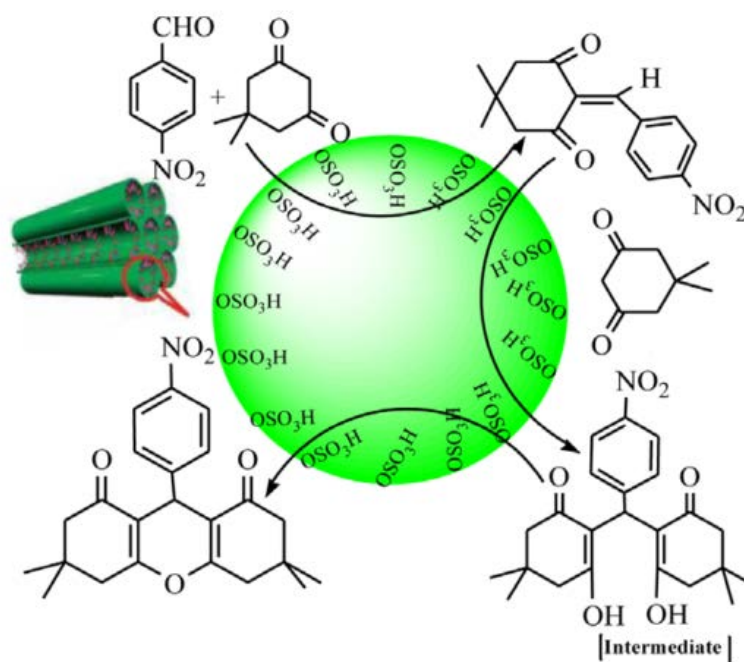
Clear evidences of the better performance of water over organic solvents as the sonochemical medium are reported for the preparation of dihydropyrano[2,3-*c*]pyrazoles (Scheme 1.27).²³⁸ Several solvents were tested and, while yields in alcohols were only slightly lower than in water, acetonitrile and less polar organic solvents such as THF and dioxane gave markedly worse results. In this study ultrasonication was applied by a 250 W medical US cleaner operating at a relatively high frequency of 40 kHz which afforded the highest reaction rate when thermostated at 50 °C. However, it is worth reminding that this is not a general principle and different organic transformations or experimental setups may lead to a different choice of solvent, as witnessed by the EtOH phase synthesis of 7,10,11,12-tetrahydrobenzo[*c*]acridin-8(9H)-one derivatives reported by Zhang and co-workers.²³⁹



Scheme 1.27 – US-enhanced preparation of dihydropyrano[2,3-*c*]pyrazoles

Rostamizadeh and co-workers suggest a synergic effect between ultrasonic waves and the nanostructured catalyst MCM-41-SO₃H due to the insertion of reactants into the sulfonic group functionalized channels of the porous material by the localized intense pressure regions deriving from cavitation.²⁴⁰ This phenomenon was exploited to promote the water phase synthesis of 1,8-dioxo-octahydroxanthene derivatives from aromatic aldehydes and dimedone (5,5-dimethyl-1,3-cyclohexanedione) (Scheme 1.28). The sonochemical reactions could be carried out at 60 °C to obtain 80% to 99% yields while in the absence of US irradiation it did not proceed (moderate yields were

attainable only by raising the temperature to 90 °C).



Scheme 1.28 - synthesis of 1,8-dioxo-octahydroanthene derivatives catalyzed by MCM-41-SO₃H under US conditions

1.6.4.2 Sonochemical polymerization reactions in aqueous solvent

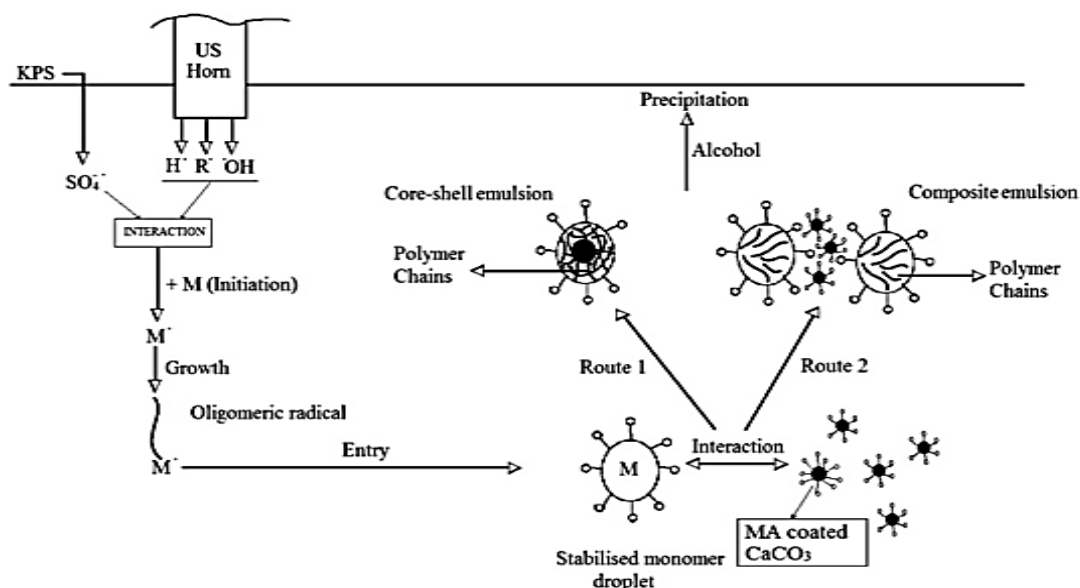
Ultrasounds have been employed to promote polymerizations since a relatively long time on account of the ability to form radical species during cavitation, hence a remarkable example of sonochemical styrene polymerization in water/sodium dodecyl sulfate (SDS) emulsion by Biggs and Grieser dates back to 1995.²⁴¹ Few years later Fujiwara and co-workers described the synthesis of poly(vinyl chloride)-*b*-poly(vinyl alcohol) copolymers resulting from the US-induced homopolymers chain scission and recombination of free radicals formed on the end groups.²⁴²

A very fast reaction rate (92% conversion after 11 min) was observed for the emulsion polymerization of *n*-butyl acrylate when sonication is used to initiate the radical mechanism instead of a conventional, thermally activated chemical initiator.²⁴³ In a very thorough study, the authors investigate the process of radical formation and highlight the marked reduction of induction time and the higher molecular weight attainable under US irradiation. Moreover, the feasibility of semi-continuous and continuous syntheses to replace batch reactions for larger scale purposes was demonstrated. Emulsions were formed, here, in the presence of SDS.

Emulsifier- and initiator-free polymerization of a butyl acrylate/styrene/acrylamide mixture performed with a sonochemical probe in aqueous phase gave ternary copolymer nanoparticles with a smaller size than observed in the corresponding silent conditions (*i.e.* 80 nm vs 140 nm).²⁴⁴ A peak in conversion was registered for an acoustic intensity of about 9.5 W/cm^3 and, although the addition of Na_2SO_4 was required for the advancing of the reaction, the concentration of the inorganic salt had roughly no influence on the rate of monomer conversion. This finding could be rationalized on the basis of two contrasting effects; the salt is responsible for the formation of an electric double layer on the surface of nanoparticles capable of preventing aggregation phenomena, on the other hand an excessive concentration would compress the double layer and destroy the emulsion.

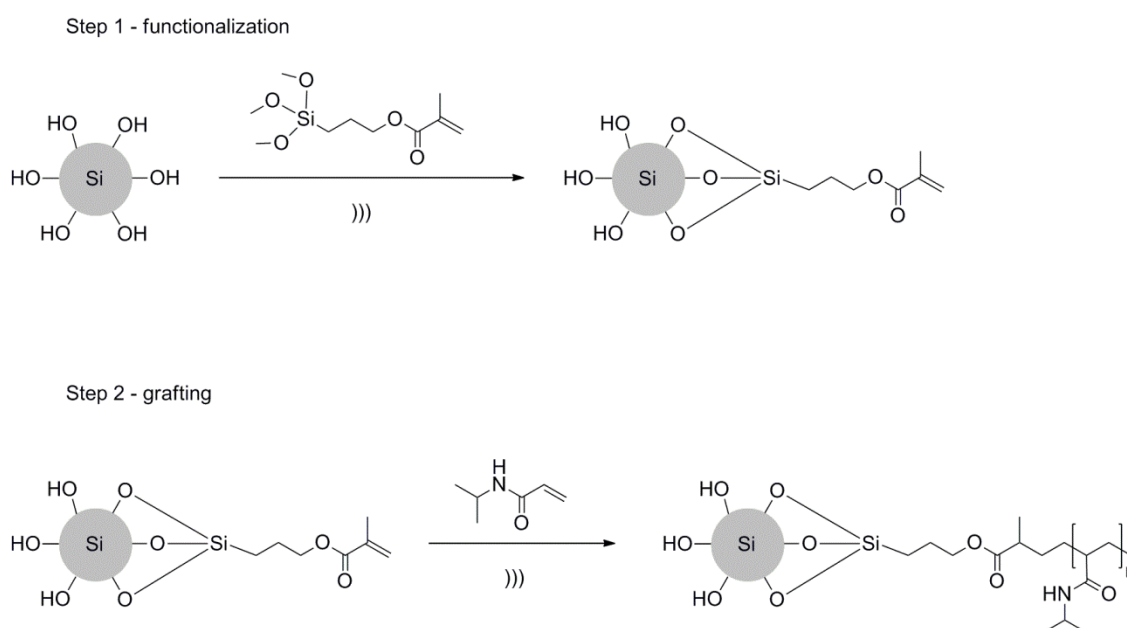
High-intensity sonication (20 kHz, 100 W/cm^2 probe reactor) of copper(II) acetate in a water solution containing aniline (1 vol%) yielded composite materials in which nanocrystalline Cu_2O particles are embedded in a poly(aniline) (PANI) matrix.²⁴⁵ It is hypothesized that, after reduction to $\text{Cu}(0)$, partial reoxidation is due to the formation of H_2O_2 or other secondary species originating from the recombination of $\text{H}\cdot$ and $\text{OH}\cdot$ radicals; accordingly, if the reaction is repeated in pure aniline as the solvent $\text{Cu}(0)$ nanoparticles are obtained. It is pointed out that particles synthesized in pure aniline are amorphous; this finding may be rationalized considering the higher temperature gradients and quenching rates generated from sonication of a solvent with a lower vapor pressure with respect to water.

The combined US/potassium persulfate (KPS) initiation of methyl methacrylate (MMA) polymerization proved to enhance the final conversion with respect to each of the two methods alone and allowed the synthesis of poly(MMA)/ CaCO_3 systems with narrow particle size distributions (Scheme 1.29).²⁴⁶ On the other hand, combined initiation unexpectedly lowered the initial polymerization rate compared to the non sonochemical process; this finding may be explained with interfering reactivity between the highly unstable $\text{SO}_4\cdot^-$ radical anion and the radicals generated from the sonolysis of water.



Scheme 1.29 – Methods for the sonochemical preparation of poly(MMA)/CaCO₃ systems

Mesoporous silica nanoparticles functionalized with 3-(trimethoxysilyl) propyl methacrylate were grafted with poly(*N*-isopropyl acrylamide) using an ultrasound induced emulsion polymerization initiated by KPS in the presence of CTABr (Scheme 1.30).²⁴⁷ The nanocomposites showed a core-shell structure with average diameter of 170 nm and demonstrated promising pH sensitivity, biocompatibility and bactericidal activity.



Scheme 1.30 – Synthetic route for the preparation of 3-(trimethoxysilyl) propyl methacrylate functionalized silica nanoparticles grafted with poly(*N*-isopropyl acrylamide)

1.6.4.3 Synthesis of inorganic nanoparticles and nanomaterials

Gold colloids are the cardinal and most thoroughly studied nanosystems; indeed, their sonochemical synthesis from HAuCl_4 in different solvents such as ethanol/water (1/1) or ethylene glycol was reported by the group of Cai already in 2003.²⁴⁸ The authors underline the dependence of nanoparticle morphology on the reaction solvent and relate this finding to the different Au^{3+} reduction rates. Sonication was performed at 0 °C in the presence of poly(vinyl pyrrolidone) (PVP) as a stabilizing agent by means of a 60 W, 40 kHz ultrasonic cleaner, hence applying a relatively low acoustic intensity of 2.4 W/cm^2 . The interest on this field has not faded with time and, recently, spherical gold nanoparticles with a relatively narrow size distribution were synthesized within very short sonication times (around 5 min) by means of a probe reactor.²⁴⁹ The use of aqueous sodium citrate dihydrate as a green reducing agent as well as mild reaction conditions makes the process environmentally favorable.

In recent past, the importance of US enhancement was emphasized for the synthesis of monodisperse magnetite nanoparticles by oxidation of a $\text{Fe}(\text{OH})_2$ precipitate (the so called ‘green rust’) since, in the heterogeneous mixture, the dissolution of iron ions is greatly accelerated by the microjet effect of sonication.²⁵⁰ The addition of ethanol to the aqueous phase has, in this study, beneficial consequences on the efficiency of the reaction. The authors rationalize this finding on the basis of ethanol decomposition during cavitation, which results in an increased concentration of the radical species responsible for Fe^{2+} oxidation. While an ethanol/water volume ratio of 20/80 proved to be the optimal solvent, a higher ratio of ethanol (*i.e.* 50/50) hampered the reaction due to the reducing properties of the alcohol.

Monodisperse Fe_3O_4 - SiO_2 core-shell nanoparticles (Figure 1.20) could also be obtained by coprecipitation of Fe(II) and Fe(III) in aqueous solution followed by alkaline hydrolysis of tetraethyl orthosilicate (TEOS) in an ethanol/water mixture.²⁵¹ When both steps were performed under power US irradiation (20 kHz) narrower size distribution of magnetite particles and higher homogeneity of the silica coating were achieved, resulting in a higher magnetization value compared to particles prepared under silent conditions.

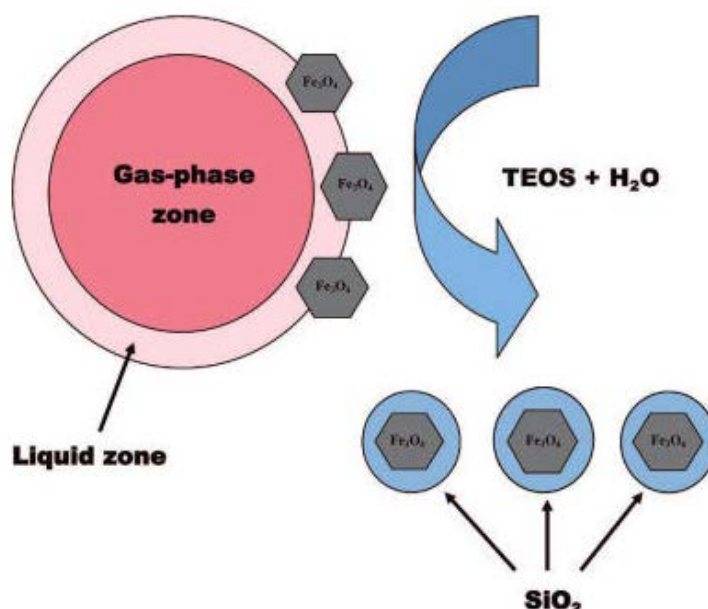


Figure 1.20 – Synthesis of monodisperse Fe_3O_4 - SiO_2 core-shell nanoparticles

$NiMoO_4$ nanorods were synthesized by a facile sonochemical procedure employing mild conditions and non-toxic materials within very short reaction times of around 30 min.²⁵² The authors describe a remarkable influence of acoustic power on morphology, observing a progressive increase in nanorods length shifting from silent conditions up to 45 W and then to 75 W US irradiation (Figure 1.21). Other interesting examples of water phase, sonochemical procedures for the synthesis of nanorods were reported in the very recent literature, witnessing the increasing interest in US as an alternative energy source in this field of chemistry.^{253,254,176}



Figure 1.21 – Increase of $NiMoO_4$ nanorods length with the increase of US power

Sonication of a $Zn(OH)_2$ in a basic aqueous solution yielded wurtzite-type crystalline ZnO which, in the presence of different soluble biopolymers (*i.e.* starch, gelatin, agar or chitosan), formed nanocomposite colloids with promising antifungal properties (Figure 1.22).²⁵⁵ Depending on the polymer employed as stabilizer and, hence, on its complexation properties, the authors observed large clusters with dimensions ranging from 200 to 600 nm containing smaller particles (around 40 nm) with spherical, rice-shaped or egg-shaped morphology. Wurtzite-type ZnO could also be obtained by high-

intensity sonication of an aqueous solution of zinc acetate containing acidic ILs with the double function of preventing aggregation of the growing ZnO nuclei and promoting their growth towards preferential directions.²⁵⁶ Indeed, different nanoparticle morphologies were observed depending on the quantity and nature of the added IL as well as on the time and frequency of the applied US field. Similarly, the sonochemical preparation of ZnO from zinc nitrate in water/ethanol basic mixture was enhanced by the addition of ethylenediamine as a chelating agent capable of promoting the crystallization process.²⁵⁷

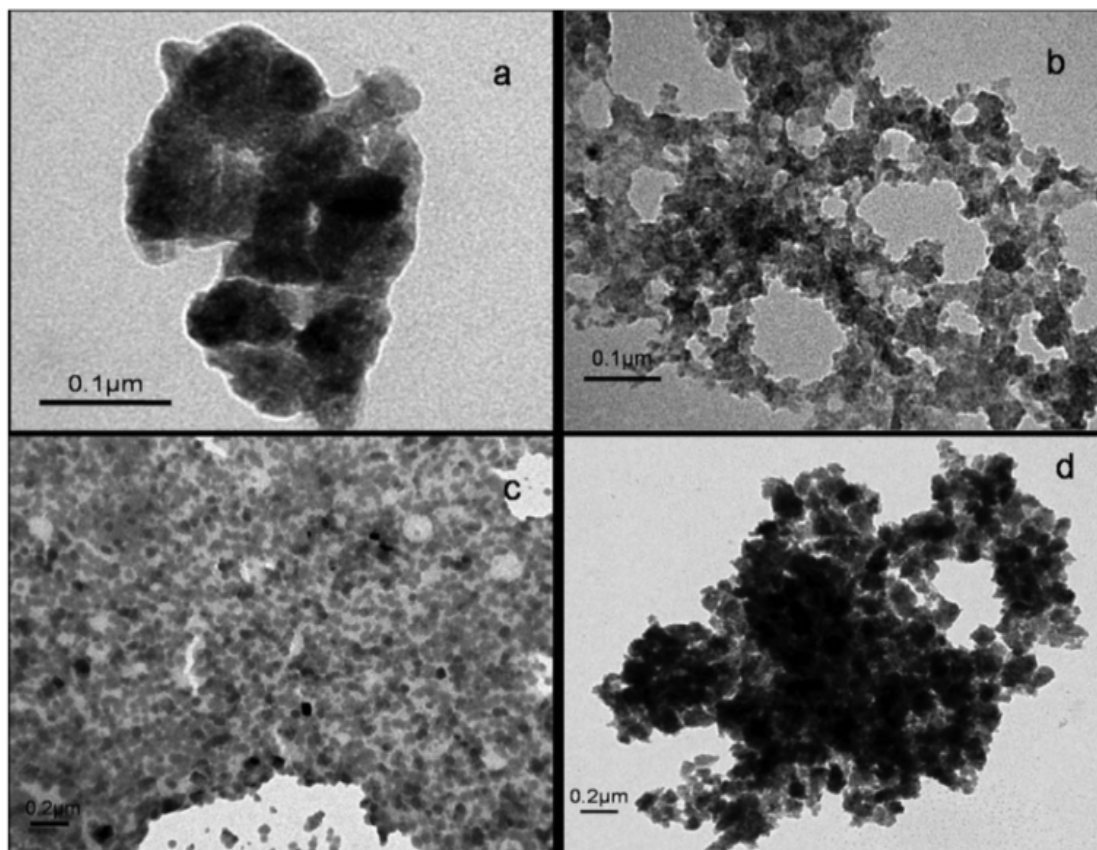


Figure 1.22 – TEM images of ZnO-biopolymer nanostructures synthesized by sonochemical method in the presence of: a) starch, b) gelatin, c) chitosan, d) agar

Selenium nanotubes were synthesized by reduction of H_2SeO_3 with hydrazine hydrate in water or EG as solvents performing US irradiation by means of different reactor setups.²⁵⁸ Interestingly, the quality of nanostructures varied with the applied US power; operating with sonication probe at 100 W yielded nanotubes with a high aspect ratio while increasing the power up to 300 W led to a progressive loss in tubular structures and to the formation of particles with very low aspect ratio, probably due to the melting of Se structures. Moreover, selenium nanowires could be obtained from the synthesized nanotubes by an aging process in solution that induces the collapse of the tubular

morphology. A more recent, alternative route to selenium nanowires was reported in which Se nanoparticles, formed *in-situ* by treatment of the metal powder with hydrazine, are sonicated in water or EG (among other screened solvents) for 1 h.²⁵⁹ It is worth noting that, when ethanol, acetone or DMF were used as solvents, nanotubes were obtained instead of nanowires, witnessing once again how the choice of the sonication medium should be considered as a crucial issue.

1.6.5 Sonochemistry in ionic liquids

ILs constitute a very interesting alternative to conventional solvents for sonochemistry on account of peculiar properties such as the extremely low vapor pressure or the relatively high heat capacity and viscosity which tend to minimize the ‘cushoning’ effect inside cavities and enhance the absorption of acoustic energy by the reaction mixture. Furthermore, simple work-up procedures and the possibility of recycling the solvent increase their appeal as green reaction media. ILs are commonly regarded as safe substances, nonetheless, concerns about their use under US irradiation derive from potential cavitation-induced degradation phenomena (*i.e.* formation of haloalkanes from SN_2 processes as well as imidazole decomposition products).²⁶⁰ Release of HF was observed under harsh conditions from some ILs containing the PF_6^- anion;^{261,262} hence, a reasoned use of these solvents should be made when applying prolonged or very high-intensity sonication.

1.6.5.1 Ionic liquid-catalyzed organic reactions

Despite the fact that ILs are usually considered as mere solvents, the interaction between their charged moieties with the functional groups of substrates can efficiently catalyze organic reactions allowing advantageous, metal-free synthetic conditions. One of the early papers in which this effect is combined with US as the energy source was published by Srinivasan and co-workers in 2003;²⁶³ the *O*-acetylation of a number of benzylic and aliphatic alcohols with acetic anhydride was carried out at room temperature by means of a 120 W, 50 kHz US cleaning bath. 1,3-di-*n*-butylimidazolium bromide ([BBIM][Br]) was chosen as the reaction medium, hence the catalytic effect is explained by the authors on the basis of the hydrogen bond interaction of the acidic H_a of the imidazolium ion with the oxygen atoms of the anhydride (Figure 1.23).

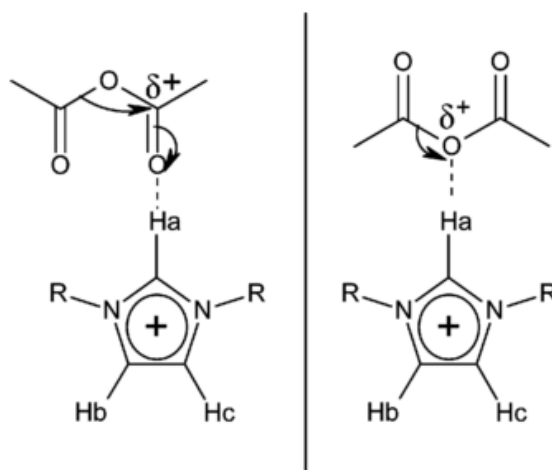
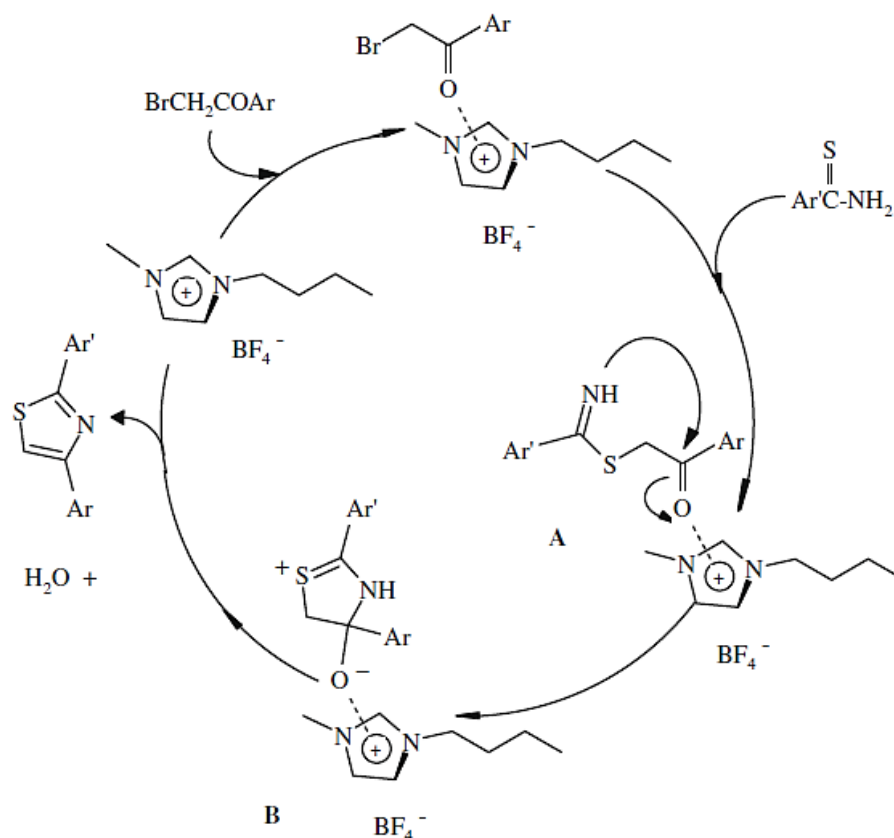


Figure 1.23 – The H_a hydrogen bond interaction of the imidazolium cation with oxygen of acetic anhydride

2,4-diarylthiazoles were obtained in very short reaction times (<10 min) from arylthioamides and α -bromoacetophenones at room temperature using [BMIM][BF₄] as the sole solvent and catalyst (Scheme 1.31) using a sonication probe operating at 140 W and 24 kHz.²⁶⁴ Lower US intensity values, as well as organic solvents were tentatively screened registering, for the model synthesis of 2-phenyl-4-(4-bromophenyl)thiazole, a marked drop in the system activity; [BMIM]-based ILs with different anions yielded, in the same conditions, only slightly worse results. Work-up consisted of a simple quench and extraction step and the products obtained after complete evaporation of the solvent did not need further purification, highlighting the environmental efficiency of this procedure.



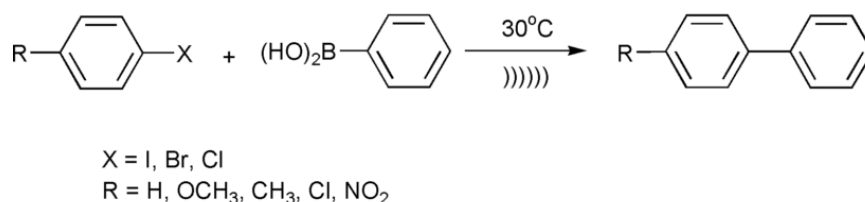
Scheme 1.31 – Proposed mechanism for the synthesis of 2,4-diaryltiazoles

The tandem addition/annulation reaction of *o*-aminoaryl ketones with α -methylene ketones yielded quinoline derivatives in very short sonication times (*i.e.* 35 min) at ambient conditions employing a thermostated cleaning bath.²⁶⁵ The IL 1-butylimidazolium tetrafluoroborate ($[\text{HBIM}][\text{BF}_4]$) afforded the best results on account of the higher basicity of its anion with respect to ClO_4^- , Br^- or Cl^- , nonetheless, optimal conditions were obtained by the addition of 25 vol% of MeOH as a cosolvent, due to the increased substrate solubility. A control reaction under silent conditions gave a very low yield (<5% vs 74% with US) and a recycle test showed that the system can be reused two times without loss of activity.

1.6.5.2 Organic reactions requiring the addition of a catalysts

Although not frequently reported, certain US-promoted organic transformations require the addition of an external catalyst even if conducted in ILs as solvents. Pd-catalyzed C-C coupling is the most investigated class of reactions in this category; for instance, an early work by the group of Srinivasan describes a brilliant US-enhanced procedure for the synthesis of olefines by fast, room temperature Heck coupling.²⁶⁶ 1,3-di-*n*-butylimidazolium bromide ($[\text{BBIM}][\text{Br}]$) and 1,3-di-*n*-butylimidazolium

tetrafluoroborate ([BBIM][BF₄]) ILs, which were used as solvents in the presence of Pd(OAc)₂ or PdCl₂ precursors, were responsible for the *in situ* formation of a Pd(II)-biscarbene complex that, in turn, is converted during olefin formation to IL-stabilized Pd(0) clusters. The whole process is promoted by sonication and, indeed, no reaction took place at all under silent conditions; similarly, no conversion could be observed replacing ILs with conventional solvents such as DMF or NMP, even with the addition of a phosphine ligand. Shortly afterwards, the same group applied the aforementioned conditions to the Suzuki cross-coupling of halobenzenes with phenylboronic acids, with the addition of MeOH as a cosolvent to optimize homogeneity (Scheme 1.32).²⁶⁷



Scheme 1.32 – Sonochemical Suzuki reaction in [bbim][BF₄]/MeOH

More recently, a sonochemical procedure for room temperature Sonogashira coupling reactions was reported emphasizing the absence of any added cocatalyst or phosphine-based ligand for the Pd-based catalyst.²⁶⁸ Various substituted aryl iodides reacted with phenylacetylene giving the corresponding alkyne in good to excellent yields and, notably, biodegradable 3-butoxycarbonyl-1-methylpyridinium bis(trifluoromethanesulfonyl)imides ILs derived from nicotinic acid were used as solvents to increase the environmental performance of the synthesis.

While ILs appear as good solvents for biocatalysts, lower enzyme activity is normally reported with respect to common organic solvents; hence, US were successfully tested as an alternative energy source with the aim of counterbalancing this negative effect. As the first example of US-enhanced enzyme catalyzed reactions in ILs, glucose transesterification with vinyl laurate by the lipase ‘Novozym 435’ was conducted at 40 °C in [BMIM][TfO] or [BMIM][PF₆]. As an industrially more attracting alternative, the glucose direct esterification with lauric acid was carried out in the same conditions by raising the temperature to 50 °C and adding a molecular sieve to remove water.²⁶⁹

1.6.5.3 Synthesis of nanoparticles and nanostructures in ionic liquids

A thiol functionalized IL was used as both solvent and stabilizer for the sonochemical

preparation of uniformly dispersed, small sized gold nanoparticles.²⁷⁰ H_2O_2 was employed as the reducing agent for HAuCl_3 in place of NaBH_4 to simplify the addition and purification steps; the authors suggest, on the basis of the poor results of the control reaction under conventional stirring, that US irradiation is indispensable for the formation of $\text{H}\cdot$ and $\text{OH}\cdot$ radical involved in the reduction mechanism as well as for the optimal dispersion of the IL-stabilized nanoparticles.

In view of their use as components for liquid magnetic marbles, a recent paper by Deng and co-workers describes the preparation of Fe_2O_3 nanoparticles by sonochemical decomposition of iron pentacarbonyl precursor under air atmosphere in 1-ethyl-3-methylimidazolium tetrafluoroborate ($[\text{EMIM}][\text{BF}_4]$) solvent at $0\text{ }^\circ\text{C}$ (Figure 1.24).²⁷¹ US were applied to the mixture for 90 min by means of a probe reactor operating at a very low power of 0.1 W; no additional stabilizer or capping agent was needed since particle aggregation and sedimentation were prevented by the IL itself.

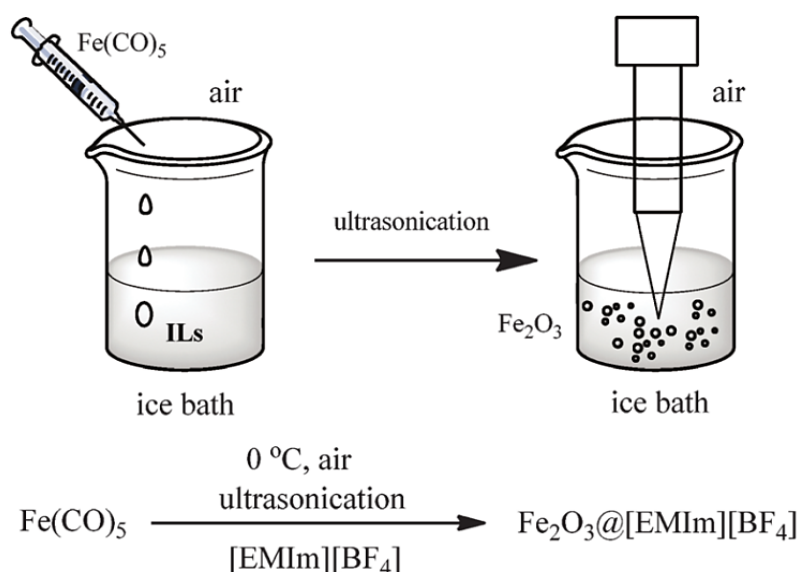


Figure 1.24 – Synthesis of iron oxide nanoparticles in $[\text{EMIM}][\text{BF}_4]$

Zinc oxide nanoparticles were obtained mixing a water solution of $\text{Zn}(\text{OH})_4^-$ ions (from basification of zinc acetate with NaOH) and 1-hexyl-3-methylimidazolium bis(trifluoromethylsulfonyl) imide ($[\text{HMIM}][\text{NTf}_2]$) IL and then sonicating the mixture (40 kHz, 50 W) for 1 h.²⁷² In the absence of US as well as of the IL the white ZnO precipitate could not be formed; the role of $[\text{HMIM}]^+$ cations in the polarization of $\text{Zn}(\text{OH})_4^-$ anions by electrostatic attraction is pointed out to explain the increased tendency towards dehydration and oxide formation.

1.6.5.4 Coordination chemistry in ionic liquids

Inorganic synthesis in ILs was rarely carried out under US irradiation, however, two interesting papers by Gedanken and co-workers describe the preparation of Fe(II)- and Ni(II)-imidazole complexes neutralized by the anion originating from the IL employed as the reaction solvent.^{273,274} More precisely, Fe(1-methylimidazole)₆(BF₄)₂ and Ni(1-methylimidazole)₆(BF₄)₂ were obtained by US-induced decomposition of the carbonyl precursors Fe(CO)₅ and Ni(CO)₄ in the presence of 1-methylimidazole and the IL [BMIM][BF₄] as solvent, while Fe(1-methylimidazole)₆(PF₆)₂ and Ni(1-methylimidazole)₆(PF₆)₂ were obtained, in the same conditions, when [BMIM][PF₆] was employed. No metal oxides were formed as byproducts and no PF₆⁻ hydrolysis took place during sonication; moreover, while only crystalline complexes were successfully synthesized in ILs, amorphous products were obtained when the same reaction was carried out in organic, non-volatile solvents.

1.6.6 Sonochemistry in other green solvents

Solvents such as EG and its oligomers (DEG; TEG and low molecular weight PEG) rather frequently employed in combination with US reactors, and some remarkable cases can be found in the literature. A phosphine-free Suzuki cross coupling was successfully performed in EG in the presence of 2.5 mol% Pd₂(dba)₃, tetrabutylammonium bromide (TBAB) and potassium carbonate as an auxiliary base employing a 47 kHz, 250 W cleaning bath.²⁷⁵ High yields of biaryls were obtained in pure EG, while water and an EG/water (20 vol%) mixture were tested as alternatives with less satisfactory results; on the other hand, recycling of the system showed a significant and progressive decrease of activity already from the second run.

Nanoparticles or nanosystems syntheses in EG are frequently described on account of the stabilizing and capping properties of this solvent; for instance, 3D flower-like bismuth sulfide nanostructures were obtained by high-intensity sonication (24 kHz, 400 W/cm²) of an EG solution of Bi(NO₃)₃•5H₂O and Na₂S₂O₃ precursors in the presence of CTABr as a surfactant.²⁷⁶ Sonication proved to be essential for the reaction rate enhancement but also for the formation of flower-like Bi₂S₃ superstructures; indeed, larger aggregates of rod-like particles were predominantly observed when the synthesis was repeated under conventional stirring (Figure 1.25). Moreover, morphology was strongly influenced by the choice of solvent; when acetylacetone or DMSO were added to EG, the product consisted in 1D rods with a low or high aspect ratio, respectively, but no 3D superstructure could be observed.

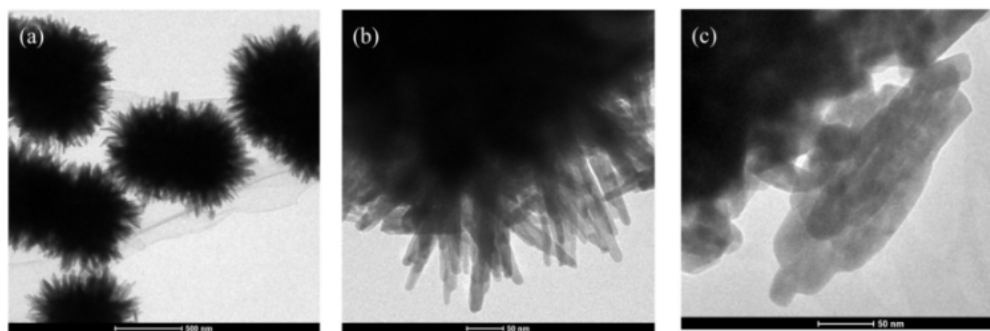


Figure 1.25 – TEM images of Bi_2S_3 structures obtained by sonochemical method (a and b) or refluxing method (c)

TEG and PEG-400 outperform EG when employed as solvents and stabilizers for the sonochemical reduction of nickel nitrate or cobalt nitrate to spherical Ni- or Co-nanoparticles.²⁷⁷ More precisely, while particles obtained in EG showed large diameters of c.a. 50 nm (Ni) and 350 nm (Co) and a tendency to precipitate shortly afterwards reaction, particles obtained in PEG-400 proved to be very small (3.2 nm and 2.3 nm respectively) and extremely stable towards aggregation and flocculation; particles obtained in TEG have properties somehow between those obtained in EG and PEG. These beneficial effects derive from the superior viscosity of PEG constituting an efficient physical barrier to nanoparticle growth after nucleation. Interestingly, the authors repeated the preparation applying an external magnetic field during the growth of the ferromagnetic particles and found that nanowires were formed in the place of spheres. Apparently the extreme conditions produced by cavitation do not hamper the particle motion and growth driven by magnetic interactions; this could stem from the fact that sonochemical reactions involving ionic species take place in the less energetic, liquid surroundings of cavities rather than in the vapor phase inside the cavity itself.

More than ten years ago, a remarkable paper described the coupling of a probe sonicator with a high pressure cell containing CO_2 at 75 bar and 10 °C as solvent for the catalyst- / initiator-free MMA radical polymerization.²⁷⁸ As the authors point out, it is necessary not to overcome the critical point of the gas since, once the phase boundary between liquid and vapor is lost, cavitation cannot physically take place; moreover, an US intensity of 25 W/cm^2 was not sufficient to induce cavitation and a higher value of 125 W/cm^2 was needed. High molecular weight PMMA could be obtained through an overall very clean procedure, nonetheless, probably due to the reactor complexity and difficult scalability, this interesting technique has not gained substantial popularity over time.

Commercial rapeseed and corn oils were used as green and safe solvents (both are edible products) for the US-promoted synthesis of highly magnetic iron nanoparticles with notable stability towards air oxidation.²⁷⁹ These vegetable oils represent good alternatives to the most common solvents in sonochemistry as they meet the fundamental requirement of low volatility; however, partial polymerization of both solvents during US irradiation was observed due to the presence of several unsaturated fats. This degradation, although hampering recyclability, favors the formation of a stabilizing matrix for the prepared iron nanoparticles which proved to be a very effective barrier against oxidation of the metal surface; indeed, poly-unsaturated rich corn oil afforded better results with respect to mono-unsaturated rich rapeseed oil.

1.6.7 Solvent-free sonochemical reactions

The absence of solvents is a highly desirable asset for an environmentally friendly chemical synthesis since large volumes of wastes as well as process complexity are often reduced significantly. Not every reaction can be carried out under these favorable conditions since the physical properties of reactants must satisfy specific requirements; this is particularly true when US irradiation is employed on account of the strong influence of viscosity, density, thermal conductivity and many other parameters on the efficiency of acoustic absorption and mass transfer. Nonetheless, during the last decade an impressive number of sonochemical organic syntheses and some polymerization reactions were successfully achieved without the addition of a solvent.

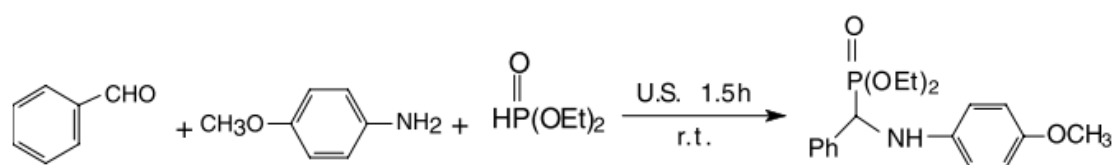
1.6.7.1 Solvent-free organic reactions

The solvent-free N-alkylation of imidazole with 1-bromobutane catalyzed by Na⁺- or Cs⁺-promoted Norit-carbon was carried out by the group of Martin-Aranda under sonochemical and thermal conditions for comparison.²⁸⁰ Utilizing the more active Cs⁺-Norit, the US rate enhancement is evident after 120 min at 40 °C (80% vs 45% yield) but becomes even larger if the reaction is run at 20 °C (71% vs 25% yield) since lower temperatures decrease the liquid phase vapor pressure and, consequently, increase the energy released by each cavity collapse.

More recently, the Knoevenagel reaction was carried out by Liu and co-workers to obtain substituted olefins from various aromatic aldehydes and ethyl cyanoacetate or malonitrile in the presence of potassium sorbate as a green, non-toxic catalyst.²⁸¹ An ultrasonic cleaner (300 W) was operated at different acoustic frequencies, observing a peak of activity for 80 kHz; under these conditions, a general rate enhancement was observed with respect to conventional stirring, although the benefit is less evident in the

case of some already fast malonitrile-based condensations.

The one-pot sonochemical synthesis of α -aminophosphonates from carbonyl compounds, amines and diethylphosphite could be successfully accomplished by a solvent- and catalyst-free procedure relying on a 40 kHz, 250 W cleaning bath as the US source.²⁸² As evidenced by a room temperature model reaction with benzaldehyde (Scheme 1.33), sonication dramatically increased the rate of the three-component coupling (97% yield within 90 min vs 18% overnight in silent conditions), although heating to 70 °C was necessary even under US irradiation when less reactive ketones were chosen as substrates. While aniline derivatives proved to be smoothly converted, aliphatic amines (above all, secondary amines like piperidine) gave unsatisfactory yields or hardly any trace of the desired products.

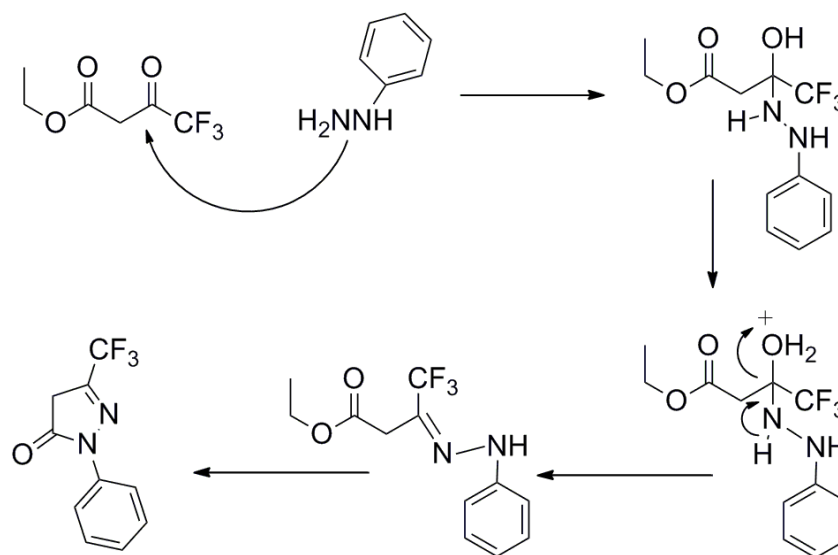


Scheme 1.33 – Model reaction for the one-pot sonochemical synthesis of α -aminophosphonates

Conventional multi-component Passerini reactions involving hindered substrate require high pressure conditions to proceed; hence, the extreme conditions generated locally during cavitation proved to accelerate the synthesis of α -acyloxyamides without the need of pressurized reactors. As an example, a very recent paper reports that a room temperature model reaction with acetone, cyclohexylisocyanide and isopentanoic acid gave comparable yields after 16.5 h at a very high pressure of 300 MPa or within only 1 h under high-intensity sonication.²⁸³ The effect of temperature was investigated, reporting a maximum of activity for 40 °C due to isonitrile decomposition upon stronger heating; interestingly the role of US intensity was also assessed observing a six-fold rate decrease by substituting the 1200 W probe reactor with a 100 W cleaning bath.

Substituted pyrazolones were prepared by Mojtahedi and his group by bulk, catalyst-free condensation of hydrazine or phenylhydrazine with various β -ketoesters carried out using a high intensity US probe (24 kHz, 460 W/cm²) as the energy source at a controlled temperature of 25 °C (Scheme 1.34).²⁸⁴ Initial optimization studies suggested to work in solvent-free conditions, while the repetition of a model reaction under conventional thermal heating (140 °C) observing unsatisfactory yields after longer times demonstrated the importance of sonication for the efficiency of the synthesis. Notably, a

relatively large scale experiment was successfully performed utilizing 50 mmol (in the place of 5 mmol) of both reactants and registering an excellent yield of 90% 1-phenyl-3-propyl-1H-pyrazol-5(4H)-one after only 25 min.



Scheme 1.34 – Mechanism of condensation of hydrazines with acetoacetates

The one-pot reaction of phthalhydrazide, dimedone and 4-nitrobenzaldehyde for the synthesis of the corresponding indazolophthalazinetrione was carried out under solvent-free conditions in the presence of (*S*)-camphorsulphonic acid as catalyst.²⁸⁵ Two alternative solvent-free procedures are described (80 °C, silent conditions or 25 °C with US-irradiation) giving very similar results in terms of yield, time and selectivity; therefore, in this case, no particular benefit other than the possibility of working at room temperature was brought by sonication. Both techniques, indeed, proved to be efficient and ecologically benign on account of the operational simplicity and atom-economy of the domino reaction.

Recently, thermal and sonochemical procedures were compared for the *p*-TSA-catalyzed synthesis of acyclic imides from anhydrides and aliphatic or aromatic nitriles in the absence of solvent.²⁸⁶ The acid catalyst, although inexpensive and relatively safe, had to be used in a quite high molar ratio of 30% for liquid nitriles and even 50% for solid nitriles; on the other hand, US-irradiation considerably shortened the range of the reaction times from 30 – 120 min to only 5 – 28 min depending on the substrates.

1.6.7.2 Bulk polymerization reactions

On account of the efficient cavitation-induced radical formation, US-promoted radical polymerizations have already been reported several years ago²⁸⁷⁻²⁸⁹ and, nowadays, are

well-established procedures. An interesting work by Kojima and co-workers described the synthesis of polystyrene (PS) by sonication of the liquid monomer at five different US frequencies (ranging from 23.4 kHz to 1 MHz) and outlined a marked influence on the characteristics of the product.²⁹⁰ More precisely, while a maximum in PS yield was observed with an acoustic frequency of 92 kHz, lower frequencies gave less satisfactory results and higher frequencies produced no conversion at all; on the other hand, PS number-average molecular weight (M_n) increased from 5.5×10^4 to 11.5×10^4 lowering the frequency from 92 kHz to 23.4 kHz. As a general trend, polydispersity indexes tended to be higher than those of analogous PS obtained by thermal heating; according to the authors, this finding is explainable on the basis of the coexistence of radical polymerization and degradation mechanisms under sonochemical conditions.

Bulk styrene polymerization was also carried out in the presence of variable amounts of multi-walled carbon nanotubes (MWCNTs) with the aim of obtaining a PS-based nanocomposite (PS-*g*-MWCNT) (Figure 1.26) with increased electrical conductivity.^{291,292} The main role of sonication, in this case, was to efficiently disperse the nanotubes by breaking the strong π -stacking interactions during polymerization; nonetheless, PS could be synthesized both in the presence or absence of a radical initiator (AIBN), witnessing how the reaction itself can easily be promoted by US irradiation. Increasing quantities of MWCNTs (up to 0.2 wt%) augmented the PDIs of the composite due to the US-induced opening of π -bonds followed chain-transfer reactions and grafting of the surface with PS or AIBN itself.

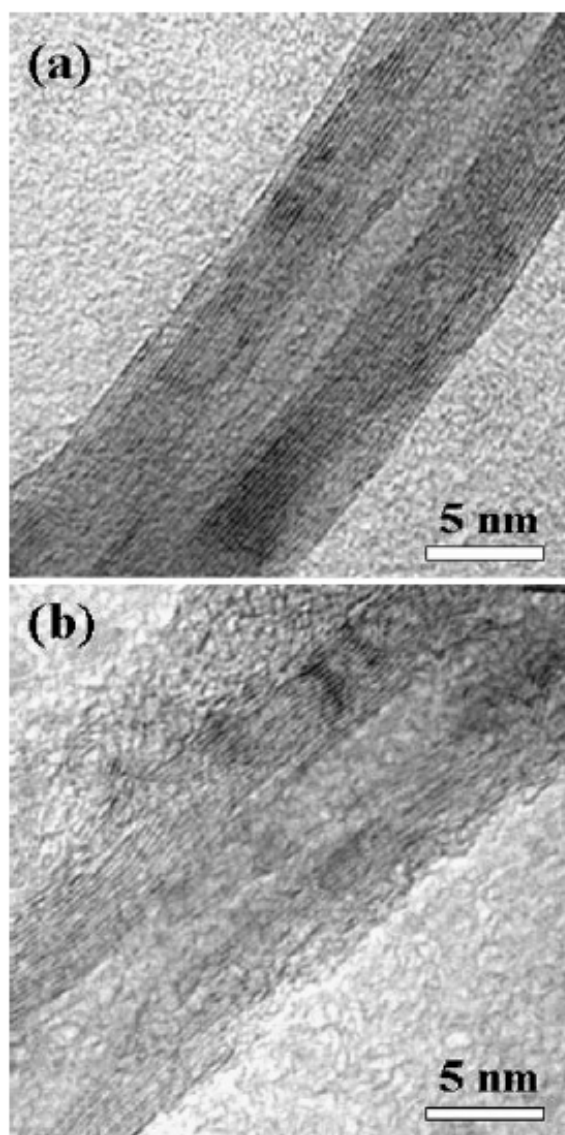


Figure 1.26 – TEM morphology of pristine MWNT (a) and PS-g-MWNT (b)

Since the efficiency of sonication depends strongly on the viscosity of the mixture, it is important to point out that the progressive increase of molecular weight during irradiation may represent a critical issue in a bulk reaction. As an example, the dibutyl tin laurate-catalyzed ring opening polymerization of ϵ -caprolactone was moderately accelerated by the use of a probe sonicator in the place of vigorous mechanical stirring; nevertheless, as an M_n of around 9500 g/mol was reached after 2.5 h, the reaction could not proceed further due to an excessive viscosity of the acoustic medium.²⁹³ The slower silent procedure, hence, produced poly(caprolactone) (PCL) with slightly higher M_n of about 10500 g/mol. When similar investigations were conducted with δ -valerolactone as the monomer, polymerization was again accelerated by the use of US. Nonetheless, depolymerization was correspondingly promoted during the late stages of the reaction and a drop in M_n was noticed after a maximum value was reached (which depends on

experimental parameters) (Figure 1.27).

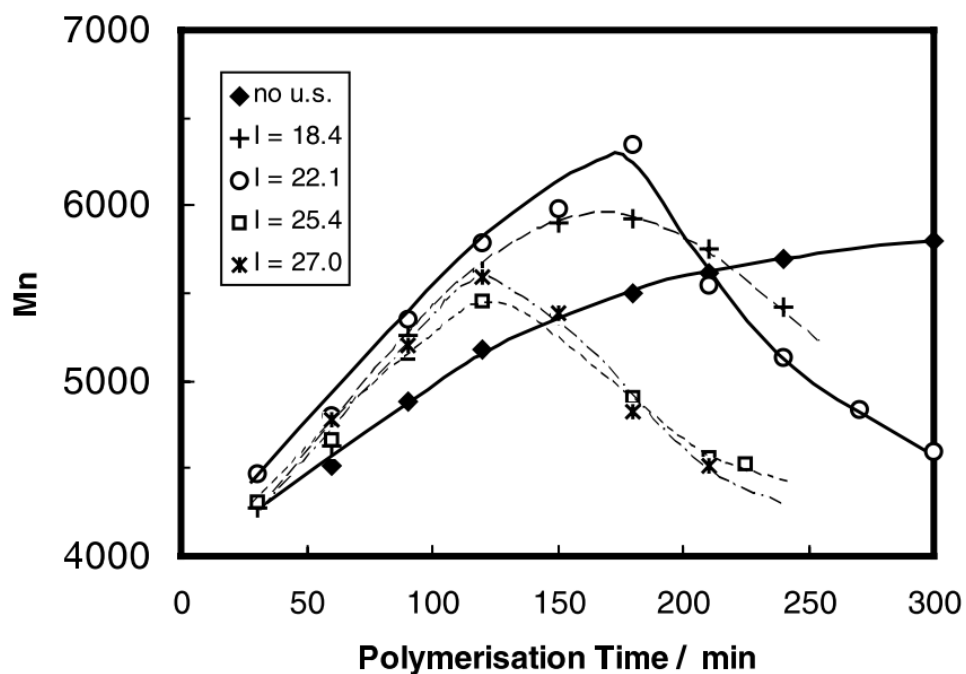


Figure 1.27 – The effect of US intensity (indicated in W/cm^2) on the molecular weight of poly(valerolactone)s polymerized at 150 °C

2 Experimental

2.1 Reagents and solvents

CuI (99,995%), Cu₂O (>99,99%), Cu nanopowder (<100µm; 99.8%), K₄[Fe(CN)₆] (>99.5%), PEG-3400, PEG-10000, Poly(ethylene glycol) monomethyl ether (M_n(GPC) = 5200 g/mol), benzyl alcohol, *n*-trioctyl amine; NaH, mesyl chloride, Na₂CO₃, *p*-toluenesulfonic acid monohydrate, Pd(OAc)₂, ε-caprolactone, Sn(Oct)₂, 4-PyCH₂OH, hexamethylene diisocyanate, BuLi (1.6 M in hexanes), PdCl₂, Ag(SbF₆) and Ag(OTs) were purchased from Sigma-Aldrich and used without further purification. *trans*-[Pd(OAc)₂(4-EtPy)₂] (**13**),¹⁵¹ [PdCl(*η*³-allyl)]₂,²⁹⁴ di-*o*-anisylphosphine²⁹⁵ and NaBAr'₄ (Ar' = 3,5-bis(trifluoromethyl)phenyl)²⁹⁶ were synthesized according to literature procedures. CuO (>99.7%) was purchased from Prolabo. L-lactide and D-lactide were purchased from Purac; *rac*-lactide was obtained as a mixture (1 : 1) of L- and D- lactide. Lactides, NaH and 4-PyCH₂OH were stored in a glove-box at room temperature under a N₂-atmosphere. CH₂Cl₂, stabilized with amylene, was purchased from Sigma-Aldrich, Panreac and J. T. Baker; DMF (anhydrous; handled under N₂ flux) and THF (HPLC-grade; BHT-stabilized; addition of molecular sieves) were purchased from VWR. *n*-Hexane was purchased from Romil-SA and Sigma-Aldrich; Et₂O (puriss. p.a. and stabilized with BHT), toluene, CHCl₃ and HPLC-grade CHCl₃ were purchased from Sigma-Aldrich. 2-propanol (purum) was purchased from Fluka Chemika; MeOH was purchased from Carlo Erba; toluene was dried over molecular sieves, all other solvents were used without further purification. Et₂O for work up of cyanation reactions was purchased from VWR and distilled before use.

CD₂Cl₂ and DMSO-d₆ were purchased from Sigma-Aldrich; CDCl₃ was purchased from Eurisotop.

2.2 Synthetic procedures

2.2.1 P(L)LA-Py (L1) and P(LD)LA-Py (L2) macroligands

In a Schlenk tube, L-lactide (for **L1**) or *rac*-lactide (for **L2**) (3.00 g, 0.021 mol) was heated at 135 °C in the presence of Sn(Oct)₂ (0.105 mmol) and 4-PyCH₂OH (109.06 mg, 0.001 mol) for 3 h under nitrogen. The reaction mixture was allowed to cool to room temperature and the crystalline lactide, that sublimed during the reaction (*i.e.* c.a. 1%) was removed mechanically. The crude reaction product was then dissolved in CHCl₃ (20.0 mL), followed by the slow addition of *n*-hexane (20.0 mL) to the latter

solution in order to precipitate the product as a powder (*i.e.* **L1**) or a dense liquid (*i.e.* **L2**). Consequently, the powdery product was separated from solution by filtration, while the liquid product was washed several times with *n*-hexane (5.0 mL), transforming it into a waxy product. Both products were dried under vacuum at room temperature. **L1**: 2.52 g (84%); M_n : 3280 g/mol; PDI: 1.33 (GPC-RI). **L2**: 2.25 g (75%); M_n : 3700 g/mol; PDI: 1.54 (GPC-RI).

2.2.2 PCL-Py (**L3**) macroligand

In a Schlenk tube, ϵ -caprolactone (10.88 g, 0.095 mmol) was heated at 135 °C in the presence of Sn(Oct)₂ (139.0 mg, 0.476 mmol) and 4-PyCH₂OH (519.0 mg, 4.760 mmol) for 3h under nitrogen. The reaction mixture was allowed to cool to room temperature and the solid residue was then dissolved in CHCl₃ (15.0 mL) and on addition of methanol (30.0 mL) to the latter solution the polymer product precipitated as off-white powder, which was successively separated from the solution by filtration and dried under vacuum (20 Torr) at room temperature for 12 h. Yield: 4.95 g (43%); M_n : 5400 g/mol (GPC - RI); PDI: 1.25.

2.2.3 MeO-PEG-Py (**L4**) macroligand

Mesylated MeO-PEG-5000 (9.10 g; 1.750 mmol), which was synthesized following a reported procedure,²⁹⁷ 4-hydroxymethyl pyridine (384.0 mg, 3.500 mmol) and NaH (84 mg; 3.500 mmol) were weighted in a round-bottom flask (250.0 mL) and dissolved in anhydrous DMF (80.0 mL) with vigorous stirring at 60 °C under N₂ atmosphere. After a reaction time of 4 h, the orange reaction mixture was cooled to room temperature and filtered through a sand layer and then through a paper filter in order to obtain a clear orange solution. After cooling the latter solution to 0 °C, cold 2-propanol (100.0 mL) was added, obtaining a pale-yellow precipitate which was separated from solution by Buchner filtration and successively washed with cold 2-propanol (50.0 mL) and *n*-hexane (20.0 mL). The white solid obtained was dried under vacuum to constant weight. Yield: 7.96 g (86%). M_n (¹H NMR)= 5200 g/mol (refers to the polymer chain).

2.2.4 (MeO-PEG-PyH⁺)OTs⁻ ((**HL4**)(**OTs**)) macroligand

L4 (500.0 mg, 0.100 mmol) and *p*-toluenesulfonic acid (37.0 mg, 0.200 mmol) were dissolved in water (5.0 mL) in a round-bottom flask and stirred at room temperature for 3 h. Then 2-propanol (20.0 mL) and cold Et₂O (40.0 mL) were added to the clear colorless reaction mixtures, causing the precipitation of the polymer product as a colorless viscous liquid. After decantation and washing with cold Et₂O (20.0 mL), the solid was dried under vacuum giving a waxy product. Yield: 451.0 mg (88%).

2.2.5 MeO-PEG-Bn (L5) macroligand

Mesylated MeO-PEG-5000 (1.14 g, 0.220 mmol), benzyl alcohol (45.5 μ L, 0.440 mmol) and NaH (11.0 mg, 0.440 mmol) were placed in a round-bottom flask and dissolved in anhydrous DMF (10.0 mL) under vigorous stirring at 60 °C under N₂ atmosphere. After a reaction time of 4 h, the pale-yellow reaction mixture was cooled to room temperature and filtered successively through a sand layer and filter paper to give a clear colorless solution. After cooling the latter solution to 0 °C, cold 2-propanol (50.0 mL) was added and the white precipitate was separated from solution by Buchner filtration and washed with cold 2-propanol (20.0 mL) and *n*-hexane (10.0 mL). The white waxy solid was dried at room temperature to constant weight under vacuum. Yield = 771.0 mg (71%). $M_n(^1\text{H NMR}) = 5200$ g/mol (refers to the polymer chain).

2.2.6 P(L)LA-*b*-P(LD)LA-Py (L6, L8) and P(D)LA-*b*-P(LD)LA-Py (L7, L9) macroligands

L2 (6.5 g, 1.75 mmol for **L6** and **L7**; 1.3 g, 0.35 mmol for **L8** and **L9**;) was dissolved in dry toluene (25.0 mL) and the obtained solution was divided into two portions. To each portion was added either L-lactide (for **L6** and **L8**) or D-lactide (for **L7** and **L9**) (5.0 g, 35.0 mmol) and Sn(Oct)₂ (85.1 mg, 0.21 mmol). The reaction mixtures were heated at reflux for 24 h under nitrogen. Afterwards the latter reaction mixtures were allowed to cool to room temperature and the products were precipitated as waxy light-orange deposits (**L6** and **L7**) white powdery solids (**L8** and **L9**) with *n*-hexane (25.0 mL), then filtered and washed with additional *n*-hexane. The crude products were dried under vacuum at room temperature for 24 h. **L6**: yield = 73%; $M_n = 5000$ g/mol (NMR), 5010 g/mol (GPC-RI), PDI = 1.25. **L7**: yield = 72%; $M_n = 5000$ g/mol (NMR), 5480 g/mol (GPC-RI), PDI = 1.21. **L8**: yield = 96%; $M_n = 11400$ g/mol (NMR), 12060 g/mol (GPC-RI), PDI = 1.59. **L9**: yield = 96%; $M_n = 11600$ g/mol (NMR), 12230 g/mol (GPC-RI), PDI = 1.53.

2.2.7 Py-P(L)LA-Py (L10) bifunctional macroligand

In a round bottom flask 2.0 g of **L1** ($M_n = 3280$ g/mol) and 5.05 mL of a dry toluene solution of hexamethylene diisocyanate (0.0678 M) were added to 10 mL of dry toluene and refluxed (110 °C) for 1 h under N₂ atmosphere. Afterwards, the clear pale-pink colored mixture was allowed to cool to room temperature noticing the precipitation of the polymer as a pale-pink granular solid. The clear liquid phase was discarded as the product was filtered on Buchner funnel and washed twice with *n*-hexane (20 mL); the polymer was dried under vacuum at room temperature for 24 h. Yield = 84%; $M_n =$

6280 g/mol, PDI = 1.17 (GPC-RI).

2.2.8 MeO-PEG-P(*o*-anisyl)₂ (L11) macroligand

Into a glovebox (N₂ atmosphere), in a round bottom flask di-*o*-anisylphosphine (1.16 g, 4.72 mmol) was dissolved in distilled THF (100 mL) and 2.95 mL of a 1.6M BuLi hexane solution (4.72 mmol) was added observing the formation of a yellow slurry which was left under stirring for 1 h. Afterwards, a solution of mesylated MeO-PEG-5000 (7.85 g, 1.57 mmol) in distilled THF (100 mL) was added dropwise to the yellow slurry containing the Li-salt of the phosphine noticing a progressive solubilisation of the slurry to form a vivid orange, clear solution, which was left under stirring for 4 h. The orange solution turns slightly turbid and is quenched with few drops of degassed distilled water, noticing the fast decoloration of the mixture; then THF is evaporated to dryness and the solid is redissolved in 250 mL of degassed CH₂Cl₂ and a slow filtration through 0.2 μm PTFE cartridges was performed. The volume of the resulting clear, colorless solution was reduced to approx. 100 mL and 100 mL of degassed 2-propanol and 300 mL of degassed Et₂O were added to precipitate the phosphine-functionalized PEG as a white powdery solid, which was separated from the liquid phase by Buchner filtration and dried under vacuum for 72 h. The obtained solid was then purified from residual free di-*o*-anisylphosphine by dissolution in 30 mL of degassed CH₂Cl₂ and precipitation with a mixture of degassed 2-propanol (40 mL) and degassed Et₂O (180 mL), followed by Buchner filtration and drying under vacuum overnight. Yield = 5.80 g (70 %); M_n = 5380 g/mol (NMR).

2.2.9 *trans*-[PdCl₂(L1)₂] (1) and *trans*-[PdCl₂(L2)₂] (2) macrocomplexes

In a round bottom flask PdCl₂ (15.0 mg, 0.084 mmol) was suspended in a 3:1 CH₂Cl₂/DMF solvent mixture (20.0 mL). To this suspension was added **L1** or **L2** (0.153 mmol). The reaction mixture was allowed to stir at room temperature for 72 h. Afterwards, the obtained yellow solutions were passed through a plug of sand, followed by addition of *n*-hexane (40.0 mL). The light brown solids were separated from the mother liquid and dried overnight under vacuum at room temperature. **1**: yield = 474.0 mg (84%); M_n (GPC-RI) = 11130 g/mol; PDI = 1.22. **2**: yield = 509.2 mg (80%); M_n (GPC-RI) = 12500 g/mol; PDI = 1.34.

2.2.10 PdCl(η³-allyl)(L1) (3) macrocomplex

In a round bottom flask [PdCl(η³-allyl)]₂ (44.0 mg, 0.120 mmol) was dissolved in

CH₂Cl₂ (25.0 mL). To this solution was added **L1** (393.6 mg, 0.120 mmol) and the resulting reaction mixture was allowed to stir at room temperature for 24 h. Afterwards, *n*-hexane (30.0 mL) was added, causing the precipitation of the product as a beige powder, which was dried overnight under vacuum at room temperature. Yield = 282.6 mg (68%).

2.2.11 *cis*-[Pd(η^3 -allyl)(L1)₂]BAr'₄ (**4**) and *cis*-[Pd(η^3 -allyl)(L1)(L2)]BAr'₄ (**5**) macrocomplexes

In a round bottom flask **3** (200.0 mg, 0.058 mmol) was dissolved in CH₂Cl₂ (10.0 mL). To the obtained clear solution **L1** or **L2** (0.058 mmol) and NaBAr'₄ (51.4 mg, 0.058 mmol) were added. The reaction mixture was allowed to stir at room temperature for 24 h, causing the precipitation of NaCl, which was separated. Upon addition of *n*-hexane (20.0 mL) the product precipitated as light brown powders which were dried overnight under vacuum at room temperature. Yield **4**: 215.2 mg (49%); yield **5**: 231.7 mg (50%).

2.2.12 [Pd(L1)₄](SbF₆)₂ (**6**); [Pd(L2)₄](SbF₆)₂ (**7**) and [Pd(L1)₂(L2)₂](SbF₆)₂ (**8**) macrocomplexes

In a Schlenk tube compound **1** or **2** (0.015 mmol) was dissolved in CH₂Cl₂ (20.0 mL). To this solution were added either **L1** or **L2** (0.030 mmol) followed by the addition of Ag(SbF₆) (0.031 mmol). The reaction mixture was allowed to stir at room temperature for 72 h. The resulting suspension was filtered through Celite and the obtained solution was centrifuged for 30 min at 2000 rpm in order to completely remove the AgCl formed. *n*-Hexane (30.0 mL) was added to the obtained clear solutions, causing the precipitation of the product as light brown powder which was dried overnight under vacuum at room temperature. **6**: yield = 115.1 mg (56%); **7**: yield = 138.4 mg (60%); **8**: yield = 98.1 mg (45%).

2.2.13 [Pd(L1)₂(L2)₂](OTs)₂ (**9**) macrocomplex

In a Schlenk tube compound **1** or **2** (0.015 mmol) was dissolved in CH₂Cl₂ (20.0 mL). To this solution were added either **L1** or **L2** (0.030 mmol) followed by the addition of Ag(OTs) (0.031 mmol). The reaction mixture was allowed to stir at room temperature for 72 h. The resulting suspension was filtered through Celite and the obtained solution was centrifuged for 30 min at 2000 rpm in order to completely remove the AgCl formed. To the obtained clear solutions was added *n*-hexane (30.0 mL), causing the precipitation of the product as light brown powder which was dried overnight under vacuum at room temperature. Yield: 101.6 g (47%).

2.2.14 *trans*-[PdCl₂(4-EtPy)₂] (4-EtPy = 4-ethylpyridine) (10) complex

PdCl₂ (20.0 mg, 0.113 mmol) was suspended in CH₂Cl₂ (15.0 mL). Afterwards, 4-ethylpyridine (25.7 μL (0.226 mmol)) was added and the resulting reaction mixture was allowed to stir at room temperature for 3 h. In the course of the reaction some of the product precipitated and on addition of diethyl ether (15.0 mL) the product was precipitated quantitatively. The product was then successively separated by filtration, washed with diethyl ether (10.0 mL) and dried under vacuum giving a slightly yellow powder. Yield: 37.6 mg (85 %). Anal. Calcd. for C₁₄H₁₈Cl₂N₂Pd: C, 42.95; H, 4.60; N, 7.15. Found: C, 42.80; H, 4.45; N, 7.03.

2.2.15 *trans*-[PdCl₂(L3)₂] (11) macrocomplex

In a round bottom flask PdCl₂ (45.9 mg, 0.258 mmol) was suspended in a 1:1 CH₂Cl₂/DMF solvent mixture (20.0 mL). L3 (0.492 mmol) was added to this suspension and the reaction mixture was allowed to stir at room temperature for 72 h. Afterwards, the yellow solution was passed through a plug of sand, followed by addition of *n*-hexane (50.0 mL). The yellow oily product was separated from the mother liquid by decantation, washed twice with additional hexane (2 x 20 mL) and dried by rotavapor (30 min; 40 °C) and then under vacuum at room temperature (72 h) obtaining a light brown solid. Yield: 2.02 g (88%); *M_n* (GPC-RI): 11690 g/mol; PDI: 1.20

2.2.16 [Pd(L3)₄](SbF₆)₂ (12) macrocomplex

In a Schlenk tube compound **11** (0.068 mmol) was dissolved in CH₂Cl₂ (20.0 mL). L3 (0.136 mmol) was added to this solution, followed by the addition of Ag(SbF₆) (0.136 mmol). The reaction mixture was allowed to stir at room temperature for 72 h. The resulting suspension was filtered through Celite and the solution was centrifuged for 30 min at 2000 rpm in order to completely remove the AgCl formed. *n*-Hexane (60.0 mL) to the clear solution, causing the precipitation of the product as a brown oil which was separated from the mother liquid by decantation and dried overnight under vacuum at room temperature. Yield: 822 mg (75%).

2.2.17 [Pd(L1)₂(L3)₂](SbF₆)₂ (13) macrocomplex

In a Schlenk tube compound **11** (0.126 mmol) was dissolved in CH₂Cl₂ (20.0 mL). L1 (0.252 mmol) was added to this solution, followed by the addition of Ag(SbF₆) (0.252 mmol). The reaction mixture was allowed to stir at room temperature for 72 h. The resulting suspension was filtered through Celite and the solution was centrifuged for 30

min at 2000 rpm in order to completely remove the AgCl formed. *n*-hexane (60.0 mL) was added to the clear solution, causing the precipitation of the product as a brown oil which was separated from the mother liquid by decantation and dried under vacuum at room temperature (72 h). Yield: 1.50 g (68%).

2.2.18 [Pd(L3)₄](OTs)₂ (14) macrocomplex

In a Schlenk tube compound **11** (0.020 mmol) was dissolved in CH₂Cl₂ (10.0 mL). **L3** (0.040 mmol) was added to this solution, followed by the addition of Ag(OTs) (0.040 mmol). The reaction mixture was allowed to stir at room temperature for 72 h. The resulting suspension was filtered through Celite and the solution was centrifuged for 30 min at 2000 rpm in order to completely remove the AgCl formed. *n*-Hexane (30.0 mL) was added to the clear solution, causing the precipitation of the product as a brown oil which was separated from the mother liquid by decantation and dried under vacuum at room temperature (72 h). Yield: 260 mg (48%).

2.2.19 [Pd(L1)₂(L3)₂](OTs)₂ (15) macrocomplex

In a Schlenk tube compound **11** (0.063 mmol) was dissolved in CH₂Cl₂ (20.0 mL). **L1** (0.126 mmol) was added to this solution, followed by the addition of Ag(OTs) (0.126 mmol). The reaction mixture was allowed to stir at room temperature for 72 h. The resulting suspension was filtered through Celite and the solution was centrifuged for 30 min at 2000 rpm in order to completely remove the AgCl formed. *n*-hexane (60.0 mL) was added to the clear solution, causing the precipitation of the product as a brown oil which was separated from the mother liquid by decantation and dried under vacuum at room temperature (72 h). Yield: 701 mg (65%).

2.2.20 [Pd(L1)₄](OTs)₂ (16) macrocomplex

In a Schlenk tube compound **1** (0.034 mmol) was dissolved in CH₂Cl₂ (10.0 mL). **L1** (0.068 mmol) was added to this solution, followed by the addition of Ag(OTs) (0.068 mmol). The reaction mixture was allowed to stir at room temperature for 72 h. The resulting suspension was filtered through Celite and the solution was centrifuged for 30 min at 2000 rpm in order to completely remove the AgCl formed. *n*-Hexane (30.0 mL) was added to the clear solution, causing the precipitation of the product as a yellow oily solid which was separated from the mother liquid by decantation and dried overnight under vacuum at room temperature. Yield: 375 mg (69%).

2.2.21 *trans*-[Pd(OAc)₂(L1)₂] (17) and *trans*-[Pd(OAc)₂(L3)₂] (18) macrocomplexes

In a round-bottom flask Pd(OAc)₂ (120.0 mg, 0.529 mmol) was dissolved in CH₂Cl₂ (35.0 mL). To this solution was added **L1** (3.60 g, 0.750 mmol) or **L3** (3.98 g, 0.750 mmol). The reaction mixture was allowed to stir at room temperature for 24h. Then *n*-hexane (40.0 mL) was added to the solution causing the precipitation of the product. The brown powder (**17**) or dark brown oil (**18**) was separated from the mother liquid by decantation. Upon washing of the crude products with *n*-hexane (5.0 mL) and drying them under vacuum (20 Torr) at room temperature, a beige (**17**) or brown (**18**) solid was obtained, respectively. **17**: yield = 3.56 g (95%); M_n = 10020 g/mol; PDI = 1.39. **18**: yield = 3.40 g (83%); M_n = 12800 g/mol; PDI = 1.68.

2.2.22 *trans*-[Pd(OAc)₂(4-EtPy)₂] (**19**) complex

trans-[Pd(OAc)₂(4-EtPy)₂] was synthesized according to a literature procedure.¹⁵¹

2.2.23 *trans*-[Pd(OAc)₂(L4)₂] (**20**) macrocomplex

L4 (4.00 g, 0.750 mmol) and Pd(OAc)₂ (87.0 mg, 0.390 mmol) were dissolved in CH₂Cl₂ (40.0 mL) and the resulting cloudy solution was stirred in air for 24 h. Afterwards, the solution was filtered through a paper filter and *n*-hexane (50.0 mL) was added to the clear yellow solution, which caused the precipitation of a brown viscous oil. The supernatant was decanted off and the brown oil was washed twice with *n*-hexane (30.0 mL) to give a brown waxy product which was dried under vacuum to constant weight yielding a beige solid: Yield: 3.33 g (82%). Pd content (ICP-OES): 0.96 wt%.

2.2.24 [Pd(L4)₄](OTs)₂ (**21**) macrocomplex

20 (910.5 mg, 0.084 mmol) and **L4** (891.7 mg, 0.168 mmol) were dissolved in CH₂Cl₂ (20 mL) under stirring by means of a magnetic stirring bar. To the clear, amber colored solution *p*-toluenesulfonic acid monohydrate (32.0 mg, 0.168 mmol) was added. After a reaction time of 24 h the solution was successively filtered through a HPLC cartridge (0.2 μm PTFE membrane) and cooled to 0 °C. Then cold 2-propanol (100 mL) was added to the latter solution and an off-white slurry was formed which was kept at 0 °C for 1 h. Afterwards, the solid was successively filtered, washed with cold 2-propanol (20.0 mL) and *n*-hexane (20.0 mL) and dried to constant weight under vacuum at room temperature. Yield: 1.47 g (81%). Pd content (ICP-OES): 0.47 wt%.

2.2.25 Pd(0)@[2(HL4)(OAc)] (**22**) and Pd(0)@[2L4 + 2(HL4) (OTs)] (**23**) stabilized Pd-nanoparticles

22 and **23** were obtained by dissolving **20** and **21** (400.0 mg) in deaerated CH₂Cl₂ (30.0

mL) at room temperature. Afterwards the clear solutions were transferred under nitrogen into a stainless steel autoclave (70.0 mL). The autoclave was charged with dihydrogen (15 bar) at room temperature and stirring started. After a reaction time of 1 h, the autoclave was successively depressurized, the black solutions transferred into a round bottom flask and concentrated to dryness, obtaining **22** and **23** as black solids. Pd content (ICP-OES): 1.1wt% (**22**) and 0.51wt% (**23**).

2.2.26 Pd(0)@[2L4 + 2(HL4) (OAc)] (24) stabilized Pd-nanoparticles

24 was obtained by dissolving **20** (400.0 mg, 0.037 mmol) in deareated CH₂Cl₂ (30.0 mL) at room temperature. Afterwards **L4** (392.8 mg, 0.074 mmol) was added to the latter solution, which was transferred into a stainless steel autoclave (70.0 mL) and pressurized with dihydrogen (15 bar). The following steps were the same as described for the syntheses of **22** and **23**. Pd content (ICP-OES): 1.2wt%.

2.2.27 Pd(0)@4L5 (25) stabilized Pd-nanoparticles

25 was obtained by dissolving **L5** (400.0 mg, 0.075 mmol) and Pd(OAc)₂ (4.3 mg, 0.019 mmol) in deareated CH₂Cl₂ (30.0 mL) at room temperature. The obtained yellow solution was stirred for half an hour and then transferred into a stainless steel autoclave (70 mL), where it was pressurized with dihydrogen (15 bar). The following steps were the same as described for the syntheses of **22** and **23**. Pd content (ICP-OES): 1.1wt%.

2.2.28 Mesylation of poly(ethylene glycol) monomethyl ether

Commercially available poly(ethylene glycol) monomethyl ether (10 g; 2 mmol ; MW = 5000 g/mol) was dried under vacuum at 70 °C for 1 hour and then dissolved under N₂ flux in CH₂Cl₂ (100 mL) in a 250 mL round-bottom flask, with magnetic stirring. Trioctyl amine (1.74 mL; 4 mmol) was added at room temperature, then the flask was cooled to 0 °C and mesyl chloride was added dropwise. After 10 minutes, the reaction mixture (transparent, colorless) was brought back to room temperature and left under continuous stirring overnight. After 20 hours the volume was reduced under vacuum to approx. 50 mL and excess Na₂CO₃ (1.5 g) was added to neutralize the ammonium chloride and enhance purification. After 4 hours (most part of the carbonate is still a white powder suspended in CH₂Cl₂) the mixture was filtered through sand and cooled to 0 °C, then cold Et₂O (100 mL) was added to precipitate the mesylated PEG as a white, finely dispersed solid. The product was recovered by Buchner filtration, washed with cold Et₂O (approx. 50 mL) and dried under vacuum overnight at room temperature to obtain a white powder. Yield: 8.82 g (83%); Mn (NMR): 5200 g/mol;

2.3 Instruments and characterization

2.3.1 ^1H , $^{13}\text{C}\{^1\text{H}\}$ and $^{31}\text{P}\{^1\text{H}\}$ NMR spectroscopy

NMR spectra were obtained with a Bruker Avance DRX-400 spectrometer acquiring spectra at 400.13 and 100.62 MHz, respectively. NMR spectra of samples **L4**, **L5**, **L10**, **L11**, **20** and **21** were obtained with a Bruker Avance DPX 300 spectrometer at 300.13 MHz and 75.47 MHz, for ^1H and ^{13}C respectively. Chemical shifts are reported in ppm (δ) with reference to TMS as an external standard. CD_2Cl_2 used for NMR experiments was purchased from Aldrich in 0.5 ml sealed glass ampules.

NMR yields for cyanation reactions were calculated from ^1H NMR analyses carried out with a Bruker Avance AM 300 MHz spectrometer in CDCl_3 . Spectra are reported in ppm with reference to TMS as an external standard using residual hydrogen of solvent as an internal reference.

2.3.1.1 NMR spectroscopic data for L1

^1H NMR (400.13 MHz, CD_2Cl_2 , 21 °C, ppm): 1.49 (d, $J = 6.8$ Hz, 3H, $\text{CH}(\text{CH}_3)\text{OH}$), 1.59 (d, $J = 6.8$ Hz, 199H, $\text{OCCH}(\text{CH}_3)\text{O}$), 4.36 (q, $J = 6.8$ Hz, 1H, $\text{CH}(\text{CH}_3)\text{OH}$), 5.20 (q, $J = 6.8$ Hz, 56H, $\text{OCCH}(\text{CH}_3)\text{O} + \text{PyCH}_2\text{O}$), 7.27 (d, $J = 6.0$ Hz, 2H, *m*-Ar-*H*), 8.62 (d, $J = 6.0$ Hz, 2H, *o*-Ar-*H*).

$^{13}\text{C}\{^1\text{H}\}$ NMR (100.62 MHz, CD_2Cl_2 , 21 °C, ppm): 16.46 (s, $\text{OCCH}(\text{CH}_3)\text{O}$), 20.29 (s, $\text{CH}(\text{CH}_3)\text{OH}$), 64.97 (s, PyCH_2O), 66.65 (s, $\text{CH}(\text{CH}_3)\text{OH}$), 68.99 (s, $\text{OCCH}(\text{CH}_3)\text{O}$), 121.84 (s, *m*-Ar-*C*), 144.67 (s, *p*-Ar-*C*), 149.61 (s, *o*-Ar-*C*), 169.49 (s, $\text{OCCH}(\text{CH}_3)\text{O}$), 174.99 (s, $\text{OCCH}(\text{CH}_3)\text{OH}$).

2.3.1.2 NMR spectroscopic data for L2

^1H NMR (400.13 MHz, CD_2Cl_2 , 21 °C, ppm): 1.47 (m, 3H, $\text{CH}(\text{CH}_3)\text{OH}$), 1.59 (br d, $J = 6.8$ Hz, 147H, $\text{OCCH}(\text{CH}_3)\text{O}$), 4.38 (br q, 1H, $\text{CH}(\text{CH}_3)\text{OH}$), 5.21 (q, $J = 6.8$ Hz, 45H, $\text{OCCH}(\text{CH}_3)\text{O} + \text{PyCH}_2\text{O}$), 7.28 (d, $J = 5.6$ Hz, 2H, *m*-Ar-*H*), 8.62 (d, $J = 5.6$ Hz, 2H *o*-Ar-*H*).

$^{13}\text{C}\{^1\text{H}\}$ NMR (100.62 MHz, CD_2Cl_2 , 21 °C, ppm): 16.46 (s, $\text{OCCH}(\text{CH}_3)\text{O}$), 20.29 (s, $\text{CH}(\text{CH}_3)\text{OH}$), 65.00 (s, PyCH_2O), 66.64 (s, $\text{CH}(\text{CH}_3)\text{OH}$), 68.99 (s, $\text{OCCH}(\text{CH}_3)\text{O}$), 121.75 (s, *m*-Ar-*C*), 144.36 (s, *p*-Ar-*C*), 149.89 (s, *o*-Ar-*C*), 169.25 and 169.31 (s, $\text{OCCH}(\text{CH}_3)\text{O}$), 174.95 (s, $\text{OCCH}(\text{CH}_3)\text{OH}$).

2.3.1.3 NMR spectroscopic data for L3

^1H NMR (400.13 MHz, CD_2Cl_2 , 21 °C, ppm): 1.41 (m, 86H,

(C(O)CH₂CH₂CH₂CH₂CH₂O)_n + (C(O)CH₂CH₂CH₂CH₂CH₂OH), 1.67 (m, 180H, (C(O)CH₂CH₂CH₂CH₂CH₂O)_n + (C(O)CH₂CH₂CH₂CH₂CH₂OH), 2.32 (t, *J* = 7.6 Hz, 86H, (C(O)CH₂CH₂CH₂CH₂CH₂O)_n, 2.45 (t, *J* = 7.6 Hz, 2H, (C(O)CH₂CH₂CH₂CH₂CH₂OH), 3.61 (t, *J* = 6.4 Hz, 2H, C(O)CH₂CH₂CH₂CH₂CH₂OH), 4.06 (t, *J* = 6.8 Hz, 86H, (C(O)CH₂CH₂CH₂CH₂CH₂O)_n), 5.19 (s, 2H, PyCH₂O), 7.28 (d, *J* = 6.4 Hz, 2H, *m*-Ar-*H*), 8.59 (d, *J* = 6.4 Hz, 4H, *o*-Ar-*H*).

¹³C{¹H} NMR (100.62 MHz, CD₂Cl₂, 21 °C, ppm): 24.6 (s, (C(O)CH₂CH₂CH₂CH₂CH₂O)_n + (C(O)CH₂CH₂CH₂CH₂CH₂OH), 25.5 (s, (C(O)CH₂CH₂CH₂CH₂CH₂O)_n + (C(O)CH₂CH₂CH₂CH₂CH₂OH), 28.3 (s, (C(O)CH₂CH₂CH₂CH₂CH₂O)_n + (C(O)CH₂CH₂CH₂CH₂CH₂OH), 32.4 (s, (C(O)CH₂CH₂CH₂CH₂CH₂OH), 34.0 (s, (C(O)CH₂CH₂CH₂CH₂CH₂O)_n), 62.3 (s, (C(O)CH₂CH₂CH₂CH₂CH₂OH), 64.0 (s, (C(O)CH₂CH₂CH₂CH₂CH₂O)_n + PyCH₂OH), 121.7 (s, *m*-Ar-*C*), 149.9 (s, *o*-Ar-*C*), 172.8 (s, C(O)CH₂CH₂CH₂CH₂CH₂OH), 173.3 (s, C(O)CH₂CH₂CH₂CH₂CH₂O)_n).

2.3.1.4 NMR spectroscopic data for L4

¹H NMR (300.13 MHz, DMSO-d₆, 21 °C, ppm): 3.36 (s, 3H, CH₂CH₂OCH₃), 3.62 (s, 464H, CH₂CH₂O), 4.59 (s, 2H, PyCH₂OCH₂CH₂), 7.29 (d, *J* = 5.6 Hz, 2H, *m*-Ar-*H*), 8.56 (d, *J* = 5.6 Hz, 2H, *o*-Ar-*H*). ¹H NMR (300.13 MHz, CD₂Cl₂, 21 °C, ppm): 3.36 (s, 3H, CH₂CH₂OCH₃), 3.62 (s, 601H, CH₂CH₂O), 4.59 (s, 2H, PyCH₂OCH₂CH₂), 7.29 (d, *J* = 5.6 Hz, 2H, *m*-Ar-*H*), 8.55 (d, *J* = 5.6 Hz, 2H, *o*-Ar-*H*).

¹³C{¹H} NMR (75.47 MHz, CD₂Cl₂, 21 °C, ppm): 58.6 (s, CH₂CH₂OCH₃), 70.5 (s, CH₂CH₂O), 71.9 (s, PyCH₂OCH₂CH₂), 121.7 (s, *m*-Ar-*C*), 147.2 (s, *p*-Ar-*C*), 149.7 (s, *o*-Ar-*C*).

2.3.1.5 NMR spectroscopic data for (HL4)(OTs)

¹H NMR (300.13 MHz, CD₂Cl₂, 21 °C, ppm): 2.39 (s, 3H, CH₃(OTs)), 3.34 (s, 3H, CH₂CH₂OCH₃), 3.61 (s, 464H, CH₂CH₂O), 4.89 (s, 2H, HyCH₂OCH₂CH₂), 7.21 (d, *J* = 8.1 Hz, 2H, *m*-Ar-*H*(OTs)), 7.74 (d, *J* = 8.1 Hz, 2H, *o*-Ar-*H*(OTs)), 7.97 (d, *J* = 6.3 Hz, 2H, *m*-Ar-*H*), 8.56 (d, *J* = 5.6 Hz, 2H, *o*-Ar-*H*).

¹³C{¹H} NMR (75.47 MHz, CD₂Cl₂, 21 °C, ppm): 21.0 (s, CH₃(OTs)), 58.6 (s, CH₂CH₂OCH₃), 70.5 (s, CH₂CH₂O), 71.9 (s, PyCH₂OCH₂CH₂), 124.1 (s, *m*-Ar-*C*), 125.9 (s, *o*-Ar-*C*(OTs)), 128.8 (s, *m*-Ar-*C*(OTs)), 140.4 (s, Ar-*C*(OTs)), 141.4 (s, *o*-Ar-*C*), 142.0 (s, *ipso*-Ar-*C*), 160.4 (s, Ar-*C*(OTs)).

2.3.1.6 NMR spectroscopic data for L5

^1H NMR (300.13 MHz, CD_2Cl_2 , 21 °C, ppm): 3.36 (s, 3H, $\text{CH}_2\text{CH}_2\text{OCH}_3$), 3.62 (s, 464H, $\text{CH}_2\text{CH}_2\text{O}$), 4.55 (s, 2H, $\text{PhCH}_2\text{OCH}_2\text{CH}_2$), 7.31 (m, 5H, Ar-H).

$^{13}\text{C}\{^1\text{H}\}$ NMR (75.47 MHz, CD_2Cl_2 , 21 °C, ppm): 58.6 (s, $\text{CH}_2\text{CH}_2\text{OCH}_3$), 70.5 (s, $\text{CH}_2\text{CH}_2\text{O}$), 73.0 (s, $\text{PhCH}_2\text{OCH}_2\text{CH}_2$), 127.4 (s, *p*-Ar-C), 147.7 (s, *m*-Ar-C), 128.2 (s, *o*-Ar-C).

2.3.1.7 NMR spectroscopic data for L6

^1H NMR (400.13 MHz, CD_2Cl_2 , 21 °C, ppm): 1.49 (d, $J = 6.8$ Hz, 3H, $\text{CH}(\text{CH}_3)\text{OH}$), 1.59 (d, $J = 6.8$ Hz, 189H, $\text{OCCH}(\text{CH}_3)\text{O}$), 4.36 (q, $J = 6.8$ Hz, 1H, $\text{CH}(\text{CH}_3)\text{OH}$), 5.20 (q, $J = 6.8$ Hz, 62H, $\text{OCCH}(\text{CH}_3)\text{O} + \text{PyCH}_2\text{O}$), 7.30 (d, $J = 6.0$ Hz, 2H, *m*-Ar-H), 8.62 (d, $J = 6.0$ Hz, 2H, *o*-Ar-H).

$^{13}\text{C}\{^1\text{H}\}$ NMR (100.62 MHz, CD_2Cl_2 , 21 °C, ppm): 16.47 (s, $\text{OCCH}(\text{CH}_3)\text{O}$), 20.29 (s, $\text{CH}(\text{CH}_3)\text{OH}$), 64.94 (s, PyCH_2O), 66.65 (s, $\text{CH}(\text{CH}_3)\text{OH}$), 68.99 (s, $\text{OCCH}(\text{CH}_3)\text{O}$), 121.90 (s, *m*-Ar-C), 144.88 (s, *p*-Ar-C), 149.45 (s, *o*-Ar-C), 169.49 (s, $\text{OCCH}(\text{CH}_3)\text{O}$), 175.00 (s, $\text{OCCH}(\text{CH}_3)\text{OH}$).

2.3.1.8 NMR spectroscopic data for L7

^1H NMR (400.13 MHz, CD_2Cl_2 , 21 °C, ppm): 1.49 (d, $J = 6.8$ Hz, 3H, $\text{CH}(\text{CH}_3)\text{OH}$), 1.59 (d, $J = 6.8$ Hz, 189H, $\text{OCCH}(\text{CH}_3)\text{O}$), 4.36 (q, $J = 6.8$ Hz, 1H, $\text{CH}(\text{CH}_3)\text{OH}$), 5.20 (q, $J = 6.8$ Hz, 62H, $\text{OCCH}(\text{CH}_3)\text{O} + \text{PyCH}_2\text{O}$), 7.30 (d, $J = 6.0$ Hz, 2H, *m*-Ar-H), 8.62 (d, $J = 6.0$ Hz, 2H, *o*-Ar-H).

$^{13}\text{C}\{^1\text{H}\}$ NMR (100.62 MHz, CD_2Cl_2 , 21 °C, ppm): 16.47 (s, $\text{OCCH}(\text{CH}_3)\text{O}$), 20.29 (s, $\text{CH}(\text{CH}_3)\text{OH}$), 64.97 (s, PyCH_2O), 66.65 (s, $\text{CH}(\text{CH}_3)\text{OH}$), 69.00 (s, $\text{OCCH}(\text{CH}_3)\text{O}$), 121.84 (s, *m*-Ar-C), 144.68 (s, *p*-Ar-C), 149.61 (s, *o*-Ar-C), 169.49 (s, $\text{OCCH}(\text{CH}_3)\text{O}$), 175.00 (s, $\text{OCCH}(\text{CH}_3)\text{OH}$).

2.3.1.9 NMR spectroscopic data for L8

^1H NMR (400.13 MHz, CD_2Cl_2 , 21 °C, ppm): 1.49 (d, $J = 6.8$ Hz, 3H, $\text{CH}(\text{CH}_3)\text{OH}$), 1.59 (d, $J = 6.8$ Hz, 436H, $\text{OCCH}(\text{CH}_3)\text{O}$), 4.36 (q, $J = 6.8$ Hz, 1H, $\text{CH}(\text{CH}_3)\text{OH}$), 5.20 (q, $J = 6.8$ Hz, 145H, $\text{OCCH}(\text{CH}_3)\text{O} + \text{PyCH}_2\text{O}$), 7.30 (d, $J = 6.0$ Hz, 2H, *m*-Ar-H), 8.62 (d, $J = 6.0$ Hz, 2H, *o*-Ar-H).

$^{13}\text{C}\{^1\text{H}\}$ NMR (100.62 MHz, CD_2Cl_2 , 21 °C, ppm): 16.47 (s, $\text{OCCH}(\text{CH}_3)\text{O}$), 20.29 (s, $\text{CH}(\text{CH}_3)\text{OH}$), 64.90 (s, PyCH_2O), 66.65 (s, $\text{CH}(\text{CH}_3)\text{OH}$), 69.00 (s, $\text{OCCH}(\text{CH}_3)\text{O}$), 121.95 (s, *m*-Ar-C), 144.60 (s, *p*-Ar-C), 149.32 (s, *o*-Ar-C), 169.48 (s, $\text{OCCH}(\text{CH}_3)\text{O}$), 174.98 (s, $\text{OCCH}(\text{CH}_3)\text{OH}$).

2.3.1.10 NMR spectroscopic data for L9

^1H NMR (400.13 MHz, CD_2Cl_2 , 21 °C, ppm): 1.49 (d, $J = 6.8$ Hz, 3H, $\text{CH}(\text{CH}_3)\text{OH}$), 1.59 (d, $J = 6.8$ Hz, 447H, $\text{OCCH}(\text{CH}_3)\text{O}$), 4.36 (q, $J = 6.8$ Hz, 1H, $\text{CH}(\text{CH}_3)\text{OH}$), 5.20 (q, $J = 6.8$ Hz, 149H, $\text{OCCH}(\text{CH}_3)\text{O} + \text{PyCH}_2\text{O}$), 7.30 (d, $J = 6.0$ Hz, 2H, *m*-Ar-*H*), 8.62 (d, $J = 6.0$ Hz, 2H, *o*-Ar-*H*).

$^{13}\text{C}\{^1\text{H}\}$ NMR (100.62 MHz, CD_2Cl_2 , 21 °C, ppm): 16.46 (s, $\text{OCCH}(\text{CH}_3)\text{O}$), 20.28 (s, $\text{CH}(\text{CH}_3)\text{OH}$), 64.90 (s, PyCH_2O), 66.65 (s, $\text{CH}(\text{CH}_3)\text{OH}$), 69.00 (s, $\text{OCCH}(\text{CH}_3)\text{O}$), 121.95 (s, *m*-Ar-*C*), 144.65 (s, *p*-Ar-*C*), 149.30 (s, *o*-Ar-*C*), 169.46 (s, $\text{OCCH}(\text{CH}_3)\text{O}$), 174.97 (s, $\text{OCCH}(\text{CH}_3)\text{OH}$).

2.3.1.11 NMR spectroscopic data for L10

^1H NMR (300.13 MHz, CD_2Cl_2 , 21 °C, ppm): 1.59 (d, $J = 6.8$ Hz, 235H, $\text{OCCH}(\text{CH}_3)\text{O} + \text{NHCH}_2(\text{CH}_2)_4\text{CH}_2\text{NH}$), 3.15 (m, 4H, $\text{NHCH}_2(\text{CH}_2)_4\text{CH}_2\text{NH}$), 5.20 (q, $J = 6.8$ Hz, 77H, $\text{OCCH}(\text{CH}_3)\text{O} + \text{PyCH}_2\text{O}$), 7.28 (d, $J = 6.0$ Hz, 2H, *m*-Ar-*H*), 8.62 (d, $J = 6.0$ Hz, 2H, *o*-Ar-*H*).

2.3.1.12 NMR spectroscopic data for L11

^1H NMR (300.13 MHz, CD_2Cl_2 , 21 °C, ppm): 2.41 (m, 2H, $\text{OCH}_2\text{CH}_2\text{P}$), 3.36 (s, 3H, $\text{CH}_2\text{CH}_2\text{OCH}_3$), 3.62 (s, 466H, $\text{CH}_2\text{CH}_2\text{O} + \text{OCH}_2\text{CH}_2\text{P}$), 3.80 (s, 6H, PhOCH_3), 6.92 (m, 4H, $\text{Ar-}H^2 + \text{Ar-}H^5$), 7.14 (m, 2H, $\text{Ar-}H^4$), 6.92 (t, $J = 3.5$ Hz, 2H, $\text{Ar-}H^3$).

$^{13}\text{C}\{^1\text{H}\}$ NMR (75.47 MHz, CD_2Cl_2 , 21 °C, ppm): 55.5 (s, $\text{C}_6\text{H}_4\text{OCH}_3$), 58.6 (s, $\text{CH}_2\text{CH}_2\text{OCH}_3$), 69.0 (d, $J = 26.3$ Hz, $\text{CH}_2\text{CH}_2\text{P}(\text{C}_6\text{H}_4\text{OCH}_3)_2$), 70.5 (s, $\text{CH}_2\text{CH}_2\text{O}$), 98.1 (s, $\text{Ar-}C^1$), 110.3 (s, $\text{Ar-}C^5$), 120.8 (s, $\text{Ar-}C^3$), 130.0 (s, $\text{Ar-}C^4$), 132.7 (s, $\text{Ar-}C^2$), 161.3 (d, $J = 13.1$ Hz, $\text{Ar-}C^6$). $^{31}\text{P}\{^1\text{H}\}$ NMR (121.5 MHz, CD_2Cl_2 , 21 °C, ppm): -40.73 (s, $\text{CH}_2\text{CH}_2\text{P}(\text{C}_6\text{H}_4\text{OCH}_3)_2$).

2.3.1.13 NMR spectroscopic data for 1 and 2

NMR signals assigned to the PLA chain did not show any significant variation upon macrocomplex formation and are hence not reported for the macrocomplexes **1-9** and **16**.

^1H NMR (400.13 MHz, CD_2Cl_2 , 21 °C, ppm): 7.34 (d, $J = 6.8$ Hz, 4H, *m*-Ar-*H*), 8.84 (d, $J = 6.8$ Hz, 4H, *o*-Ar-*H*). $^{13}\text{C}\{^1\text{H}\}$ NMR (100.62 MHz, CD_2Cl_2 , 21 °C, ppm): 122.61 (s, *m*-Ar-*C*), 147.96 (s, *p*-Ar-*C*), 153.25 (s, *o*-Ar-*C*).

2.3.1.14 NMR spectroscopic data for 3

NMR signals assigned to the PLA chain did not show any significant variation upon

macrocomplex formation and are hence not reported for the macrocomplexes **1-9** and **16**.

^1H NMR (400.13 MHz, CD_2Cl_2 , 21 °C, ppm): 3.15 (br s, 2H, allyl(CH_2)), 4.02 (d, $J = 6.8$ Hz, 2H, allyl(CH_2)), 5.68 (m, 1H, allyl(CH)), 7.37 (d, $J = 5.6$ Hz, 2H, *m*-Ar-*H*), 8.80 (br s, 2H, *o*-Ar-*H*). ^1H NMR (400.13 MHz, CD_2Cl_2 , -60 °C, ppm): 2.99 (d, $J = 12.4$ Hz, 1H, allyl(CH_2)), 3.23 (d, $J = 12.4$ Hz, 1H, allyl(CH_2)), 3.97 (d, $J = 6.4$ Hz, 1H, allyl(CH_2)), 4.02 (d, $J = 6.4$ Hz, 1H, allyl(CH_2)), 5.68 (m, 1H, allyl(CH)), 7.37 (d, $J = 5.6$ Hz, 2H, *m*-Ar-*H*), 8.76 (d, $J = 5.6$ Hz, 2H, *o*-Ar-*H*).

$^{13}\text{C}\{^1\text{H}\}$ NMR (100.62 MHz, CD_2Cl_2 , -60 °C): 58.20 (s, allyl(CH_2)), 64.49 (s, allyl(CH_2)), 115.05 (s, allyl(CH)), 122.62 (s, *m*-Ar-*C*), 146.99 (s, *p*-Ar-*C*), 153.02 (s, *o*-Ar-*C*).

2.3.1.15 NMR spectroscopic data for 4

NMR signals assigned to the PLA chain did not show any significant variation upon macrocomplex formation and are hence not reported for the macrocomplexes **1-9** and **16**.

^1H NMR (400.13 MHz, CD_2Cl_2 , 21 °C, ppm): 3.32 (d, $J = 12.4$ Hz, 2H, allyl(CH_2)), 4.13 (d, $J = 6.8$ Hz, 2H, allyl(CH_2)), 5.93 (m, 1H, allyl(CH)), 7.45 (d, $J = 5.6$ Hz, 4H, *m*-Ar-*H*(Py)), 7.59 (s, 4H, *p*-Ar-*H*(BAr'₄)), 7.75 (s, 8H, *o*-Ar-*H*(BAr'₄)), 8.48 (br s, 4H, *o*-Ar-*H*(Py)).

$^{13}\text{C}\{^1\text{H}\}$ NMR (100.62 MHz, CD_2Cl_2 , 21 °C, ppm): 63.04 (s, allyl(CH_2)), 117.45 (s, *p*-Ar-*C*(BAr'₄)), 120.51 (s, allyl(CH)), 123.41 (s, *m*-Ar-*C*(Py)), 124.54 (q, $J = 272.5$ Hz, CF_3), 129.99 (q, $J = 38.7$ Hz, *m*-Ar-*C*(BAr'₄)), 134.77 (s, *o*-Ar-*C*(BAr'₄)), 148.71 (br s, *p*-Ar-*C*(Py)), 150.59 (s, *o*-Ar-*C*(Py)), 161.62 (m, *ipso*-Ar-*C*(BAr'))).

2.3.1.16 NMR spectroscopic data for 5

NMR signals assigned to the PLA chain did not show any significant variation upon macrocomplex formation and are hence not reported for the macrocomplexes **1-9** and **16**.

^1H NMR (400.13 MHz, CD_2Cl_2 , 21 °C, ppm): 3.30 (d, $J = 12.2$ Hz, 2H, allyl(CH_2)), 4.11 (d, $J = 6.8$ Hz, 2H, allyl(CH_2)), 5.89 (m, 1H, allyl(CH)), 7.42 (d, $J = 5.6$ Hz, 4H, *m*-Ar-*H*(Py)), 7.59 (s, 4H, *p*-Ar-*H*(BAr'₄)), 7.75 (s, 8H, *o*-Ar-*H*(BAr'₄)), 8.51 (br s, 4H, *o*-Ar-*H*(Py)). ^1H NMR (400.13 MHz, CD_2Cl_2 , -60 °C, ppm): 3.28 (d, $J = 12.0$ Hz, 4H, allyl(CH_2)), 4.08 d, $J = 6.4$ Hz, 4H, allyl(CH_2)), 5.88 (m, 1H, allyl(CH)), 7.42 (d, $J = 5.6$ Hz, 4H, *m*-Ar-*H*(Py)), 7.57 (s, 4H, *p*-Ar-*H*(BAr'₄)), 7.75 (s, 8 H, *o*-Ar-*H*(BAr'₄)), 8.33

(br. s, 4H, *o*-Ar-*H*(Py)).

$^{13}\text{C}\{^1\text{H}\}$ NMR (100.62 MHz, CD_2Cl_2 , $-60\text{ }^\circ\text{C}$, ppm): 63.11 (s, allyl(CH_2)), 117.64 (s, *p*-Ar-C(BAr'_4)), 120.12 (s, allyl(CH)), 123.47 (s, *m*-Ar-C(Py)), 124.50 (q, $J = 272.5\text{ Hz}$, CF_3), 128.54 (q, $J = 38.7\text{ Hz}$, *m*-Ar-C(BAr'_4)), 134.69 (s, *o*-Ar-C(BAr'_4)), 149.10 (br. s, *p*-Ar-C(Py)), 151.69 (s, *o*-Ar-C(Py)), 161.43 (m, *ipso*-Ar-C(BAr')).

2.3.1.17 NMR spectroscopic data for 6 – 8

NMR signals assigned to the PLA chain did not show any significant variation upon macrocomplex formation and are hence not reported for the macrocomplexes **1-9** and **16**.

^1H NMR (400.13 MHz, CD_2Cl_2 , $21\text{ }^\circ\text{C}$, ppm): 7.49 (d, $J = 6.4\text{ Hz}$, 8H, *m*-Ar-*H*), 8.88 (d, $J = 6.4\text{ Hz}$, 8H, *o*-Ar-*H*).

$^{13}\text{C}\{^1\text{H}\}$ NMR (100.62 MHz, CD_2Cl_2 , $21\text{ }^\circ\text{C}$, ppm): δ 124.85 (s, *m*-Ar-C), 150.76 (s, *p*-Ar-C), 150.99 (s, *o*-Ar-C).

2.3.1.18 NMR spectroscopic data for 9

NMR signals assigned to the PLA chain did not show any significant variation upon macrocomplex formation and are hence not reported for the macrocomplexes **1-9** and **16**.

^1H NMR (400.13 MHz, CD_2Cl_2 , $21\text{ }^\circ\text{C}$, ppm): 2.42 (s, 6H, $\text{CH}_3\text{C}_6\text{H}_4\text{SO}_3^-$), 7.32 (m, 12H, *m*-Ar-*H*(Py) + Ar-*H*(OTs)), 7.97 (d, $J = 8.0\text{ Hz}$, 4H, Ar-*H*(OTs)), 9.76 (d, $J = 5.6\text{ Hz}$, 8H, *o*-Ar-*H*(Py)).

$^{13}\text{C}\{^1\text{H}\}$ NMR (100.62 MHz, CD_2Cl_2 , $21\text{ }^\circ\text{C}$, ppm): 21.05 (s, CH_3), 123.90 (s, *m*-Ar-C(Py)), 125.94 (s, Ar-C(OTs)), 128.83 (s, Ar-C(OTs)), 139.73 (s, Ar-C(OTs)), 144.67 (s, Ar-C(OTs)), 148.76 (s, *p*-Ar-C(Py)), 152.42 (s, *o*-Ar-C(Py)).

2.3.1.19 NMR spectroscopic data for 10

^1H NMR (400.13 MHz, CD_2Cl_2 , $21\text{ }^\circ\text{C}$, ppm): 1.28 (t, $J = 8.0\text{ Hz}$, 6H, CH_3), 2.74 (q, $J = 8.0\text{ Hz}$, 4H, CH_2), 7.23 (d, $J = 6.0\text{ Hz}$, 4H, *m*-Ar-*H*), 8.67 (d, $J = 6.0\text{ Hz}$, 4H, *o*-Ar-*H*).

$^{13}\text{C}\{^1\text{H}\}$ NMR (100.62 MHz, CD_2Cl_2 , $21\text{ }^\circ\text{C}$, ppm): 13.65 (s, CH_3), 28.05 (s, CH_2), 124.57 (s, *m*-Ar-C), 152.54 (s, *o*-Ar-C), 156.77 (s, *p*-Ar-C).

2.3.1.20 NMR spectroscopic data for 11

^1H NMR (400.13 MHz, CD_2Cl_2 , $21\text{ }^\circ\text{C}$, ppm): 1.41 (m, 96H, $(\text{C}(\text{O})\text{CH}_2\text{CH}_2\text{CH}_2\text{CH}_2\text{CH}_2\text{O})_n + \text{C}(\text{O})\text{CH}_2\text{CH}_2\text{CH}_2\text{CH}_2\text{CH}_2\text{OH}$), 1.66 (m, 192H,

(C(O)CH₂CH₂CH₂CH₂CH₂O)_n + C(O)CH₂CH₂CH₂CH₂CH₂OH), 2.32 (t, *J* = 7.6 Hz, 94H, (C(O)CH₂CH₂CH₂CH₂CH₂O)_n, 2.45 (t, *J* = 7.6 Hz, 4H, C(O)CH₂CH₂CH₂CH₂CH₂OH), 3.61 (t, *J* = 6.4 Hz, 2H, C(O)CH₂CH₂CH₂CH₂CH₂OH), 4.06 (t, *J* = 6.8 Hz, 94H, (C(O)CH₂CH₂CH₂CH₂CH₂O)_n), 5.35 (s, 4H, PyCH₂O), 7.35 (d, *J* = 6.4 Hz, 2H, *m*-Ar-*H*), 8.81 (d, *J* = 6.4 Hz, 4H, *o*-Ar-*H*).

¹³C{¹H} NMR (100.62 MHz, CD₂Cl₂, 21 °C, ppm): 24.7 (s, (C(O)CH₂CH₂CH₂CH₂CH₂O)_n + C(O)CH₂CH₂CH₂CH₂CH₂OH), 25.4 (s, (C(O)CH₂CH₂CH₂CH₂CH₂O)_n + C(O)CH₂CH₂CH₂CH₂CH₂OH), 28.3 (s, (C(O)CH₂CH₂CH₂CH₂CH₂O)_n + C(O)CH₂CH₂CH₂CH₂CH₂OH), 32.4 (s, C(O)CH₂CH₂CH₂CH₂CH₂OH), 34.0 (s, (C(O)CH₂CH₂CH₂CH₂CH₂O)_n), 62.3 (s, PyCH₂OH), 63.1 (s, C(O)CH₂CH₂CH₂CH₂CH₂OH), 64.0 (s, (C(O)CH₂CH₂CH₂CH₂CH₂O)_n), 122.7 (s, *m*-Ar-*C*), 148.9 (s, *p*-Ar-*C*), 153.1 (s, *o*-Ar-*C*), 172.6 (s, C(O)CH₂CH₂CH₂CH₂CH₂OH), 173.3 (s, (C(O)CH₂CH₂CH₂CH₂CH₂O)_n).

2.3.1.21 NMR spectroscopic data for 12

¹H NMR (400.13 MHz, CD₂Cl₂, 21 °C, ppm): 1.41 (m, 65H, (C(O)CH₂CH₂CH₂CH₂CH₂O)_n + C(O)CH₂CH₂CH₂CH₂CH₂OH), 1.66 (m, 130H, (C(O)CH₂CH₂CH₂CH₂CH₂O)_n + C(O)CH₂CH₂CH₂CH₂CH₂OH), 2.32 (t, *J* = 7.6 Hz, 65H, (C(O)CH₂CH₂CH₂CH₂CH₂O)_n, 2.45 (t, *J* = 7.6 Hz, 4H, C(O)CH₂CH₂CH₂CH₂CH₂OH), 3.63 (t, *J* = 6.4 Hz, 2H, C(O)CH₂CH₂CH₂CH₂CH₂OH), 4.07 (t, *J* = 6.8 Hz, 94H, (C(O)CH₂CH₂CH₂CH₂CH₂O)_n), 5.15 (s, 2H, PyCH₂O), 7.48 (d, *J* = 6.4 Hz, 2H, *m*-Ar-*H*), 8.88 (d, *J* = 6.4 Hz, 4H, *o*-Ar-*H*).

¹³C{¹H} NMR (100.62 MHz, CD₂Cl₂, 21 °C, ppm): 24.5 (s, (C(O)CH₂CH₂CH₂CH₂CH₂O)_n + C(O)CH₂CH₂CH₂CH₂CH₂OH), 25.4 (s, (C(O)CH₂CH₂CH₂CH₂CH₂O)_n + C(O)CH₂CH₂CH₂CH₂CH₂OH), 28.3 (s, (C(O)CH₂CH₂CH₂CH₂CH₂O)_n + C(O)CH₂CH₂CH₂CH₂CH₂OH), 32.4 (s, C(O)CH₂CH₂CH₂CH₂CH₂OH), 34.0 (s, (C(O)CH₂CH₂CH₂CH₂CH₂O)_n), 62.5 (s, C(O)CH₂CH₂CH₂CH₂CH₂OH), 63.5 (s, (C(O)CH₂CH₂CH₂CH₂CH₂O)_n + PyCH₂OH), 124.9 (s, *m*-Ar-*C*), 151.8 (s, *p*-Ar-*C*), 151.0 (s, *o*-Ar-*C*), 172.5 (s, C(O)CH₂CH₂CH₂CH₂CH₂OH), 173.3 (s, (C(O)CH₂CH₂CH₂CH₂CH₂O)_n).

2.3.1.22 NMR spectroscopic data for 13

¹H NMR (400.13 MHz, CD₂Cl₂, 21 °C, ppm): 1.41 (m, CH(CH₃)OH + (C(O)CH₂CH₂CH₂CH₂CH₂O)_n + C(O)CH₂CH₂CH₂CH₂CH₂OH), 1.65 (m, (OCCH(CH₃)O)_n + (C(O)CH₂CH₂CH₂CH₂CH₂O)_n + C(O)CH₂CH₂CH₂CH₂CH₂OH),

2.32 (t, $J = 7.6$ Hz, 94H, $(\text{C}(\text{O})\text{CH}_2\text{CH}_2\text{CH}_2\text{CH}_2\text{CH}_2\text{O})_n$), 2.45 (t, $J = 7.6$ Hz, 4H, $\text{C}(\text{O})\text{CH}_2\text{CH}_2\text{CH}_2\text{CH}_2\text{CH}_2\text{OH}$), 3.63 (t, $J = 6.4$ Hz, 2H, $\text{C}(\text{O})\text{CH}_2\text{CH}_2\text{CH}_2\text{CH}_2\text{CH}_2\text{OH}$), 4.07 (t, $J = 6.8$ Hz, 94H, $(\text{C}(\text{O})\text{CH}_2\text{CH}_2\text{CH}_2\text{CH}_2\text{CH}_2\text{O})_n$), 4.36 (q, $J = 6.8$ Hz, 1H, $\text{CH}(\text{CH}_3)\text{OH}$), 5.20 (q, $J = 6.8$ Hz, 45H, $(\text{OCCH}(\text{CH}_3)\text{O})_n + \text{PyCH}_2\text{O}$), 7.48 (d, $J = 6.4$ Hz, 2H, *m*-Ar-*H*), 8.88 (d, $J = 6.4$ Hz, 4H, *o*-Ar-*H*).

$^{13}\text{C}\{^1\text{H}\}$ NMR (100.62 MHz, CD_2Cl_2 , 21 °C, ppm): 16.45 (s, $(\text{OCCH}(\text{CH}_3)\text{O})_n$), 20.27 (s, $\text{CH}(\text{CH}_3)\text{OH}$), 24.5 (s, $(\text{C}(\text{O})\text{CH}_2\text{CH}_2\text{CH}_2\text{CH}_2\text{CH}_2\text{O})_n + \text{C}(\text{O})\text{CH}_2\text{CH}_2\text{CH}_2\text{CH}_2\text{CH}_2\text{OH}$), 25.4 (s, $(\text{C}(\text{O})\text{CH}_2\text{CH}_2\text{CH}_2\text{CH}_2\text{CH}_2\text{O})_n + \text{C}(\text{O})\text{CH}_2\text{CH}_2\text{CH}_2\text{CH}_2\text{CH}_2\text{OH}$), 28.3 (s, $(\text{C}(\text{O})\text{CH}_2\text{CH}_2\text{CH}_2\text{CH}_2\text{CH}_2\text{O})_n + \text{C}(\text{O})\text{CH}_2\text{CH}_2\text{CH}_2\text{CH}_2\text{CH}_2\text{OH}$), 32.4 (s, $\text{C}(\text{O})\text{CH}_2\text{CH}_2\text{CH}_2\text{CH}_2\text{CH}_2\text{OH}$), 34.0 (s, $(\text{C}(\text{O})\text{CH}_2\text{CH}_2\text{CH}_2\text{CH}_2\text{CH}_2\text{O})_n$), 62.5 (s, $\text{C}(\text{O})\text{CH}_2\text{CH}_2\text{CH}_2\text{CH}_2\text{CH}_2\text{OH}$), 63.5 (s, $(\text{C}(\text{O})\text{CH}_2\text{CH}_2\text{CH}_2\text{CH}_2\text{CH}_2\text{O})_n + \text{PyCH}_2\text{OH}$), 66.6 (s, $\text{CH}(\text{CH}_3)\text{OH}$), 68.9 (s, $(\text{OCCH}(\text{CH}_3)\text{O})_n$), 124.9 (s, *m*-Ar-*C*), 151.8 (s, *p*-Ar-*C*), 151.0 (s, *o*-Ar-*C*), 169.4 (s, $(\text{OCCH}(\text{CH}_3)\text{O})_n$), 172.5 (s, $\text{C}(\text{O})\text{CH}_2\text{CH}_2\text{CH}_2\text{CH}_2\text{CH}_2\text{OH}$), 173.3 (s, $(\text{C}(\text{O})\text{CH}_2\text{CH}_2\text{CH}_2\text{CH}_2\text{CH}_2\text{O})_n$), 174.9 (s, $\text{OCCH}(\text{CH}_3)\text{OH}$).

2.3.1.23 NMR spectroscopic data for 14

^1H NMR (400.13 MHz, CD_2Cl_2 , 21 °C, ppm): 1.41 (m, 65H, $(\text{C}(\text{O})\text{CH}_2\text{CH}_2\text{CH}_2\text{CH}_2\text{CH}_2\text{O})_n + \text{C}(\text{O})\text{CH}_2\text{CH}_2\text{CH}_2\text{CH}_2\text{CH}_2\text{OH}$), 1.66 (m, 130H, $(\text{C}(\text{O})\text{CH}_2\text{CH}_2\text{CH}_2\text{CH}_2\text{CH}_2\text{O})_n + \text{C}(\text{O})\text{CH}_2\text{CH}_2\text{CH}_2\text{CH}_2\text{CH}_2\text{OH}$), 2.32 (t, $J = 7.6$ Hz, $\text{CH}_3\text{C}_6\text{H}_4\text{SO}_3^- + (\text{C}(\text{O})\text{CH}_2\text{CH}_2\text{CH}_2\text{CH}_2\text{CH}_2\text{O})_n$), 2.45 (t, $J = 7.6$ Hz, 4H, $\text{C}(\text{O})\text{CH}_2\text{CH}_2\text{CH}_2\text{CH}_2\text{CH}_2\text{OH}$), 3.63 (t, $J = 6.4$ Hz, 2H, $\text{C}(\text{O})\text{CH}_2\text{CH}_2\text{CH}_2\text{CH}_2\text{CH}_2\text{OH}$), 4.07 (t, $J = 6.8$ Hz, 65H, $(\text{C}(\text{O})\text{CH}_2\text{CH}_2\text{CH}_2\text{CH}_2\text{CH}_2\text{O})_n$), 5.10 (s, 2H, PyCH_2O), 7.32 (m, 12H, *m*-Ar-*H*(Py) + Ar-*H*(OTs)), 7.96 (sb, 4H, Ar-*H*(OTs)), 9.75 (d, $J = 5.6$ Hz, 8H, *o*-Ar-*H*(Py)).

$^{13}\text{C}\{^1\text{H}\}$ NMR (100.62 MHz, CD_2Cl_2 , 21 °C, ppm): 21.05 (s, $\text{CH}_3\text{C}_6\text{H}_4\text{SO}_3^-$), 24.5 (s, $(\text{C}(\text{O})\text{CH}_2\text{CH}_2\text{CH}_2\text{CH}_2\text{CH}_2\text{O})_n + \text{C}(\text{O})\text{CH}_2\text{CH}_2\text{CH}_2\text{CH}_2\text{CH}_2\text{OH}$), 25.3 (s, $(\text{C}(\text{O})\text{CH}_2\text{CH}_2\text{CH}_2\text{CH}_2\text{CH}_2\text{O})_n + \text{C}(\text{O})\text{CH}_2\text{CH}_2\text{CH}_2\text{CH}_2\text{CH}_2\text{OH}$), 28.3 (s, $(\text{C}(\text{O})\text{CH}_2\text{CH}_2\text{CH}_2\text{CH}_2\text{CH}_2\text{O})_n + \text{C}(\text{O})\text{CH}_2\text{CH}_2\text{CH}_2\text{CH}_2\text{CH}_2\text{OH}$), 32.4 (s, $\text{C}(\text{O})\text{CH}_2\text{CH}_2\text{CH}_2\text{CH}_2\text{CH}_2\text{OH}$), 34.0 (s, $(\text{C}(\text{O})\text{CH}_2\text{CH}_2\text{CH}_2\text{CH}_2\text{CH}_2\text{O})_n$), 62.4 (s, $\text{C}(\text{O})\text{CH}_2\text{CH}_2\text{CH}_2\text{CH}_2\text{CH}_2\text{OH}$), 64.0 (s, $(\text{C}(\text{O})\text{CH}_2\text{CH}_2\text{CH}_2\text{CH}_2\text{CH}_2\text{O})_n + \text{PyCH}_2\text{OH}$), 123.9 (s, *m*-Ar-*C*), 125.9 (s, Ar-*C*(OTs)), 128.8 (s, Ar-*C*(OTs)), 148.7 (s, Ar-*C*(OTs)), 149.9 (s, Ar-*C*(OTs)), 152.2 (s, *p*-Ar-*C*), 152.4 (s, *o*-Ar-*C*), 172.5 (s, $\text{C}(\text{O})\text{CH}_2\text{CH}_2\text{CH}_2\text{CH}_2\text{CH}_2\text{OH}$), 173.3 (s, $(\text{C}(\text{O})\text{CH}_2\text{CH}_2\text{CH}_2\text{CH}_2\text{CH}_2\text{O})_n$).

2.3.1.24 NMR spectroscopic data for 15

^1H NMR (400.13 MHz, CD_2Cl_2 , 21 °C, ppm): 1.41 (m, $\text{CH}(\text{CH}_3)\text{OH}$ + $(\text{C}(\text{O})\text{CH}_2\text{CH}_2\text{CH}_2\text{CH}_2\text{CH}_2\text{O})_n$ + $\text{C}(\text{O})\text{CH}_2\text{CH}_2\text{CH}_2\text{CH}_2\text{CH}_2\text{OH}$), 1.65 (m, $(\text{OCCH}(\text{CH}_3)\text{O})_n$ + $(\text{C}(\text{O})\text{CH}_2\text{CH}_2\text{CH}_2\text{CH}_2\text{CH}_2\text{O})_n$ + $\text{C}(\text{O})\text{CH}_2\text{CH}_2\text{CH}_2\text{CH}_2\text{CH}_2\text{OH}$), 2.32 (t, $J = 7.6$ Hz, $\text{CH}_3\text{C}_6\text{H}_4\text{SO}_3^-$ + $(\text{C}(\text{O})\text{CH}_2\text{CH}_2\text{CH}_2\text{CH}_2\text{CH}_2\text{O})_n$), 2.45 (t, $J = 7.6$ Hz, 4H, $\text{C}(\text{O})\text{CH}_2\text{CH}_2\text{CH}_2\text{CH}_2\text{CH}_2\text{OH}$), 3.61 (t, $J = 6.4$ Hz, 2H, $\text{C}(\text{O})\text{CH}_2\text{CH}_2\text{CH}_2\text{CH}_2\text{CH}_2\text{OH}$), 4.07 (t, $J = 6.8$ Hz, 94H, $(\text{C}(\text{O})\text{CH}_2\text{CH}_2\text{CH}_2\text{CH}_2\text{CH}_2\text{O})_n$), 4.36 (q, $J = 6.8$ Hz, 1H, $\text{CH}(\text{CH}_3)\text{OH}$), 5.10 (s, 8H, PyCH_2O), 5.20 (q, $J = 6.8$ Hz, 45H, $(\text{OCCH}(\text{CH}_3)\text{O})_n$ + PyCH_2O), 7.33 (m, 12H, $m\text{-Ar-H}(\text{Py})$ + $\text{Ar-H}(\text{OTs})$), 7.98 (sb, 4H, $\text{Ar-H}(\text{OTs})$), 9.74 (d, $J = 5.6$ Hz, 8H, $o\text{-Ar-H}(\text{Py})$).

$^{13}\text{C}\{^1\text{H}\}$ NMR (100.62 MHz, CD_2Cl_2 , 21 °C, ppm): 16.4 (s, $(\text{OCCH}(\text{CH}_3)\text{O})_n$), 20.27 (s, $\text{CH}(\text{CH}_3)\text{OH}$), 21.05 (s, $\text{CH}_3\text{C}_6\text{H}_4\text{SO}_3^-$), 24.5 (s, $(\text{C}(\text{O})\text{CH}_2\text{CH}_2\text{CH}_2\text{CH}_2\text{CH}_2\text{O})_n$ + $\text{C}(\text{O})\text{CH}_2\text{CH}_2\text{CH}_2\text{CH}_2\text{CH}_2\text{OH}$), 25.4 (s, $(\text{C}(\text{O})\text{CH}_2\text{CH}_2\text{CH}_2\text{CH}_2\text{CH}_2\text{O})_n$ + $\text{C}(\text{O})\text{CH}_2\text{CH}_2\text{CH}_2\text{CH}_2\text{CH}_2\text{OH}$), 28.3 (s, $(\text{C}(\text{O})\text{CH}_2\text{CH}_2\text{CH}_2\text{CH}_2\text{CH}_2\text{O})_n$ + $\text{C}(\text{O})\text{CH}_2\text{CH}_2\text{CH}_2\text{CH}_2\text{CH}_2\text{OH}$), 32.4 (s, $\text{C}(\text{O})\text{CH}_2\text{CH}_2\text{CH}_2\text{CH}_2\text{CH}_2\text{OH}$), 34.0 (s, $(\text{C}(\text{O})\text{CH}_2\text{CH}_2\text{CH}_2\text{CH}_2\text{CH}_2\text{O})_n$), 62.5 (s, $\text{C}(\text{O})\text{CH}_2\text{CH}_2\text{CH}_2\text{CH}_2\text{CH}_2\text{OH}$), 63.5 (s, $(\text{C}(\text{O})\text{CH}_2\text{CH}_2\text{CH}_2\text{CH}_2\text{CH}_2\text{O})_n$ + PyCH_2OH), 66.6 (s, $\text{CH}(\text{CH}_3)\text{OH}$), 68.9 (s, $(\text{OCCH}(\text{CH}_3)\text{O})_n$), 123.9 (s, $m\text{-Ar-C}$), 125.9 (s, $\text{Ar-C}(\text{OTs})$), 128.8 (s, $\text{Ar-C}(\text{OTs})$), 148.7 (s, $\text{Ar-C}(\text{OTs})$), 149.9 (s, $\text{Ar-C}(\text{OTs})$), 151.8 (s, $p\text{-Ar-C}$), 151.0 (s, $o\text{-Ar-C}$), 169.4 (s, $(\text{OCCH}(\text{CH}_3)\text{O})_n$), 172.5 (s, $\text{C}(\text{O})\text{CH}_2\text{CH}_2\text{CH}_2\text{CH}_2\text{CH}_2\text{OH}$), 173.3 (s, $(\text{C}(\text{O})\text{CH}_2\text{CH}_2\text{CH}_2\text{CH}_2\text{CH}_2\text{O})_n$), 174.9 (s, $\text{OCCH}(\text{CH}_3)\text{OH}$).

2.3.1.25 NMR spectroscopic data for 16

NMR signals assigned to the PLA chain did not show any significant variation upon macrocomplex formation and are hence not reported for the macrocomplexes **1-9** and **16**.

^1H NMR (400.13 MHz, CD_2Cl_2 , 21 °C, ppm): 2.45 (s, 6H, CH_3), 7.32 (m, 12H, $m\text{-Ar-H}(\text{Py})$ + $\text{Ar-H}(\text{OTs})$), 7.98 (d, $J = 8.0$ Hz, 4H, $\text{Ar-H}(\text{OTs})$), 9.77 (d, $J = 5.6$ Hz, 8H, $o\text{-Ar-H}(\text{Py})$).

$^{13}\text{C}\{^1\text{H}\}$ NMR (100.62 MHz, CD_2Cl_2 , 21 °C, ppm): 21.05 (s, $\text{CH}_3\text{C}_6\text{H}_4\text{SO}_3^-$), 123.90 (s, $m\text{-Ar-C}(\text{Py})$), 125.94 (s, $\text{Ar-C}(\text{OTs})$), 128.83 (s, $\text{Ar-C}(\text{OTs})$), 139.73 (s, $\text{Ar-C}(\text{OTs})$), 144.67 (s, $\text{Ar-C}(\text{OTs})$), 148.76 (s, $p\text{-Ar-C}(\text{Py})$), 152.42 (s, $o\text{-Ar-C}(\text{Py})$).

2.3.1.26 NMR spectroscopic data for 17

^1H NMR (400.13 MHz, CD_2Cl_2 , 21 °C, ppm): 1.49 (d, $J = 6.8$ Hz, 3H, $\text{CH}(\text{CH}_3)\text{OH}$), 1.59 (d, $J = 6.8$ Hz, 264H, $\text{OCCH}(\text{CH}_3)\text{O}$), 1.83 (s, 6H CH_3CO_2^-), 4.36 (q, $J = 6.8$ Hz,

2H, $CH(CH_3)OH$), 5.20 (q, $J = 6.8$ Hz, 88H, $OCCH(CH_3)O$), 5.25 (s, 4H, $PyCH_2O$), 7.34 (d, $J = 6.0$ Hz, 4H, *m*-Ar-*H*), 8.64 (d, $J = 6.0$ Hz, 4H, *o*-Ar-*H*). $^{13}C\{^1H\}$ NMR (100.62 MHz, CD_2Cl_2 , 21 °C, ppm): 16.5 (s, $OCCH(CH_3)O$), 20.3 (s, $CH(CH_3)OH$), 22.8 (s, $CH_3CO_2^-$), 64.1 (s, $PyCH_2O$), 66.6 (s, $CH(CH_3)OH$), 69.0 (s, $OCCH(CH_3)O$), 122.6 (s, *m*-Ar-*C*), 147.8 (s, *p*-Ar-*C*), 151.4 (s, *o*-Ar-*C*), 169.5 (s, $OCCH(CH_3)O$), 175.0 (s, $OCCH(CH_3)OH$), 177.5 (s, $CH_3CO_2^-$).

2.3.1.27 NMR spectroscopic data for 18

1H NMR (400.13 MHz, CD_2Cl_2 , 21 °C, ppm): 1.38 (m, 292H, $(C(O)CH_2CH_2CH_2CH_2CH_2O)_n + C(O)CH_2CH_2CH_2CH_2CH_2OH$), 1.65 (m, 584H, $(C(O)CH_2CH_2CH_2CH_2CH_2O)_n + C(O)CH_2CH_2CH_2CH_2CH_2OH$), 1.82 (s, 6H, $CH_3CO_2^-$), 2.32 (t, $J = 7.6$ Hz, 288H, $(C(O)CH_2CH_2CH_2CH_2CH_2O)_n$), 2.48 (t, $J = 7.6$ Hz, 4H, $C(O)CH_2CH_2CH_2CH_2CH_2OH$), 3.62 (t, $J = 6.4$ Hz, 4H, $C(O)CH_2CH_2CH_2CH_2CH_2OH$), 4.07 (t, $J = 6.8$ Hz, $(C(O)CH_2CH_2CH_2CH_2CH_2O)_n$), 5.20 (s, 4H, $PyCH_2O$), 7.36 (d, $J = 6.4$ Hz, 4H, *m*-Ar-*H*), 8.61 (d, $J = 6.4$ Hz, 4H, *o*-Ar-*H*).

$^{13}C\{^1H\}$ NMR (100.62 MHz, CD_2Cl_2 , 21 °C, ppm): 22.5 (s, $CH_3CO_2^-$), 24.6 (s, $(C(O)CH_2CH_2CH_2CH_2CH_2O)_n + C(O)CH_2CH_2CH_2CH_2CH_2OH$), 25.5 (s, $(C(O)CH_2CH_2CH_2CH_2CH_2O)_n + C(O)CH_2CH_2CH_2CH_2CH_2OH$), 28.3 (s, $(C(O)CH_2CH_2CH_2CH_2CH_2O)_n + C(O)CH_2CH_2CH_2CH_2CH_2OH$), 33.1 (s, $C(O)CH_2CH_2CH_2CH_2CH_2OH$), 34.0 (s, $(C(O)CH_2CH_2CH_2CH_2CH_2O)_n$), 62.4 (s, $C(O)CH_2CH_2CH_2CH_2CH_2OH$), 63.1 (s, $PyCH_2OH$), 64.0 (s, $(C(O)CH_2CH_2CH_2CH_2CH_2O)_n$), 122.7 (s, *m*-Ar-*C*), 148.8 (s, *p*-Ar-*C*), 151.3 (s, *o*-Ar-*C*), 172.6 (s, $C(O)CH_2CH_2CH_2CH_2CH_2OH$), 173.3 (s, $C(O)CH_2CH_2CH_2CH_2CH_2O)_n$), 177.6 (s, $CH_3CO_2^-$).

2.3.1.28 NMR spectroscopic data for 20

1H NMR (300.13 MHz, CD_2Cl_2 , 21 °C, ppm): 1.82 (s, 6H, CH_3COO^-), 3.37 (s, 6H, $CH_2CH_2OCH_3$), 3.63 (s, 928H, CH_2CH_2O), 4.66 (s, 4H, $PyCH_2OCH_2CH_2$), 7.38 (d, $J = 6.8$ Hz, 4H, *m*-Ar-*H*), 8.58 (d, $J = 6.8$ Hz, 4H, *o*-Ar-*H*).

$^{13}C\{^1H\}$ NMR (75.47 MHz, CD_2Cl_2 , 21 °C, ppm): 22.9 (s, CH_3COO^-), 58.6 (s, $CH_2CH_2OCH_3$), 70.5 (s, CH_2CH_2O), 71.9 (s, $PyCH_2OCH_2CH_2$), 122.5 (s, *m*-Ar-*C*), 151.0 (s, *o*-Ar-*C*), 151.6 (s, *p*-Ar-*C*), 177.5 (s, CH_3COO^-).

2.3.1.29 NMR spectroscopic data for 21

1H NMR (300.13 MHz, CD_2Cl_2 , 21 °C, ppm): 2.42 (s, 6H, $CH_3(OTs)$), 3.37 (s, 12H, $CH_2CH_2OCH_3$), 3.63 (s, 1856H, CH_2CH_2O), 4.53 (s, 8H, $PyCH_2OCH_2CH_2$), 7.28 (d, $J =$

7.2 Hz, 4H, *m*-Ar-*H*(OTs)), 7.33 (d, $J = 6.4$ Hz, 8H, *m*-Ar-*H*(Py)), 7.97 (d, $J = 7.2$ Hz, 4H, *o*-Ar-*H*(OTs)), 9.64 (d, $J = 6.4$ Hz, 8H, *o*-Ar-*H*(Py)).

$^{13}\text{C}\{^1\text{H}\}$ NMR (75.47 MHz, CD_2Cl_2 , 21 °C, ppm): 21.0 (s, $\text{CH}_3(\text{OTs})$), 58.6 (s, $\text{CH}_2\text{CH}_2\text{OCH}_3$), 70.5 (s, $\text{CH}_2\text{CH}_2\text{O}$), 71.9 (s, $\text{PyCH}_2\text{OCH}_2\text{CH}_2$), 123.8 (s, *m*-Ar-*C*(Py)), 126.0 (s, *o*-Ar-*C*(OTs)), 128.7 (s, *m*-Ar-*C* (OTs)), 139.3 (s, *p*-Ar-*C* (OTs)), 126.0 (s, *ipso*-Ar-*C*(OTs)), 151.9 (s, *o*-Ar-*C*(Py)), 152.4 (s, *p*-Ar-*C*(Py)).

2.3.1.30 ^1H NMR data for cyanation products

4-Methoxybenzotrile [CAS: 874-90-8]

δ_{H} (ppm) (300 MHz; CDCl_3) 3.87 (s, 3 H, OCH_3), 6.96 (d, $J = 9$ Hz, 2H, $\text{H}_{\text{AA}'}$), 7.59 (d, $J = 9$ Hz, 2H, $\text{H}_{\text{XX}'}$). ESI-MS(+) m/z 134 ($[\text{M}+\text{H}]^+$, 100%), 130 (45), 122 (15), 102 (20), 94 (40).

4-Methylbenzotrile [CAS: 104-85-8]

δ_{H} (ppm) (300 MHz; CDCl_3) 2.44 (s, 3 H, CH_3), 7.28 (d, $J = 9$ Hz, 2 H, $\text{H}_{\text{XX}'}$), 7.55 (d, $J = 9$ Hz, 2 H, $\text{H}_{\text{AA}'}$). ESI-MS(+) m/z 118 ($[\text{M}+\text{H}]^+$, 100%), 91 (30), 64 (15), 40 (15).

4-Aminobenzotrile [CAS: 873-74-5]

δ_{H} (ppm) (300 MHz; CDCl_3) 2.25 (sb, 2 H, NH_2), 6.66 (d, $J = 9$ Hz, 2H, $\text{H}_{\text{AA}'}$), 7.40 (d, $J = 9$ Hz, 2H, $\text{H}_{\text{XX}'}$). ESI-MS(+) m/z 119 ($[\text{M}+\text{H}]^+$, 100%), 83 (10).

9-Cyanophenanthrene [CAS: 2510-55-6]

δ_{H} (ppm) (300 MHz; CDCl_3) 7.63-7.79 (m, 4H, $\text{H}_{2,3,6,7}$), 7.90 (d, $J = 8$ Hz, 1H, H_8), 8.18 (s, 1H, H_{10}), 8.27 (d, $J = 8$ Hz, 1H, H_1), 8.27 (m, 2H, $\text{H}_{4,5}$). ESI-MS(+) m/z 204 ($[\text{M}+\text{H}]^+$, 100%), 130 (30), 108 (20), 94 (95).

3-Cyanobenzyl alcohol [CAS: 626-17-5]

δ_{H} (ppm) (300 MHz; CDCl_3) 4.74 (s, 1H, CH_2), 7.47 (t, $J = 9$ Hz, 1H, H_5), 7.59 (m, 2 H, $\text{H}_{4,6}$), 7.67 (s, 1H, H_2). ESI-MS(+) m/z 134 ($[\text{M}+\text{H}]^+$, 100%).

1,4-Dicyanobenzene [CAS: 623-26-7]

δ_{H} (ppm) (300 MHz; CDCl_3) 7.81 (s, 4H, H_{Ar}). ESI-MS(+) m/z 129 ($[\text{M}+\text{H}]^+$, 100%).

1,3-Dicyanobenzene [CAS: 626-17-5]

δ_{H} (ppm) (300 MHz; CDCl_3) 7.65 (t, $J = 9$ Hz, 1H, H_5), 7.92 (d, $J = 9$ Hz, 2H, $\text{H}_{4,6}$), 7.98 (s, 1H, H_2). ESI-MS(+) m/z 129 ($[\text{M}+\text{H}]^+$, 100%).

1,2-Dicyanobenzene [CAS: 91-15-6]

δ_H (ppm) (300 MHz; CDCl_3) 7.75-7.90 (m, 4H, H_{Ar}). ESI-MS(+) m/z 129 ($[\text{M}+\text{H}]^+$, 100%).

2-Cyanonaphthalene [CAS: 613-46-7]

δ_H (ppm) (300 MHz; CDCl_3) 7.55-7.70 (m, 3H, $\text{H}_{3,6,7}$), 7.80-7.95 (m, 3H, $\text{H}_{4,5,8}$), 8.23 (s, 1H, H_{10}). ESI-MS(+) m/z 154 ($[\text{M}+\text{H}]^+$, 100%), 141 (12), 99 (50), 94 (25).

3-Cyanoquinoline [CAS: 34846-64-5]

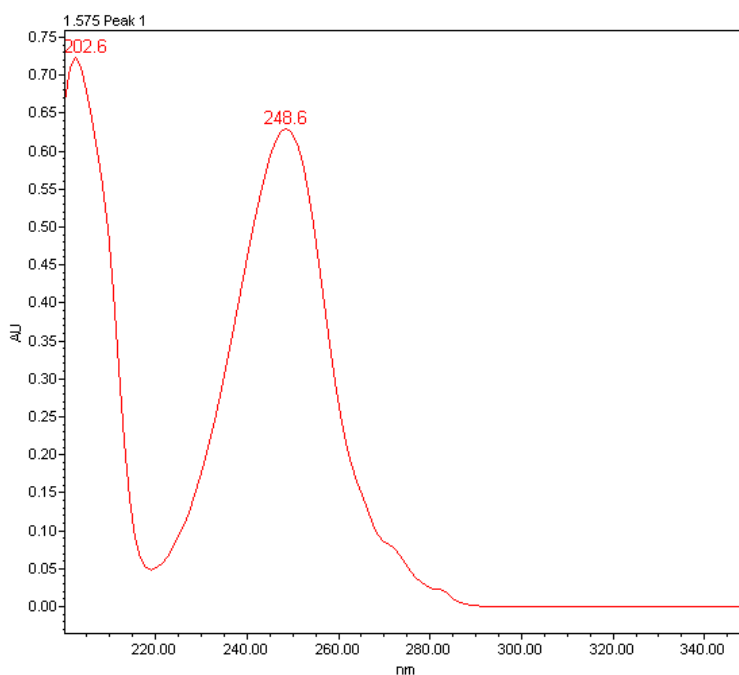
δ_H (ppm) (300 MHz; CDCl_3) 7.71 (t, $J = 8$ Hz, 1H, H_6), 7.91 (m, 2 H, $\text{H}_{5,7}$), 8.19 (d, $J = 6$ Hz, 1H, H_8), 8.56 (s, 1H, H_4), 9.05 (s, 1H, H_2). ESI-MS(+) m/z 155 ($[\text{M}+\text{H}]^+$, 100%).

2.3.2 HPLC-UV

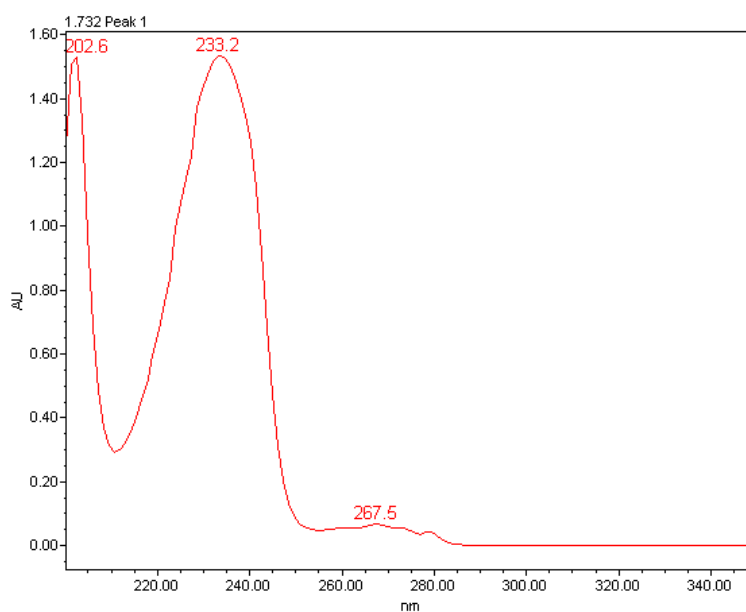
Analytical high performance liquid chromatography (HPLC) was performed on a Waters Millennium 717 equipped with Autosampler, with a variable wavelength diode detector using a CHROMOLITH RP18 column (50 x 4,6 mm), flow 5 mL/min, linear gradient CH_3CN in water 0–100% (+0.1% TFA) in 4.5 min. UV spectra were recorded by the HPLC detector for chromatographic peaks.

2.3.2.1 UV spectra of HPLC peaks of cyanation products

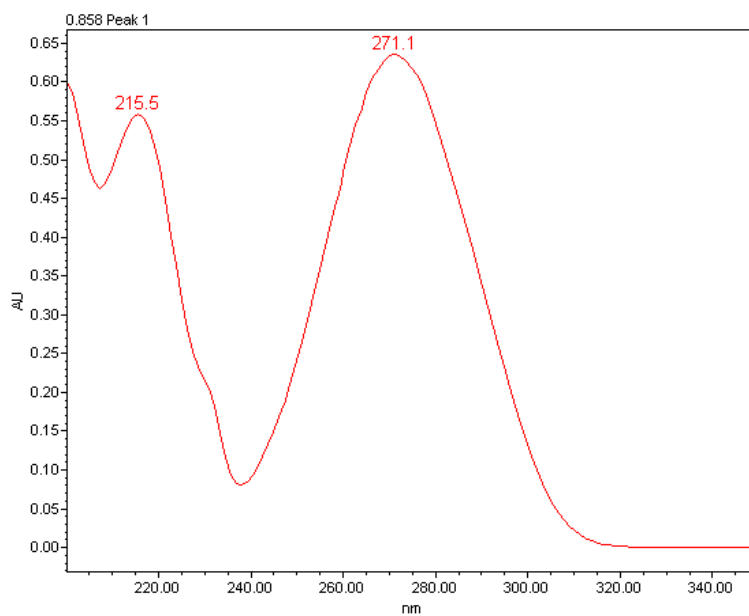
4-Methoxybenzonitrile [CAS: 874-90-8]



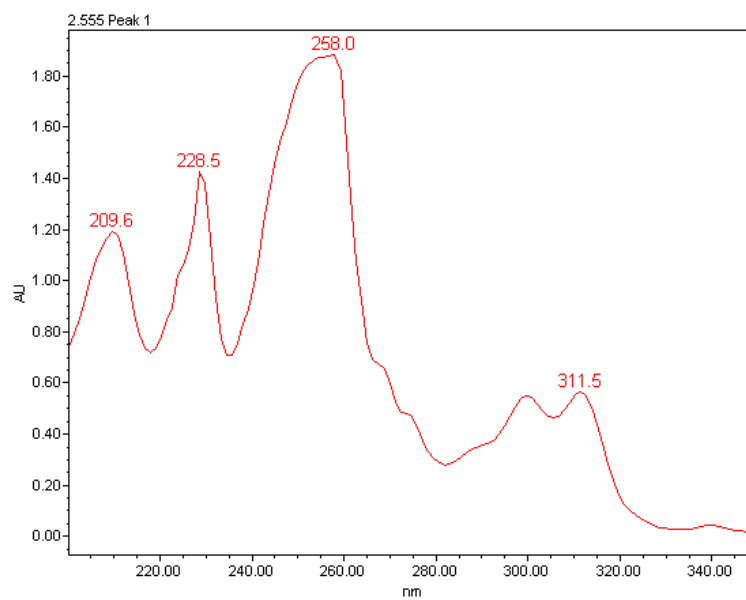
4-Methylbenzonitrile [CAS: 104-85-8]



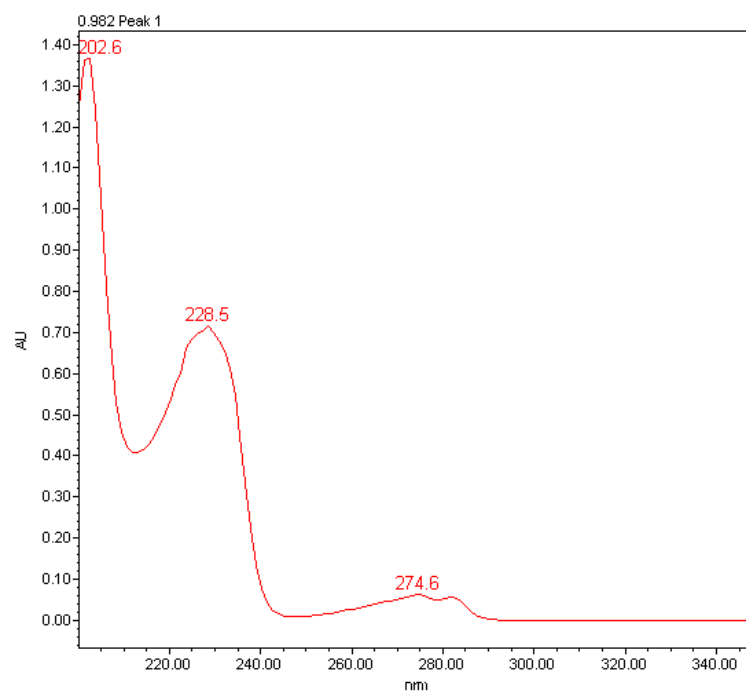
4-Aminobenzonitrile [CAS: 873-74-5]



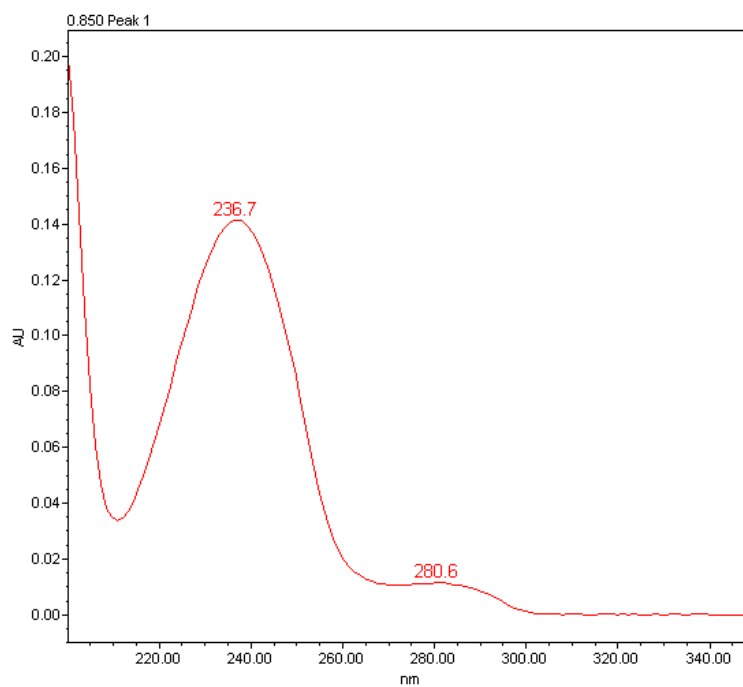
9-Cyanophenanthrene [CAS: 2510-55-6]



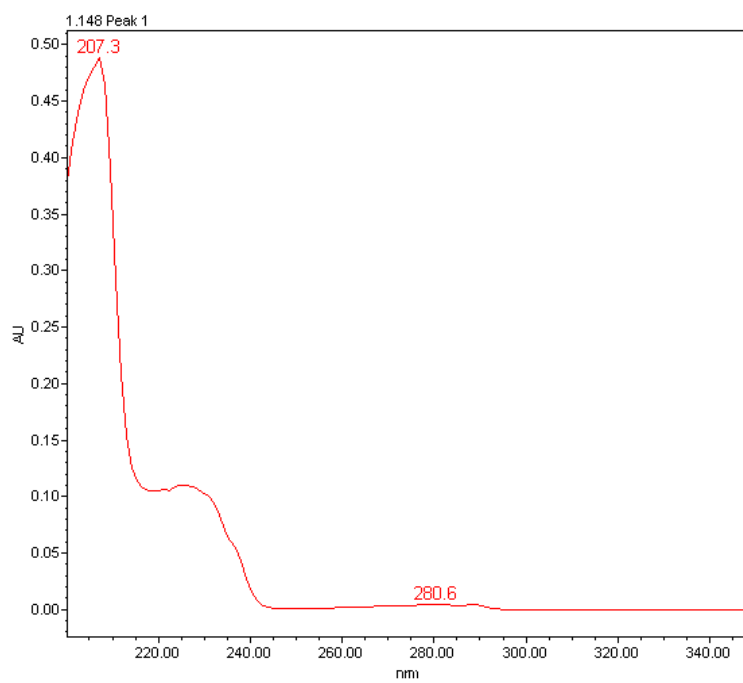
3-Cyanobenzyl alcohol [CAS: 626-17-5]



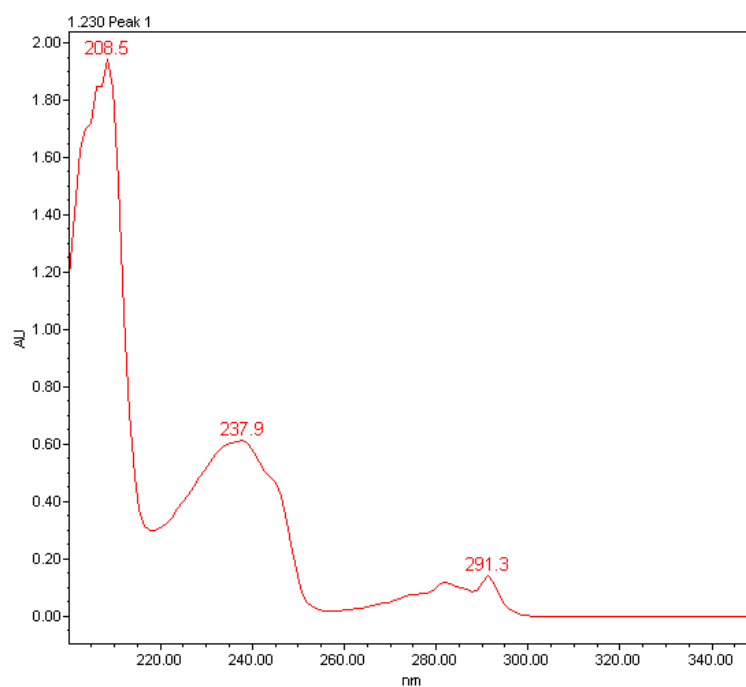
1,4-Dicyanobenzene [CAS: 623-26-7]



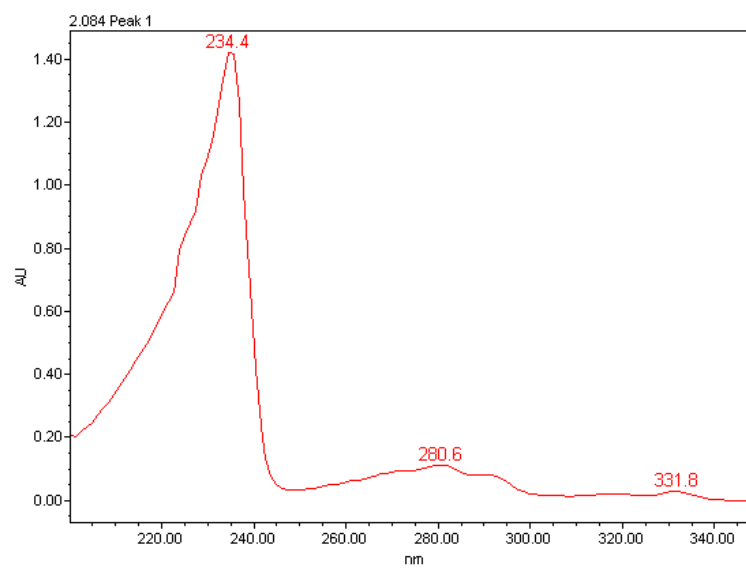
1,3-Dicyanobenzene [CAS: 626-17-5]



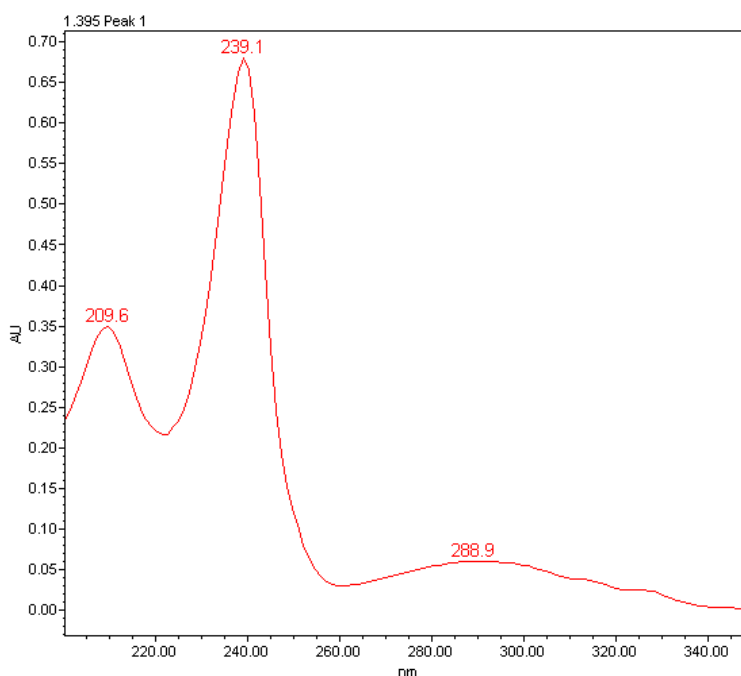
1,2-Dicyanobenzene [CAS: 91-15-6]



2-Cyanonaphthalene [CAS: 613-46-7]



3-Cyanoquinoline [CAS: 34846-64-5]



2.3.3 Gel Permeation Chromatography (GPC)

GPC analyses were carried out with a SEC-GPC system, equipped with a *Waters 'Binary HPLC 1525'* pump; a manual injector with a 6-way valve and a 200 μL loop; three in-series connected *Shodex KF-802.5; KF-803 and KF-804* columns (length: 300 mm each; inner diameter: 8.0 mm; 24500 theoretical plates; exclusion limit for PS: up to 400000 g/mol); a RI detector (*Waters, mod. 2414*; for samples **L4**, **L5**, and **20** a *Wyatt Optilab T-rEX* was used) and an UV-Vis detector (*Waters, mod. 2489*). HPLC-grade CHCl_3 or THF with a water content of 0.1 vol% (max.) was used as eluent at a constant flux of 1 mL/min, keeping the columns thermostated at 30 $^{\circ}\text{C}$. The GPC system was calibrated using polystyrene standards.

2.3.4 UV-Vis spectroscopy

UV-Vis spectra of **1** (1.79×10^{-4} mol/l) **10** (5.10×10^{-3} mol/l) and **L1** (6.0×10^{-4} mol/l) were recorded on a Varian-Cary 4000 UV-Vis spectrophotometer, using HPLC-grade CHCl_3 and a quartz cuvette with a 10 mm optical pathlength.

Measurements on PEG-containing samples **L4**, **L5** and **20 – 25** were carried out on deionized water solutions using a concentration of 0.3 mg/mL.

2.3.5 Differential Scanning Calorimetry (DSC)

For **L1**, **L2**, and **1-9**: DSC-measurements were carried out under nitrogen with a Perkin-Elmer DSC 7 instrument calibrated with In and Pb as standard references. Each sample was subjected to two heating cycles in the temperature range from 40.0 to 200.0 $^{\circ}\text{C}$, employing the following heating program: (i) sample at 40.0 $^{\circ}\text{C}$ for 1 min; (ii) heating

the sample from 40.0 to 200.0 °C with a heating rate of 20.0 °C/min; (iii) sample at 200.0 °C for 1 min; (iv) cooling the sample to 40.0 °C with a cooling rate of -20.0 °C/min; (v) sample at 40.0 °C for 5 min followed by a second heating run repeating steps (ii) and (iii).

For **L1**, **L3**, **17** and **18**: (DSC) analysis were carried out under an atmosphere of nitrogen with a DSC Exstar 7020 SEIKO instrument, calibrated with In and Pb applying a heating rate of 10 °C/min. The following heating programs were applied:

- 1) For **L1** and **17**: 1st heating: 20 to 200 °C (holding this temperature for 2 min) followed by cooling the sample to -10 °C; 2nd heating: -10 to 200 °C; heating rate: 10 °C/min.
- 2) For **L2** and **18**: 1st heating: 20 to 120 °C (holding this temperature for 5 min) followed by cooling the sample to -100 °C (holding this temperature for 5 min); 2nd heating: -100 to 100 °C; heating rate: 10 °C/min.

2.3.6 Thermo-Gravimetric Analysis (TGA)

Thermo-gravimetric (TG) analyses were performed with a Mettler Toledo Star System TGA/SDTA 851e Module between 30 and 600 °C at a standard heating rate of 10 °C/min under thermo oxidative atmosphere.

TG analyses on samples **L4**, **L5** and **20 – 25** were performed under an air flux (200 ml/min) by using a SEIKO TG/DTA 7200 instrument calibrated with In as reference sample. Measurements were carried out in the temperature interval from 30 to 700 °C with a heating rate of 10 °C/min.

2.3.7 X-Ray Powder Diffraction (XRPD)

XRPD spectra were acquired on a X'Pert PRO (PANalytical) powder diffractometer in a 2 θ range from 5 to 80 ° (10 to 60 ° for samples **L4**, **L5** and **20 – 25**) with a step size of 0.1050 °, using Cu K α radiation (1.541874 Å).

2.3.8 X-Ray Photoelectron Spectroscopy (XPS)

XPS analyses were performed with a Thermo Electron ESCALAB 250 working with an excitation source Al K α (1486.6 eV). The analyzed surface has a diameter of 400 μ m; photoelectron spectra are calibrated referring the binding energy of the C-C component of Carbon C1s at 284.8 eV. The charge is compensated by an electron beam (-2eV).

2.3.9 Gas Chromatography (GC-FID / GC-MS)

GC-FID analyses were performed with a Shimadzu 2010 gas chromatograph equipped

with a flame ionization detector using a 30 m (0.25 mm i.d., 0.25 μm film thickness) VF-WAXms capillary column and *n*-decane as internal standard. GC-MS analyses were performed with a Shimadzu QP 5000 apparatus, equipped with a 30 m (0.32 mm i.d., 0.50 μm film thickness) CP-WAX 52 CB WCOT-fused silica column.

2.3.10 Transmission Electron Microscopy (TEM)

TEM analyses were carried out on a TEM CM PHILIPS, equipped with an OLYMPUS Megaview G2 camera and using an accelerating voltage of 80 keV. Samples for TEM analyses were prepared by depositing a drop of the water solution of the corresponding sample on a Lacey carbon Cu grid, followed by solvent evaporation.

TEM analyses on cyanation catalysts were performed with a JEOL 1200EX2 microscope operating at 100 kV (point resolution of 0.4 nm; reseaux resolution 0.2 nm). Images were captured with an SIS Olympus Quemesa camera; the digital camera has an 11 Mpixel CCD.

HR-TEM analyses on cyanation catalysts were performed with a JEOL 2200FS microscope (acceleration voltage of 200 kV; point resolution of 0.23 nm). EDS analyses were performed with a JEOL DRY SD30GV (Silicon Drift Diode detector; surface of 30 mm^2 ; resolution of 133 eV [Fe: 5.9 keV at 1000 CPS]).

2.3.11 Inductively Coupled Plasma (ICP)

ICP-MS analyses were carried out on a Thermo ICP-MS XSeries 2.

ICP-OES analyses were carried out on an ICP apparatus of the type Perkin Elmer Optima 2000 OES DV.

2.3.12 X-ray crystallographic study of complex 10

Diffraction data for **10** were collected on an Oxford Diffraction CCD diffractometer, using Mo $K\alpha$ radiation ($\lambda = 0.71069 \text{ \AA}$) and corrected for Lorentz and polarization effects. Absorption correction was performed using the XABS2 program.²⁹⁸ The structure (Figure 2.1) was solved by direct methods using SHELXS-97²⁹⁹ and refined by full-matrix least squares methods against F^2 using the WINGX³⁰⁰ software package. All non hydrogen atoms were refined anisotropically, while hydrogen atoms were added at calculated positions and refined applying a riding model with isotropic U values depending on the U_{eq} of the adjacent carbon atom. CCDC 815906 contains the supplementary crystallographic data. These data can be obtained free of charge from the Cambridge Crystallographic Data Centre via www.ccdc.cam.ac.uk/data_request/cif.

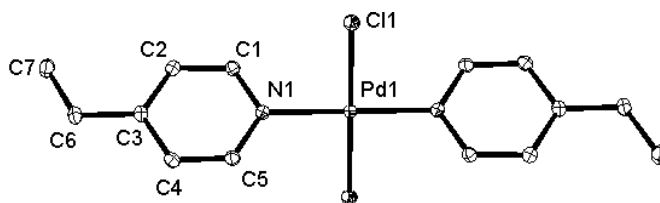


Figure 2.1 – ORTEP-plot of **10**. Hydrogen atoms are omitted and the thermal ellipsoids are shown at the 30% probability level. Only the atoms belonging to the asymmetric unit are labeled. Selected bond distances (Å) and angles (°): Pd1-N1 2.0199(13); Pd-Cl1 2.3026(4); Cl1-Pd1-N1 90.15(4)

Crystallographic Data and Refinement Details for **10**:

Empirical formula	C ₁₄ H ₁₈ Cl ₂ N ₂ Pd
Molecular weight (g/mol)	391.60
Crystal habit	yellow prism
Crystal size (mm)	0.30×0.20×0.10
Temperature (K)	150(2)
Wavelength (Å)	0.71069
Crystal system	Monoclinic
Space group	P2(1)/c
<i>a</i> (Å)	7.8580(3)
<i>b</i> (Å)	13.3651(5)
<i>c</i> (Å)	7.1402(2)
β (°)	96.055(3)
<i>V</i> (Å ³)	745.70(5)
<i>Z</i>	2
<i>D</i> _{calc} (g/cm ³)	1.744
<i>F</i> (000)	392
θ range (°)	4.19-32.34
μ (mm ⁻¹)	1.59
Number of reflections collected	2402
Number of unique reflections	2402
Number of parameters	89
Final <i>R</i> indices [<i>I</i> >2 σ (<i>I</i>)]	R1 = 0.0224 wR2 = 0.0512
<i>R</i> indices (all data)	R1 = 0.0299 wR2 = 0.0525

Largest diff peak, hole ($e/\text{\AA}^3$)

0.486, -0.917

2.3.13 NMR experiments of stepwise macroligand dissociation from macrocomplexes **4** and **6**

Compound **4** (20.0 mg (0.0026 mmol)) was dissolved in CD_2Cl_2 (0.8 mL), followed by the acquisition of an ^1H NMR spectrum at room temperature. Afterwards, $[\text{N}(n\text{-Bu})_4]\text{Cl}$ (0.72 mg (0.0026 mmol)) was added to the latter solution, followed by the successive acquisition of an ^1H NMR spectrum at room temperature and at $-70\text{ }^\circ\text{C}$. In a separate NMR experiment, dppe (1.04 mg (0.0026 mmol)) was added to an identical CD_2Cl_2 solution of **4**, followed by the acquisition of ^1H and $^{31}\text{P}\{^1\text{H}\}$ NMR spectra at room temperature.

Compound **6** (20.0 mg (0.001 mmol)) was dissolved in CD_2Cl_2 (0.7 mL) and an ^1H NMR spectrum was acquired at room temperature. To this latter solution $[\text{N}(n\text{-Bu})_4]\text{Cl}$ (0.55 mg (0.002 mmol)) was added at room temperature, followed by the acquisition of an ^1H NMR spectrum at the same temperature. Afterwards, PPh_3 (0.52 mg, 0.002 mmol) was added to the latter NMR solution, followed by the acquisition of ^1H and $^{31}\text{P}\{^1\text{H}\}$ NMR spectra at room temperature.

2.3.14 Centrifugation experiments with water solutions of **23** and **25**

Water solutions of **23** and **25** of identical concentration (10 mg/mL) were centrifuged at 6000 rpm for 6 h. During this time period a black powder separated from the water solution of **25**. The black solid was successively separated from solution, washed with deionized water, dried under vacuum at room temperature and analyzed by X-ray powder diffraction (XRPD). In the case of **23** no precipitate formation was observed even after doubling the centrifugation time (12 h at 6000 rpm).

2.4 Catalysis

2.4.1 Aerobic oxidations in toluene catalyzed by **17** – **19**

A stainless steel autoclaves (80.0 mL) was successively charged at room temperature with precatalyst **17-19** (0.005 mmol) or with a mixture of precatalyst **17/19** (0.005 mmol) and the corresponding ligand (**L1** or 4-EtPy) (0.010 mmol), toluene (5.0 mL) and substrate (8.00 mmol). The autoclave was sealed at room temperature and then heated to $70\text{ }^\circ\text{C}$ with an oil bath. Once the latter temperature was reached, air (4 bar) was introduced and magnetic stirring was started. After the desired reaction time, the autoclave was rapidly cooled to room temperature by means of an ice / water bath, the

air pressure released, and the reaction solution analyzed by GC-FID and GC-MS analyses. In **17**- and **18**-catalyzed oxidation reactions, methanol (12.0 mL) was added to the toluene solution in order to quantitatively precipitate the polymer, which was filtered off. The solution was analyzed by ICP-MS to determine the amount of residual palladium in solution.

2.4.2 Stability test of L1 and L3 carried out under aerobic oxidation conditions

A stainless steel autoclave (80.0 mL) was successively charged at room temperature with **L1** or **L3** (0.005 mmol), toluene (5.0 mL) and alcohol (*i.e.* benzyl alcohol or 1-hexanol or cinnamyl alcohol) (8.0 mmol). Afterwards, the autoclave was sealed, heated to 70 °C with an oil bath and, once the temperature was reached, air (4 bar) was introduced and magnetic stirring was started. After 36 h the autoclave was cooled to room temperature, the air pressure released, and the content of the autoclave was transferred into a Schlenk tube. The reaction solution was concentrated to dryness under vacuum at room temperature. The obtained solid was completely redissolved in CH₂Cl₂ (1.0 mL) and to the latter solution, methanol (8.0 mL) was added in order to quantitatively precipitate the polymer, which was successively separated by filtration and dried under vacuum (10 Torr) at room temperature. The isolated polymer was analyzed by ¹H NMR spectroscopy and GPC, performed in CD₂Cl₂ and THF, respectively.

2.4.3 Recycling experiments with 17+2L1 and benzyl alcohol

A typical reaction cycle was carried out as follows: A stainless steel autoclave (80.0 mL) was successively charged at room temperature with **17** (0.010 mmol), **L1** (0.020 mmol), toluene (5.0 mL) and benzyl alcohol (1.00 mmol). Afterwards, the autoclave was sealed and heated to 70 °C with an oil bath. Once the reaction temperature was reached, air (4 bar) was introduced and stirring was started. After a reaction time of 2 h, the autoclave was rapidly cooled to room temperature with an ice/water bath. The air pressure was then released and the reaction solution analyzed by GC. Afterwards the autoclave was sealed again and the solvent removed under vacuum. The solid residue was completely dissolved in CH₂Cl₂ (1.0 mL) and diethyl ether (15.0 mL) was added to the vigorously stirred yellow solution. Afterwards the supernatant was separated from the polymeric material by decantation; the isolated solid was dried under vacuum (10 Torr) at room temperature for half an hour and then used as catalyst for the next catalytic run.

2.4.4 Aerobic oxidations in water catalyzed by 20 – 25

A stainless steel autoclave (80.0 mL) was successively charged with water (5.0 mL), the desired amount of catalyst, substrate and K_2CO_3 (where used), then the autoclave was sealed and heated to 60 °C with an oil bath. Once the reaction temperature was reached, air (30 bars) was introduced and magnetic stirring was started. After the desired reaction time, the autoclave was cooled to room temperature with an ice-water bath and the air pressure released. To the crude reaction mixture was transferred into a separation funnel and the water suspension was extracted with Et_2O (3×8.0 mL). The combined organic phases were analyzed by GC-FID and GC-MS analyses.

2.4.5 Stability test of L4 performed under basic aerobic oxidation conditions

L4 (70.0 mg, 0.013 mmol) and K_2CO_3 (34.0 mg, 0.25 mmol) were dissolved in water (5.0 mL) and the solution was transferred into a stainless steel autoclave, which was successively sealed, pressurized with 30 bar of air and heated at 60 °C under stirring for 14 h. Afterwards, the autoclave was cooled to room temperature, the air pressure released and to the colorless water solution was added 2-propanol (20.0 mL) and Et_2O (50.0 mL), causing the precipitation of the polymer as a finely dispersed white solid which was separated from solution, washed with Et_2O (15.0 mL) and dried under vacuum at room temperature. The solid was dissolved in HPLC-grade THF for GPC-RI analysis. **L4**: (a) as synthesized; $M_n = 7750$ g/mol, PDI = 1.05; (b) after the stability test; $M_n = 8300$ g/mol, PDI = 1.08.

2.4.6 Recycling experiments with 23 and cinnamyl alcohol

A stainless steel autoclave (80.0 mL) was charged with **23** (65.0 mg, 0.003 mmol), cinnamyl alcohol (100.0 μ L, 0.778 mmol) and water (5.0 mL) at room temperature. The autoclave was then sealed, heated to 60 °C with an oil bath and charged with air (30 bar). After a reaction time of 2 h the autoclave was cooled to room temperature, the air pressure released, and the suspension transferred into a separation funnel. The water phase was extracted with Et_2O (3×8.0 mL). Afterwards, the water phase was placed again in the autoclave and cinnamyl alcohol (100.0 μ L, 778 mmol) added. The second, third and fourth catalytic cycle were carried out as described for the first cycle.

2.4.7 Cu-catalyzed cyanation of aryl halides under sonochemical conditions

Cyanation reactions were carried out with a 400 W Bioblock Scientific *Vibracell 72408* sonicator equipped with a 12 mm diameter titanium alloy probe and a rubber septum;

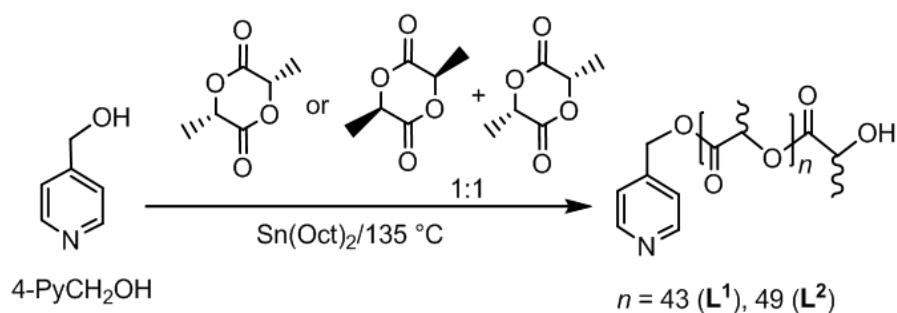
sonication was pulsed (on/off = 5 sec/5 sec) and wave amplitude was set at 70%. PEG (20.0 g) was slowly melted in a 25 ml round-bottom flask by means of a hot air gun under vacuum/N₂ cycles, then substrate (4 mmol), catalyst and K₄[Fe(CN)₆] were added under N₂ flux and the probe was inserted into the flask. As the rubber septum was applied on the flask neck, the N₂ flux was stopped and sonication started. After sonication, raw product was analyzed by HPLC-UV, then CH₂Cl₂ (100 ml) was used to recover product from probe and dissolve the mixture, eventually 10.0 ml of solution were carefully withdrawn and transferred dropwise into 250 ml of Et₂O (only 1/10 of the total volume was purified to avoid the use of 2.5 l of Et₂O per reaction). The light-grey slurry was kept at -16°C for 4 h and then filtered through a frit (porosity 3). The clear, liquid phase was evaporated to dryness and the product was re-dissolved in CDCl₃ for NMR and HPLC-UV analysis. Conversions and yields were calculated adding CH₂Br₂ (0.712 mmol, 50.0 μL) as internal standard.

3 Results and discussion

3.1 Synthesis of PLA- and PCL-based Pd macrocomplexes

3.1.1 Macrocomplexes combining P(L)LA- and P(LD)LA-based macroligands

The Ring Opening Polymerization of L- and racemic (*rac*)-lactide was carried out in bulk in the presence of 4-PyCH₂OH and catalyzed by Sn(Oct)₂ giving the 4-pyridinemethylene-end-capped P(L)LA macroligand **L1** ($M_n = 3280$ g/mol, PDI = 1.33) and the P(LD)LA macroligand **L2** ($M_n = 3700$ g/mol, PDI = 1.54) in 84 and 75% yield, respectively (Scheme 3.1).



Scheme 3.1 – Synthesis of pyridine functionalized macroligands

The esterification of 4-PyCH₂OH has been proved by ¹³C NMR spectroscopy. The corresponding ¹³C NMR spectrum showed a singlet centered at 64.97 ppm, which was assigned to the 4-PyCH₂O carbon atom. In addition, the absence of the ¹³C NMR singlet assigned to the carboxylic acid carbon atom at 171.60 ppm³⁰¹ combined with lack of a ¹H NMR singlet at 4.74 ppm assigned to PyCH₂OH is a further valuable proof of the occurred end-capping of PLA (Figure 3.1).

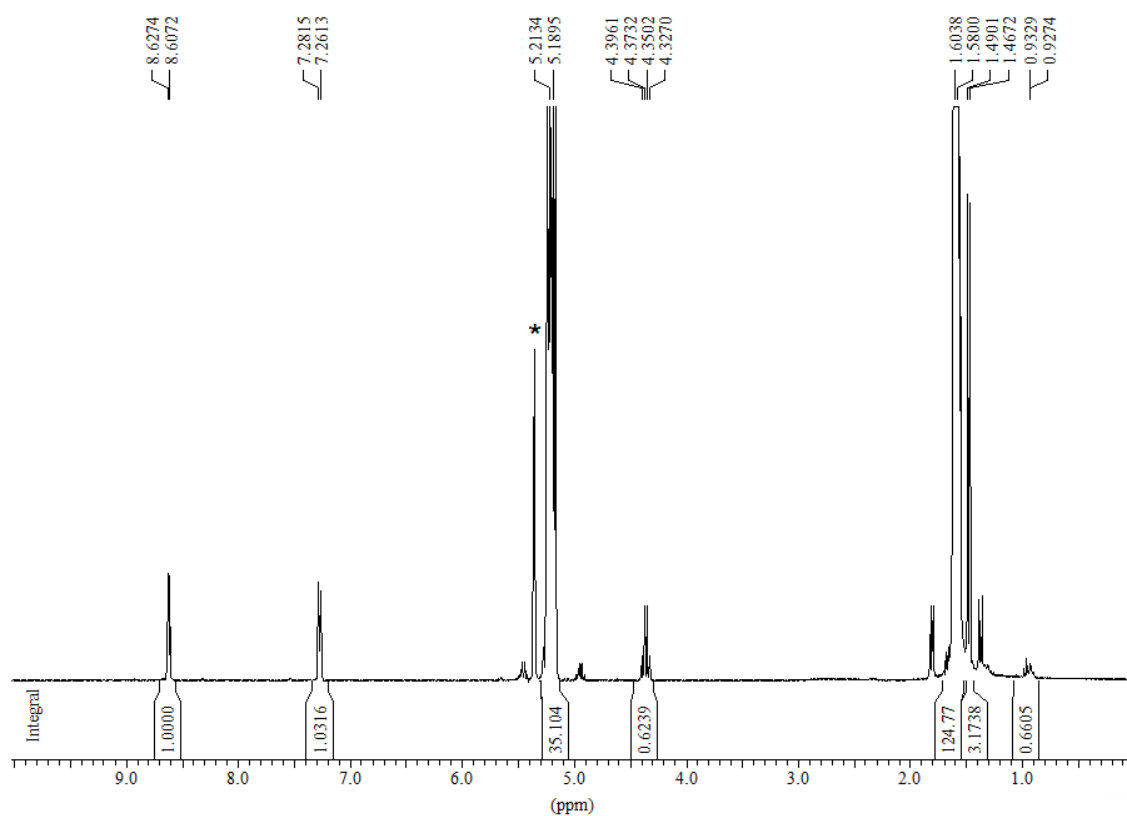
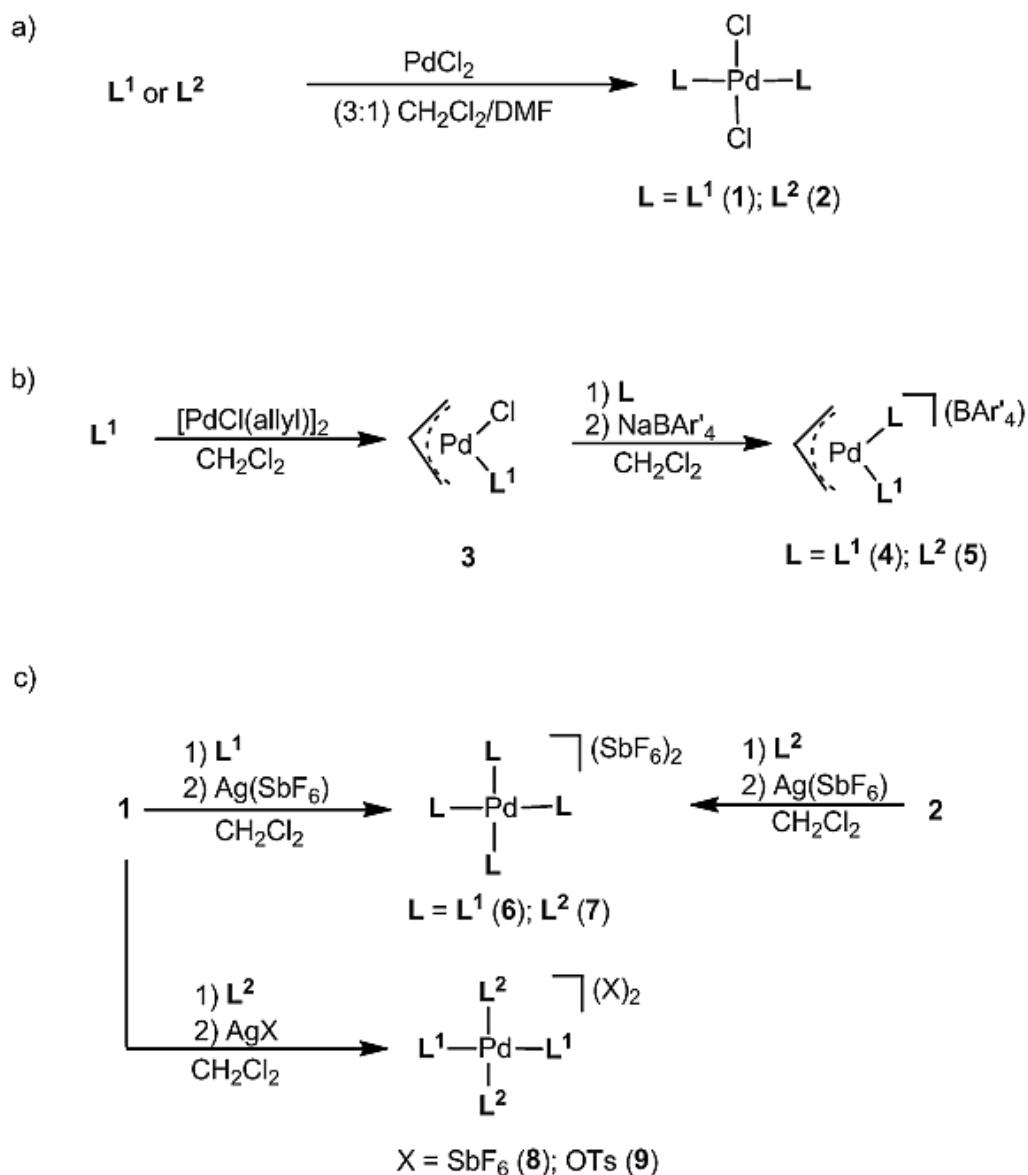


Figure 3.1 – ^1H NMR spectrum of PLA-based macroligand **L1**

The 1:2 stoichiometric reaction between PdCl_2 and **L1** or **L2** was carried out in a 3:1 solvent mixture of CH_2Cl_2 and DMF giving *trans*- $[\text{PdCl}_2(\mathbf{L1})_2]$ (**1**) and *trans*- $[\text{PdCl}_2(\mathbf{L2})_2]$ (**2**), respectively (Scheme 3.2/a) as light brown powders with c.a. 80% yield.



Scheme 3.2 – Synthesis of Pd(II)-PLA macrocomplexes

^1H NMR and $^{13}\text{C}\{^1\text{H}\}$ NMR spectra of **1** and **2**, acquired in CD_2Cl_2 , showed mainly for the *ortho*-hydrogen atoms of the pyridine moiety a coordination shift (c.a. 0.2 ppm for ^1H NMR) (Figure 3.2).

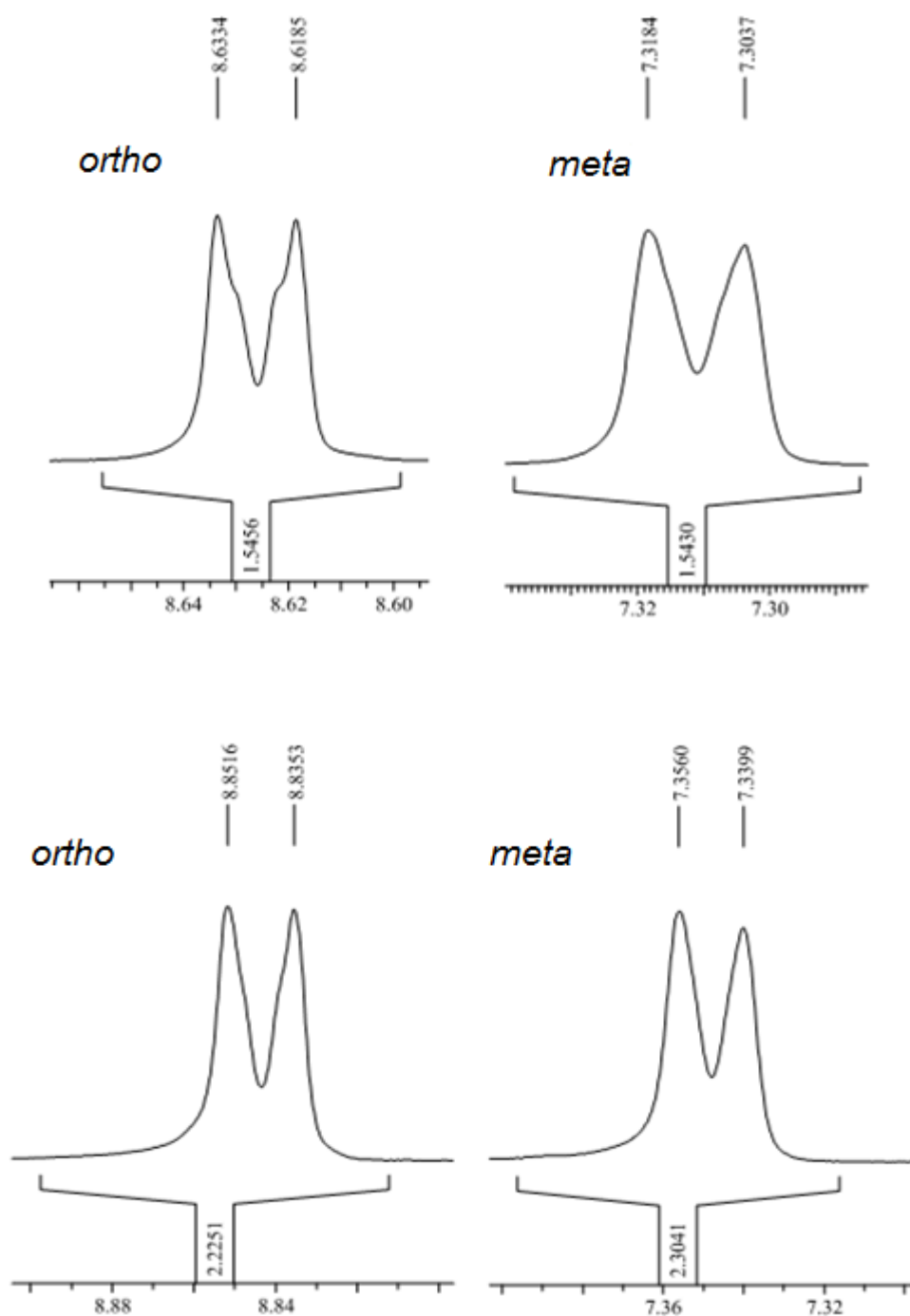


Figure 3.2 – Enlargement of NMR signals relative to the aromatic protons in L2 (top) and 2 (bottom)

Furthermore, GPC measurements carried out on CHCl_3 solutions of **1** (Figure 3.3) and **2** proved a two-fold increase of the molecular weight compared to the corresponding uncoordinated macroligand. It is also worth noting how the presence of the complex induces a strong increase in the UV absorption coefficient at 240, as witnessed by GPC-UV analyses on **L1** and **1**.

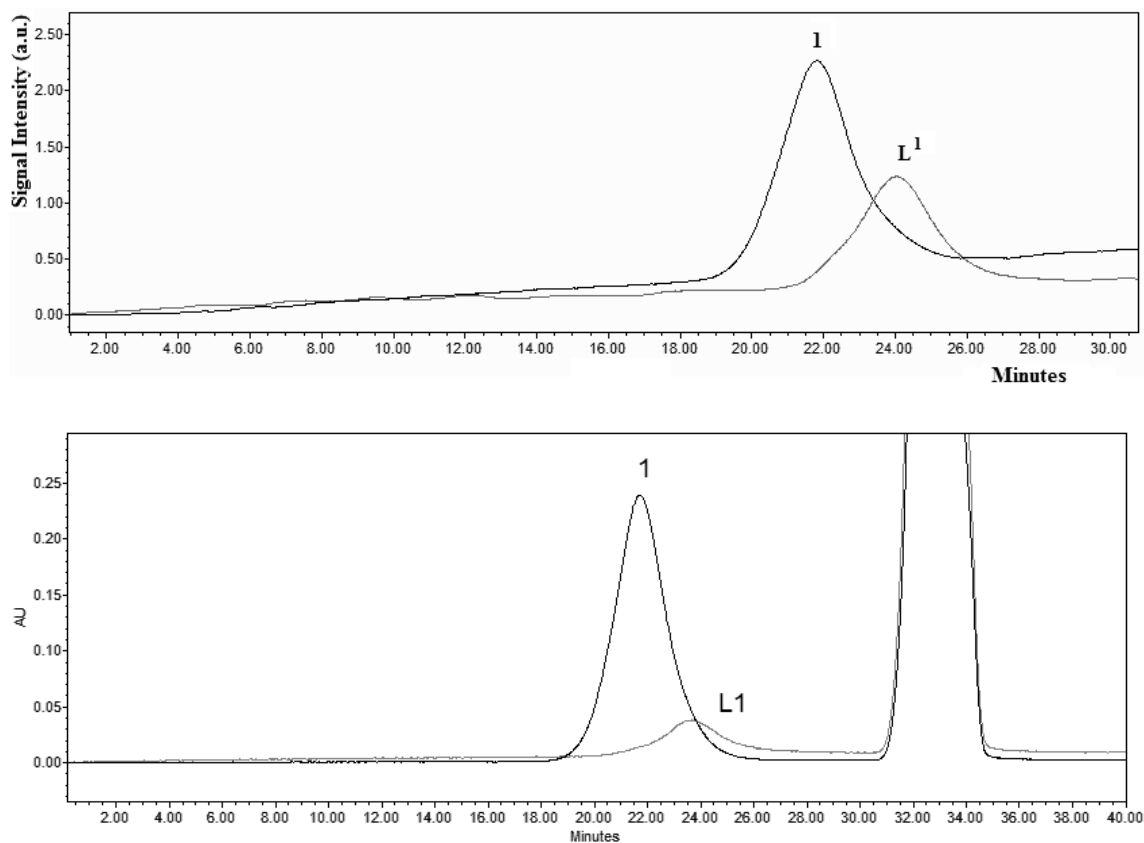


Figure 3.3 – GPC-curves of **1** and **L1** acquired with a RI-detector (top) and with an UV-detector set at 240 nm wavelength (enlargement) (bottom)

The coordination of the pyridine moieties *trans* to each other in **1** and **2** has been confirmed by comparing the UV-Vis spectrum of **1** with that of the reference compound *trans*-[PdCl₂(4-EtPy)₂] (4-EtPy = 4-ethylpyridine) (**10**) (Figure 3.4). The stereochemistry of the latter compound has been proved by a single crystal X-ray structure analysis (see experimental part).

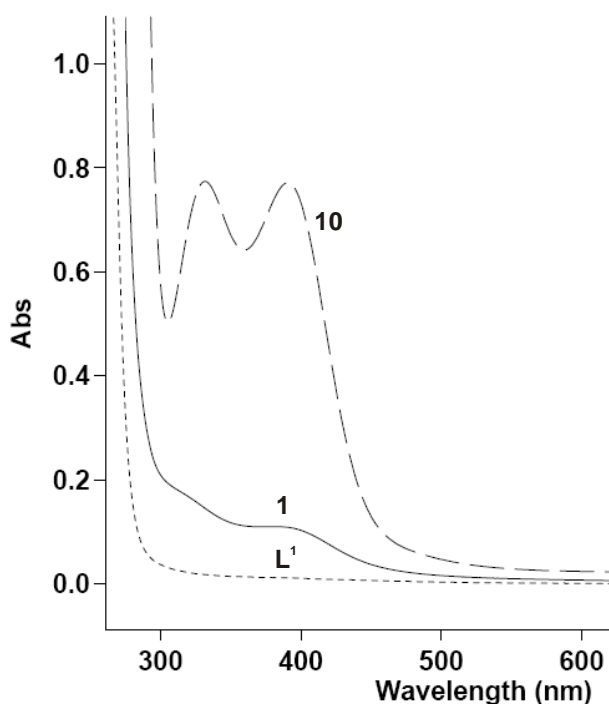


Figure 3.4 – UV-Vis spectra of **1**, **L1** and **10**, acquired in CHCl_3

Unlike **L1**, **1** and **10** share the metal to ligand charge transfer (MLCT) absorption bands at 332.0 and 391.0 nm.³⁰² The shoulder centred at 332.0 nm of **1**, is the sum of the absorption of the second MLCT absorption band centred at 332.0 nm and the small UV-absorption of the polymer chain in the region between 350 to 300 nm.

The 1:1 stoichiometric reaction between $[\text{PdCl}(\eta^3\text{-ally})]_2$ and **L1** gave **3** as beige powder with 68% yield (Scheme 3.2/b). ^1H and ^{13}C NMR spectra for **3**, acquired in CD_2Cl_2 at room temperature and -60°C confirmed the asymmetric coordination of the allyl-moiety, due to the presence of different ligands (*i.e.* chloride and pyridine) coordinating *trans* to it.¹⁵¹ The reaction of **3** with either **L1** or **L2** in the presence of NaBAr'_4 ($\text{Ar}' = 3,5\text{-bis(trifluoromethyl)phenyl}$) gave the monocationic, V-shaped homo- and heteroleptic macrocomplexes **4** and **5**, respectively. The successful substitution of the chloride ligand in **3** by **L1** or **L2** was confirmed by ^1H and $^{13}\text{C}\{^1\text{H}\}$ NMR spectra, acquired at room temperature and at -60°C .

The homoleptic star-shaped Pd(II) macrocomplexes (*i.e.* **6** and **7**) were obtained upon reaction of **1** and **2** with two molequiv. of **L1** and **L2**, respectively, in the presence of $\text{Ag}(\text{SbF}_6)$, while the heteroleptic macrocomplexes (*i.e.* **8** and **9**) were obtained by the reaction of **1** with two molequiv. of **L2** in the presence of either $\text{Ag}(\text{SbF}_6)$ or $\text{Ag}(\text{OTs})$ ($\text{OTs} = p\text{-Toluenesulfonate}$) (Scheme 3.2/c). All star-shaped macrocomplexes were

obtained as light brown powders with yields ranging from 45 to 60%. ^1H and $^{13}\text{C}\{^1\text{H}\}$ NMR spectra acquired for the star-shaped macrocomplexes confirmed the symmetric coordination of the pyridine moieties to the metal centre. The successful coordination of four macroligands to the same Pd(II) centre has been proved by: (i) the ^1H NMR integral ratio between the aromatic tosylate and pyridine hydrogen atoms in **9** (Figure 3.5); (ii) the reaction of **6** with two molequiv. of 1,2-bis(diphenylphosphanyl)ethane (dppe) in CD_2Cl_2 leading to uncoordinated **L1** and $[\text{Pd}(\text{dppe})_2](\text{SbF}_6)_2$,³⁰³ which was the only phosphorus containing compound. Unfortunately, the charged complexes like **4** and **5**, **6-9** proved to be not stable during GPC-analysis, due to the presence of strong shear forces stemming from high-performance packing in size exclusion chromatography.³⁰⁴

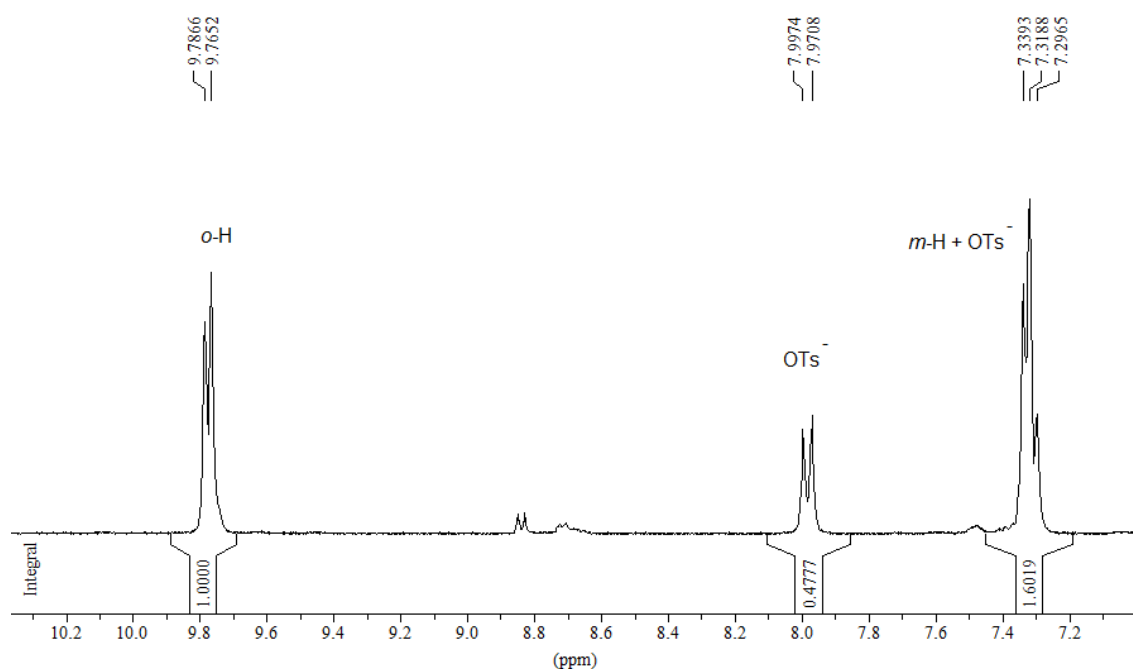


Figure 3.5 – ^1H NMR spectrum (enlargement) of macrocomplex **9**

The stepwise de-coordination of macroligands from V- and star-shaped macrocomplexes has been studied by means of NMR spectroscopy. To this purpose, **4** was reacted with one molequiv. of $[\text{N}(n\text{-Bu})_4]\text{Cl}$ in CD_2Cl_2 to give a 1:1 mixture of **3** and uncoordinated **L1**. The corresponding ^1H NMR spectrum, acquired at room temperature, showed for the pyridine moiety two broad singlets centred at 7.35 and 8.72 ppm (Figure 3.6, trace b), due to a dynamic equilibrium between **3** and **L1** at room temperature.

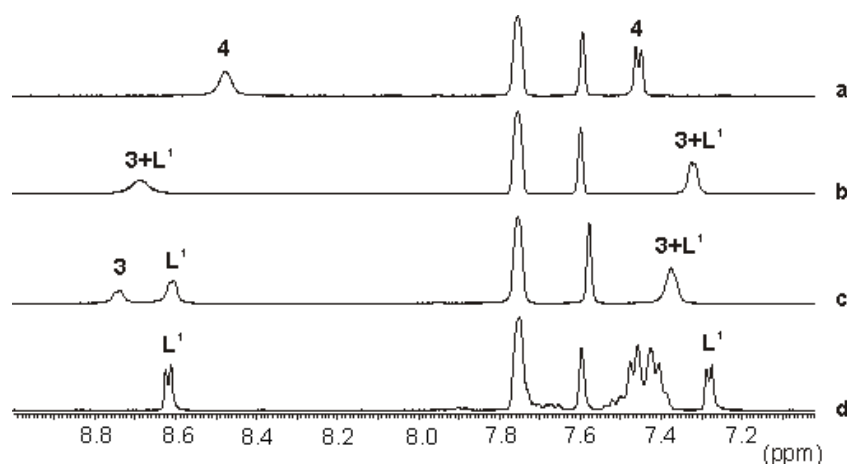


Figure 3.6 – Sequence of ^1H NMR spectra, acquired in CD_2Cl_2 at room temperature, in the chemical shift range from 7.00 to 9.00 ppm: (a) **4** at room temperature; (b) after addition of one molequiv. of $[\text{N}(\text{n-Bu})_4]\text{Cl}$ at room temperature; (c) cooling the latter NMR solution to $-70\text{ }^\circ\text{C}$; (d) after addition of one molequiv. of *dppe* at room temperature

Accordingly, the corresponding ^1H NMR spectrum, acquired at $-70\text{ }^\circ\text{C}$, showed for the *ortho*-hydrogen atoms of **3** and **L1** two distinct ^1H NMR doublets at 8.77 and 8.62 ppm, respectively (Figure 3.6, trace c). Upon reaction of **4** with one molequiv. of *dppe*, $[\text{Pd}(\eta^3\text{-allyl})(\text{dppe})]\text{BAR}'_4$ ³⁰⁵ was formed under the quantitative release of **L1** as proved by the corresponding ^1H NMR spectrum (Figure 3.6, trace d).

The addition of two molequiv. of $[\text{N}(\text{n-Bu})_4]\text{Cl}$ to a CD_2Cl_2 solution of **6** led to a 1:1 mixture of **1** and uncoordinated **L1** (Figure 3.7, trace b).

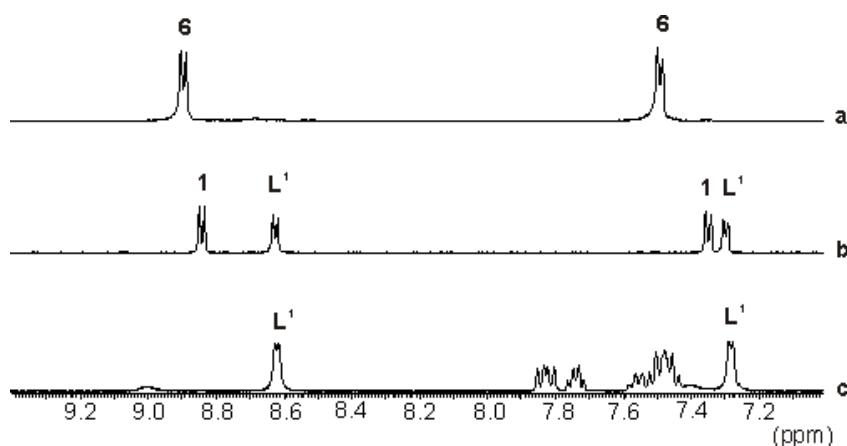


Figure 3.7 – Sequence of ^1H NMR spectra, acquired in CD_2Cl_2 at room temperature, in the chemical shift range from 7.10 to 9.30 ppm: (a) **6**; (b) after addition of two molequiv. of $[\text{N}(\text{n-Bu})_4]\text{Cl}$; (c) after addition of two molequiv. of PPh_3 to the 1:1 mixture of **1** and **L1**

The successive addition of two molequiv. of PPh_3 to the latter NMR solution brought about the quantitative transformation of **1** into *trans*- $[\text{PdCl}_2(\text{PPh}_3)_2]$ ³⁰⁶ and uncoordinated **L1** (Figure 3.7, trace c).

The thermal behaviour of the macroligands and the corresponding Pd(II)-macrocomplexes has been analyzed by DSC and the results are reported in Table 3.1.

Entry ^a	Sample	T _m (°C)	T _c (°C)	ΔH _m (J/g)	ΔH _c (J/g)	χ _c (%) ^b
1	L1	139.8	96.8	46.8	-31.9	84.1
2^c	L2	-	-	-	-	-
3	1	141.2	115.3	38.2	-35.1	78.3
4	4	143.7	110.0	38.9	-38.1	82.3
5	5	142.7	117.8	9.1	-9.2	19.5
6	6	143.4	120.3	26.7	-24.3	54.5
7^c	7	-	-	-	-	-
8^c	8	-	-	-	-	-

^a Second heating carried out in the temperature range from 40.0 to 200.0 °C with a heating rate of 20.0 °C/min. ^b Crystallinity calculated applying the formula: $100 \times (\Delta H_m - \Delta H_c) / \Delta H_m^0$ with $\Delta H_m^0 = 93.6 \text{ J/g}$.³⁰⁷ ^c Amorphous material.

Table 3.1 – DSC analysis of L1, L2, 1 and 4-8

From a perusal of Table 1 arises that: (i) the homoleptic macrocomplexes containing **L1** (*i.e.* **1**, **4** and **6**) showed a higher melting (T_m) and crystallization temperature (T_c) compared to **L1**, due to an increase of the molecular weight upon macrocomplex formation; (ii) **6** showed the lowest crystallinity (χ_c), which is mainly due to the higher number of end groups present in **6** compared to **1** and **4** and to the presence of two counter-ions per palladium (Table 3.1, entry 6 vs 3 and 4);³⁰⁸ (iii) the heteroleptic macrocomplexes (**5**, **7** and **8**) showed a significantly lower value of crystallinity compared to the corresponding homoleptic counterpart (Table 3.1, entry 5 vs 4 and 8 vs 6; Figure 3.8), confirming the influence of **L2** on the crystallization behaviour of **L1** in the macrocomplexes;³⁰⁹ (iv) **L2** and **7** were found to be, as expected, completely amorphous.

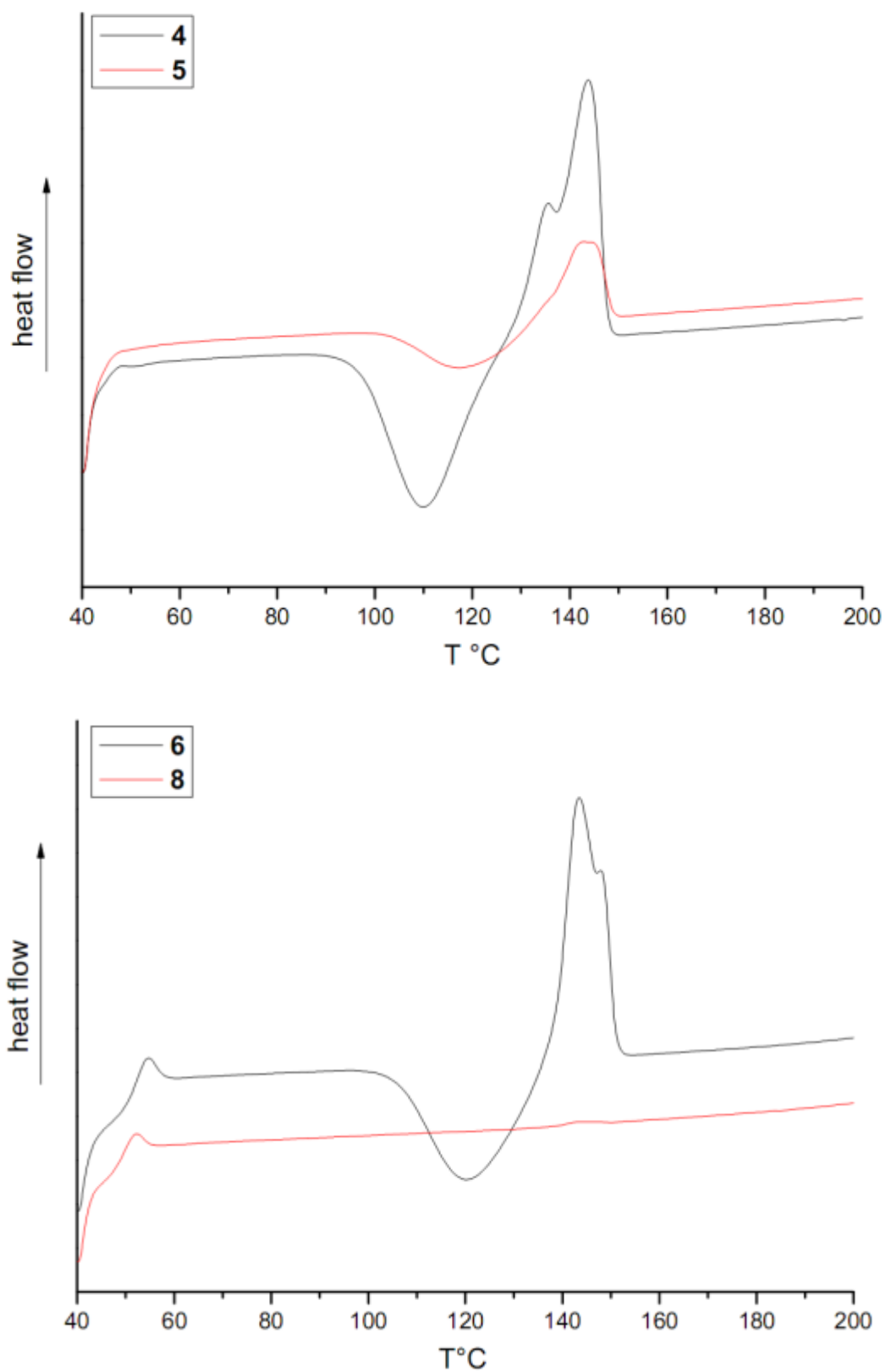


Figure 3.8 – DSC analysis (2nd heating) of 4/5 (top) and 6/8 (bottom)

Preliminary morphologic studies have been carried out on crude samples of **1** and **8** by means of transition electron microscopy. Representative TEM images for both samples

are shown in Figure 3.9.

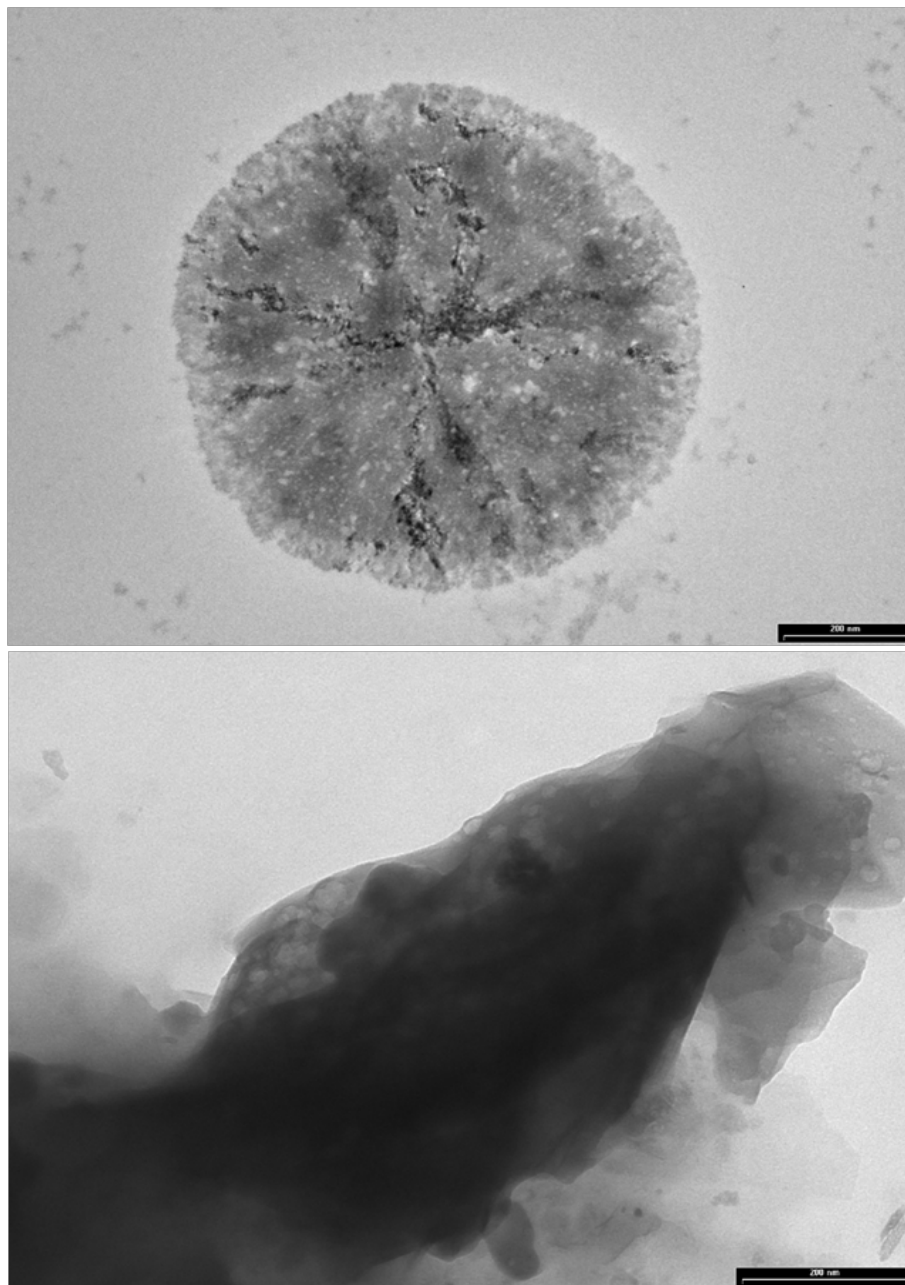


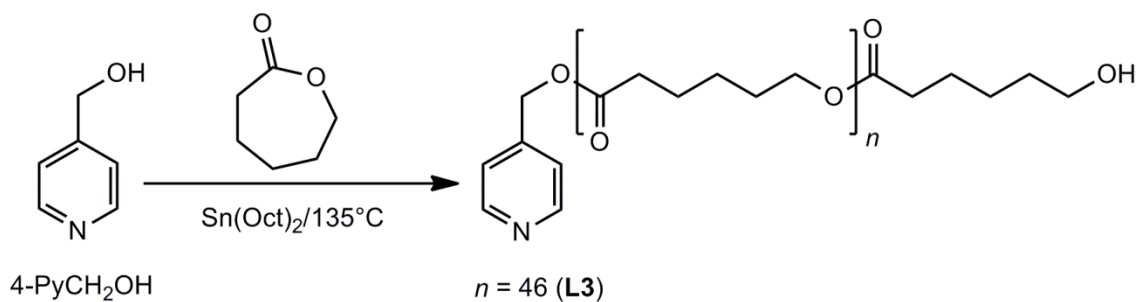
Figure 3.9 – TEM images of **1** (top) and **8** (bottom); scale bar = 200 nm.

The crystalline compound **1** consisted of spherulites (*i.e.* three-dimensional assembly composed of crystalline and amorphous regions),³¹⁰ whereas **8** proved to be featureless, which is in accordance with the lack of crystallinity.

3.1.2 Macrocomplexes combining P(L)LA- and PCL-based macroligands

The Ring Opening Polymerization of ϵ -caprolactone carried out in bulk in the presence of 4-PyCH₂OH and catalyzed by Sn(Oct)₂ gave the 4-pyridinemethylene-end-capped

PCL-based macroligand **L3** ($M_n = 5400$ g/mol, PDI = 1.25) (Scheme 3.3). The synthetic procedure resembles closely the one described for PLA as the ROP mechanism is analogous for any cyclic lactone. Nonetheless, a slight modification in the work-up procedure was necessary to obtain suitably pure PCL: hexane was replaced by methanol as the non-solvent for the polymer precipitation. Indeed, when alkanes were employed to precipitate PCL a small amount (*i.e.* about 10%) of unreacted 4-PyCH₂OH precipitated too and contaminated the product; on the other hand, methanol was miscible enough with the free oxydrylic initiator to avoid contamination of the precipitate. The reason for the decreased reactivity of 4-PyCH₂OH should be further investigated and may be related to the different thermodynamic parameters involved in the ROP of PCL with respect to PLA. As already described for PLA, in PCL obtained by methanol precipitation, the successful end-capping of the polymer chains with a 4-pyridinemethylene moiety was proved by ¹H- and ¹³C NMR spectroscopy (Figure 3.10). As a result, a high-frequency shift of the ¹H and ¹³C NMR singlet, assigned to PyCH₂O-Poly compared to PyCH₂OH was observed (*i.e.* from 4.73 / 62.5 ppm to 5.14 / 64.0 ppm).



Scheme 3.3 –ROP of ϵ -caprolactone for the synthesis of macroligand **L3**

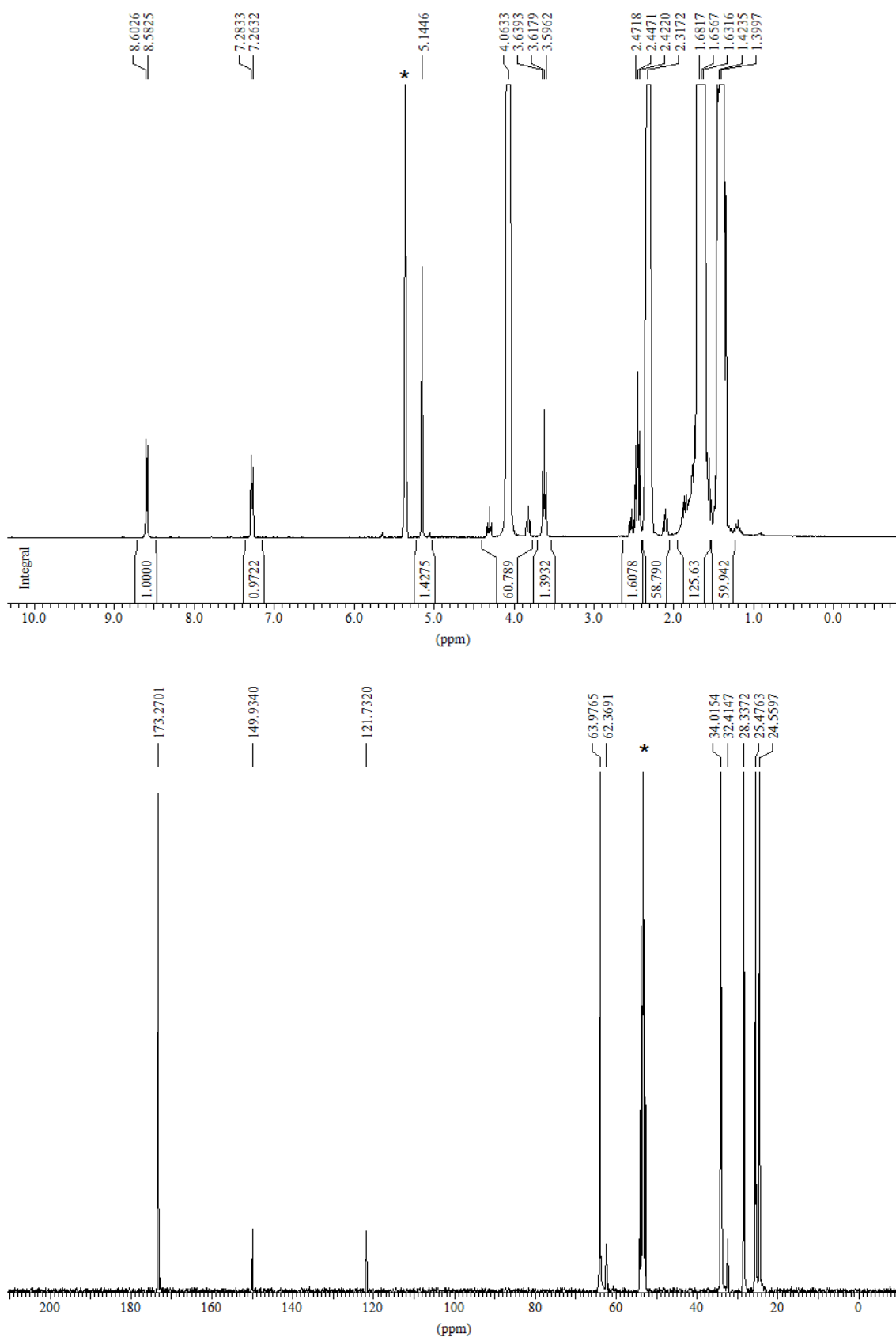
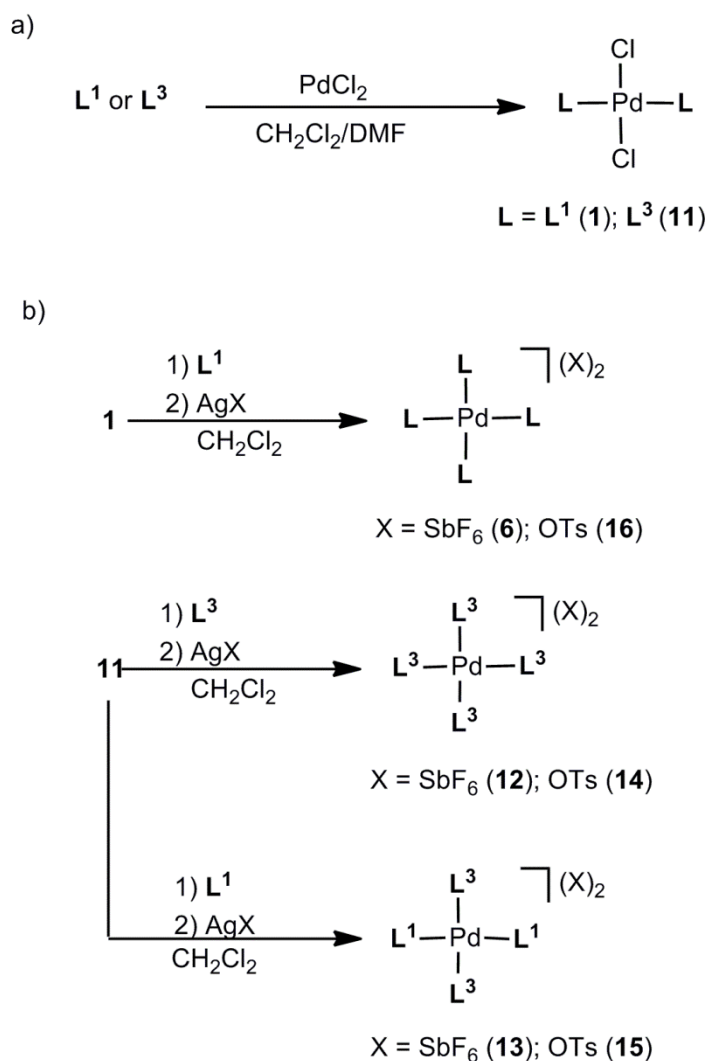


Figure 3.10 – ¹H NMR (top) and ¹³C NMR (bottom) spectra of PCL-based macroligand L3 in CD₂Cl₂

The 1:2 stoichiometric reaction between PdCl₂ and L3 carried out in a 3:1 solvent

mixture of CH_2Cl_2 and DMF gave *trans*- $[\text{PdCl}_2(\text{L}3)_2]$ (**11**) (Scheme 3.4/a) as a light brown flaky solid with 88% yield. The homoleptic star-shaped PCL-based Pd(II) macrocomplexes (*i.e.* **12** and **14**) were obtained upon reaction of **11** with two molequiv. of **L3** in the presence of $\text{Ag}(\text{SbF}_6)$ or $\text{Ag}(\text{OTs})$ respectively, while the heteroleptic macrocomplexes (*i.e.* **13** and **15**) were obtained by the reaction of **11** with two molequiv. of **L1** in the presence of either $\text{Ag}(\text{SbF}_6)$ or $\text{Ag}(\text{OTs})$ ($\text{OTs} = p\text{-Toluenesulfonate}$). Additionally, in order to complete the available combination possibilities and better investigate the influence of the anion on thermal properties, the homoleptic star-shaped PLA-based macrocomplex **16** was obtained upon reaction of **1** with two molequiv. of **L1** in the presence of $\text{Ag}(\text{OTs})$ (Scheme 3.4/b). All star-shaped macrocomplexes were obtained as light brown powders with yields ranging from 50 to 75%.



Scheme 3.4 – Synthesis of Pd(II) macrocomplexes bearing P(L)LA- and PCL-based macroligands

GPC-RI measurements carried out on **11** ($M_n = 11690$ g/mol, PDI = 1.20) proved a two-

fold increase of the molecular weight compared to the corresponding uncoordinated macroligand **L3**, maintaining a low PDI and confirming the observations reported for the behaviour of the two PLA-based counterparts **1** and **L1** (Figure 3.11).

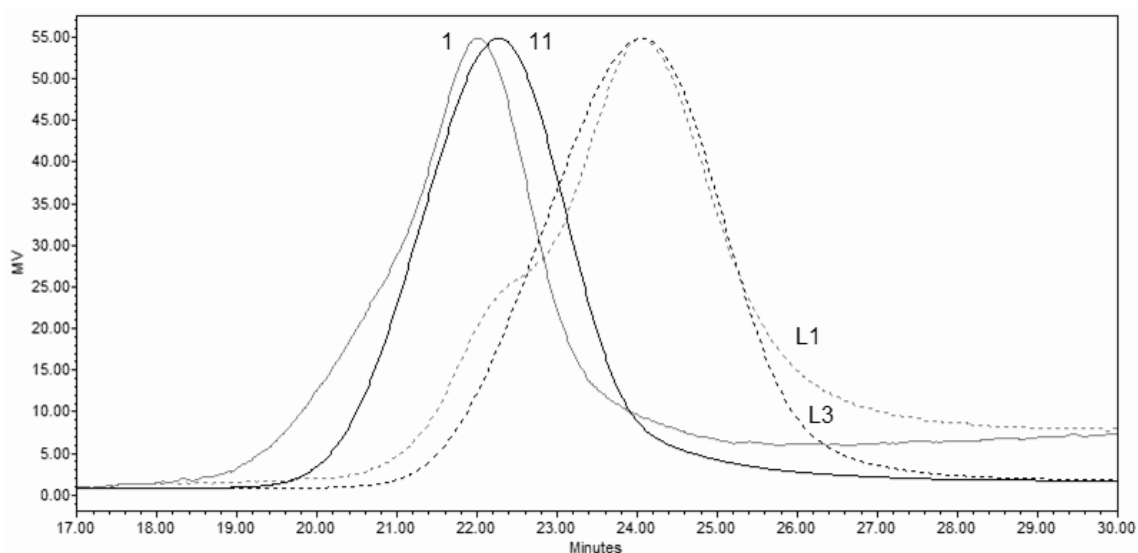
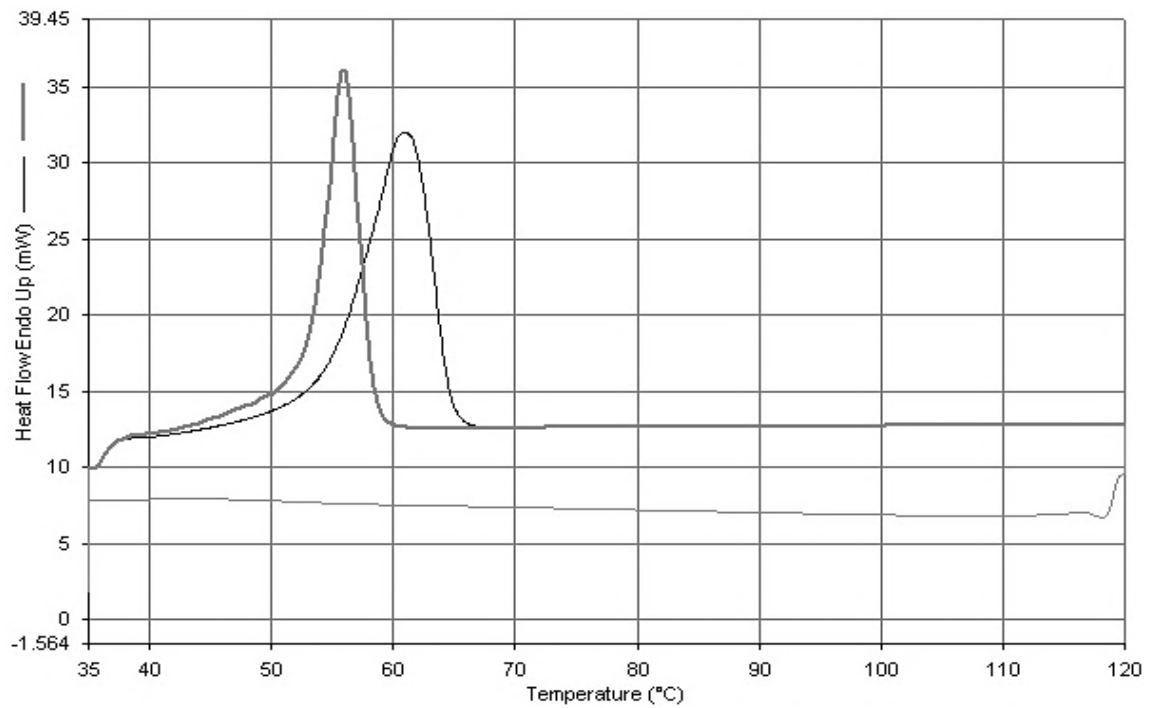
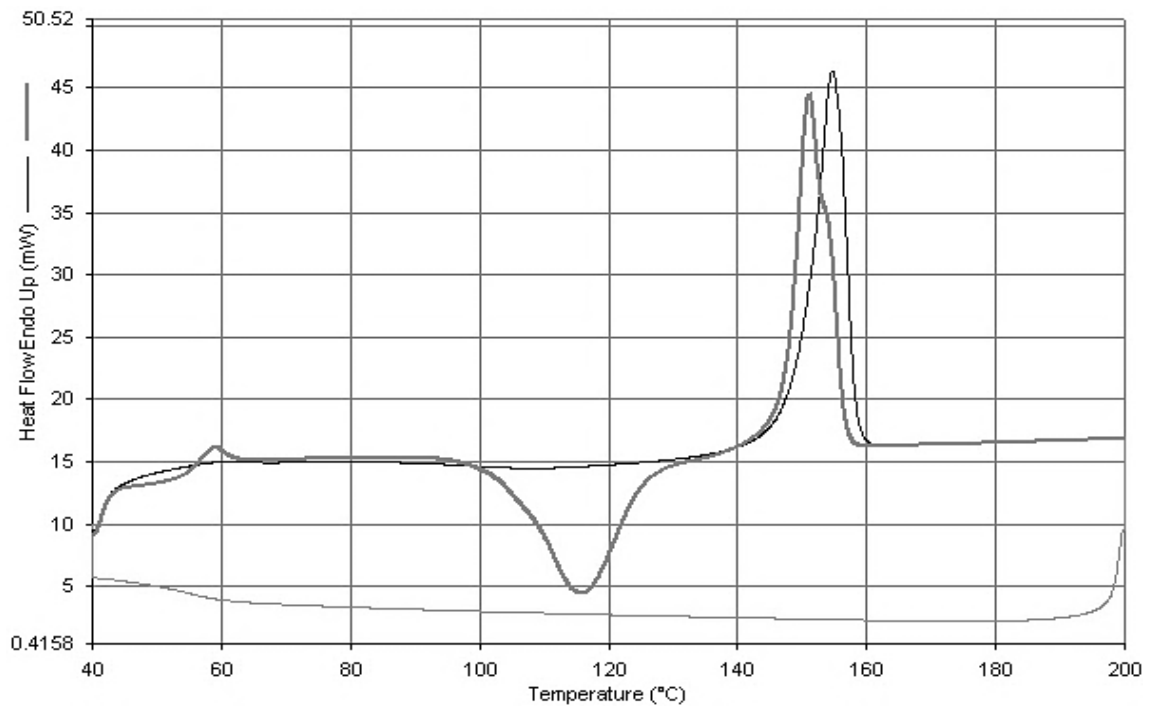


Figure 3.11 – GPC curves of **1**, **11**, **L1** and **L3** acquired with a RI-detector

The chief aim of combining macroligands based on polymers with different chemical nature was to investigate the effect of heteroleptic complexation (which yields a star-shaped PCL-PLA copolymer) on the crystallinity and thermal properties of the resulting products. As a result, according to DSC analyses (Figure 3.12; Table 3.4): (i) the neutral macrocomplexes **1** and **11** have an analogous degree of crystallinity compared to the PLA- or PCL-based macroligands **L1** and **L3**, while the homoleptic star-shaped complexes show a markedly lower crystallinity (**12** and **13** vs **L3**, **6** and **16** vs **L1**), probably on account of the hindered anions surrounding the charged complex; on the other hand, transition temperatures are similar; (ii) the heteroleptic complexes **13** and **15** show properties that are quite similar to those of a 1:1 mix of **1** and **11** demonstrating how micro-phase separation does not hamper the organization of P(L)LA and PCL chains into crystalline domains which are formed even after the supramolecular copolymer is synthesized by complexation to Pd(II); (iii) the difference in crystallinity due to the replacement of SbF_6^- with OTs^- appears to be very small and non univocal (Table 3.2, samples **6** vs **16**, **12** vs **14** and **13** vs **15**).



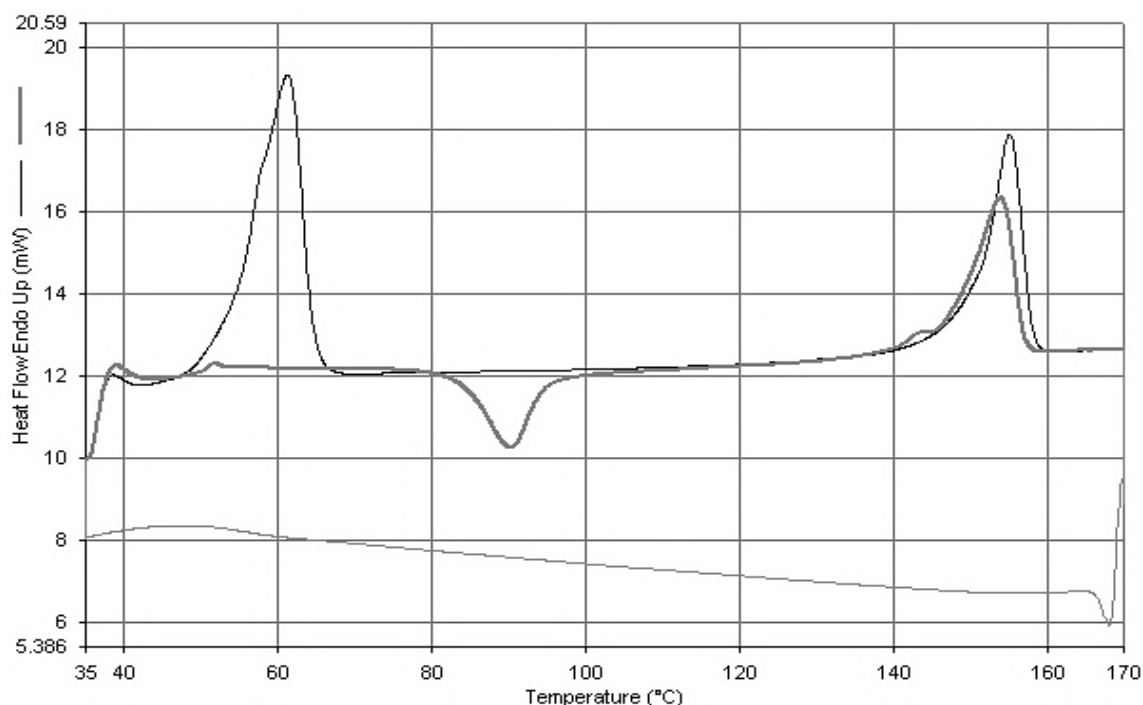


Figure 3.12 – DSC curves of **6** (top), **12** (middle) and of **15** (bottom); 1st heating (black), 2nd heating (grey) and cooling (light grey)

Sample	T_{c2} (°C)**	T_{m1} (°C)*	T_{m2} (°C)**	χ_c (%)#
L1	86.9	153.0	149.0	71.6
L3	-	59.7	52.3	79.1
L1+L3 (1:1)	-	150.1 + 59.8	151.7 + 50.9	33.5 + 45.1
1	113.6	154.3	148.0	68.2
11	-	62.9	53.0	78.2
6	123.3	154.3	150.4	57.4
16	115.8	154.7	151.2	62.4
12	-	60.9	56.1	69.5
14	-	62.1	55.7	67.8
13	92.6	155.0 + 59.0	153.7 + 51.8	29.7 + 43.6
15	90.3	155.1 + 61.2	154.0	28.3 + 45.2

* first heating; ** second heating; # $100 \times (\Delta H_m - \Delta H_c) / \Delta H^0_m$, on first heating, with $\Delta H^0_m = 93.6$ J/g and 139.3 J/g for 100% crystalline PLA and PCL, respectively.

Table 3.2 – Melting and crystallization temperatures and degree of crystallinity of P(L)LA- and PCL-based macroligands and macrocomplexes

Interestingly, it was possible to confirm the crystalline structure of P(L)LA and PCL domains of **13** and **15** (Figure 3.13, top to bottom) while following their sequential melting by means of XRPD analyses at variable temperature under protected (N_2)

atmosphere. At room temperature, the sample contains both P(L)LA and PCL crystalline domains, as witnessed by the typical XRPD peaks at $2\theta = 16.5^\circ$; 18.8° (PLA) and $2\theta = 21.1^\circ$; 23.5° (PCL). As the temperature is progressively increased (heating rate = $20^\circ\text{C}/\text{min}$; one XRPD scan every 20°C) PCL melts completely and independently from PLA; while at 65°C only PLA remains crystalline, at 165°C the product is completely melted and no XRPD peak is visible anymore. Upon cooling to 25°C (cooling rate = $20^\circ\text{C}/\text{min}$; steps of 20°C) only PCL crystallizes while PLA solidifies retaining an amorphous structure, indicating how crystallization kinetics differ between the two polymers (the more flexible PCL chains appear to crystallize more rapidly). It is worth noting that ^1H NMR spectra recorded after 2 heating / cooling cycles from 25°C to 165°C showed that the signals of both complexes (*i.e.* **13** and **15**) remained practically unchanged and no significant decomplexation took place with the treatment.

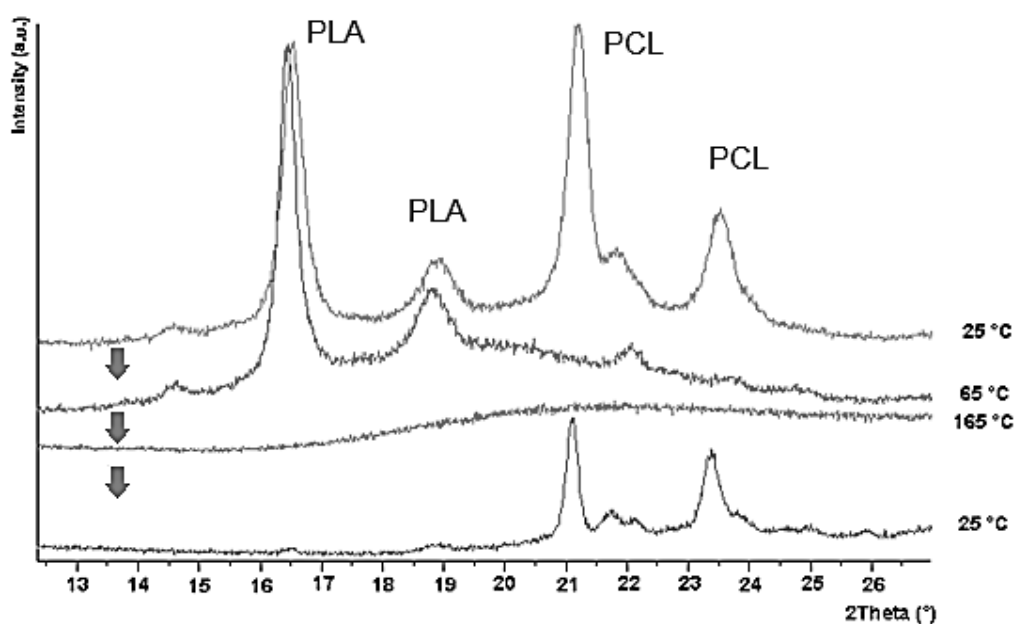
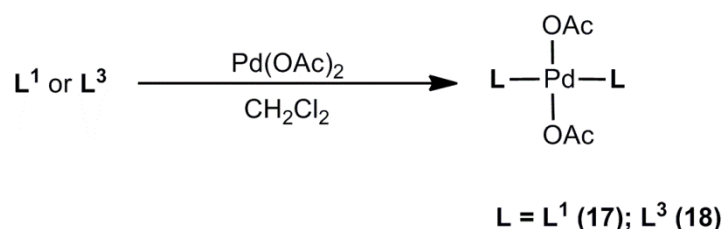


Figure 3.13 – XRPD spectra of **15** obtained by heating the sample to 165°C and consequently cooling to 25°C

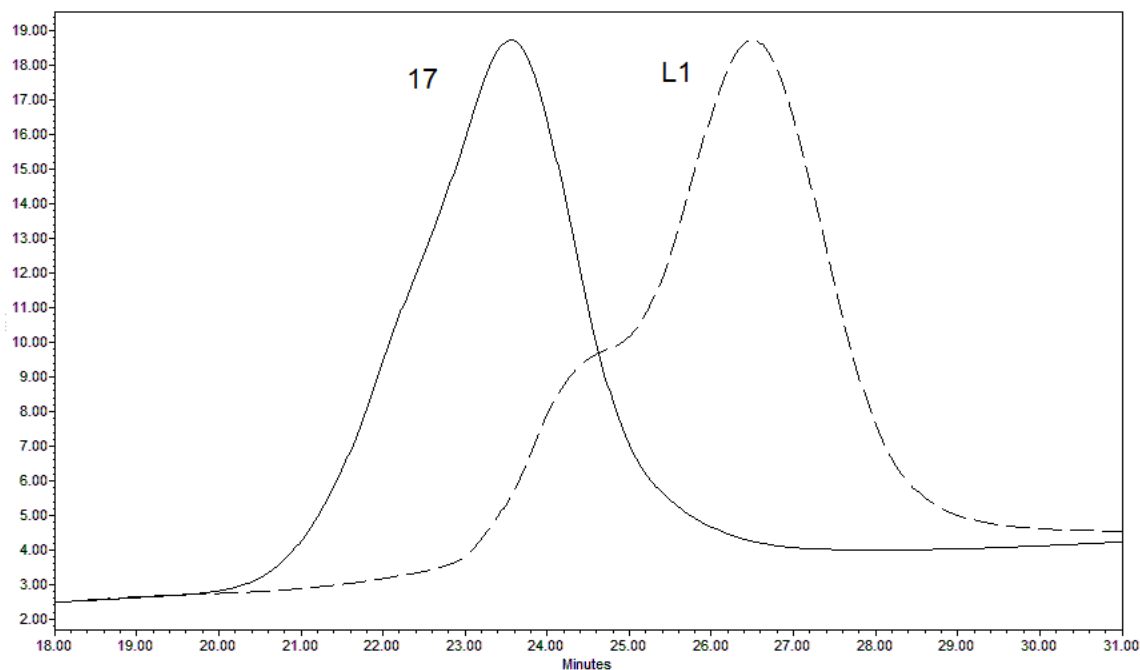
3.2 Aerobic oxidation of alcohols catalyzed by PLA-based Pd macrocomplexes

The P(L)LA- and PCL-based macroligands **L1** and **L3** described in the previous paragraphs were used to coordinate $\text{Pd}(\text{OAc})_2$ in CH_2Cl_2 , obtaining the corresponding macrocomplexes of the formula *trans*- $[\text{Pd}(\text{OAc})_2(\text{L1})_2]$ (**17**) and *trans*- $[\text{Pd}(\text{OAc})_2(\text{L3})_2]$ (**18**) (Scheme 3.5) as beige and brown powders with 95 and 83% yield, respectively. The formation of either complex in CH_2Cl_2 was followed by UV-Vis spectroscopy, showing for both macroligands a rapid $\text{Pd}(\text{OAc})_2$ coordination (*i.e.* c.a. 80% $\text{Pd}(\text{OAc})_2$

coordination within the first 3 min of reaction time). GPC analyses carried out on **17** and **18** (Figure 3.14) showed, roughly, a doubling of the molecular weight compared to the corresponding macroligands (**L1**: M_n : 3280 g/mol; PDI: 1.33. **L3**: M_n : 5400 g/mol; PDI: 1.25. **17**: M_n : 10020 g/mol; PDI: 1.39. **18**: M_n : 12800 g/mol; PDI: 1.68). Furthermore, the acquisition of the corresponding ^1H NMR spectra in CD_2Cl_2 exhibited a small high frequency shift of the doublets assigned to the *ortho* and *meta* pyridine-hydrogen atoms, (c.a. 0.03 ppm (*o*) and 0.08 ppm (*m*)) compared to **L1** (Figure 3.15) and **L3** as well as the appearance of the singlet related to the methyl group of acetate at about 1.82 ppm (Figure 3.16).



Scheme 3.5 – Synthesis of *trans*-[Pd(OAc)₂(L1)₂] (**17**) and *trans*-[Pd(OAc)₂(L3)₂] (**18**) macrocomplexes



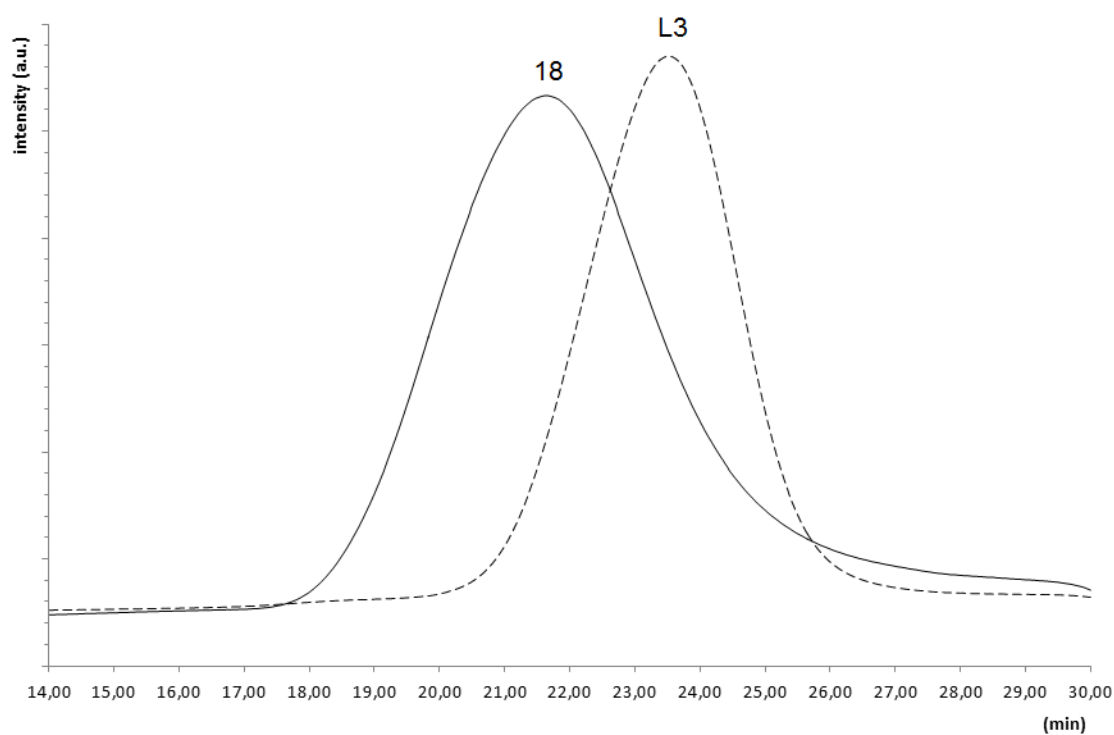


Figure 3.14 – GPC-curves of 17 vs L1 (top) and 18 vs L3 (bottom) acquired with a RI-detector

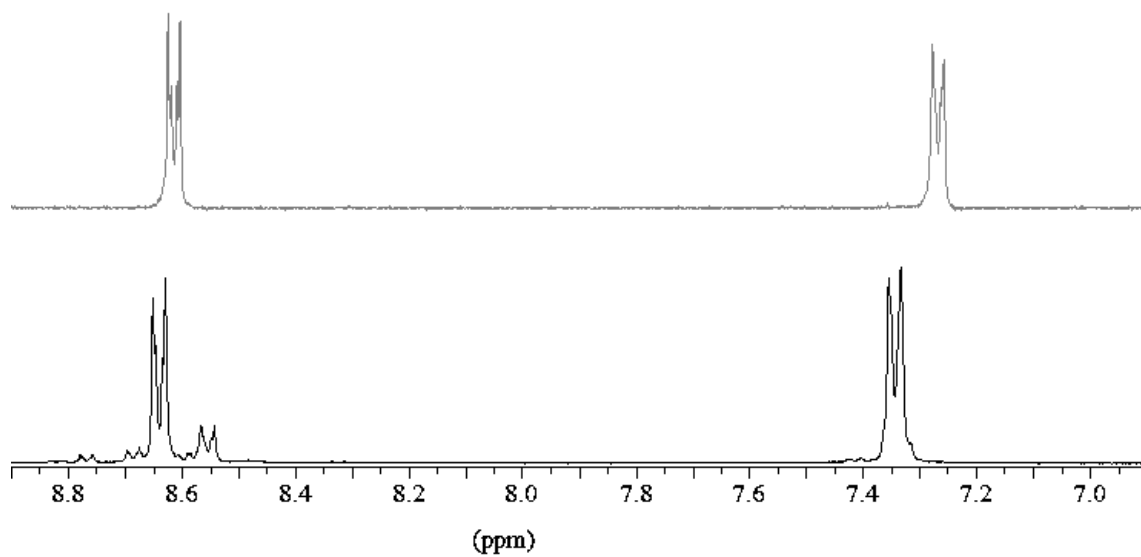


Figure 3.15 – ^1H NMR signals of the ortho and meta aromatic protons in L1 (top) and 17 (bottom)

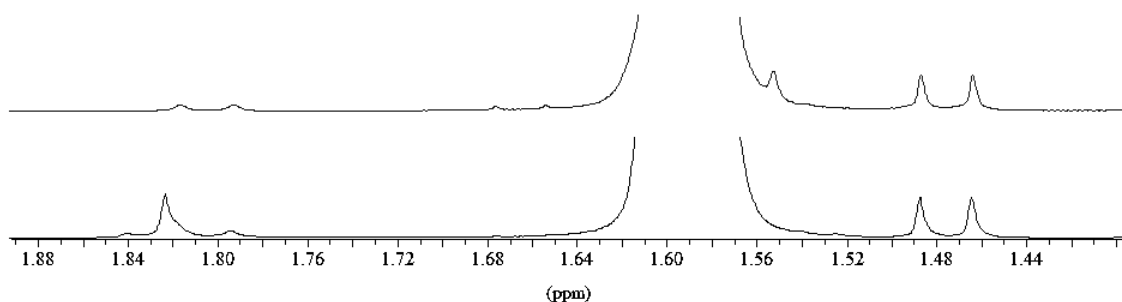


Figure 3.16 – ^1H NMR signals of **L1** (top) and **17** (bottom) in the 1.4 – 1.9 ppm spectral region

The *trans*-coordination of the macroligands to each other in **17** and **18** has been confirmed by UV-Vis spectroscopy (Figure 3.17) and corresponds to what has been found for the related PdCl_2 -based macrocomplexes. In fact, UV-Vis spectra of CHCl_3 solutions of **17** and **18** showed a shoulder centered at c.a. 330 nm which matches the absorption peak of *trans*- $[\text{Pd}(\text{OAc})_2(4\text{-EtPy})_2]$ (4-EtPy = 4-ethylpyridine) (**19**).¹⁵¹ The UV-Vis absorption of **18** at c.a. 310 nm (shoulder) stems from **L3** which, unlike **L1**, shows a weak UV-Vis absorption shoulder at the latter wavelength.

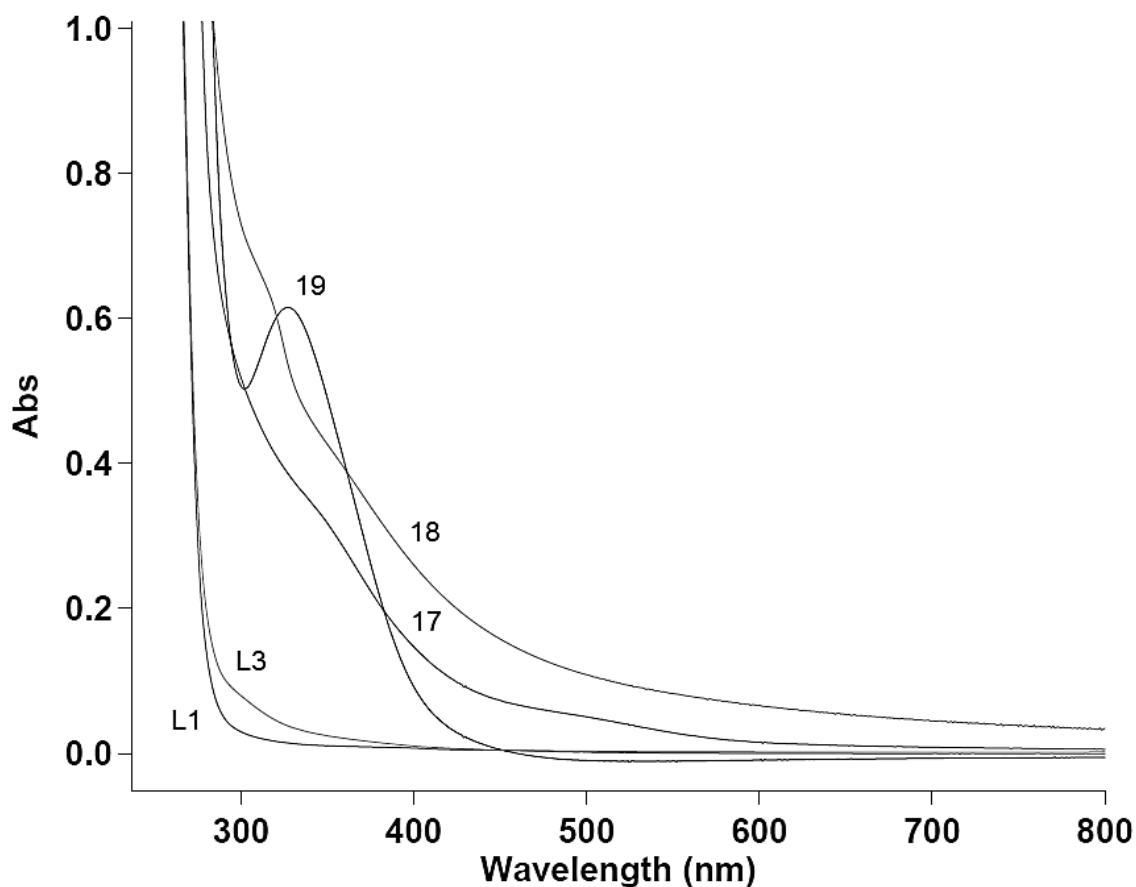


Figure 3.17 - UV-Vis spectra of **L1**, **L3**, **17-19** acquired in CHCl_3

The complexation reaction between the pyridine end group of macroligands and $\text{Pd}(\text{OAc})_2$ was quite rapid, as demonstrated by UV-Vis analyses carried out shortly after the mixing of the two reactants (Figure 3.18). Indeed, the evolution in the UV-Vis absorption spectrum during the first 3 minutes of reaction was much greater than the evolution of the system during the following 27 min.

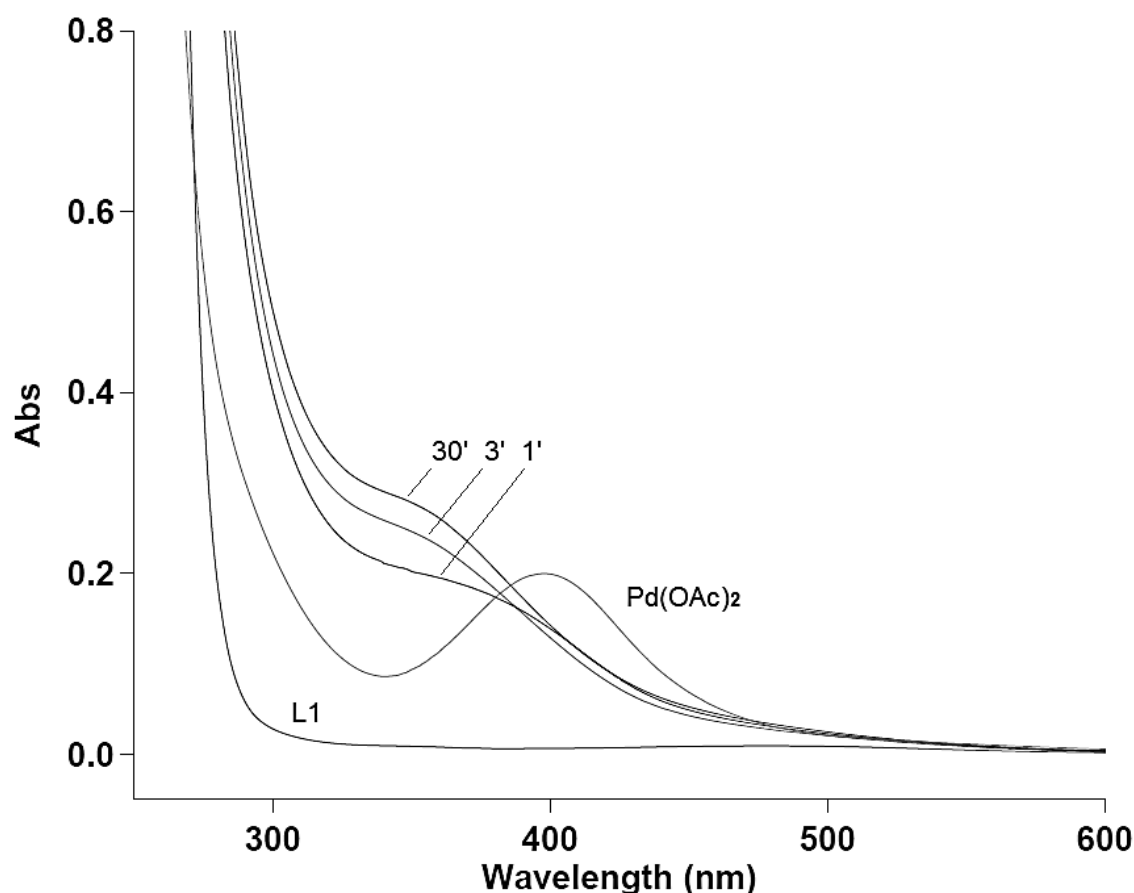


Figure 3.18 – UV-Vis spectra of L1, Pd(OAc)₂, and the resulting complex 17 acquired in CHCl₃ after 1, 3 and 30 min from the mixing time

The thermal behaviour of **L1**, **L3**, **17** and **18** has been studied by TG and DSC analyses. TG analyses were carried out in the temperature range from 30 to 600 °C and in the presence of air, showing for **L1** and **L2** a degradation temperature (T_d) of c.a. 288 and 373 °C, respectively. Interestingly, the corresponding macrocomplexes showed an even higher T_d of c.a. 353 °C (**17**) and 403 °C (**18**) (Figure 3.19; Table 3.3). This experimental finding corroborates the fact that, unlike Sn, Zn and Fe species,³¹¹ Pd does not catalyse intra- and intermolecular transesterification reactions in the solid state,^{312,313} which would lead to the formation of short chain polyesters characterized by a significantly lower T_d compared to **L1** and **L3**.

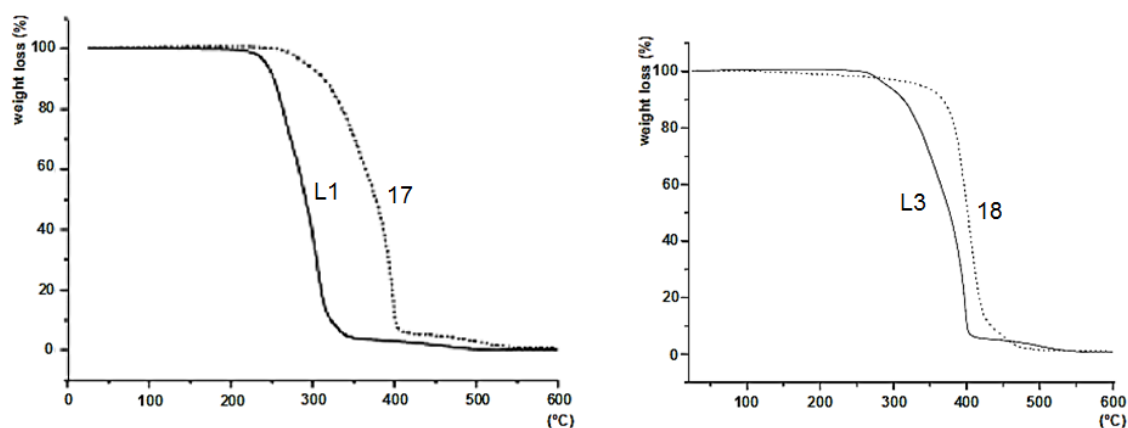


Figure 3.19 – TGA curves of 17 vs L1 (left) and of 18 vs L3 (right)

Sample	T _d (mid-point) (°C)	Residue (%)
L1	287.8	0.15
L3	372.7	0.77
17	353.4	3.20
18	402.9	1.04

Table 3.3 – TG analyses of L1, L3, 17 and 18

ICP-MS analyses showed a Pd content of 1.52 wt% and of 0.94 wt% for **17** and **18**, respectively. DSC measurements of **L1**, **L3**, **17** and **18** revealed the typical thermal behaviour of PLA³⁰⁷ and PCL.³¹⁴ The degree of crystallinity of the macrocomplexes revealed to be slightly higher compared to the corresponding macroligand: 45.8% (**L1**) vs 57.7% (**17**) and 45.7% (**L2**) vs 50.2% (**18**), indicating that the presence of the polymer chain-linking Pd(OAc)₂ unit does not significantly alter the crystallization behaviour of PLA and PCL (Table 3.4).

Sample	T _g (°C)	T _c (°C)	T _m (°C)	ΔH _m (J/g)	ΔH _c (J/g)	χ _c (%) ^b
L1	n.d.	99.8	149.6	42.9	-38.0	45.8
17	49.7	96.0	147.3	54.0	-34.0	57.7
L3	-68.6	34.3	54.5	63.7	-57.8	45.7
18	-66.2	31.4	54.8	70.0	-60.6	50.2

^a Second heating carried out in the temperature range from -10.0 to 200 °C (**L1** and **17**) and from -100.0 to 120 °C (**L3** and **18**) applying a heating rate of 10 °C/min. ^b The degree of crystallinity (χ_c) expressed in percentage was calculated applying the formula: χ_c = 100 × ΔH_m/ΔH^o_m, with ΔH^o_m = 93.6 J/g and 139.3 J/g for 100% crystalline PLA and PCL, respectively.

Table 3.4 – DSC analyses of L1, L3, 17 and 18

In order to ascertain the stability of the macroligands against transesterification,³¹² hydrolysis^{310,315} and alcoholysis reactions, **L1** and **L3** were tested under real catalytic aerobic oxidation conditions (*i.e.* 70 °C, toluene, air (4 bar)) in the presence of various non-dried alcohols (benzyl alcohol or cinnamyl alcohol or 1-hexanol) using an alcohol : macroligand molar ratio of 1600 : 1. Stability tests were performed by GPC analysis and ¹H NMR spectroscopy and the outcome was not significantly influenced by the type of alcohol employed. A comparison of GPC traces before and after treatment of **L1** and **L3** with benzyl alcohol under real catalytic conditions is shown in Figure 3.20.

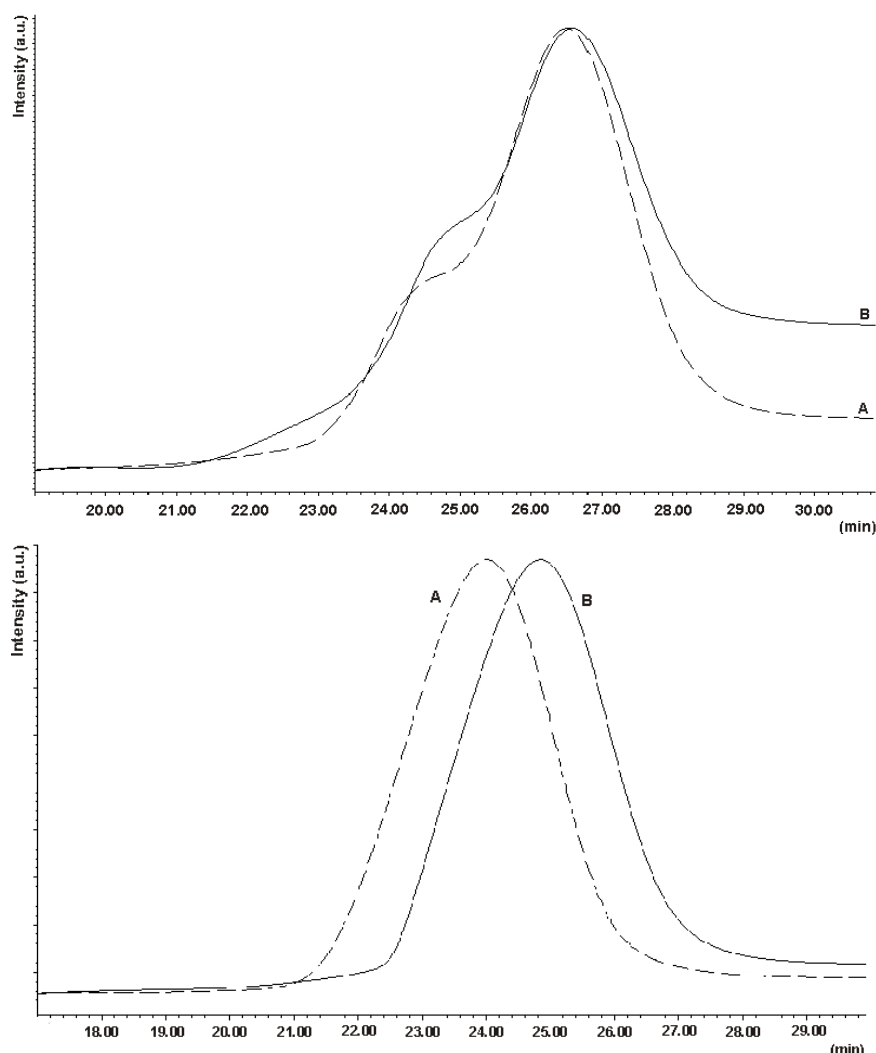
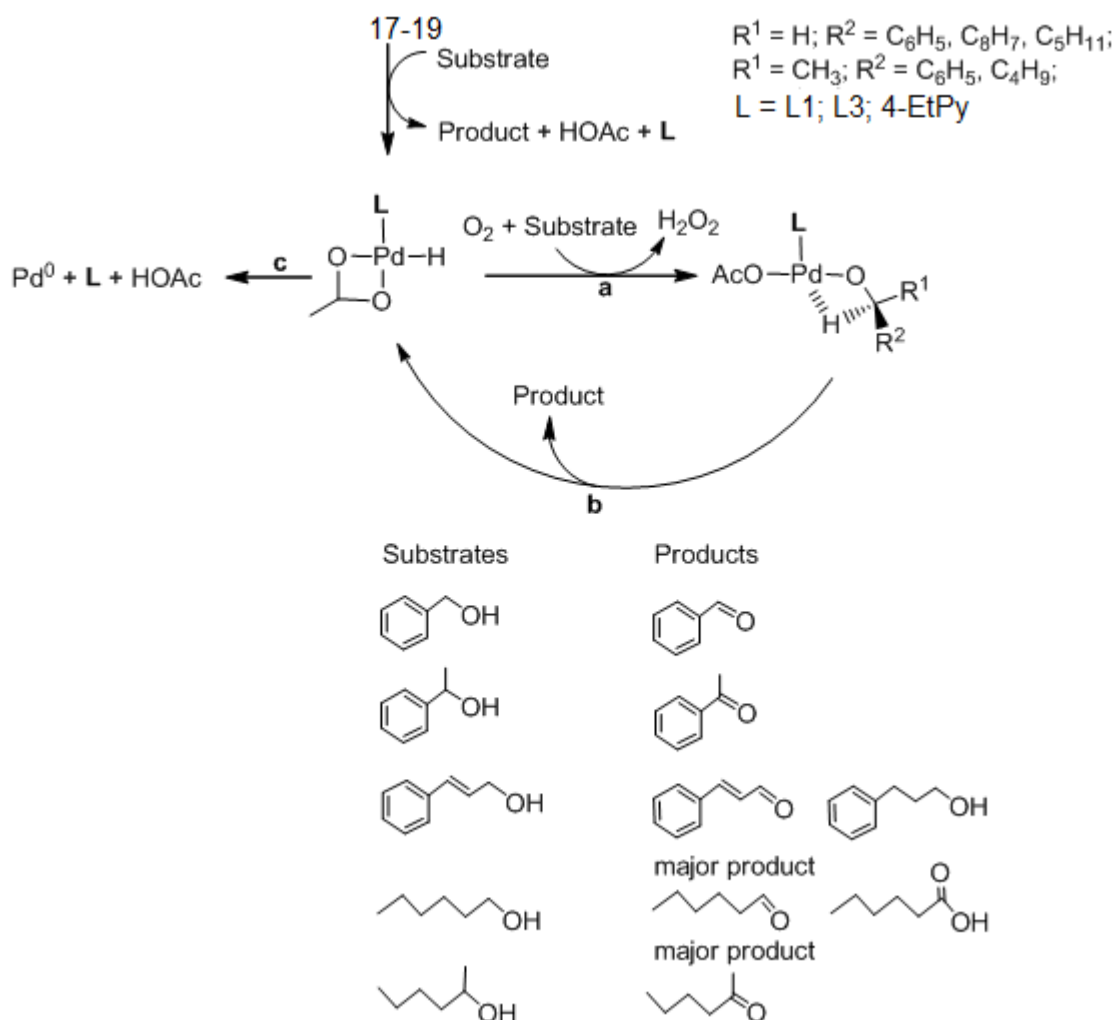


Figure 3.20 – GPC traces of **L1** (top) and **L3** (bottom): (A) **L1** and **L3** as-synthesized; (B) after treatment with benzyl alcohol under real catalytic conditions

As a result, **L1** was stable under real catalytic conditions (Figure 3.20, top), whereas in the case of **L3** the maximum of the molar mass distribution was shifted, after the test reaction, to higher retention time compared to untreated **L3** (Figure 3.20, bottom). This

experimental finding is in accordance with a decrease of M_n from 5400 to 4470 g/mol in the case of **L3**. An analogous test reaction with **L3** carried out in the absence of an alcohol substrate led to an identical experimental outcome, confirming that the decrease of M_n in the case of **L3** is due to transesterification and to alcoholysis reactions. The integration of the ^1H NMR spectra of **L1** and **L3** completely supported the outcome of the GPC analyses. Furthermore, all ^1H NMR spectra of treated **L1** and **L3** witnessed the presence of the end-capping 4-pyridinemethylene moiety in the polymer chain.

Macrocomplexes **17** and **18** were used to catalyse the aerobic oxidation of selected primary and secondary alcohols to aldehydes (major compound) and ketones, respectively (Scheme 3.6). In the case of cinnamyl alcohol and 1-hexanol, 3-phenyl propanol and 1-hexanoic acid have been obtained as minor products, respectively. In order to evaluate the catalytic performance of **17** and **18** under homogeneous catalytic conditions (*i.e.* **17** and **18** are completely soluble under catalytic conditions: toluene, 70 °C, air (4bar)), **19** was introduced as reference catalytic system and all catalytic reactions were carried out in the same experimental conditions. The results of the comparative catalytic study are reported in Table 3.5.



Scheme 3.6 – Aerobic alcohol oxidation catalyzed by 17-19

Entry ^a	Precatalyst	Substrate	Conv (%) / TOF ^b		Sel (%)	
			18 h	36 h	18 h	36 h
1	17	Benzyl alcohol	47	70		
2	18	Benzyl alcohol	15	28		
3	19	Benzyl alcohol	47	60		
4	17+2L1	Benzyl alcohol	23/20	44/20		
5	19+2(4-EtPy)	Benzyl alcohol	21/19	29/13		
6	17	1-Phenylethanol	47	69		
7	18	1-Phenylethanol	12	20		
8	19	1-Phenylethanol	43	62		
9	17+2L1	1-Phenylethanol	24/21	47/21		
10	19+2(4-EtPy)	1-Phenylethanol	28/25	35/15		
11	17	Cinnamyl alcohol	38	77	94 ^c	88 ^c

12	19	Cinnamyl alcohol	40	52	93 ^c	85 ^c
13	17+2L1	Cinnamyl alcohol	22/20	43/19	97 ^c	97 ^c
14	19+2(4-EtPy)	Cinnamyl alcohol	16/14	22/10	94 ^c	87 ^c
15	17	1-Hexanol	10	21	72 ^d	53 ^d
16	19	1-Hexanol	12	16	84 ^d	71 ^d
17	17+2L1	1-Hexanol	8/7	15/7	78 ^d	64 ^d
18	19+2(4-EtPy)	1-Hexanol	10/9	11/5	88 ^d	83 ^d
19	17	2-Hexanol	23	46		
20	19	2-Hexanol	23	38		
21	17+2L1	2-Hexanol	20/18	38/17		
22	19+2(4-EtPy)	2-Hexanol	22/20	29/13		

^a Catalytic conditions: Precatalyst (0.005 mmol), substrate (8.00 mmol), T (70 °C), toluene (5 mL), p(air) (4 bar). ^b TOF expressed in h⁻¹. ^c Selectivity referred to cinnamyl aldehyde. ^d Selectivity referred to 1-hexanal.

Table 3.5 – Aerobic oxidation of alcohols catalyzed by 17-19

Table 3.5 shows that **17**-catalyzed aerobic oxidation reactions led to much higher substrate conversion compared to **18** (Table 3.5, entries 1 and 6 vs 2 and 7). This experimental finding, which is reported here only for benzyl alcohol and 1-phenylethanol, applied also to the other alcohols studied herein. The much lower catalytic performance of **18** compared to **17** may be ascribed to the much more flexible polyester chain in **L3** compared to **L1**, which might hinder the substrate access to the palladium centre.

Regardless of the substrate employed, **17**-catalyzed aerobic oxidation reactions showed, mainly after a long reaction time of 36 h, a substrate conversion which is higher than that of **19** (Table 3.5, 1 vs 3, 6 vs 8, 11 vs 12, 15 vs 16, 19 vs 20). Nevertheless in all cases a drop of catalytic activity in **17**- and **19**-catalyzed reactions was observed, due to the formation of palladium black, which is almost inactive under the chosen catalytic conditions. While **19**-catalyzed reactions showed a black precipitation after a reaction time of 36 h, analogous **17**-catalyzed reactions gave, after the same reaction time, a black homogenous toluene solution from which a grey-black solid precipitated after addition of methanol or *n*-pentane to the catalytic solution, while the supernatant was transparent. A comparison of XRPD spectra acquired of the latter polymer material (Figure 3.21, trace a) and of as-synthesized **17** (trace d) showed the presence of a broad Bragg reflection centred at $2\Theta = 38.7^\circ$ (*i.e.* Pd(111), face centred cubic palladium³¹⁶),

confirming the formation of Pd-nanoparticles.

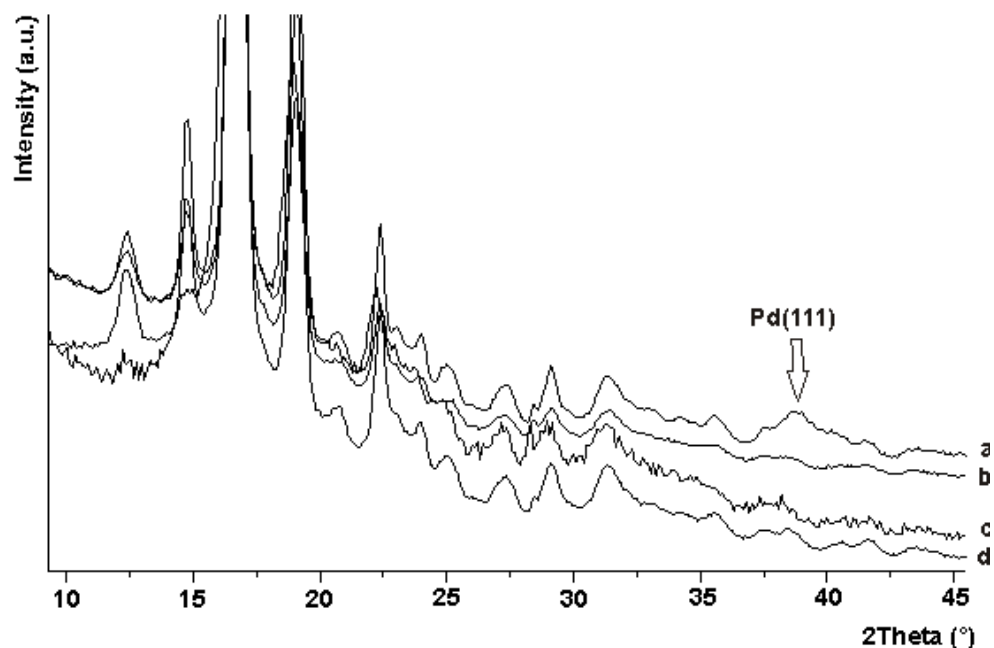


Figure 3.21 – XRPD spectra: (a) **17** after catalysis (36h); (b) **17+2L1** after catalysis (1st cycle); (c) **17+2L1** after catalysis (4th cycle); (d) **17** as-synthesized

In order to increase the stability of the palladium centre in **17** against Pd-black formation (Scheme 3.6/c), analogous catalytic reactions were carried out in the presence of 2 molequivalents of additional **L1** (*i.e.* denoted as **17+2L1**). A comparison of UV-Vis spectra of CHCl_3 solutions of **17** and **17+2L1** (Figure 3.22) clearly showed that, due to the strong coordination of acetate to palladium,⁴ the addition of **2L1** to **17** simply led to a dilution of **17** and not to the formation of a charged palladium complexes of the formula $[\text{Pd}(\mathbf{L1})_4](\text{OAc})_2$.

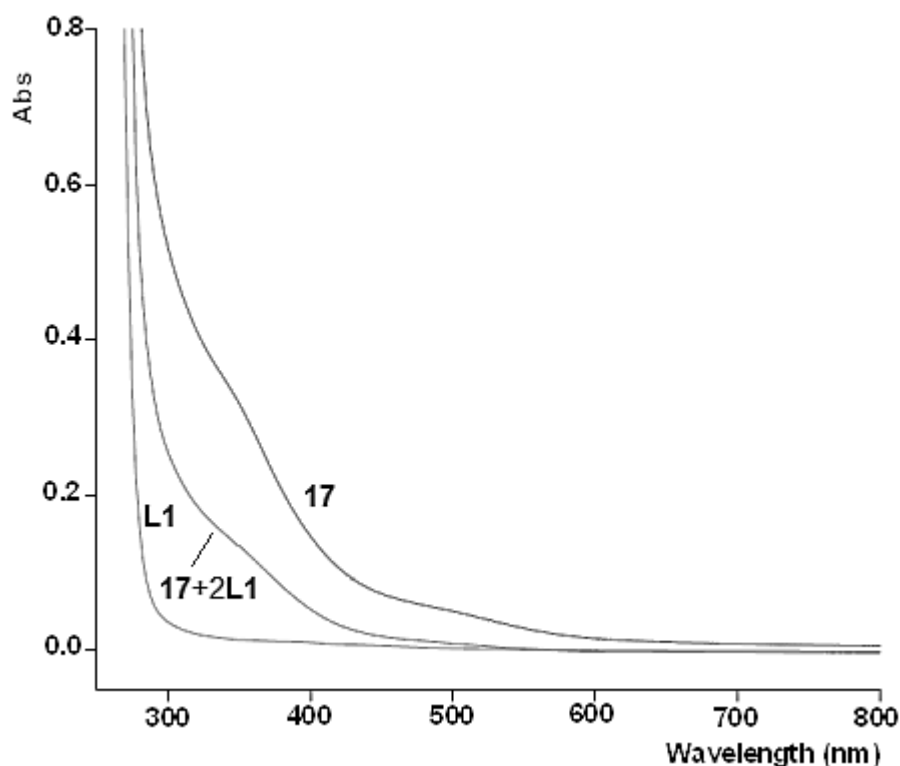


Figure 3.22 – UV-Vis spectra of **17**, **L1** and **17+2L1** acquired in CHCl_3

A ^1H NMR spectrum of **17+2L1** acquired in CD_2Cl_2 was in full agreement with the corresponding UV-Vis spectrum, showing the contemporary presence of two doublets assigned to palladium-coordinating pyridine moieties (*i.e.* 8.64 ppm, $^2J = 6.0$ Hz (*ortho*-H); 7.34 ppm, $^2J = 6.0$ Hz (*meta*-H)) and two doublets assigned to non-coordinating pyridine moieties (*i.e.* 8.61 ppm, $^3J = 6.0$ Hz (*ortho*-H); 7.27 ppm, $^3J = 6.0$ Hz (*meta*-H)).

Regardless of the substrate employed, (**17+2L1**)-catalyzed reactions showed a high stability against Pd black formation (Table 3.5). It is reported, that a pyridine to metal atom ratio of 4 in Pd-based aerobic oxidation catalysts stabilizes the metal centre on the expense of substrate conversion, since two molequivalents of pyridine have to be removed from palladium centre by the substrate.^{145,151} A comparison of the reported TOF values for (**17+2L1**)-catalyzed reactions lasting 18 h and 36 h nicely showed the catalyst stability with time, while the reference system (**19+2(4-EtPy)**) decomposed under analogous conditions. Unlike **17**-catalyzed reactions, (**17+2L1**)-catalyzed reactions showed, after a reaction time of 36 h, a yellowish solution that yielded an off-white solid after addition of *n*-pentane or methanol (Figure 3.23).

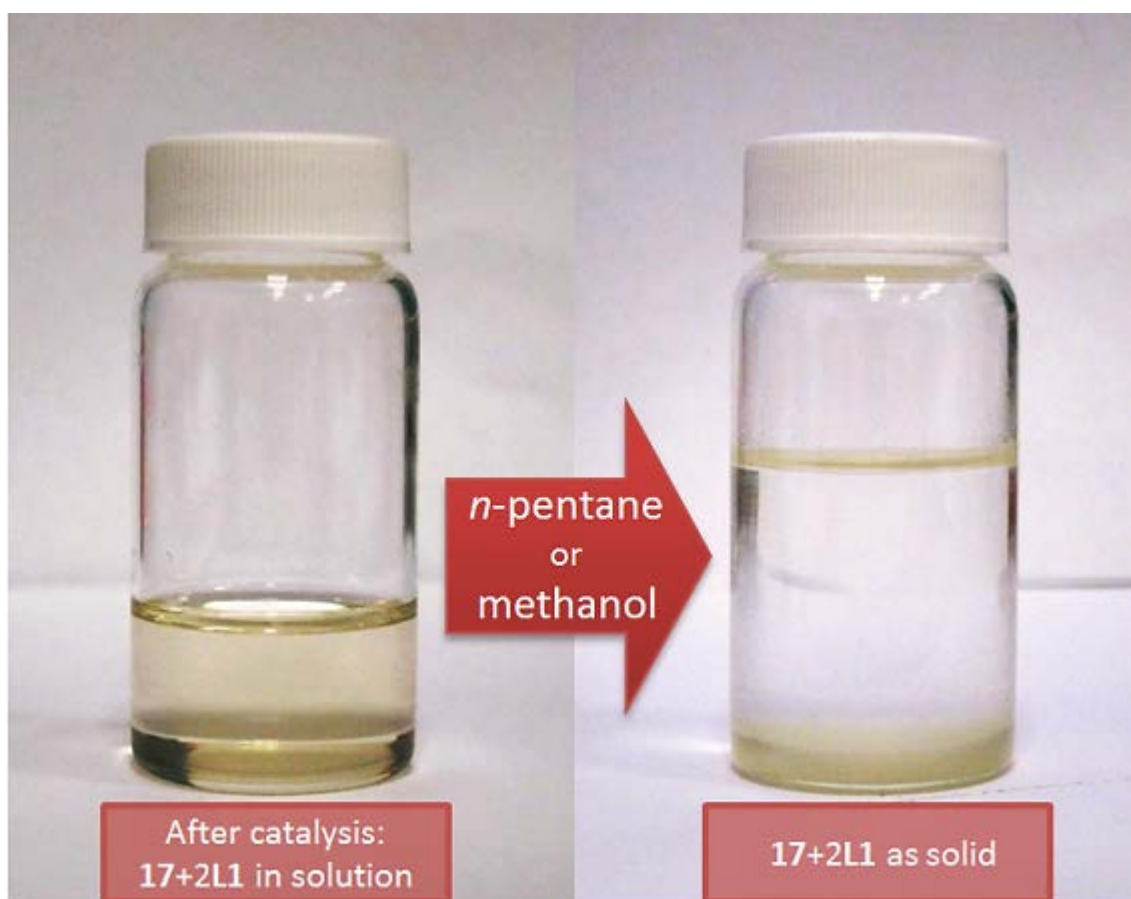


Figure 3.23 – Recovery of the 17+2L1 by precipitation with a non-solvent for P(L)LA

An (ICP-MS) analysis of the latter solution showed a Pd content of <1 ppm and a parallel catalytic run with the latter solution, without adding catalyst, showed almost no catalytic activity (*i.e.* substrate conversion of <1%). Moreover, a XRPD spectrum acquired on the recovered polymer-anchored catalyst (*i.e.* **17+2L1**) showed a pattern which was identical to that of as-synthesized **17** (Figure 3.21, trace b vs d), excluding the presence of XRPD-detectable palladium nanoparticles. Encouraged by the promising results obtained from (**17+2L1**)-catalyzed oxidations, we employed the latter catalytic system for four consecutive recycling experiments carried out with benzyl alcohol and substrate to precatalyst ratio of 100. The substrate conversions obtained after each cycle are reported in Figure 3.24.

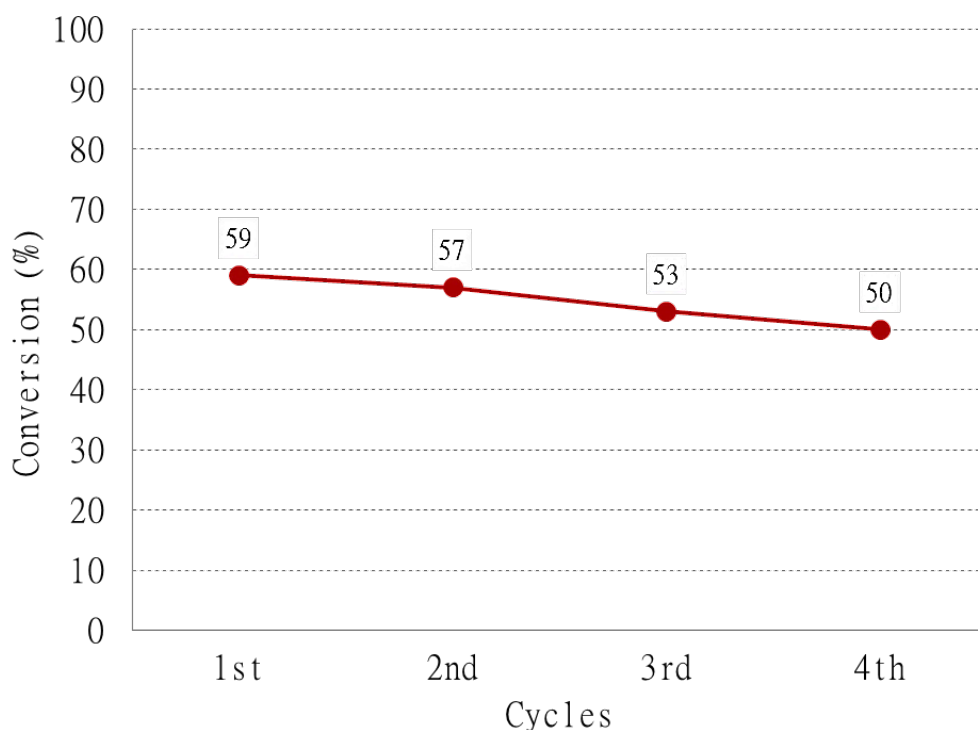
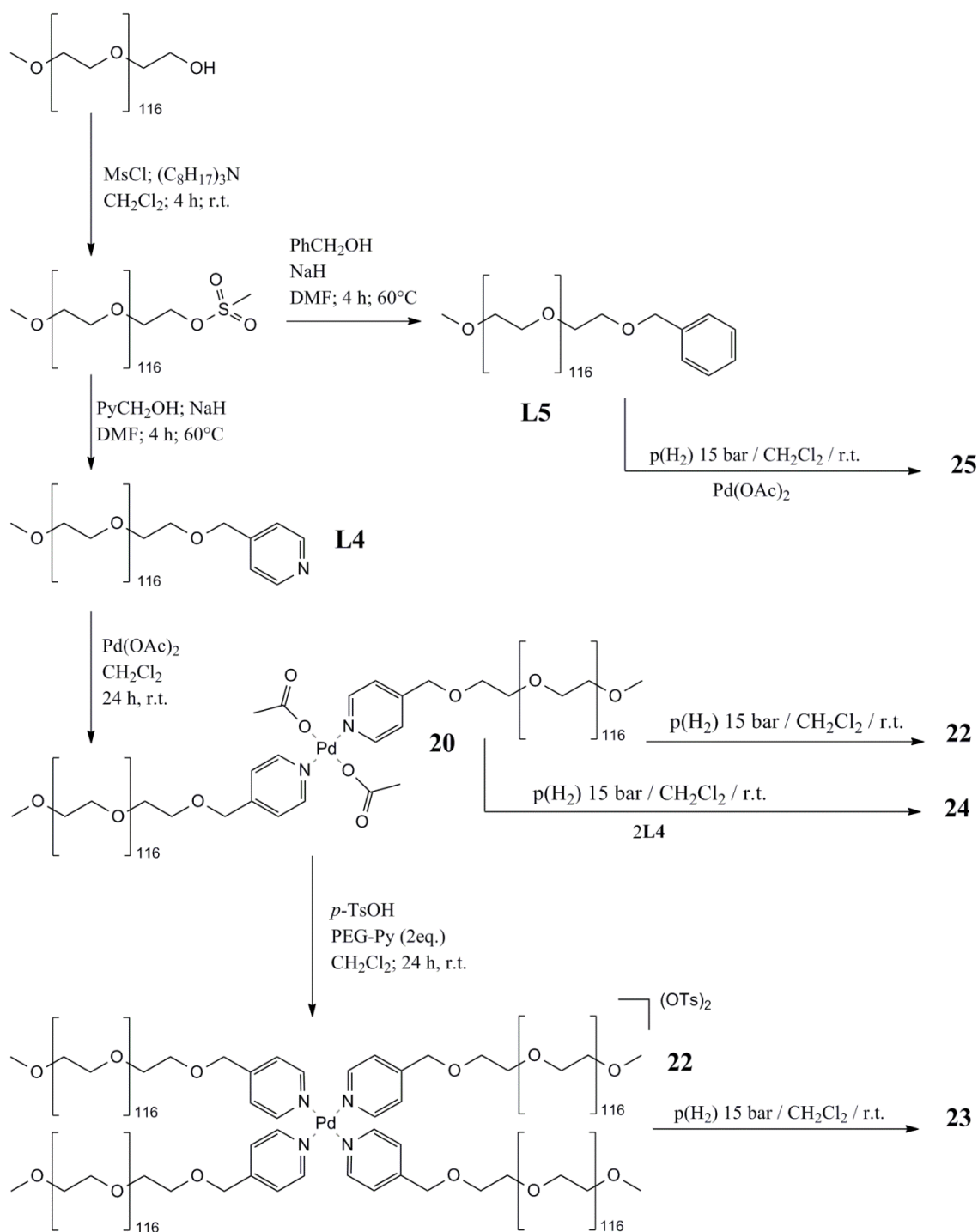


Figure 3.24 – Conversion of benzyl alcohol after recycling of 17+2L1 catalyst. Catalytic conditions: 17 (0.010 mmol), L1 (0.020 mmol), benzyl alcohol (1.00 mmol), toluene (5 mL), 70 °C, 2 h, air (4 bar)

In order to prove the absence of XRPD-detectable Pd-nanoparticles in the isolated catalytic polymer material after each catalytic cycle, corresponding XRPD spectra were acquired. The patterns of all spectra acquired after each catalytic cycle were identical, hence only the XRPD pattern registered after the 4th cycle is shown (Figure 3.21, trace c).

3.3 Water phase aerobic oxidation of alcohols catalyzed by PEG-stabilized Pd nanoparticles

The macroligands of the formula $\text{MeO}-(\text{CH}_2\text{CH}_2\text{O})_{16}\text{CH}_2\text{CH}_2\text{OR}$ with R = 4-pyridinemethylene (**L4**) and benzyl (**L5**) were straightforwardly obtained by a mesylation reaction of commercial MeO-PEG-OH followed by the reaction of the isolated mesylate with NaH in dry DMF in the presence of the corresponding alcohol (*i.e.* 4-hydroxymethylpyridine or benzyl alcohol) (Scheme 3.7). **L4** and **L5** were obtained as white solids in 86 and 71% yield, respectively.



Scheme 3.7 – Synthesis of PEG-based macroligands, Pd(II) macrocomplexes and Pd-NPs

The successful end-functionalization of PEG was proved by ^1H NMR spectroscopy. As a result, the ^1H NMR spectra of **L4** (Figure 3.25) and **L5**, acquired in CD_2Cl_2 , showed for the benzylic hydrogen atoms a singlet at 4.59 and 4.55 ppm, respectively, which is slightly shifted to lower frequency compared to the analogous ^1H NMR signal of PyCH_2OH (4.73 ppm) and PhCH_2OH (4.66 ppm). Moreover, in the ^1H NMR spectra of **L4** and **L5** ($\text{DMSO}-d_6$) the triplet signal centered at 4.56 ppm ($J = 5.2$ Hz), which was assigned to the terminal MeO-PEG-OH ,³¹⁷ was absent. The number-averaged molecular

weight (M_n) of **L4** and **L5** was determined by ^1H NMR spectroscopy ($M_n = 5200$ g/mol) by integration of the singlets assigned to the $(\text{CH}_2\text{CH}_2\text{O})_n$ moiety (3.60 ppm) and to the terminal CH_3O unit (3.36 ppm). GPC analyses in THF were also carried out in order to determine polydispersity indexes of the two macroligands (**L4** and **L5**: $M_n = 7750$ g/mol; PDI = 1.05). The molar mass values determined by ^1H NMR integration and GPC analysis were significantly different; this observation is due to the use of polystyrene to calibrate GPC columns.³¹⁸

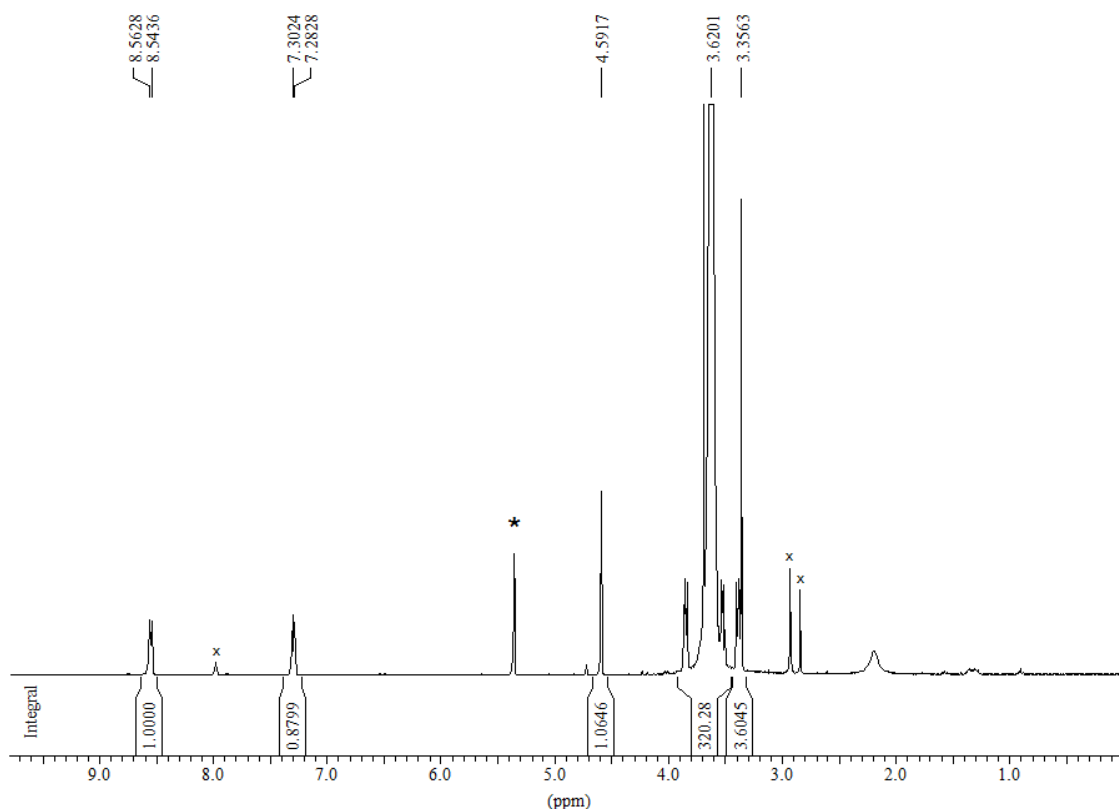


Figure 3.25 – ^1H NMR spectrum of PEG-based macroligand **L4** in CD_2Cl_2 (x = traces of residual DMF)

Macroligand **L4** was used to coordinate $\text{Pd}(\text{OAc})_2$ in CH_2Cl_2 , yielding the neutral Pd(II) macrocomplex of the formula $\text{trans}[\text{Pd}(\text{OAc})_2(\text{L4})_2]$ (**20**). The addition of two molequivalents of **L4** to a CH_2Cl_2 solution of **20** in the presence of *p*-toluenesulfonic acid (*p*-TsOH) gave the bis-cationic Pd(II) macrocomplex of the formula $[\text{Pd}(\text{L4})_4](\text{OTs})_2$ (**21**) (Scheme 3.7). Both latter macrocomplexes were isolated in around 80% yield, as yellowish (**20**) and beige (**21**) powders. The occurred coordination of **L4** to Pd(II) in **20** and **21** has been proved by ^1H NMR and UV-Vis spectroscopy. As a result, the ^1H NMR spectrum of **20** showed a doublet at 7.38 ppm (*i.e.* *meta*-H atoms of the pyridine unit) which was shifted to higher frequency compared to that of **L4** (7.29 ppm), while the *ortho*-pyridine hydrogen atoms of **21** were centered at 9.64 ppm, which

was diagnostic for their interaction with the oxygen atoms of *p*-toluenesulfonate as shown for related Pd(II) compound.^{151,140} UV-Vis spectra, acquired in water, showed for **20** an adsorption shoulder centered at 225 nm due to the Pd-pyridine interaction, which is absent in the spectrum of **L4** (Figure 3.26, left). In **21** this feature is masked by the absorption peak at 228 nm, which stems from tosylate anion, as confirmed by the UV-Vis spectrum of (HL4)(OTs) (Figure 3.26, right).

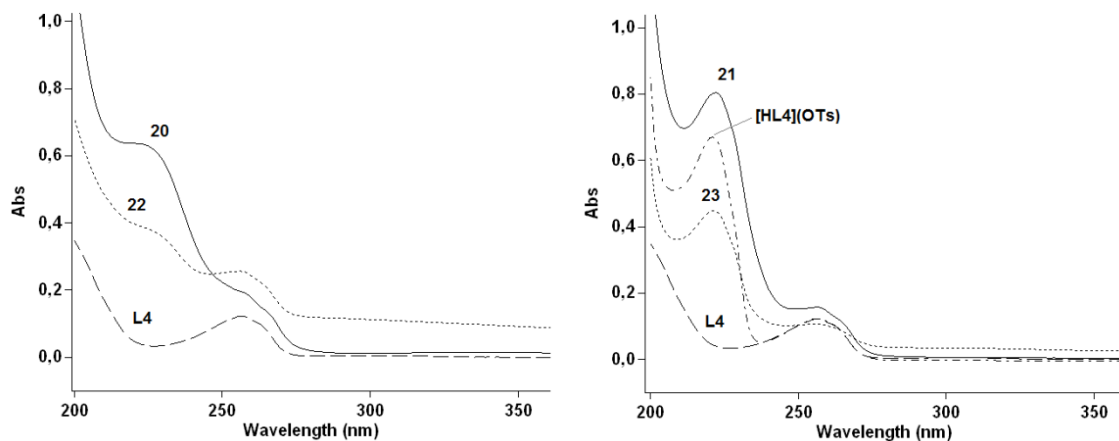


Figure 3.26 – UV-Vis spectra (H_2O) of: **L4**, **20** and **22** (left); **L4**, (HL4)(OTs), **21** and **23** (right)

The macrocomplexes **20** and **21** were reduced with dihydrogen (15 bar) in solution (*i.e.* CH_2Cl_2) at room temperature, yielding Pd-NPs stabilized by (HL4)(OAc) (**22**); by **L4** and (HL4)(OAc) in a 1 : 1 molar ratio (**24**) or by **L4** and (HL4)(OTs) in a 1 : 1 molar ratio (**23**) (Scheme 3.7). Both latter pyridinium salts were obtained upon protonation of the corresponding free acid (*i.e.*, AcOH and *p*-TsOH, generated by the reduction of $Pd(OAc)_2$ and $Pd(OTs)_2$) with **L4**. In contrast, Pd-NPs in **24** and **25** were obtained by *in-situ* reductions of **20** in the presence of 2**L4** and of $Pd(OAc)_2$ in the presence of **L5**, respectively

UV-Vis spectra acquired in water, showed for **22** and **23** a significantly lower absorption in the region from 200 to 245 nm, due to the absence of the MLCT contribution. The latter was replaced by a rather featureless broad spectral band due to the scattering of radiation by nm-sized colloidal palladium.³¹⁹ In this context it is interesting to note that **22** showed a significantly more intense UV scattering in the range from 280 to 360 nm compared to **23**, which is due to the higher Pd(0) content in **22** (1.1 wt%) than in **23** (0.51 wt%).

The Pd-NPs size and their degree of aggregation have been revealed by TEM analysis. Representative TEM images of **22** and **23**, (Figure 3.27) clearly proved for **23** the

occurrence of spherical and well-separated Pd-NPs with an average size of 6.33 ± 1.40 nm (Figure 3.27/b), whereas **22** showed non-defined worm-like aggregates (Figure 3.27/a).

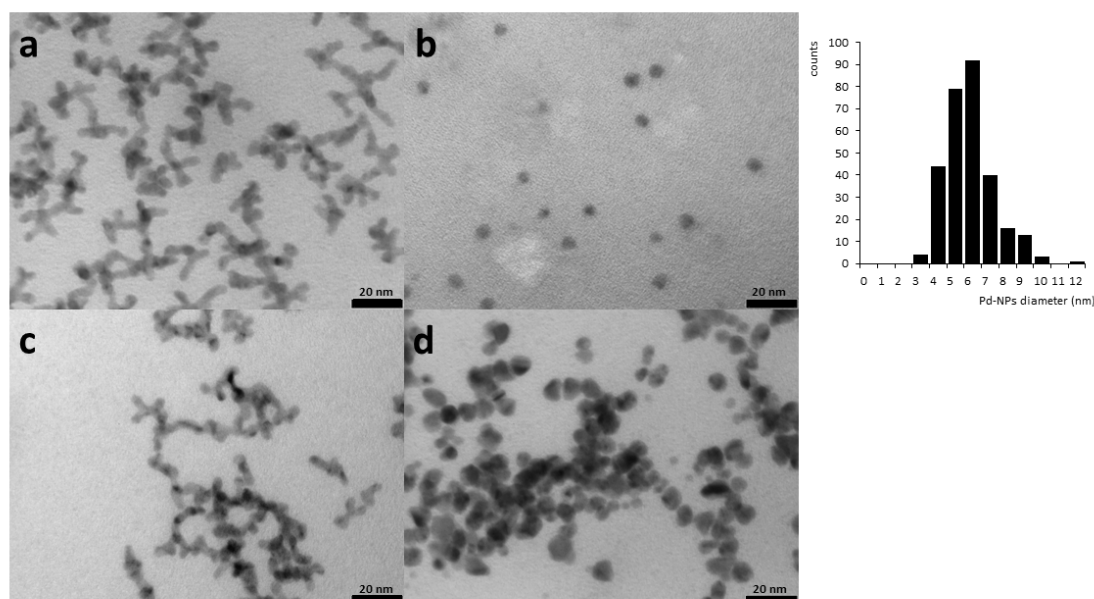


Figure 3.27 – TEM images of: (a) **22**, (b) **23**, (c) **24** and (d) **25**

The degree of Pd-NPs aggregation found in **24** was comparable to that of **22** (Figure 3.27/c), while the highest degree of particle aggregation was encountered in **25** (Figure 3.27/d) which contains the benzyl-functionalized macroligand **L5**. Since **23** and **25** were the two extreme cases of optimal and least efficient NPs separation, we tested the ability of the corresponding macroligands to stabilize Pd-NPs. To this purpose we carried out centrifugation experiments with water solutions of **23** and **25** under identical experimental conditions. As a result, while **23** gave no precipitate, from the water solution of **25** a black solid precipitate was formed, which was identified by means of XRPD analysis as polymer-free Pd-NPs with a mean diameter of 6.0 nm (determined by the Debye-Scherrer method³²⁰ using the Pd(111) Bragg reflex of the XRPD pattern; Figure 3.28, trace b) in good agreement with TEM observations.

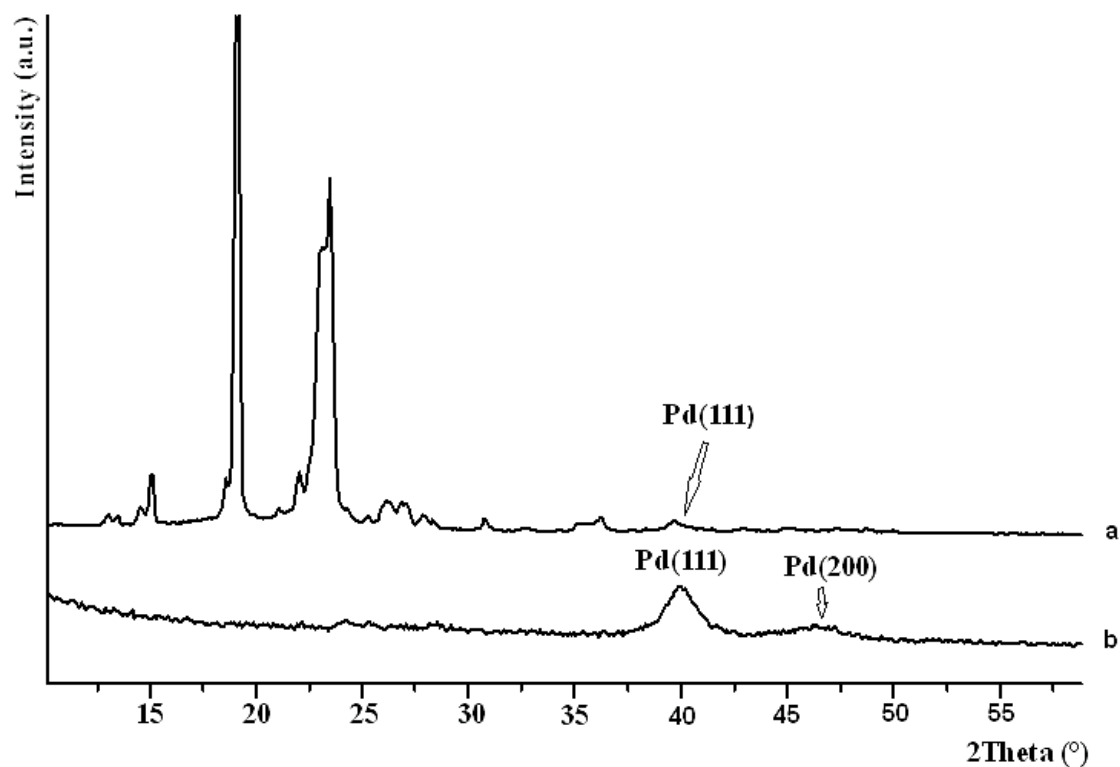


Figure 3.28 – XRPD spectra of: (a) **25** and (b) Pd-NPs isolated from centrifugation experiment carried out on **25**

In order to compare the oxidative thermal degradation behavior of **L4** and **L5** with that of **22**, **23** and **25** in the solid state, thermogravimetric analyses (TGA) have been carried out in a temperature range from 30 to 700 °C and in the presence of an air flux.³²¹ The results are shown in Figure 3.29, which presents the complete TGA curves of all compounds (top) and the weight loss in an interval from 5% (onset) to 50% (bottom).

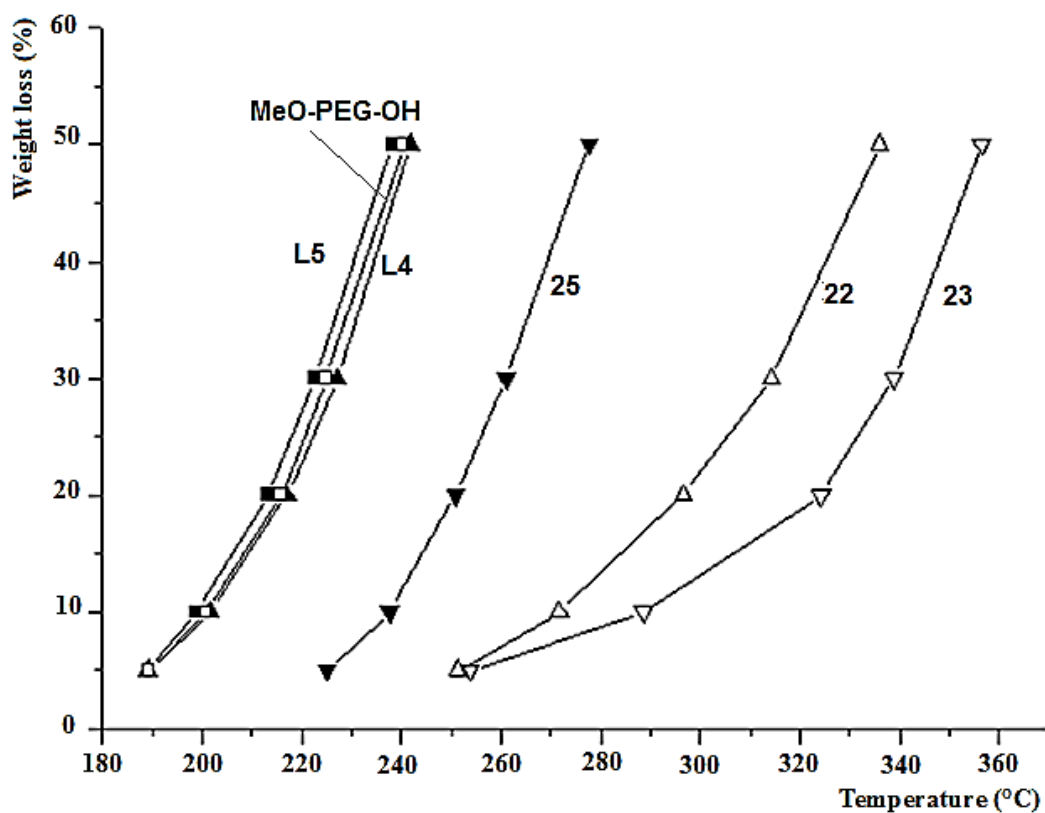
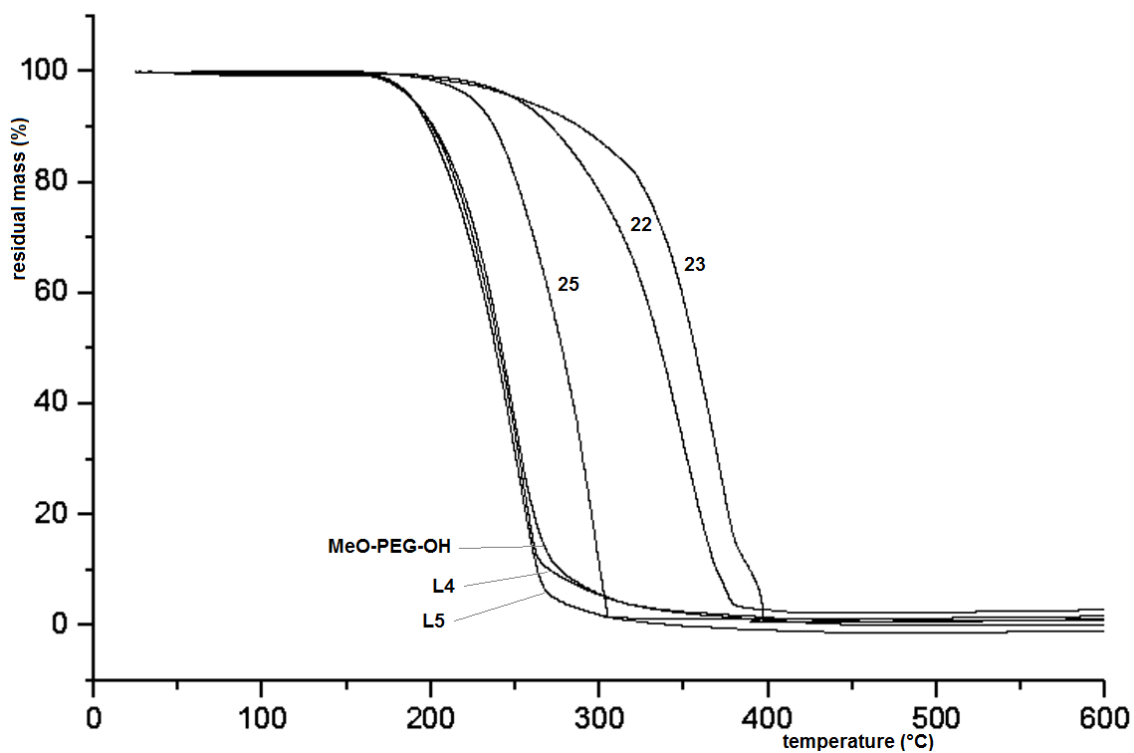


Figure 3.29 – TGA-curves (top) and weight loss data (bottom) of MeO-PEG-OH, L4, L5, 22, 23 and 25 carried out in air atmosphere

Sample	T(°C) at 5% w. loss (onset)	T(°C) at 10% w. loss	T(°C) at 20% w. loss	T(°C) at 30% w. loss	T(°C) at 50% w. loss (mid-point)
MeO-PEG-OH	189.2	201.6	217.0	227.2	241.8
L4	189.4	200.8	215.0	224.9	240.3
L5	189.2	198.8	213.3	222.6	238.2
22	251.4	271.6	296.5	314.2	336.1
23	253.9	288.6	324.2	338.9	356.4
25	225.1	237.6	250.9	261.0	277.6

Table 3.6 – TGA Data for MeO-PEG-OH, L4, L5, 22, 23 and 25

From an analysis of the TGA data (Table 3.6) emerged that: (i) the thermal behavior of **L4** and **L5** is comparable to that of commercial MeO-PEG-OH, which is indicative for a degradation mechanism of random scission of the polyether and not for an unzipping of the polymer chain starting from the terminal groups;⁷⁴ (ii) the presence of Pd-NPs in the polymer matrix exerts a stabilizing effect on the macroligands against thermal degradation as proved by the corresponding onset temperatures for the degradation process (see also Figure 3.29: **22** and **23** vs **L4**; **25** vs **L5**); (iii) the degree of Pd-NP aggregation, which determines the contact surface area between polymer and NP, is crucial for the thermal stability of the PEG-based macroligands. As a consequence, the stability against thermal oxidative degradation increases in the order **25** < **22** < **23**.

The stability of **L4** in solution against oxidative degradation has been tested by applying real oxidative catalytic conditions (*i.e.* water solution of **L4** was heated at 60 °C in the presence of K₂CO₃ and 30 bar of air for 14 h) and analyzed by GPC (Figure 3.30). As a result, **L4** was not degraded significantly under the chosen experimental conditions since variations in both M_n and PD are within typical GPC experimental errors (*i.e.* **L4**: M_n = 7750 g/mol, PDI = 1.05; after treatment under oxidative conditions: M_n = 8300 g/mol, PDI = 1.08).

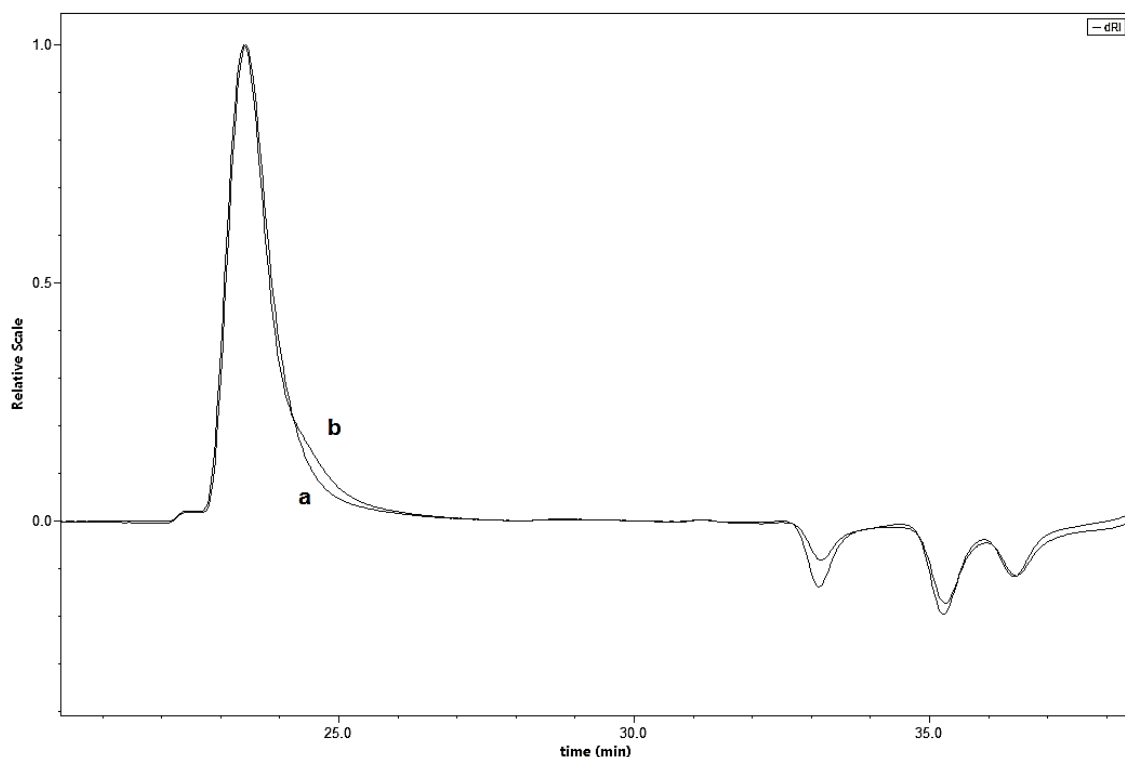
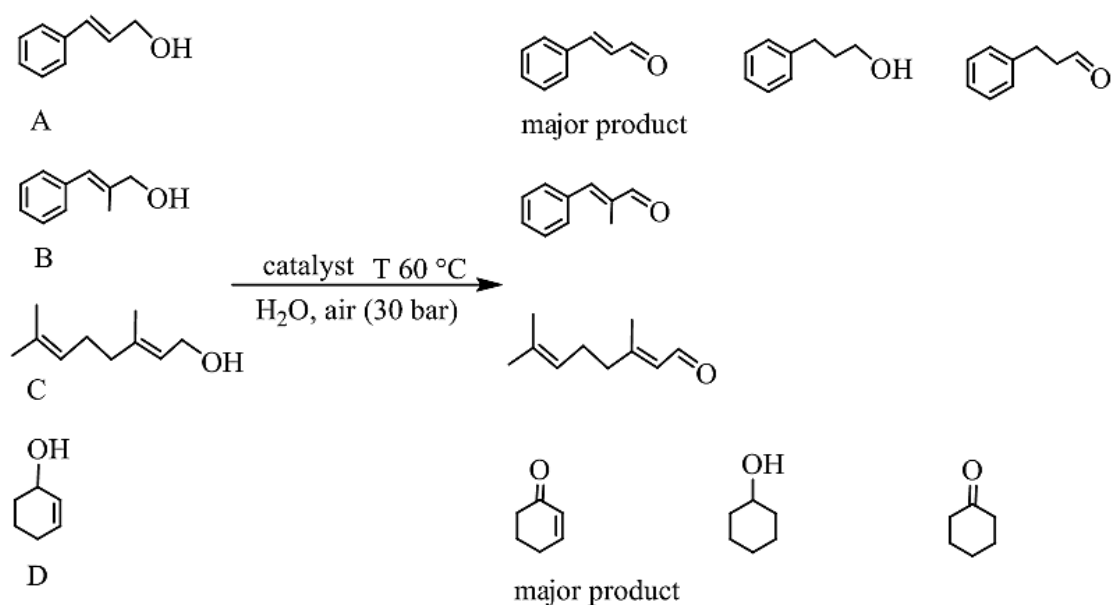


Figure 3.30 – GPC traces of L4: (a) before and (b) after the stability test

The Pd(II) macrocomplexes **20** and **21** and the macroligand-stabilized Pd-NPs **22**, **23**, **24** and **25** were used to catalyse the aerobic oxidation (*i.e.* 30 bar of air) of selected α,β -unsaturated alcohols (*i.e.* cinnamyl alcohol (A), *trans*-2-methylcinnamyl alcohol (B), geraniol (C) and 2-cyclohexen-1-ol (D)) in water, giving the corresponding α,β -unsaturated carbonyl compound as major product (Scheme 3.8).



Scheme 3.8 – Aerobic oxidation of α,β -unsaturated alcohols in water

The performance of the catalysts was screened using cinnamyl alcohol as substrate. The amount of catalyst used for the oxidative reactions was based on their Pd content which was determined by ICP-OES.

As far as the catalytic activity is concerned, the Pd-NPs-based catalysts showed an almost ten times higher activity compared to the Pd(II)-based macrocomplexes. As a consequence, a substrate to Pd molar ratio of 2600 was applied in **22**, **23**, **24** and **25**-catalyzed reactions, while **20** and **21** gave acceptable substrate conversions only with a substrate to Pd molar ratio of 100 (Table 3.7, entries 6,7, 15 and 16 vs entries 1 and 3). The performance of the latter Pd(II) catalysts in terms of activity is comparable to that of Pd(OAc)₂(bathoneocuproine-disulfonate-disodium) (**26**), which is one of the most efficient Pd(II) catalysts for the aerobic oxidation of alcohols in water.³²² All Pd(II)-based catalysts decreased their activity with time, which is in accordance with the formation of Pd-black in the course of the catalytic reaction (Table 3.7, entries 1-5).

Entry ^a	Catalyst	Substrate	Conv (%) / TOF ^b			Sel (%) ^c		
			2 h	4 h	14 h	2 h	4 h	14 h
Pd(II)^d								
1	20	A	57/29	78/20		98	99	
2^e	20	A	83/41			99		
3	21	A	52/26	78/20		96	95	
4^e	21	A	87/43			99		
5	26	A	71/36	85/21		85	85	
Pd(0)^f								
6	22	A		30/200	76/145		93	91
7	23	A		29/193	99/189		90	89
8^g	23	A		30/200	98/187		77	75
9^e	23	A		27/180	88/177		98	98
10^h	23	A	98/127			95		
11^{h,i}	23	A	97/126			94		
12	23	B		27/180	88/168		100	100
13	23	C		4/27	14/27		100	100
14	23	D		29/193	90/171		99	98
15	24	A		40/267	79/150		91	93
16	25	A		30/200	70/133		94	88

17^e	25	A		21/140	61/116		99	99
^a Catalytic conditions: 60 °C, water (5.0 mL), air (30 bar). ^b TOF expressed in h ⁻¹ . ^c Chemoselectivity referred to the α,β -unsaturated aldehyde. ^d Pd amount (0.01 mmol), substrate (1.00 mmol). ^e Addition of K ₂ CO ₃ (0.25 mmol). ^f Pd amount (0.003 mmol), substrate (8.00 mmol). ^g Air (1 bar). ^h Substrate (0.778 mmol). ⁱ 4 th catalytic cycle.								

Table 3.7 – Aerobic Oxidation of α,β -unsaturated alcohols in water catalyzed by 20 – 26

The Pd-NPs-based catalysts showed a cinnamyl alcohol conversion which was comparable for a reaction time of 4 h (Table 1, entries 6, 7, 15 and 16) and in the range of activity found for a Pt/Bi-catalyst supported on alumina (*i.e.* TOF 144 h⁻¹), which is one of the most active and chemoselective heterogeneous catalysts for the oxidation of this substrate in water in the presence of a detergent.^{204,323}

By carrying out analogous catalytic reactions lasting 14 h, TOF values decreased significantly, except for **23**, which showed the highest catalyst stability with time regardless of the substrate employed (Table 3.7, entries 7, 12, 13 and 14). TEM images, acquired on recovered **23** after catalytic reactions lasting 4 h (Figure 3.31/a) and 14 h (Figure 3.31/b), showed a size distribution for Pd-NPs which is comparable to as-synthesized **23** (*i.e.* 6.33 ± 1.40 nm (before catalysis), 6.11 ± 0.93 nm (after 4 h catalysis) and 5.65 ± 1.38 nm (after 14 h catalysis)), corroborating the superior catalyst longevity of **23**.

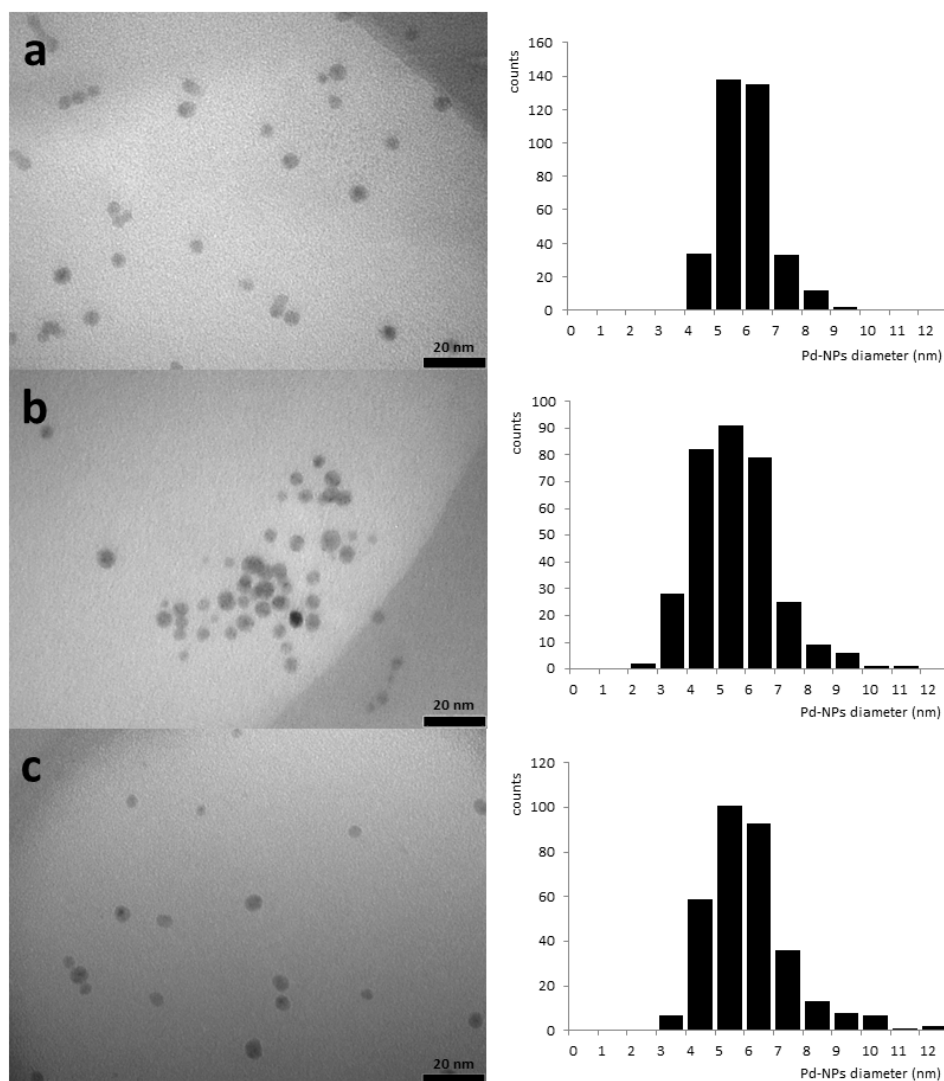


Figure 3.31 – TEM images of **23**: (a) after 4 h, (b) after 14 h of catalysis without K_2CO_3 and (c) after 4 h catalysis in the presence of K_2CO_3

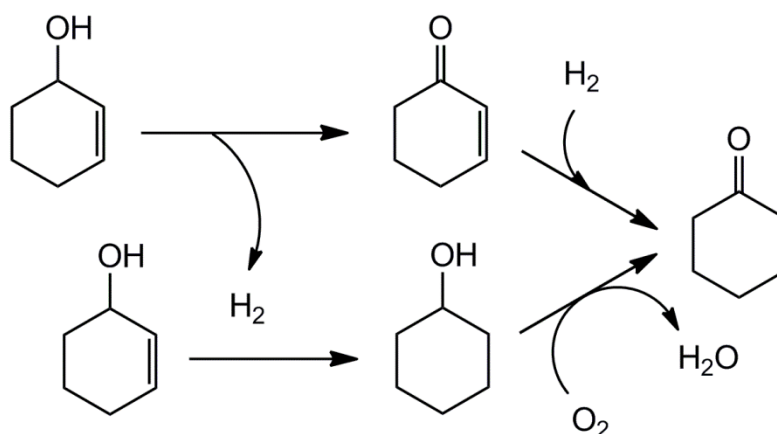
The rather low conversion of geraniol (substrate D) by **23** is probably due to the weak interaction of the aliphatic substrate with the surface of the Pd-NPs, which is a prerequisite for the oxidative addition of the alcohol functionality at a low coordinated Pd atom located at the edge or corner of the Pd-NPs.²⁰⁰

For what concerns the chemoselectivity of catalytic oxidation reactions, substrates B and C were converted into the corresponding α,β -unsaturated carbonyl compound with a chemoselectivity of 100%. Conversely, the oxidation of substrates A and D gave the corresponding α,β -unsaturated carbonyl compound as major product (Scheme 3.8) with selectivity in the range from 75% to 99%. The formation of the corresponding saturated alcohols and carbonyl compounds as minor products is the result of a hydrogen transfer

reaction between two molecules of substrate or a molecule of substrate and a molecule of product (Scheme 3.9), which is in competition with the reduction of oxygen to water. If the adsorption probability of substrate or product on the Pd-NP surface is higher, then the chemoselectivity for the unsaturated carbonyl compound is lower.^{324,323}

As a consequence, catalytic reactions carried out in the presence of only 1 bar of air gave a very low chemoselectivity (*i.e.* 75 - 77%) for the α,β -unsaturated carbonyl compound, while the substrate conversion remained comparable to that obtained in the presence of 30 bar of air (Table 3.7, entry 8 vs 7). This latter experimental result is in accordance with the role of oxygen in these catalytic reactions as dihydrogen acceptor and not as scavenger of strongly Pd-NPs-adsorbing compounds, such as CO.³²⁴

The chemoselectivity of the oxidation reactions with substrate A was positively altered in the presence of a Brønsted base such as K_2CO_3 , regardless of the catalyst employed (Table 3.7). The associated catalyst activity increases in the case of **20** and **21**, and decreases in the case of **23** and **25** compared to catalytic reactions carried out in the absence of base. The catalytic results in the case of **20** and **21** may be due to the role of K_2CO_3 as an external base, stabilizing the Pd(II) catalyst. The negative effect of the base on the catalytic activity of **23** (Table 3.7, entry 9 vs 7) and **25** (Table 3.7, entry 17 vs 16) might be ascribed to a coverage of the Pd-NP surface with (OH)-groups which may hamper the access of substrate and product to the particle surface. As a consequence, the chemoselectivity of the oxidation reaction is increased at the expense of catalytic activity.³²⁴ It is important to mention at this point, that the mean size of the Pd-NPs of **23** did not change significantly during catalysis carried out in the presence of K_2CO_3 (*i.e.* 6.26 ± 1.51 nm after 14 h vs 6.33 ± 1.40 nm before catalysis) as shown by the corresponding TEM image (Figure 3.31/c).

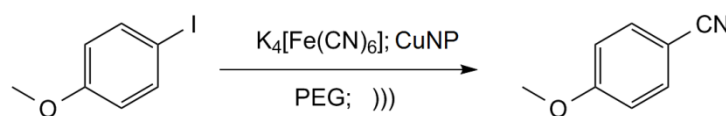


Scheme 3.9 – Formation of saturated alcohols and carbonyl compounds as byproducts of aerobic oxidation reactions

Recycling experiments were carried out with **23** in the presence of cinnamyl alcohol (at a substrate to Pd molar ratio of 260) extracting products from the aqueous phase with diethyl ether at the end of each catalytic test and reusing the aqueous solution for the following cycle. Four consecutive catalytic reactions showed a constant substrate conversion (*i.e.* 98%) and chemoselectivity (*i.e.* 95%) (Table 3.7, entries 10 and 11). Importantly, the leaching of Pd into the organic phase was determined after each catalytic cycle by ICP-OES, which showed a Pd-content of c.a. 25 ppb.

3.4 PEG as solvent for the Cu-catalyzed cyanation of aryl halides under sonochemical conditions

Preliminary tests performed with polymers having low molecular weight (*i.e.* PEG-250-(OMe)₂, PEG-300 or MeO-PEG-1100-OH) gave no conversion of starting material under ultrasound (US) irradiation. Our first purpose was to determine the influence of the weight-average molecular weight (M_w) of PEG on reaction conversion and yield, using 4-iodo-anisole and 5 mol% commercial Cu-nanopowder (Cu-NP) as benchmark substrate and catalyst, respectively. We fine-tuned the M_w of the polymer by varying the ratio of a PEG-3400 / PEG-10000 mixture. Based on previous findings,³²⁵ the reaction mixture was sonicated in a pulsed fashion (*i.e.* on/off = 5 sec/5 sec) in order to enhance homogeneity of irradiation and a total reaction time of 20 min (*i.e.* 10 min total sonication) was chosen. As a result, we observed a marked dependence of conversion and yield on the M_w of the PEG mixture. A set of PEGs with different M_w s at narrow intervals was screened by mixing PEG-3400 and PEG-10000 in different proportions to obtain a total of 20 g of mixture per reaction, showing a maximum of catalytic activity for PEG-5600 (Figure 3.32; Table 3.8, entries 1-9).



Entry ^a	PEG M_w (g/mol)	PEG-3400 (g)	PEG-10000 (g)	Time ^b (min)	Conversion ^c (%)	Yield ^d (%)
1	3400	20.00	0.00	20	18	18
2 ^c	4200	17.58	2.42	20	26	24
3 ^c	5000	15.15	4.85	20	74	63
4 ^c	5300	14.24	5.76	20	86	72

5 ^e	5600	13.33	6.76	20	94	81
6 ^e	5900	12.42	7.58	20	99	75
7 ^f	6000	-	-	20	70	67
8 ^e	6200	11.52	8.48	20	89	72
9 ^e	7000	10.91	9.09	20	98	73
10 ^g	5000	-	-	20	73	62
11 ^h	5000	-	-	40	0	0

^a 4-Iodo-anisole (4.0 mmol), K₄[Fe(CN)₆] (2.4 mmol), Cu-NP (0.2 mmol), melted PEG (20.0 g), N₂ atmosphere, US amplitude (A) = 70%, US frequency = 20 KHz; ^b Minutes of pulsed sonication (on / off = 5 sec / 5 sec); ^c Conversion was determined by HPLC and ¹H NMR; ^d Determined by ¹H NMR using CH₂Br₂ as internal standard; ^e PEG-3400 / PEG-10000 weighted mixture; ^f Commercially available PEG-6000 was used; ^g Commercially available MeO-PEG-5000 was used; ^h 20 weight% MeO-PEG-5000 water solution (20.0 g).

Table 3.8 – Cu-NP-catalyzed cyanation of 4-iodo-anisole in melted PEG

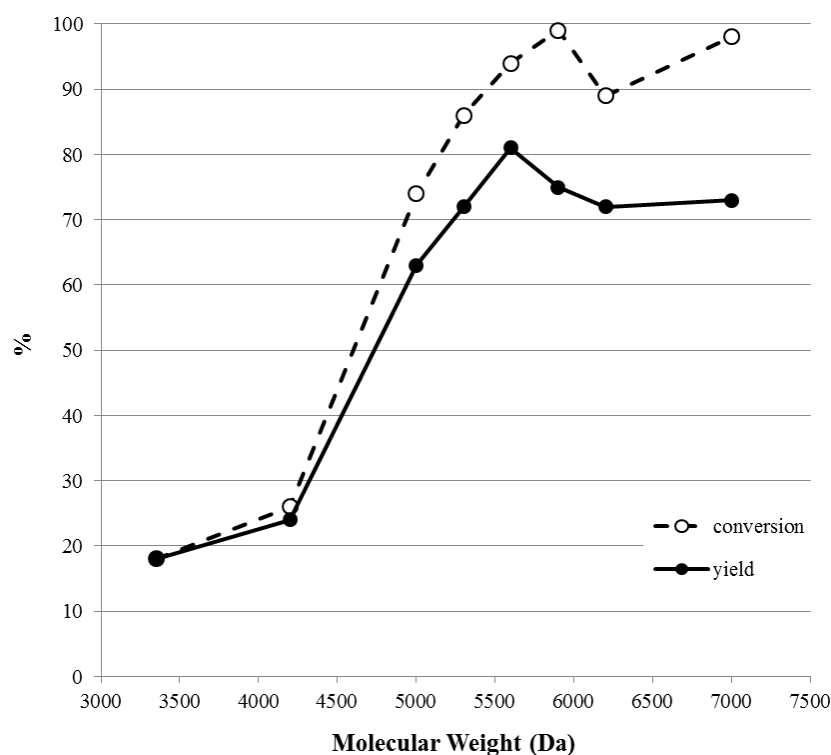


Figure 3.32 – Cu-NP catalyzed cyanation of 4-iodo-anisole in melted PEG; conversion (dashed) and yield (solid) vs Mw of the PEG mixture

The poor substrate conversions observed for low M_w PEGs may be rationalized on the basis of the mathematical equation which describes the attenuation of acoustic waves:²²⁴

$$I = I_0 \exp(-2\alpha l)$$

I is the acoustic intensity, *l* corresponds to the distance of the emitting probe and α is the

absorption coefficient, which depends on the viscosity of the medium (η_s) as given by the Stoke equation:

$$\alpha = \frac{8\pi^2 f^2}{3\rho c^3} \eta_s$$

where f is the ultrasonic frequency, ρ is the density of the medium and c is the speed of sound through the medium. Throughout our experiments f is kept constant (*i.e.* 20 KHz), while the variation of ρ within the screened M_w interval is negligible. Hence, it is reasonable to assume that the increase in melt viscosity (which is markedly molecular weight-dependent)³²⁶ plays a major role in enhancing the absorption of acoustic energy and, consequently, determines a more efficient energy transfer to the molecules of reactants.

On the other hand, melted PEGs with M_w higher than 6000 g/mol (Table 3.8, entry 7) up to 20000 g/mol, were probably too viscous liquids to allow an efficient diffusion of reactants. When PEG-7000 was employed, agitation was visibly difficult and our reactor was pushed to work at a power level close to overload; the lower homogeneity resulted in a decreased selectivity with 4,4'-dimethoxybiphenyl and 4-methoxybenzylamine as main byproducts. The results obtained from a reaction in pure MeO-PEG-5000, which were similar to those with the PEG-5000 mixture (Table 3.8, entry 10 *vs* 3) suggested that the effect of mixing high and low molecular weight PEGs is not chiefly important. A 20 weight% MeO-PEG-5000 / water solution was tested as solvent in the same conditions and no conversion was obtained even after prolonged sonication (Table 3.8, entry 11). This finding suggests that water may hamper reactivity by lowering the viscosity of the mixture and limiting the reaction temperature by partial evaporation. This clearly showed the peculiar effect of ultrasounds in promoting the cyanation reaction in pure PEG, which proved completely ineffective when microwave activation was used,³²⁷ and succeeded only in PEG / water mixtures.^{327,222}

Given the strong influence of PEG M_w on the efficacy of the whole reaction system, it is chiefly important to evaluate the stability of the polymer backbone under our US-assisted cyanation reaction conditions. To this purpose we recovered the PEG-5600 phase after work-up, reused it in a second run and performed a GPC analysis on native, recovered and recycled polymer phases. As a result, no M_w and polydispersion index variation exceeding experimental error was registered (Figure 3.33; Table 3.9).

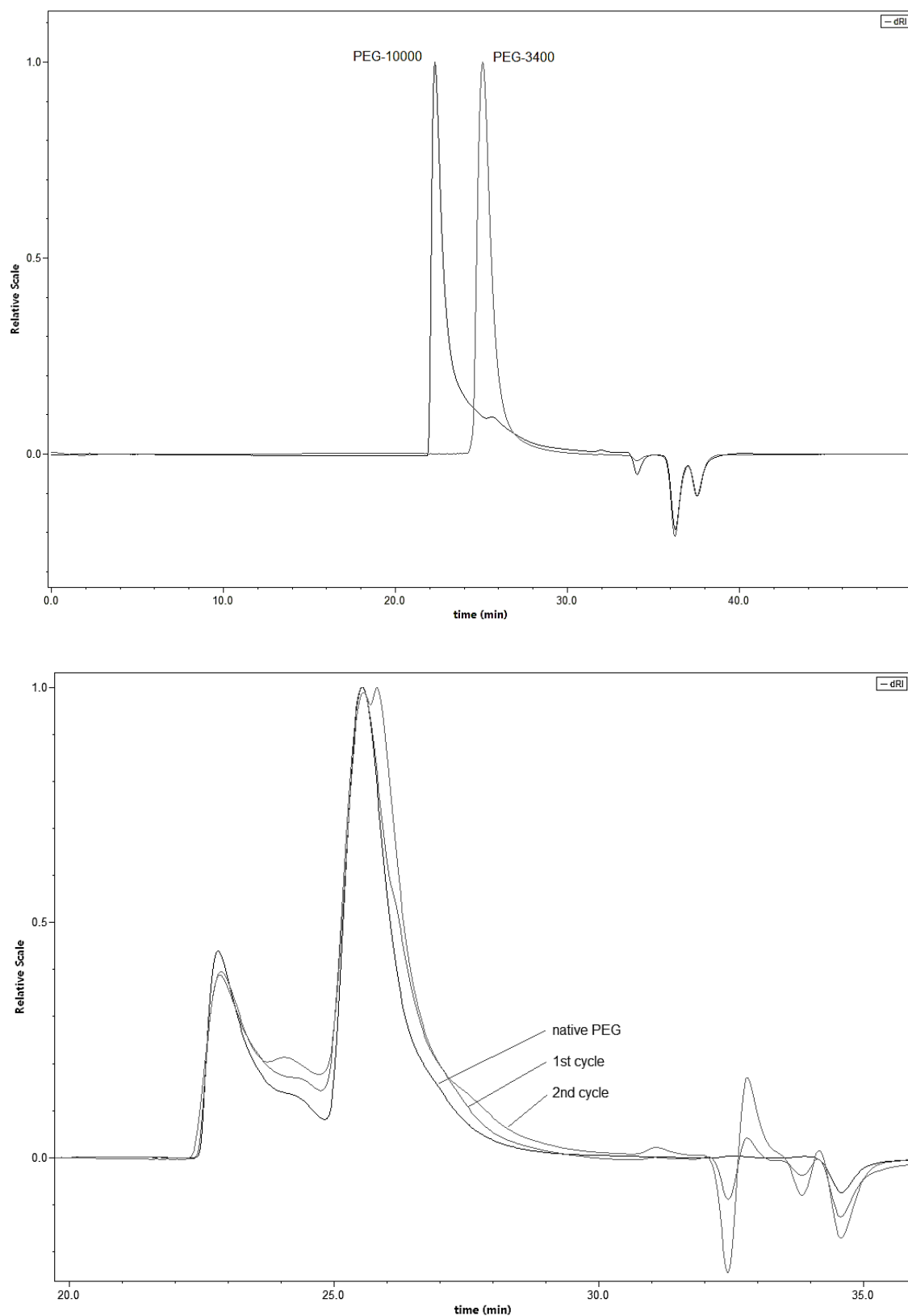


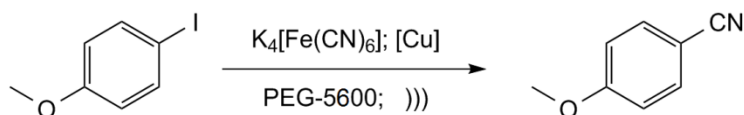
Figure 3.33 – GPC-RI analyses on commercial PEG-3400 and PEG-10000 (top); GPC-RI analyses (enlarged) on native and recycled PEG-3400 / PEG-10000 mixture (bottom)

Sample	M_w^a (g/mol)	Error	PDI
Native PEG-5600 ^b	8978	+/- 9.5%	1.27

Cycle 1	8908	+/- 9.4%	1.28
Cycle 2	8659	+/- 9.4%	1.31
^a Calibration with PS standards introduces a systematic bias into MW values (c.a. 1,2X for PEG samples). ^b Obtained as a weighted blend of PEG-3400 and PEG-10000.			

Table 3.9 – GPC-RI analyses on native and recycled PEG-3400 / PEG-10000 mixtures

After selecting the polymer blend with optimal M_w and melt viscosity (*i.e.* PEG-5600), we tested the activity of some copper species at different oxidation states (Table 3.10, entries 1-4). As a result, Cu-NP and CuI proved to be the most promising catalysts, giving almost complete conversions and very good yields even at a catalyst loading of 5 mol%. On the other hand Cu(I) and Cu(II) oxides showed moderate or poor activity, respectively.



Entry ^a	Catalyst	[Cat] mol%	Time ^b (min)	Conversion ^c (%)	Yield ^d (%)
1	Cu-NP	5	20	94	81
2	CuI	5	20	92	84
3	Cu ₂ O	5	20	68	57
4	CuO	5	20	42	33
5 ^e	CuI	5	20	97	84
6	Cu-NP	15	15	>99	94
7	CuI	15	15	>99	92
8 ^f	CuI	5	20	64	54
9 ^g	Pd(OAc) ₂	1	12	>99	75
10 ^{g,h}	Pd(OAc) ₂	5	120	0	0
11	-	0	30	0	0
12	CuI + L4 ⁱ	5	20	59	51

^a 4-Iodo-anisole (4.0 mmol), K₄[Fe(CN)₆] (2.4 mmol), melted PEG-5600 as a PEG-3400 / PEG-10000 weighted mixture (20.0 g), N₂ atmosphere, US amplitude (A) = 70%, US frequency = 20 KHz; ^b Pulsed sonication (on / off = 5 sec / 5 sec); ^c Conversion was determined by HPLC and ¹H NMR; ^d Yield was determined by ¹H NMR using CH₂Br₂ as internal standard; ^e 4-Iodo-anisole (12.0 mmol), K₄[Fe(CN)₆] (7.2 mmol), melted PEG-5600 (16.0 g); ^f 2nd cycle; ^g Addition of Na₂CO₃ (4.0 mmol); ^h The reaction was performed under microwave activation in a sealed vessel at 140°C using Na₂CO₃ (4.0 mmol). ⁱ CuI (0.2 mmol) and **L4** (0.2 mmol, 1.0 g) were dissolved in CH₂Cl₂, stirred overnight, then precipitated with Et₂O and dried prior to the addition to a melted PEG mixture (19.0 g).

Table 3.10 – Cu- and Pd-catalyzed cyanation of 4-iodo-anisole in melted PEG-5600

A test was repeated employing a triple concentration of reactants in PEG and gave nearly identical results (Table 3.10, entry 5 vs 2), suggesting that the throughput of the synthesis might be easily scaled up. As expected, conversion and yield could be further increased by raising the amount of catalyst to 15 mol% (Table 3.10, entries 6 and 7). Once again, Cu-NP and CuI showed a very similar catalytic performance.

A reaction was carried out adding the PEG-based macroligand **L4** to CuI in an equimolar amount in order to assess the performance of the copper catalyst in the presence of a coordinating pyridine end-group. **L4** was chosen in the place of a common low MW ligand to exploit the advantage that the covalent binding of the pyridine moiety to the PEG chain prevents its migration into the product phase as a contaminant during workup. Unfortunately, the activity of the catalyst system appeared to be significantly reduced (Table 3.10, entry 12) with respect to macroligand-free conditions, suggesting that, in this case, coordination reduces the accessibility of substrates to the metal center lowering the turnover frequency. Indeed, the issue of reagents diffusion may be particularly relevant in the presence of such a highly viscous solvent system, outbalancing any potential benefit brought by the particles-stabilizing effect of the macroligand (which played a role in the aforementioned toluene- or water-phase Pd-based catalyses).

To further investigate the nature of the active catalytic species we performed an XPS analysis on both 15 mol% Cu-NP and CuI containing pre-reaction mixtures and post-reaction PEG phases recovered after work up (*i.e.* precipitation and filtration)^{102,328,329} (Figure 3.34).

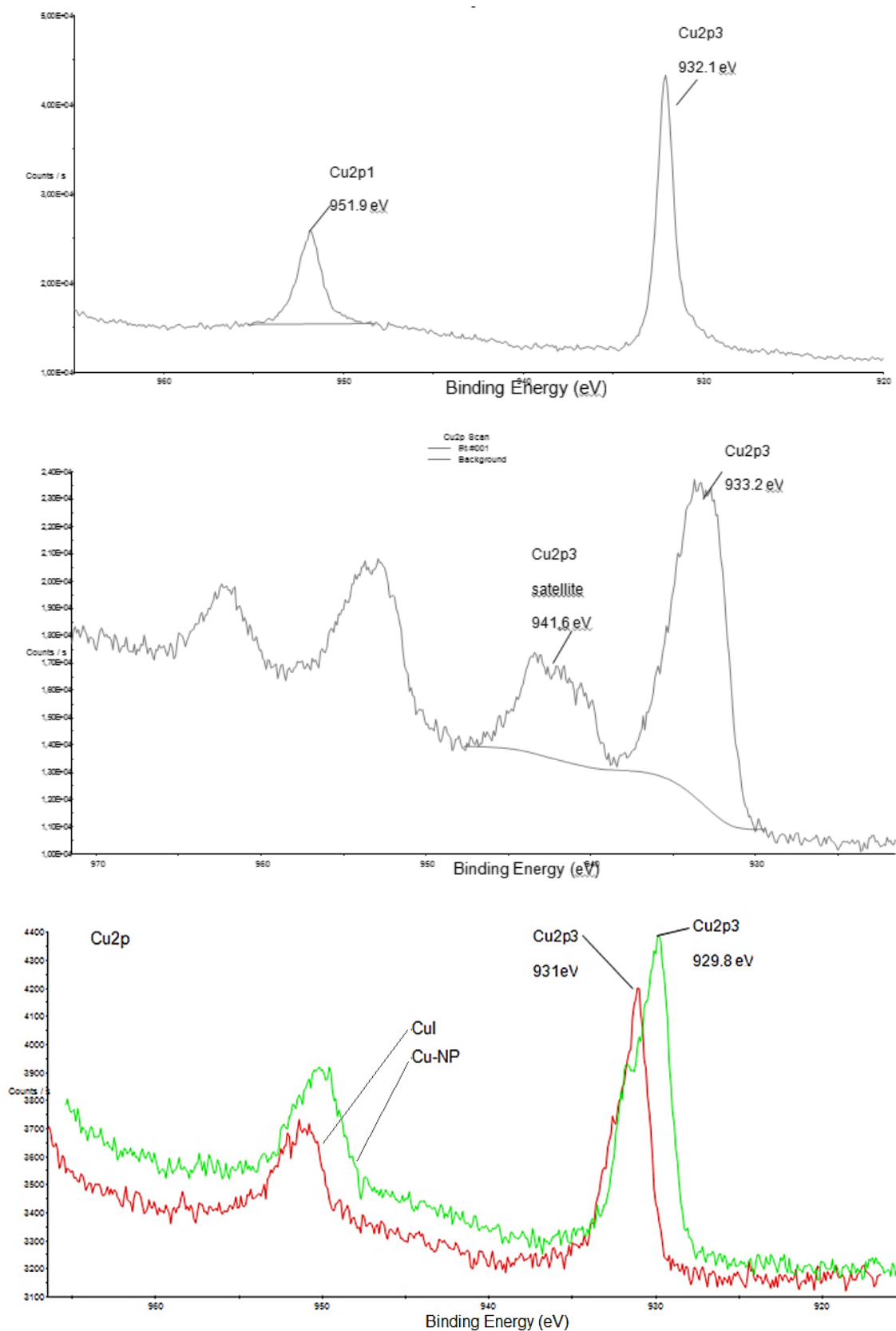
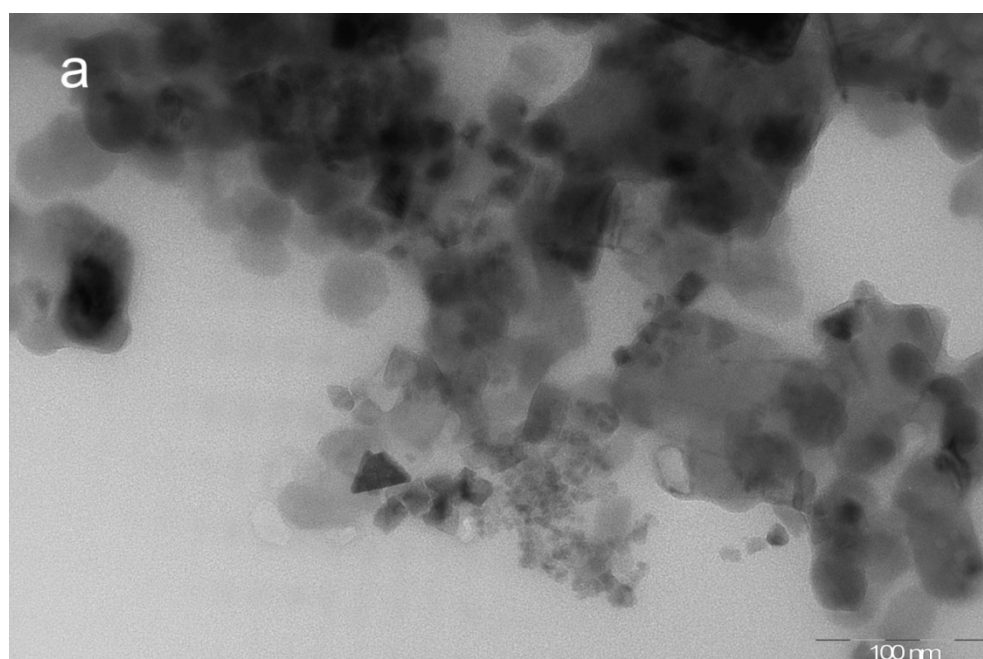


Figure 3.34 – XPS spectra (Cu₂p region) of native CuI (top), native Cu-NP (middle) and the two catalysts in the PEG phase recovered after reaction (bottom)

While the easily recognizable Cu(II) satellite peaks (942 eV and 962 eV) indicated surface oxidation in native Cu-NP, the two PEG phases did not contain Cu(II) after

reaction, ruling out the latter as the active oxidation state in agreement with the low performance observed for CuO (Table 3.10, entry 4). On the other hand, the close characteristic binding energies and very low concentration of copper in PEG made an unambiguously discrimination between Cu(0) and Cu(I) species impossible. Auger signals could have been useful to discriminate between Cu(I) and Cu(0) but did not show a satisfactory signal to noise ratio and hence could not be utilized. While the presence of Cu(II) after reaction can be excluded, the difference of *c.a.* 1 eV between the two catalytic systems can be due to different oxidation states but also to differences in charge compensation.

TEM investigations on PEG phases after catalysis showed, for both 5 mol% Cu-NP and CuI catalyzed reactions, aggregates of quite similar morphology (Figure 3.35) in which geometrical and spherical shaped particles with highly variable size (approximately from 10 to 50 nm) appear to coexist in large clusters. An HR-TEM / EDS analysis (Figure 3.36) suggests the presence of major quantities of residual $K_4[Fe(CN)_6]$ and Fe(0) obtained from the redox process involving the reduction of the latter by the hydroxyl end groups of polyol PEG,^{98,97} as well as a minor amount of copper (in accordance with the reaction stoichiometry). While clarifying the fate of iron in the cyanation reaction, these observations leave some uncertainty about the identification of the catalytically active copper species, for which more thorough characterization will be needed.



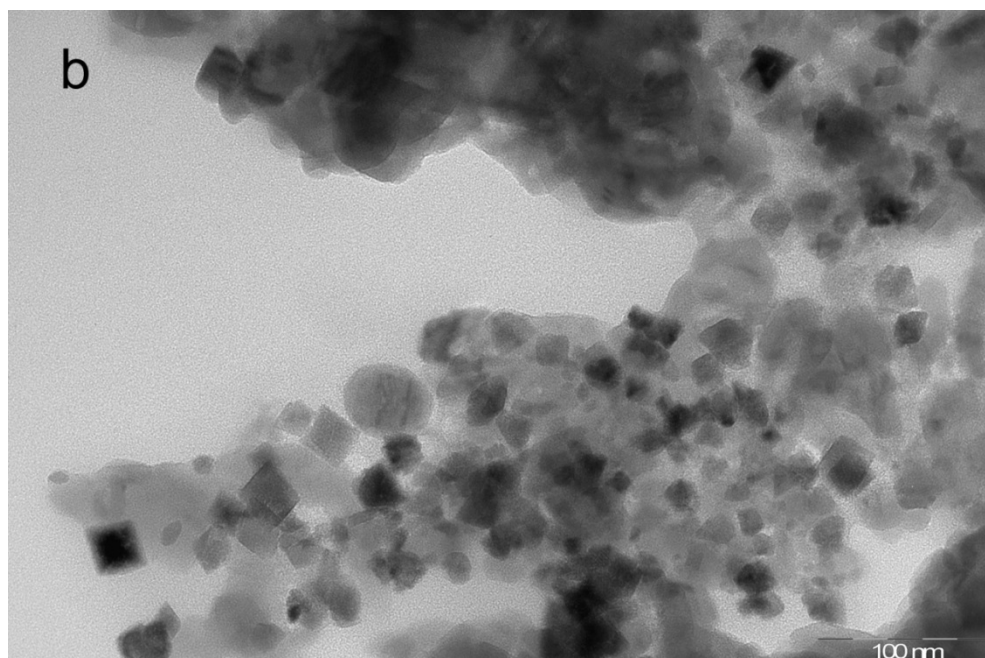
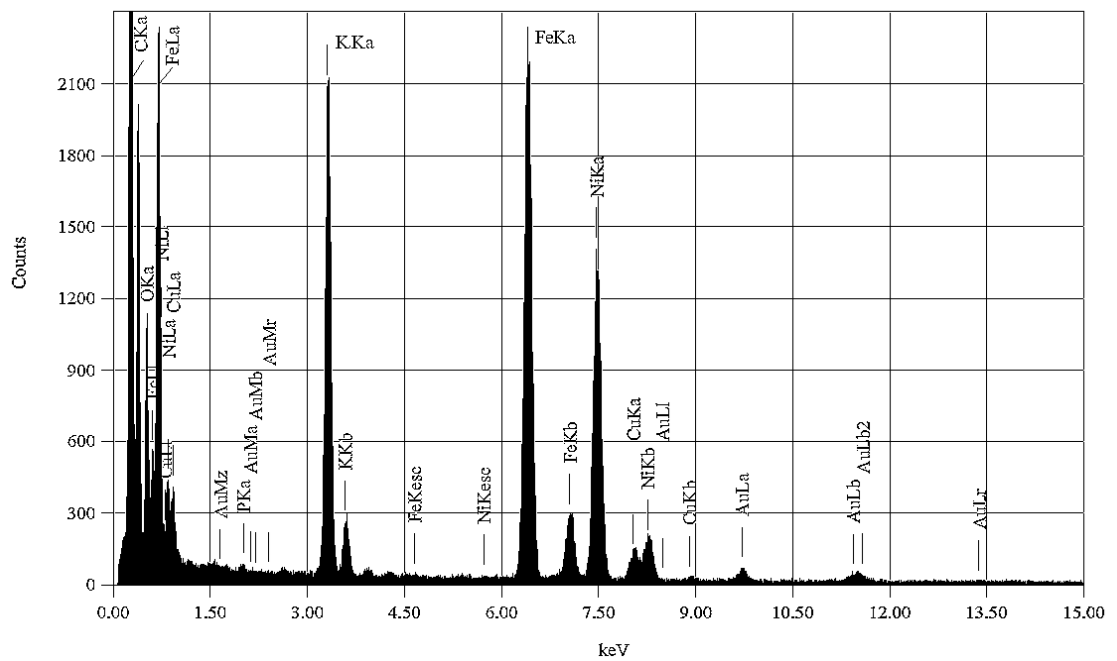
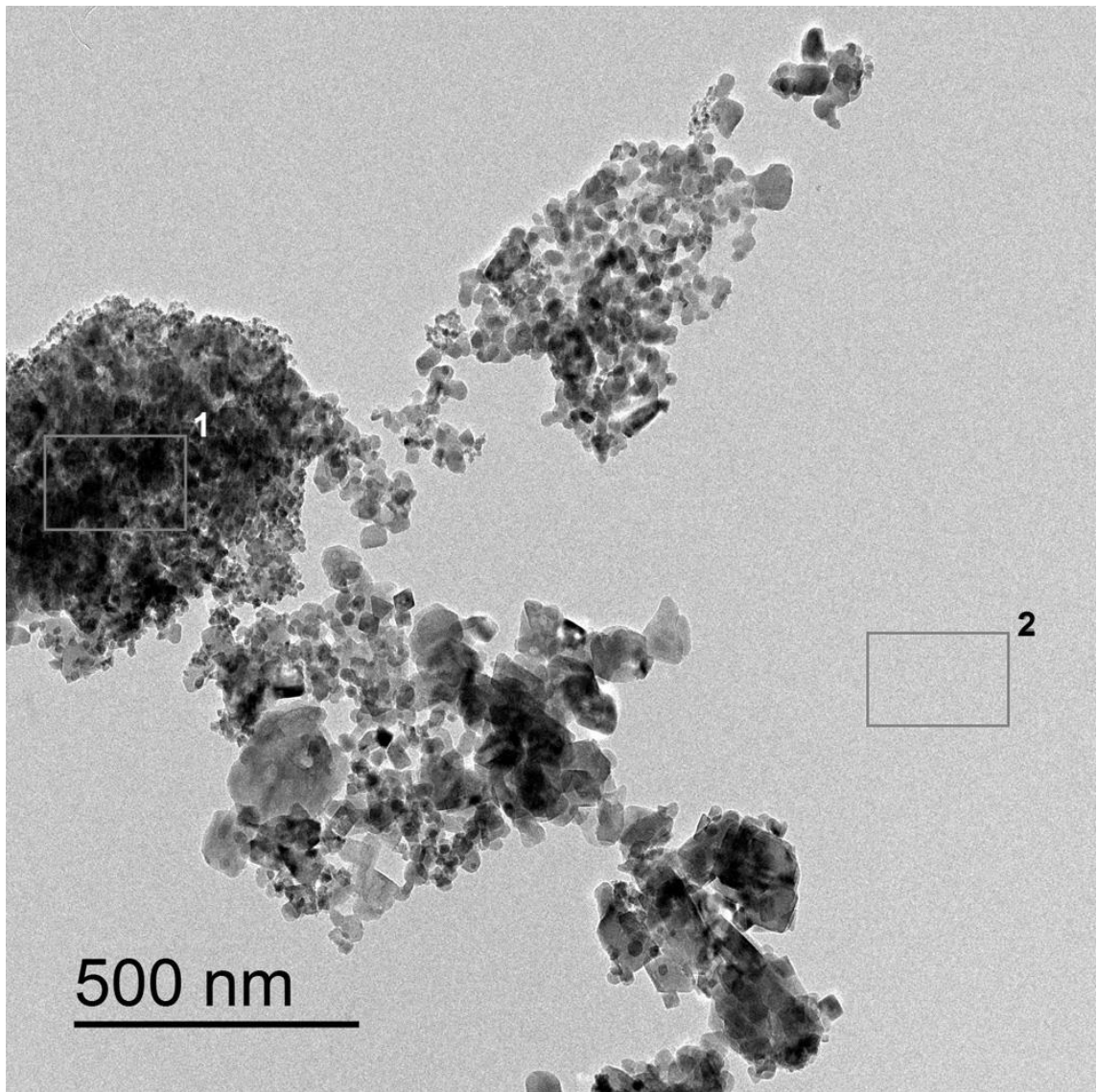


Figure 3.35 – TEM images of PEG phases recovered after reactions catalyzed by: (a) Cu-NP and (b) CuI



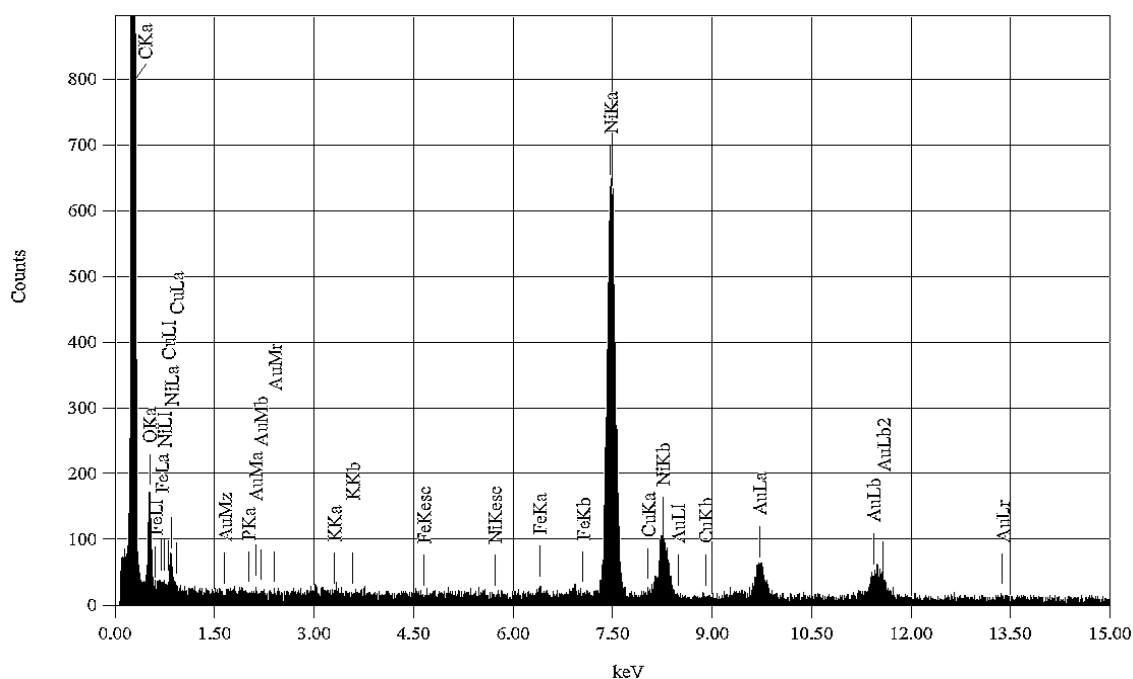
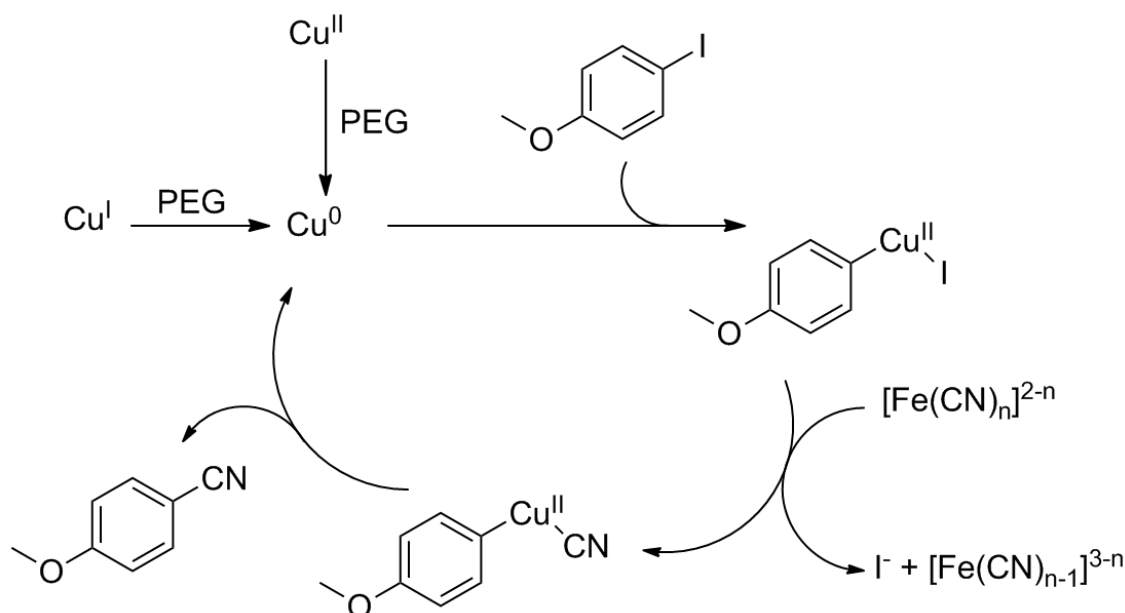


Figure 3.36 – HR-TEM image of the PEG phase recovered after a Cu-NP-catalyzed reaction (top); EDS analysis of targets ‘1’(middle) and ‘2’(blank) (bottom)

ICP-OES measurements performed on PEG recovered from the CuI-catalyzed (*i.e.* 5 mol%) 4-iodoanisole cyanation reaction showed copper concentrations of 570 ppm and 63 ppm in the polymer and product phase respectively, confirming hence a copper leaching of 10% into the organic phase. As a consequence, the organic product contamination is far from exceeding or even approaching the threshold levels for human copper intake (*i.e.* tolerable upper intake level = 10 mg/day).³³⁰ Iron concentrations of 2800 ppm and <0.01 ppm were found in the polymer phase and product respectively. This experimental result indicates that roughly half of the stoichiometric amount of $K_4[Fe(CN)_6]$ is effectively available for the cyanation reaction in melted PEG. In addition, this latter finding is in agreement with the visual observation that mechanical segregation of the salt to the flask neck occurred during the first minutes of sonication. This experimental problem might be resolved by developing a more sophisticated reactor setup, placing for example an ultrasound probe-dedicated tight septum between the probe and the neck, recycling of the segregated salt during sonication. The recycling of the polymer-based catalytic system was performed by melting the recovered PEG phase and adding fresh substrate and $K_4[Fe(CN)_6]$ to the polymer melt. As a result, a drop of the catalytic substrate conversion was registered for the second cycle (Table 3.10, entry 8 vs 2) probably due to the notable Cu-NPs aggregation displayed by TEM analyses. Based on these observations, we propose a reaction mechanism based on copper reduction by the polymer end groups followed by oxidative addition of the aryl

halide, coordination of the cyanide group with release of the halide and a reductive elimination yielding the benzonitrile product (Scheme 3.10). The intermediate Cu(0) and Cu(II) species can be easily stabilized by PEG matrix. The formation of stable $\text{Cu}_2[\text{Fe}(\text{CN})_6]$ complexes as well as the high affinity of cyanide ions towards copper-based catalysts could be responsible of a fast deactivation of the catalytic system.²¹² PEG polymer acts not only as the reaction solvent or reducing agent, but also as metal stabilizing protective matrix, thus avoiding high catalyst loading. Indeed, chelation of potassium cations thanks to its crown-ether like effect⁹² could be responsible for the improved reactivity of the ‘naked’ $[\text{Fe}(\text{CN})_6]^{4-}$ counter-ion under ultrasound activation.



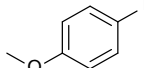
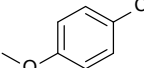
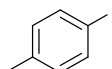
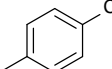
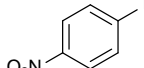
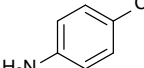
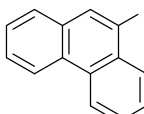
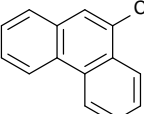
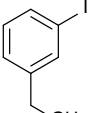
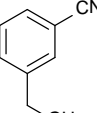
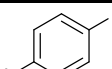
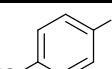
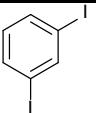
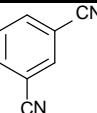
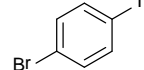
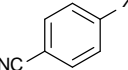
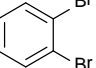
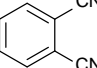
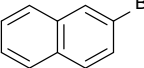
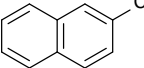
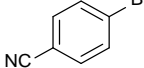
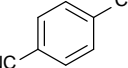
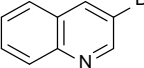
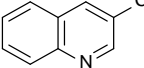
Scheme 3.10 – Proposed reaction mechanism for copper-catalyzed cyanation reactions with $\text{K}_4[\text{Fe}(\text{CN})_6]$ in melted PEG

It is worth noting that $\text{Pd}(\text{OAc})_2$ (1 mol%) could be employed as catalyst with good results under sonochemical conditions (Table 3.10, entry 9) while in recent attempts by our group (Table 3.10, entry 10), as well as in previous literature,³²⁷ Pd-based species failed to give satisfactory yields when microwaves were utilized as the energy source in the presence of bulk PEG. A blank reaction (*i.e.* with 0 mol% $[\text{Cu}]$) was carried out in order to exclude reagents or PEGs contamination by any catalytic species; no conversion was observed even after prolonged sonication (Table 3.10, entry 11).

On the basis of its good catalytic performance, inexpensive and environmentally benign CuI was selected as the optimal catalyst and used to study the reaction scope with a number of mono and bi-functional aryl iodides and bromides. Throughout this screening, a significantly lower amount of copper catalyst (*i.e.* 5 mol%) was employed

compared to literature reports (*i.e.* from 10 mol% to 30 mol%), obtaining good to excellent yields in relatively short reaction times. As a result, aryl iodides (Table 3.11, entries 1-7) were cyanated smoothly regardless of the electronic nature of substituents with the exception of *p*-nitro-iodobenzene which showed total conversion but only a moderate yield. With the latter substrate, the reduction of the nitro group occurs quantitatively.³³¹ assuming that a copper hydride species might be generated during the reaction course in the presence of hydroxyl (-OH) functional groups as previously described with other metals,³³² and stabilized by the presence of polyoxygenated PEG polymer backbone. Indeed, the extraction of the cyanoaniline from PEG phase is probably hampered by the affinity between oxygen atoms in the polymer chain and the polar -NH₂ / -NH₃⁺ groups of the product.³³³

In the presence of KI (60% molar ratio), electron-poor or neutral aryl bromides gave high yields too, although longer sonication times were needed compared to iodides (Table 3.11, entries 9-12); on the other hand, electron-rich aryl bromides proved typically less active. The reaction with *p*-bromo-iodobenzene (Table 3.11, entry 8) exhibited high conversion but low chemoselectivity as cyanation occurred at the iodide group (prevalently), bromide group or both, even without the addition of KI. Cyanation of 3-chloroanisole was tentatively performed under these conditions but conversion into benzonitrile failed even after 1 h of sonication.

Entry ^a	Substrate	Product	Time ^b (min)	Conversion ^c (%)	Yield ^d (%)
1			20	92	84
2			20	87	80
3			20	>99	57 ^e
4			20	97	97
5			20	94	91
6 ^f			20	>99	88
7 ^f			20	>99	95
8			20	87	87 ^g
9 ^{f,h}			60	>99	70
10 ^h			90	90	88
11 ^h			60	95	75
12 ^h			60	86	82

^a Arylhalide (4.0 mmol), K₄[Fe(CN)₆] (2.4 mmol), CuI (0.2 mmol), melted PEG-5600 as a PEG-3400 / PEG-10000 weighted mixture (20.0 g), N₂ atmosphere, US amplitude (A) = 70%, US frequency = 20 KHz; ^b Pulsed sonication (on / off = 5 sec / 5 sec); ^c Conversion was determined by HPLC and ¹H NMR; ^d Yield was determined by ¹H NMR using CH₂Br₂ as internal standard; ^e No 4-Nitrobenzonitrile was obtained; ^f Arylhalide (2.0 mmol), K₄[Fe(CN)₆] (2.4 mmol), CuI (0.2 mmol), melted PEG-5600 (20.0 g), N₂ atmosphere; ^g Product is a mix of X = Br (44%), X = CN (24%) and X = I (19%); ^h KI (2.4 mmol) was used.

Table 3.11 – CuI-catalyzed cyanation of arylhalides in melted PEG-5600

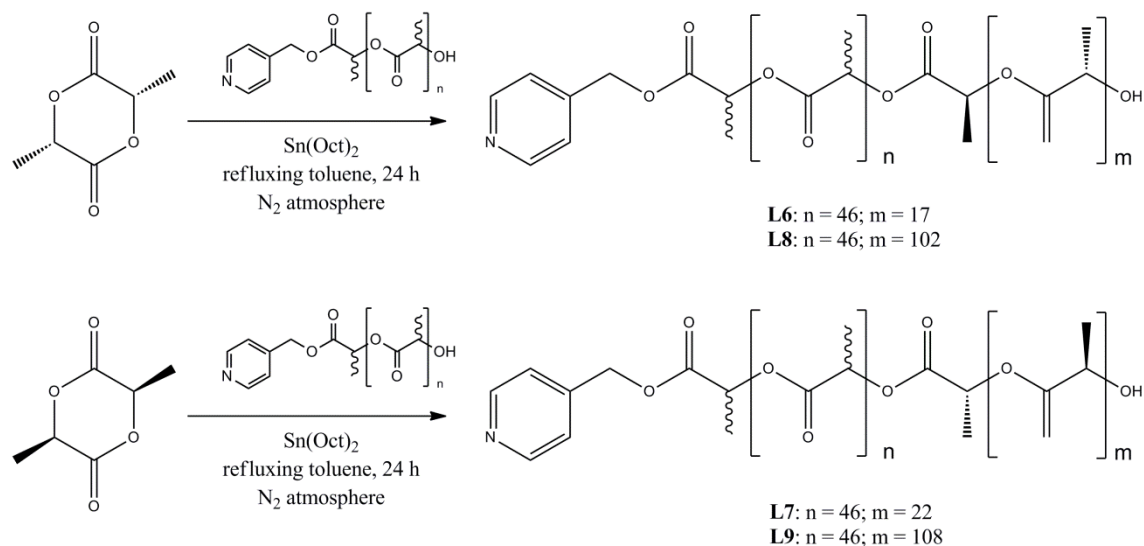
3.5 Synthesis of PLA- and PEG-based macroligands for future developments

With the aim of expanding the range of available macroligands for future applications in the fields of supported catalysis and material science, further syntheses were carried out

focusing on (i) copolymers bearing PLA with different tacticity, (ii) coupling reactions between preformed PLA-Py macroligands or (iii) the functionalization of PEG with a phosphinic moiety.

3.5.1 Synthesis of PLA-based stereoblock copolymers

The use of the –OH end group of P(LD)LA-based macroligand **L2** ($M_n = 3700$ g/mol) as the initiator for the polymerization of L- or D-LA allowed to obtain Py-functionalized stereoblock copolymers **L6** – **L9** bearing an atactic, amorphous block covalently linked to an isotactic, crystalline block with L (**L6**, **L8**) or D (**L7**, **L9**) configuration (Scheme 3.11). In order to optimize homogeneity in the presence of the bulky polymeric macroinitiator, refluxing toluene was needed as the polymerization solvent in the place of the previously described ROP procedure in the melt, while the amount of Sn(Oct)₂ was kept constant (*i.e.* 0.5 mol%). Isotactic blocks with different molecular weights could be obtained by tuning the LA : **L2** ratio; more precisely, a 20 : 1 ratio was used to synthesize an L- (**L6**) or D-block (**L7**) with M_n of approximately 1500 g/mol, while a ratio of 100 : 1 yielded an L- (**L8**) or D-block (**L9**) with M_n of approximately 8000 g/mol, as evaluated by GPC and ¹H NMR measures.



Scheme 3.11 – Synthesis of PLA-based stereoblock copolymers **L6** – **L9** from macroligand **L2**

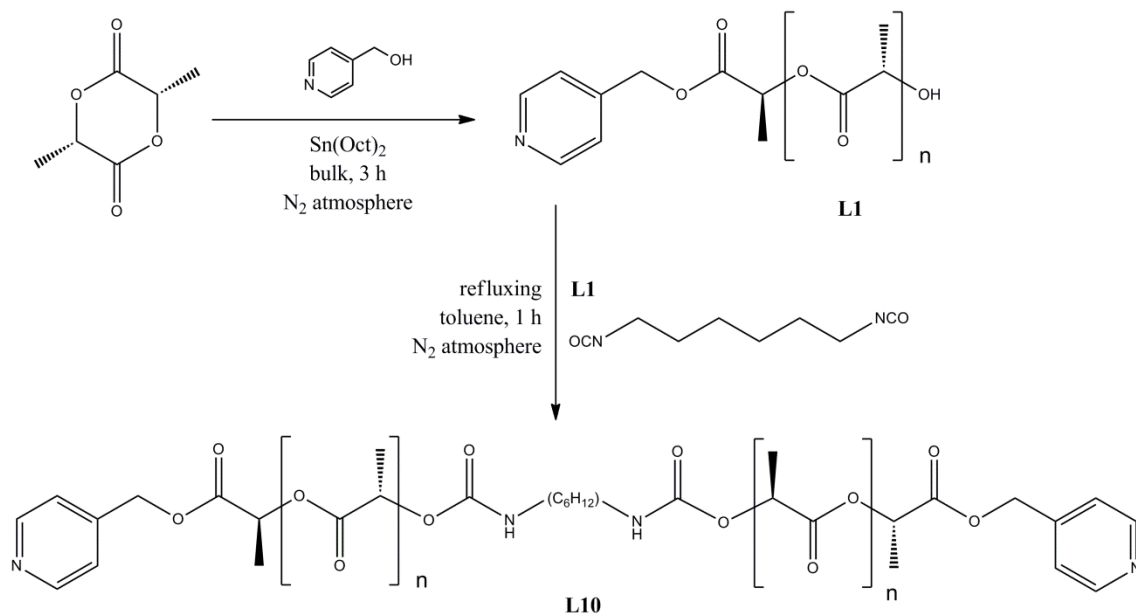
This class of macroligands was synthesized with the aim of supporting a catalyst to polymer chains bearing isotactic blocks of opposed configuration, which in solution (*e.g.* in toluene) form a stereocomplex with markedly decreased solubility with respect to the atactic block. Hence, the system is engineered to expose the metal binding groups towards the organic solution at high temperature and, subsequently, to restore a PLA stereocomplex core at low temperature allowing to precipitate the polymer-bound

catalyst without the addition of a non-solvent. Hence, preliminary solubility tests were performed by adding equimolar amounts of **L6** and **L7** to toluene (200 mg of **L6** / **L7** mixture in 10 mL) and comparing the response to temperature variations with those of a solution containing pure **L6**. As a result, the **L6** / **L7** mixture gave a slightly turbid, colorless liquid phase at room temperature while **L6** dissolved completely to form a clear, pale-pink solution. When the temperature was raised to 70 °C, the turbidity of the **L6** / **L7** mixture decreased progressively to give, after 5 min, a clear solution resembling pure **L6**; lowering the temperature back to 25 °C, the **L6** / **L7** mixture turned turbid again reverting to the initial appearance. Upon 15 minutes of centrifugation (3000 rpm) a pale-pink powdery precipitate separated from the clear colorless toluene phase and could be recovered and dried; on the other hand the solution containing pure **L6** remained clear. Although the observations of high temperature dissolution and low temperature aggregation appeared promising, the recovered mass of polymer was only 80% of the initial quantity. Longer isotactic blocks induce stronger stereocomplexation and reduce the overall solubility of macroligands; indeed, when the solubility test was repeated employing a **L8** / **L9** mixture vs pure **L8** a temperature of 90 °C in the place of 70 °C was needed to obtain a clear solution for both samples. After cooling to room temperature both the **L8** / **L9** mixture and pure **L8** turned turbid, nonetheless, upon centrifugation (15 min at 3000 rpm) the **L8** / **L9** mixture separated neatly from the clear toluene phase while pure **L8** remained in the turbid liquid phase with only a minor amount of precipitate. In contrast with the previous test, in the case of the **L8** / **L9** mixture a complete recovery of dry polymer was achieved, demonstrating the important influence of the M_n of P(L)LA and P(D)LA isotactic blocks on the macroligand solubility.

3.5.2 Synthesis of Py-P(L)LA-Py difunctional macroligand

The difunctional macroligand **L10** could be obtained from two equivalents of **L1** by a chain coupling reaction between the –OH tail groups of the preformed Py-functionalized P(L)LA chains and hexamethylene diisocyanate (Scheme 3.12). The reaction was carried out in refluxing toluene under rigorously dry conditions and N₂ atmosphere to avoid the formation of single-chain adducts which would require a difficult and inefficient purification step. The coupling completion and the purity of the bifunctional macroligand were verified by means of a proton NMR spectrum, showing the absence of the quartet signal at 4.36 ppm related to unreacted CH(CH₃)OH tail groups. Moreover, the spectrum shows the appearance of a multiplet at 3.15 ppm which can be assigned to the methylene groups in α position with respect to the urethane moieties and,

hence, witnesses the binding of the linker to the polymer chains. A GPC-RI analysis comparing **L10** and **L1** evidences an approximate doubling of the macroligand M_n (*i.e.* 6280 g/mol vs 3280 g/mol) as well as a reduction in polydispersity from 1.33 to 1.17, (Figure 3.37) which are both indicative evidences of an effective coupling.



Scheme 3.12 – Synthesis of Py-P(L)LA-Py difunctional macroligand **L10** by chain coupling of **L1** with hexamethylene diisocyanate

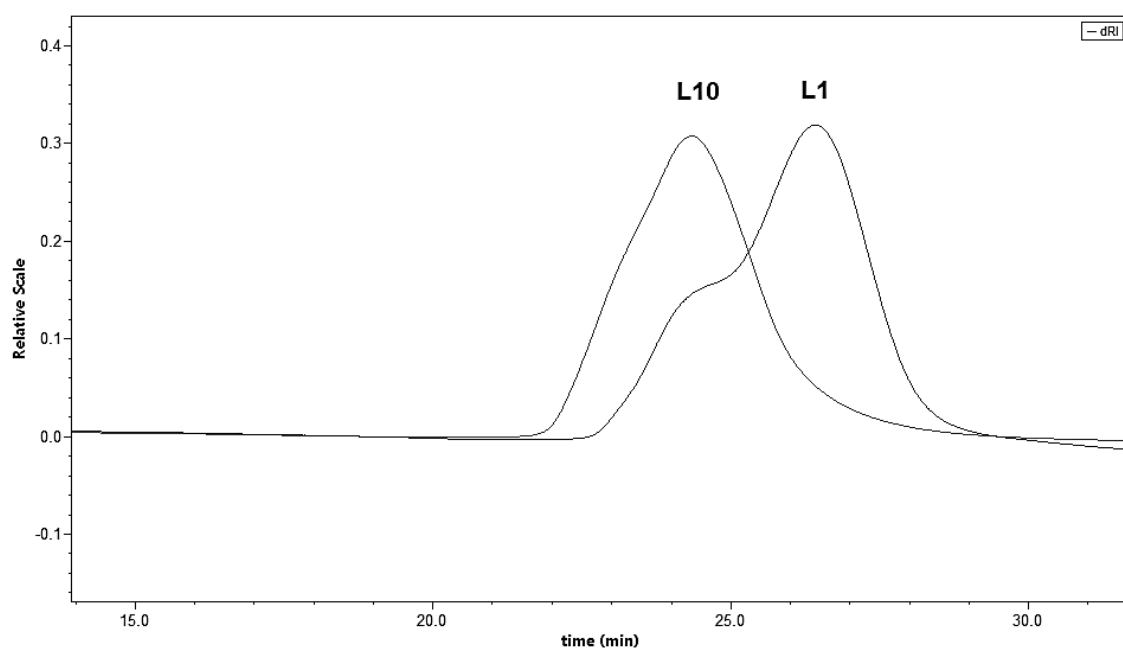


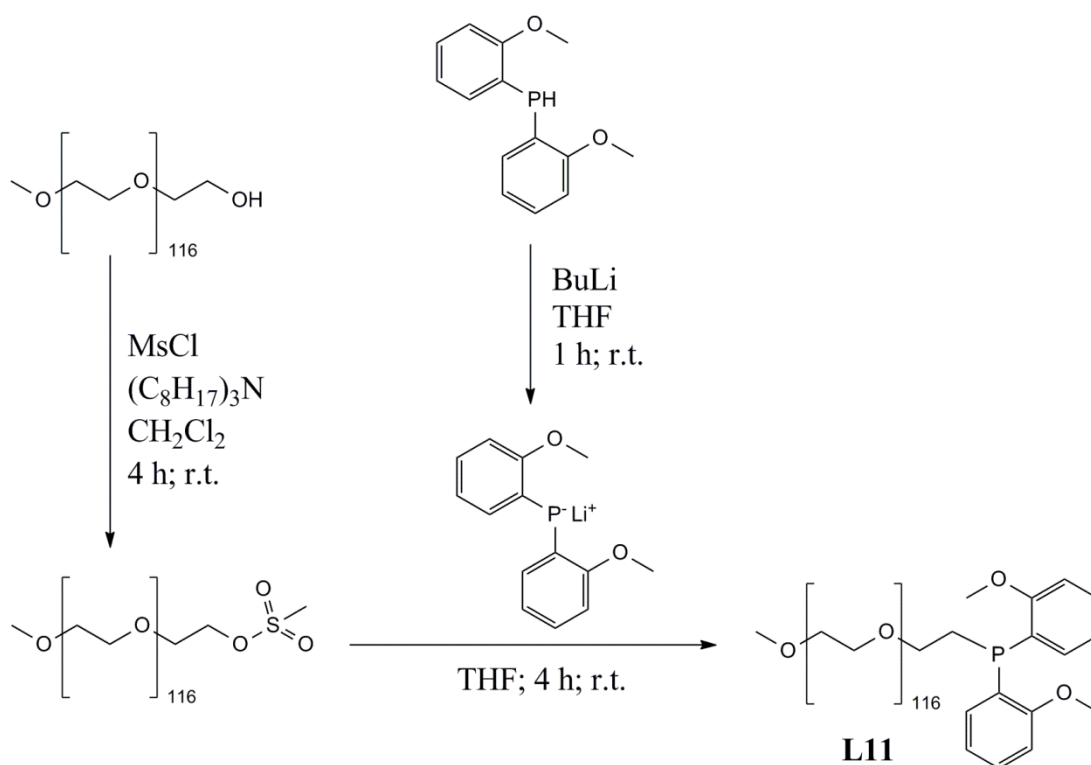
Figure 3.37 – GPC-RI curves of P(L)LA-based macroligands **L1** and **L10**

L10 was synthesized with the aim of expanding future research towards the field of polycondensation-type macrocomplexes, for which a linear polymer chain bearing a

pyridine group at each end could be an ideal “macromonomer”. Unfortunately, when **L10** was employed for preliminary tests and tentatively reacted with PdCl₂ or Pd(OAc)₂, a mixture of complexes was obtained with a very high polydispersion index. This finding suggests that future efforts will be necessary to control the molecular weight of the polycondensation-type product by adjusting the conditions of the metal coordination step.

3.5.3 Synthesis of phosphine end-capped PEG methyl ether (**L11**)

The functionalization of PEG with di-*o*-anisylphosphine requires a first step in which the Li salt of the phosphine is formed in THF solution followed by the reaction of the latter (which is used in large excess of 3 : 1) with a solution of mesylated MeO-PEG-5000 in the same solvent (Scheme 3.13). The achieved functionalization was proved by means of ¹H NMR spectroscopy (the -OSO₂CH₃ singlet at 3.09 ppm is replaced by the -C₆H₄OCH₃ singlet at 3.80 ppm) (Figure 3.38) and ³¹P NMR spectroscopy (the singlet for PEG-*P(o-anisyl)*₂ at -40.73 ppm is the only signal of the spectrum and signals for PH at -72.80 ppm or P=O at -27.54 ppm are not visible).



Scheme 3.13 – Synthesis of the phosphine-functionalized macroligand L11

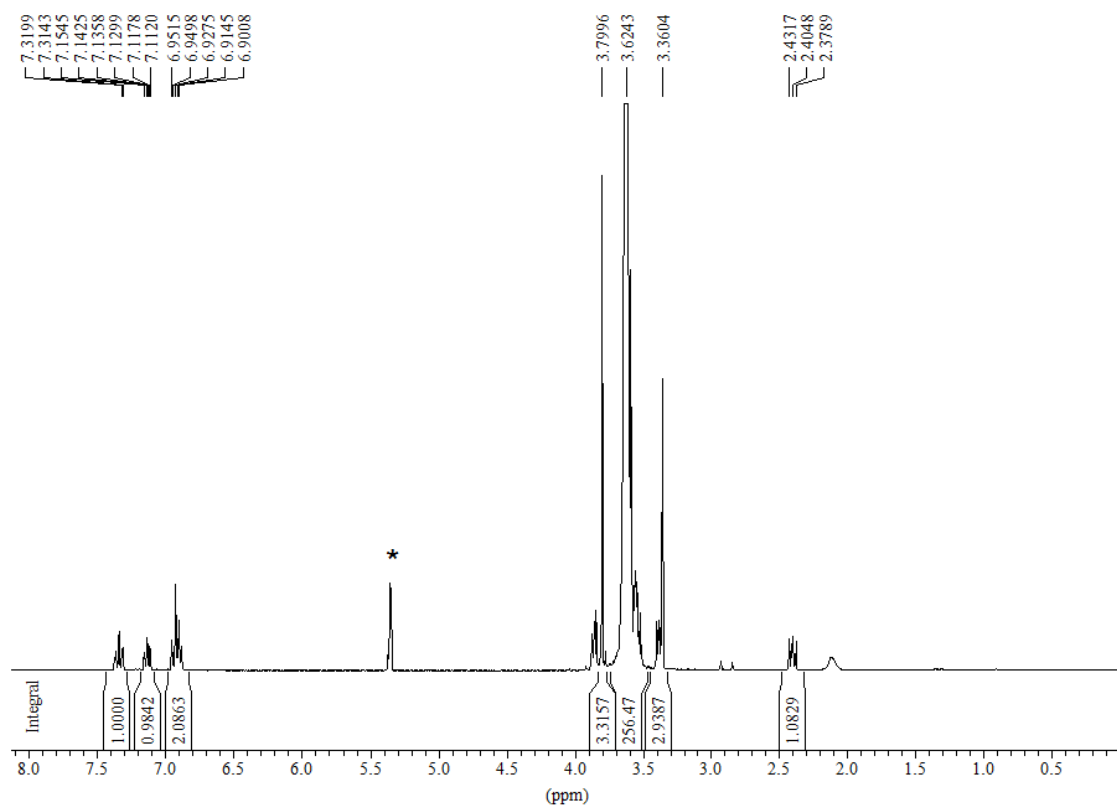


Figure 3.38 – ^1H NMR spectrum of PEG-based macroligand **L11** in CD_2Cl_2

It was chiefly important to work constantly under a dry, N_2 atmosphere as well as to utilize distilled THF and carefully degassed solvents to avoid the formation of unwanted $\text{P}=\text{O}$ byproducts or the deactivation of BuLi and the lithium salt of the phosphine. Nonetheless, the workup procedure could be performed outside the glovebox without detrimental effects on the macroligand. An additional purification step (*i.e.* reprecipitation from dichloromethane with a 2-propanol / diethyl ether mixture) was necessary to eliminate some residual unreacted phosphine from the macroligand; anyhow, in spite of the time-consuming and relatively complex synthesis, **L11** was obtained with a good overall yield of 70 % and excellent purity. **L11** may be a useful building block for the synthesis of novel macrocomplexes in which the presence of phosphine-based ligands is required for catalytic applications as well as if a donor group with a different hard / soft character with respect to pyridines will be needed. Potential research advances include the combined use of P- and N-based macroligands to coordinate metal ions with a different affinity, allowing the exchange between macroligands and, hence, the development of materials with reversible or stimuli-responsive properties.

4 Conclusions

The present thesis describes the synthesis and characterization of PLA-, PCL- and PEG-based macroligands and the metal-polymer macrocomplexes obtained by coordination of macroligands to metal ions, with particular reference to Pd(II). The use of macroligands and macrocomplexes and the role of the related polymers in catalytic systems for organic syntheses are also investigated and discussed.

Firstly, the macroligands **L1**, **L2** and **L3**, bearing an end-capping 4-pyridinemethylene moiety, were obtained by a Sn(Oct)₂-catalyzed ROP of L-lactide, racemic lactide and ϵ -caprolactone, respectively. These macroligands were coordinated for the first time to Pd(II) to obtain macrocomplexes with neutral, linear (**1**, **2**, **11**) or monocationic, V-shaped (**4**, **5**) or bis-cationic star-shaped (**6** – **9**, **12** – **16**) structures. This range of novel metal-polymer coordination compounds has been characterized in solution by NMR and UV-Vis spectroscopy and GPC analyses as well as in the solid state by DSC and variable-temperature XRD analyses. The reversibility of the macroligand coordination was demonstrated upon reactions of the macrocomplexes with appropriate ligands (*i.e.* chloride and phosphanes), while the stepwise synthesis of the Pd-macrocomplexes allowed the easy formation of both homo- and heteroleptic species. The latter contained combinations of poly(lactic acid) of different stereochemistry and PCL leading to materials with different physical and thermal properties compared to both the homoleptic counterparts and the free macroligands.

Furthermore, in order to exploit the Pd-anchored polymer as a soluble and recoverable catalyst, macroligands **L1** and **L3** were coordinated to Pd(OAc)₂ in a *trans* configuration yielding, respectively, the homoleptic, linear macrocomplexes **17** and **18**. These complexes were tested as supported homogeneous catalysts for the aerobic oxidation of alcohols in toluene (70 °C); unlike **L3**, **L1** showed high stability against polymer chain degradation under the required catalytic conditions. From a screening of the catalytic performance of **17** and **18** vs a reference system (*i.e.* *trans*-[Pd(OAc)₂(4-EtPy)₂] (4-EtPy = 4-ethylpyridine)) emerged that: (i) **17** is superior to **18** concerning substrate conversion, which might be due to the different chain flexibility between PLA- and PCL-based macroligands, influencing the access of the substrate to the palladium centre; (ii) the addition of two molequivalents of **L1** to **17**-catalyzed reactions (*i.e.* **17**+2**L1**) led to a catalytic system that showed a superior stability against Pd-black

formation compared to the analogous reference system, due to an efficient polymer chain-assisted separation of the metal centers that prevents agglomeration of Pd in the course of the catalytic reaction; (iii) unlike the reference system, **17+2L1** can be recovered from the reaction solution by simple precipitation of the polymer and reused for several consecutive catalytic runs with only a moderate loss of activity.

With the aim of expanding the catalytic possibilities to water-phase reactions, a PEG-based macroligand **L4** was synthesized by mesylation and, successively, pyridine end-functionalization of commercial poly(ethylene glycol) monomethyl ether. **L4** was then employed to stabilize Pd(II) in well-defined neutral, linear (**20**) and bis-cationic, star-shaped (**21**) macrocomplexes with a **L4** : Pd molar ratio of 2 :1 and 4 :1, respectively. Unlike **20**, **21** revealed to be a suitable molecular precursor for the generation of stabilized and well-dispersed Pd-NPs (**23**) (mean diameter of 6.33 ± 1.40 nm) by reduction of the metal center with H₂. Interestingly, TG analyses proved that the homogeneous distribution of Pd-NPs in **23** exerted a significant stabilizing effect on **L4** against the oxidative thermal degradation of the PEG chain. From a screening of the Pd(II)- and Pd-NPs-based catalysts in the aerobic oxidation reaction of α,β -unsaturated alcohols in water (60 °C; 30 bar of air), **23** emerged as the most stable catalyst, maintaining TOF values up to 200 h⁻¹ and high selectivity throughout prolonged reaction times. This catalytic system was recyclable upon extraction of products with diethyl ether and showed an extremely low Pd leaching (c.a. 25 ppb) into the organic phase.

On the other hand, when the pyridine-end capped **L4** was combined with non functionalized PEG and utilized as solvent for the sonochemically enhanced cyanation of aryl halides, the Cu-based catalyst showed a decreased activity compared to ligand-free conditions, probably due to the steric hindrance of the macroligand. Nonetheless, driven by the environmentally benign characteristics of PEG, we demonstrated the feasibility and effectiveness of the reaction in melted, non functionalized PEG-5600 and proved that, in order to maximize conversions and yields, the viscosity of the sonication medium was a parameter of chief importance. Under these conditions, aryl iodides and electron-poor aryl bromides could be converted to nitriles employing K₄[Fe(CN)₆] as the cyanide source and a relatively low amount (*i.e.* 5% molar ratio) of safe and inexpensive CuI as catalyst. The reaction proved to be fast and selective, although the activity of the catalytic system decreased upon recycling; the quantity of copper leached into benzonitrile products was far from troublesome limits, suggesting the procedure as potentially suitable for food or pharmaceutical applications.

Lastly, with the aim of expanding the range of available macroligands for future applications in the fields of supported catalysis and material science, further syntheses were carried out focusing on (i) stereoblock copolymers combining PLA with different tacticity (*i.e.* **L6** – **L9**), (ii) the coupling reaction between preformed **L1** to obtain a di-functional Py-PLA-Py type macroligand (*i.e.* **L10**) or (iii) the functionalization of PEG with a phosphinic donor group (*i.e.* **L11**).

5 References

1. Kaplan, D. L.; Hartman, H. M. "High Molecular Weight Polylactic Acid Polymers", in: *Biopolymers from Renewable Resources, 1st edition*, Ed. Springer Berlin **1998**, 367.
2. Auras, R.; Harte, B.; Selke, S. *Macromol. Biosci.* **2004**, *4*, 835.
3. Witzke, D. R. *PhD thesis, Michigan State University, East Lansing, MI* **1997**, 398.
4. Hoogstein, W.; Postema, A. R.; Pennings, A. J.; Brinke, G. T.; Zugenmaier, P. *Macromolecules* **1990**, *23*, 634.
5. Nature Works; www.natureworks.com.
6. Perego, G.; Cella, G. D.; Bastioli, C. *J. Appl. Polym. Sci.* **1996**, *59*, 37.
7. Doi, Y.; Fukuda, K. *Biodegradable Plastics and Polymers: Proceedings of the Third International Scientific Workshop on Biodegradable Plastics and Polymers, Osaka, Japan (Studies in Polymer Science, 12)*, Elsevier Science, New York **1994**, 464.
8. Auras, R. *PhD Thesis, Michigan State University, East Lansing, MI* **2004**, 268.
9. Stiles, M. E.; Holzappel, W. H. *J. Food. Microbiol.* **1977**, *36*, 1.
10. Ramirez-Lopez, C. A.; Ochoa-Gomez, J. R.; Torricella-Soria, J. *Ind. Eng. Chem. Res.* **2010**, *49*, 6270.
11. Sentisiran, A.; Arasaratnam, V.; Balasubramaniam, K. *J. Natl. Sci. Found. Sri Lanka* **1999**, *27*, 107.
12. Dubois, P.; Coulembier, O.; Raquez, J. *Handbook of Ring Opening Polymerization, Wiley-VCH* **2009**.
13. Yin, M.; Baker, G. L. *Macromolecules* **1999**, *32*, 7711.
14. Gruber, P. R.; Hall, E. S.; Kolstad, J. H.; Iwen, M. L.; Benson, R. D.; Borchardt, R. L. *US Patent 5142023* **1992**.
15. Kricheldorf, H. R.; Dunsing, R. *Die Makromol. Chem.* **1986**, *187*, 1611.
16. Kricheldorf, H. R.; Kreiser-Saunders, I. *Die Makromol. Chem.* **1990**, *191*, 1057.
17. Dechy-Cabaret, O.; Martin-Vaca, B.; Bourissou, D. *Chem. Rev.* **2004**, *104*, 6147.
18. Kim, Y.; Verkade, J. G. *Macromol. Symp.* **2005**, *224*.
19. Kowalski, A.; Duda, A.; Penczek, S. *Macromolecules* **2000**, *33*, 7359.
20. Kricheldorf, H. R.; Berl, M.; Schannagl, N. *Macromolecules* **1988**, *21*, 286.
21. Dubois, P.; Jerome, R.; Teyssie, P. *Die Makromol. Chem.* **1991**, *42*, 103.
22. Stevels, W. M.; Ankone, M. J. K.; Dijkstra, P. J.; Feijen, J. *Macromolecules* **1996**, *29*, 8296.
23. Culkin, D. A.; Jeong, W.; Csihony, S.; Gomez, E. D.; Balsara, N. P.; Hendrick, J. L.; Waymouth, R. M. *Angew. Chem. Int. Ed.* **2007**, *46*, 2627.
24. Coulembier, O.; Lohmeijer, B. G. G.; Dove, A. P.; Pratt, R. C.; Mespouille, L.; Culkin, D. A.; Benight, S. J.; Dubois, P.; Waymouth, R. M.; Hedrick, J. L. *Macromolecules* **2006**, *39*.
25. Dove, A. P.; Li, H.; Pratt, R. C.; Lohmeijer, B. G. G.; Culkin, D. A.; Waymouth, R. M. *Chem. Commun.* **2006**, 2881.
26. Kricheldorf, H. R.; Schwarz, G. *Macromol. Rapid Commun.* **2003**, *24*, 359.
27. Dattaa, R.; Tsaia, S. P.; Bonsignorea, P.; Moona, S. H.; Frank, J. R. *FEMS Microbiol. Rev.* **1995**, *16*, 221.
28. Whiteman, N. "2000 Polymers, Laminations and Coatings Conference" - Chicago, IL **2000**, 631.
29. Vink, E. T. H.; Ràbago, K. R.; Glassner, D. A.; Springs, B.; O'Connor, R. P.; Kolstad, J. J.; Gruber, P. *Macromol. Biosci.* **2004**, *4*, 551.

30. Li, D.; Frey, W.; Baeumner, A. J. *J. Memb. Sci.* **2006**, *279*, 354.
31. Kawahima, N.; Ogawa, S.; Obuchi, S.; Matsuo, M.; Yagi, T. "Polylactic acid "LACEA"", in: *Biopolymers. Polyesters III. Applications and Commercial Products, 1st edition*, Y. Doi, A. Steinbuchel, Eds., Wiley-VCH Verlag GmbH, Weinheim **2002**, 251.
32. Biela, T.; Duda, A.; Penczek, S. *Macromolecules* **2006**, *39*, 3710.
33. Spinu, M.; Gardner, K. H. *Polym. Mater. Sci. Eng.* **1994**, *74*, 19.
34. Radano, C. P.; Baker, G. L.; Smith, M. R. J. *J. Am. Chem. Soc.* **2000**, *122*, 1552.
35. Younes, H.; Cohn, D. *Eur. Polym.* **1988**, *24*, 765.
36. Wang, J. D.; Mandel, F. S.; Popov, V. K.; Howdel, S. M. *Ceram. Trans.* **2000**, *107*, 97.
37. Zheng, X.; Zhou, S.; Li, X.; Weng, J. *Biomaterials* **2006**, *27*, 4288.
38. Samyn, C.; Van Beylen, M. *Makromol. Chem., Macromol. Symp.* **1988**, *19*, 225.
39. Yamamoto, Y.; Nagasaki, Y.; Kato, M.; K., K. *Biointerfaces* **1999**, *16*, 135.
40. Van Natta, F. J.; Hill, J. W.; Carruthers, W. H. *J. Am. Chem. Soc.* **1934**, *56*, 455.
41. Huang, S. In: *Encyclopedia of Polymer Science and Engineering*. New York; John Wiley and Sons **1985**, 220.
42. Pitt, C. G. In: *biodegradable polymers as drug delivery systems*. New York; Marcel Dekker **1990**, 71.
43. Okada, M. *Progr. Polym. Sci.* **2002**, *27*, 87.
44. Nair, L. S.; Laurencin, C. T. *Biomaterials* **2007**, *32*, 762.
45. Chandra, R.; Rustgi, R. *Progr. Polym. Sci.* **1998**, *23*, 1273.
46. Zein, I.; Hutmacher, D. W.; Tan, K. C.; Teo, S. H. *Biomaterials* **2002**, *23*, 1169.
47. Huang, H.; Oizumi, S.; Kojima, N.; Niino, T.; Sakai, Y. *Biomaterials* **2007**, *28*, 3815.
48. Marrazzo, C.; Di Maio, E.; Iannace, S. *Polym. Eng, Sci.* **2008**, *48*, 336.
49. Lee, K. H.; Kim, H. Y.; Khil, M. S.; Ra, Y. M.; Lee, D. R. *Polymer* **2003**, *44*, 1287.
50. Luciani, A.; Coccoli, V.; Orsi, S.; Ambrosio, L.; Netti, P. A. *Biomaterials* **2008**, *29*, 4800.
51. Storey, R. F.; Taylor, A. E. *Abstr. Pap. Am. Chem. Soc.* **1996**, *211*, 114.
52. Hayashi, T. *Progr. Polym. Sci.* **1994**, *19*, 663.
53. Coulembier, O.; Degee, P.; Hedrick, J. L.; Dubois, P. *Progr. Polym. Sci.* **2006**, *31*, 723.
54. Koleske, J. In: *Polymer blends*. New York; Academic Press Inc. **1978**, 369.
55. Vert, M. *J. Mater. Sci. Mater. Med.* **2009**, *20*, 437.
56. Gunatillake, P. A.; Adhikari, R. *Eur. Cells Mater.* **2003**, *5*, 1.
57. Middleton, J. C.; Tipton, A. J. *Biomaterials* **2000**, *21*, 2335.
58. Hollande, S. J.; Tighe, B. J. In: *Advances in Pharmaceutical Science*, vol. 6. London; Accademic Press Inc. **1992**, 101.
59. Chen, D. R.; Bei, J. Z.; Wang, S. G. *Polym. Degrad. Stab.* **2000**, *67*, 455.
60. Persenaire, O.; Alexandre, M.; Degee, P.; Dubois, P. *Biomacromolecules* **2001**, *2*, 288.
61. Pitt, C. G.; Gratzl, M. M.; Kimmel, G. L.; Surles, J.; Schindler, A. *Biomaterials* **1981**, *2*.
62. Ye, W. P.; Du, F. S.; Jin, W. H.; Yang, J. Y.; Xu, Y. *React. Funct. Polym.* **1997**, *32*, 1997.
63. Huang, M. H.; Li, S. M.; Hutmacher, D. W.; Coudane, J.; Vert, M. *J. Appl. Polym. Sci.* **2006**, *102*, 1681.
64. Albertsson, A. C.; Karlsson, S. In: *Macromolecular design of polymeric materials*. New York/Basel/Hong Kong; Marcel Dekker Inc. **1997**, 739.
65. Vert, M. *Progr. Polym. Sci.* **2007**, *32*, 755.

66. Woodward, S. C.; Brewer, P. S.; Moatamed, F.; Schindler, A.; Pitt, C. G. *J. Biomed. Mater. Res.* **1985**, *19*.
67. *Toxicological Evaluation of Certain Food Additives, WHO - Food Additive Series 14.* **1979**.
68. Harris, J. M. *Poly(ethylene glycol) chemistry, in: Biotechnical and Biomedical Applications, Plenum Press, New York/London.* **1992**.
69. Knop, K.; Hoogenboom, R.; Fischer, D.; Schubert, U. S. *Angew. Chem. Int. Ed.* **2010**, *49*, 6288.
70. Milton Harris, J.; Zalipsky, S. *Poly(ethylene glycol): Chemistry and Biological Applications, ACS, Washington.* **1997**.
71. Gravert, D. J.; Janda, K. D. *Chem. Rev.* **1997**, *97*, 489.
72. Bailey Jr, F. E.; Koleske, J. *Poly(ethylene oxide), Academic Press, New York.* **1976**.
73. Haldebrant, D. J.; Jessop, P. G. *J. Am. Chem. Soc.* **2003**, *125*, 5600.
74. Wang, J. Q.; He, L. N.; Miao, C. X.; Gao, J. *ChemSusChem* **2009**, *2*, 755.
75. Pielichowski, K.; K., F. *Polym. Adv. Technol.* **2002**, *13*, 690.
76. Totten, G. E.; Clinton, N. A.; Matlock, J. J. *Macromol. Sci. Rev. Macromol. Chem. Phys.* **1998**, *38*, 77.
77. Pasut, G.; Veronese, F. M. *Progr. Polym. Sci.* **2007**, *32*.
78. Duncan, R.; Vicent, M. J.; Greco, F.; Nicholson, R. I. *Endocr. Relat. Cancer* **2005**, *12*, S189.
79. Allen, T. M.; Cullis, P. R. *Science* **2004**, *303*, 1818.
80. Torchilin, V. P.; Trubetskoy, V. S. *Adv. Drug Delivery Rev.* **1995**, *16*, 141.
81. Luxenhofer, R.; Bezen, M.; Jordan, R. *Macromol. Rapid Commun.* **2008**, *29*, 1509.
82. Grayson, S. M.; Godbey, W. T. *J. Drug Targeting* **2008**, *16*, 329.
83. Veronese, F. M.; Pasut, G. *Drug Discovery Today* **2005**, *10*, 1451.
84. Passirani, C.; Benoit, J. P. *Biomaterials for Targeting of Proteins and Nucleic Acids, CRC, Boca Raton, FL* **2005**.
85. Petersen, H.; Fechner, P. M.; Fischer, D.; Kissel, T. *Macromolecules* **2002**, *35*, 6867.
86. Torchilin, V. P. *J. Microencapsulation* **1998**, *15*, 1.
87. Hinds, K. D. *Biomaterials for Delivering and Targeting of Proteins and Nucleic Acids, CRC, Boca Raton, FL.* **2005**.
88. Herold, D. A.; Keil, K.; Bruns, D. E. *Biochem. Pharmacol.* **1989**, *38*, 73.
89. Moghimi, S. M.; Hunter, A. C.; Murray, J. C. *Pharmacol. Rev.* **2001**, *52*, 283.
90. Y., T.; Takagi, A.; Hashida, M.; Sezaki, H. *Pharm. Res.* **1987**, *4*, 293.
91. Torchilin, V. P. *Adv. Drug Delivery Rev.* **2006**, *58*, 1532.
92. Chen, J.; Spear, S. K.; Huddleston, J. G.; Rogers, R. D. *Green Chem.* **2005**, *7*, 64.
93. Zhao, Y.; Zhu, J. J.; Hong, J. M.; Bian, N.; Chen, H. Y. *Chem. Eur. J. Inorg. Chem.* **2004**, 4072.
94. Figlartz, M.; Fievet, F.; Lagier, J. P. *Fr. Pat. 8551483 (1985); Eur. Pat. 0113281 (1987); USA Pat. 4539041 (1985); Jap. Pat. 24303783 (1992).*
95. Fievet, F.; Lagier, J. P. *Solid State Ionics* **1989**, *32*, 198.
96. Feldman, C. *Adv. Funct. Mater.* **2003**, *13*, 101.
97. Bonet, F.; Guéry, C.; Guyomard, D.; Herrera Urbina, R.; Tekaiia-Elhsissen, K.; Tarascon, J. M. *Solid State Ionics* **1999**, *126*, 337.
98. Bonet, F.; Guéry, C.; Guyomard, D.; Herrera Urbina, R.; Tekaiia-Elhsissen, K.; Tarascon, J. M. *Int. J. Inorg. Mater.* **1999**, *1*, 47.
99. Ma, X.; Jiang, T.; Han, B.; Zhang, J.; Miao, S.; Ding, K.; An, G.; Xie, Y. X.; Zhou, Y.; Zhu, A. *Catal. Commun.* **2008**, *9*, 70.

100. Luo, C. C.; Zhang, Y. H.; Wang, Y. G. *J. Mol. Catal. A: Chem.* **2005**, *229*, 7.
101. Mao, J.; Guo, J.; Fang, F.; Ji, S. J. *Tetrahedron* **2008**, *64*, 3905.
102. Colacino, E.; Daich, L.; Martinez, J.; Lamaty, F. *Synlett* **2007**, 1279.
103. Mao, J.; Guo, J.; Ji, S. J. *J. Mol. Catal. A: Chem.* **2008**, *284*, 85.
104. Sreedhar, B.; Reddy, P. S.; Kumar, N. S. *Tetrahedron* **2006**, *47*, 3055.
105. Colacino, E.; Villebrun, L.; Martinez, J.; Lamaty, F. *Tetrahedron* **2010**, *66*, 3730.
106. Perrier, S.; Gemici, H.; Li, S. *Chem. Commun.* **2004**, 604.
107. Hu, Z.; Shen, X.; Qiu, H.; Lai, G.; Wu, J.; Li, W. *Eur. Polym. J.* **2009**, *45*, 2313.
108. Chandrasekar, S.; Narsihmulu, C.; Sultana, S. S.; Reddy, N. R. *Org. Lett.* **2002**, *4*, 4399.
109. Xu, L.; Chen, W.; Ross, J.; Xiao, J. *Org. Lett.* **2001**, *3*, 295.
110. Larhed, M.; Hallberg, A. *J. Org. Chem.* **1997**, *62*, 7858.
111. Cabri, W.; Candiani, I. *Acc. Chem. Res.* **1995**, *28*, 2.
112. Haimov, A.; Neumann, R. *Chem. Commun.* **2002**, 876.
113. Feng, B.; Hua, L.; Hou, Z.; Yang, H.; Hu, Y.; Li, H.; Zhao, X. *Catal. Commun.* **2009**, *10*, 1542.
114. Urgoitia, G.; SanMartin, R.; Herrero, M. T.; Dominguez, E. *Green Chem.* **2011**, *13*, 2161.
115. Schubert, U. S.; Eschbaumer, C.; Hien, O. *Macromol. Rapid Commun.* **2000**, *21*, 1156.
116. Schubert, U. S.; Eschbaumer, C. *Macromol. Symp.* **2001**, *163*, 177.
117. Guerrero-Sanchez, C.; Lohmeijer, B. G. G.; Meier, M. A. R.; Schubert, U. S. *Macromolecules* **2005**, *38*, 10388.
118. Zhou, G.; Harruna, I. I. *Macromolecules* **2005**, *38*, 4114.
119. Lohmeijer, B. G. G.; Schubert, U. S. *J. Polym. Sci., Part A: Polym. Chem.* **2005**, *43*, 6331.
120. Lohmeijer, B. G. G.; Schubert, U. S. *J. Polym. Sci., Part A: Polym. Chem.* **2004**, *42*, 4016.
121. Lohmeijer, B. G. G.; Schubert, U. S. *J. Polym. Sci., Part A: Polym. Chem.* **2003**, *41*, 1413.
122. Gohy, J. F.; Lohmeijer, B. G. G.; Varshney, S. K.; Schubert, U. S. *Macromolecules* **2002**, *35*, 7427.
123. Fustin, C. A.; Guillet, P.; Schubert, U. S.; Gohy, J. F. *Adv. Mater.* **2007**, *19*.
124. Heller, M.; Schubert, U. S. *e-Polymers* **2002**, 27.
125. Smith, A. P.; Fraser, C. L. *Macromolecules* **2003**, *36*, 5520.
126. Fraser, C. L.; Smith, A. P.; Wu, X. *J. Am. Chem. Soc.* **2000**, *122*, 9026.
127. Smith, A. P.; Fraser, C. L. *Macromolecules* **2002**, *35*, 594.
128. Corbin, P. S.; Webb, M. P.; McAlvin, J. E.; Fraser, C. L. *Biomacromolecules* **2001**, *2*, 223.
129. Johnson, R. M.; Fraser, C. L. *Macromolecules* **2004**, *37*, 2718.
130. Johnson, R. M.; Fraser, C. L. *Biomacromolecules* **2004**, *5*, 580.
131. McAlvin, J. E.; Fraser, C. L. *Macromolecules* **1999**, *32*, 1341.
132. Chen, J.; Gorczynski, J. L.; Zhang, G.; Fraser, C. L. *Macromolecules* **2010**, *43*, 4909.
133. Chen, J.; Gorczynski, J. L.; Fraser, C. L. *Macromol. Chem. Phys.* **2010**, *211*, 1272.
134. Hoogenboom, R.; Moore, B. C.; Schubert, U. S. *Macromol. Rapid Commun.* **2010**, *31*, 840.
135. Smith, A. P.; Fraser, C. L. *Macromol. Chem. Phys.* **2010**, *211*, 1246.
136. Yu, S. C.; Kwok, C. C.; Chan, W. K.; Che, C. M. *Adv. Mater.* **2003**, *15*, 1643.
137. Chen, Y. Y.; Yun, H. C. *J. Polym. Sci., Part A: Polym. Chem.* **2007**, *45*, 3243.
138. Holder, E.; Marin, V.; Kozodaev, D.; Meier, M. A. R.; Lohmeijer, B. G. G.;

- Schubert, U. S. *Macromol. Chem. Phys.* **2005**, *206*, 989.
139. Zhao, S.; Liu, S. J.; Huang, W. *Macromol. Rapid Commun.* **2010**, *31*, 794.
140. Giachi, G.; Frediani, M.; Oberhauser, W.; Passaglia, E. *J. Polym. Sci., Part A: Polym. Chem.* **2011**, *49*, 4708.
141. Gohy, J. F.; Lohmeijer, B. G. G.; Schubert, U. S. *Chem. Eur. J.* **2003**, *9*, 3472.
142. Gohy, J. F.; Lohmeijer, B. G. G.; Schubert, U. S. *Macromol. Rapid Commun.* **2002**, *23*, 555.
143. Horing, S.; Manners, I.; Newkome, G. R.; Schubert, U. S. *Macromol. Rapid Commun.* **2010**, *31*, 771.
144. Sheldon, R. A.; Arends, I. W. C. E.; Dijkstra, A. *Catal. Today* **2000**, *57*, 157.
145. Stahl, S. S. *Angew. Chem. Int. Ed. Engl.* **2004**, *43*, 3400.
146. Blackburn, T. F.; Schwartz, J. J. *J. Chem. Soc. Chem. Commun.* **1978**, 632.
147. Blackburn, T. F.; Schwartz, J. J. *J. Chem. Soc. Chem. Commun.* **1977**, 157.
148. Peterson, K. P.; Larock, R. C. *J. Org. Chem.* **1998**, *63*, 3185.
149. Nishimura, T.; Onoue, T.; Ohe, K.; Uemura, S. *J. Org. Chem.* **1999**, *64*, 6750.
150. Komano, T.; Iwasawa, T.; Tokunaga, M.; Obora, Y.; Tsuji, Y. *Org. Lett.* **2005**, *7*, 4677.
151. Bettucci, L.; Bianchini, C.; Filippi, J.; Lavacchi, A.; Oberhauser, W. *Eur. J. Inorg. Chem.* **2011**, 1797.
152. Iwasawa, T.; Tokunaga, M.; Obora, Y.; Tsuji, Y. *J. Am. Chem. Soc.* **2004**, *126*, 6554.
153. Ye, X.; Johnson, M. D.; Diao, T.; Yates, M. H.; Stahl, S. S. *Green Chem.* **2010**, *12*, 1180.
154. Kakiuchi, N.; Maeda, Y.; Nishimura, T.; Uemura, S. *J. Org. Chem.* **2001**, *66*, 6620.
155. Giachi, G.; Frediani, M.; Oberhauser, W.; Passaglia, E. *J. Polym. Sci., Part A: Polym. Chem.* **2012**, *50*, 2725.
156. Lu, J.; Toy, P. H. *Chem. Rev.* **2009**, *109*, 815.
157. Bergbreiter, D. E.; Tian, J.; Hongfa, C. *Chem. Rev.* **2009**, *109*, 530.
158. Tanyeli, C.; Gumus, A. *Tetrahedron Lett.* **2003**, *44*, 1639.
159. Pozzi, G.; Cavazzini, M.; Quici, S.; Benaglia, M.; Dell'Anna, G. *Org. Lett.* **2004**, *6*, 441.
160. Chung, C. W. Y.; Toy, P. H. *Comb. Chem.* **2007**.
161. Dijkstra, A.; Arends, I. W. C. E.; Sheldon, R. A. *Chem. Commun.* **2000**, 271.
162. Ferreira, P.; Hayes, W.; Phillips, E.; Rippon, D.; Tsang, S. C. *Green Chem.* **2004**, *6*, 310.
163. Nlate, S.; Astruc, D.; Neumann, R. *Adv. Synth. Catal.* **2004**, *346*, 1445.
164. Hamamoto, H.; Suzuki, Y.; Yamada, Y. M. A.; Tabata, H.; Takahashi, H.; Ikegami, S. *Angew. Chem. Int. Ed. Engl.* **2005**, *44*, 4536.
165. Harris, J. M.; Liu, Y.; Chai, S.; Andrews, M. D.; Vederas, J. C. *J. Org. Chem.* **1998**, *63*, 2409.
166. Ten Brink, G. J.; Arends, I. W. C. E.; Sheldon, R. A. *Science* **2000**, *287*, 1636.
167. Jensen, D. R.; Pugsley, J. S.; Sigman, M. S. *J. Am. Chem. Soc.* **2001**, *123*.
168. Ferreira, E. M.; Stoltz, B. M. *J. Am. Chem. Soc.* **2001**, *123*, 7725.
169. Hallman, K.; Moberg, C. *Adv. Synth. Catal.* **2001**, *343*, 260.
170. Schultz, M. J.; Park, C. C.; Sigman, M. S. *Chem. Commun.* **2002**, 3034.
171. Jensen, D. R.; Schultz, M. J.; Mueller, J. A.; Sigman, M. S. *Angew. Chem. Int. Ed.* **2003**, *42*, 3810.
172. Astruc, D.; Feng, L.; Ruiz Aranzaes, J. *Angew. Chem. Int. Ed.* **2005**, *44*, 7852.
173. Feng, B.; Hou, Z.; Yang, H.; Wang, X.; Hu, Y.; Li, H.; Qiao, Y.; Zhao, X.; Huang, Q. *Langmuir* **2010**, *26*, 2505.
174. Gittins, D. I.; Caruso, F. *Angew. Chem. Int. Ed.* **2001**, *40*, 3001.

175. Haruta, M. *J. New Mater. Electrochem. Syst.* **2004**, *7*, 163.
176. Banerjee, P.; Chakrabarti, S.; Maitra, S.; Dutta, B. K. *Ultrason. Sonochem.* **2012**, *19*, 85.
177. Nemamcha, A.; Moumeni, H.; Rehspringer, J. L. *Phys.Procedia* **2009**, *2*, 713.
178. Hwang, C. B.; Fu, Y. S.; Lu, Y. L.; Jang, S. W.; Chou, P. T.; Wang, R.; Yu, S. J. *J. Catal.* **2000**, *195*, 336.
179. Paulus, U. A.; Endruschat, U.; Feldmeyer, G. J.; Schmidt, T. J.; Bonnemann, H.; Behm, J. J. *J. Catal.* **2000**, *195*, 383.
180. Han, Y. F.; Kumar, D.; Goodman, D. W. *J. Catal.* **2005**, *230*, 353.
181. Bars, J. L.; Specht, U.; Bradley, J. S.; Blackmond, D. G. *Langmuir* **1999**, *15*, 7621.
182. Li, Y.; Boone, E.; El-sayed, M. A. *Langmuir* **2002**, *18*, 4921.
183. Veisz, B.; Király, Z.; Tóth, L.; Pècz, B. *Chem. Mater.* **2002**, *14*.
184. Choudary, B. M.; Madhi, S.; Chowdary, N. S.; Kantam, M. L.; Sreedhar, B. J. *Am. Chem. Soc.* **2002**, *124*, 14127.
185. Le Bars, J.; Specht, U.; Bradley, J. S.; Blackmond, D. G. *15* **1999**, 7621.
186. Augustine, R. L.; O'Leary, S. T. *J. Mol. Catal. A: Chem.* **1995**, *277*, 95.
187. Kaneda, K.; Higushi, M.; Himanaka, T. *J. Mol. Catal. A: Chem.* **2001**, *63*, L33.
188. Prockl, S.; Kleist, W.; Gruber, M. A.; Kohler, K. *Angew. Chem. Int. Ed.* **2004**, *43*.
189. Djakovitch, L.; Kohler, K. *J. Am. Chem. Soc.* **2001**, *123*, 5990.
190. Julia, M.; Duteil, M.; Grard, C.; Kunz, E. *Bull. Soc. Chim. Fr.* **1993**, 2791.
191. Reetz, M. T.; Westermann, E. *Angew. Chem. Int. Ed.* **2000**, *39*.
192. Reetz, M. T.; de Vries, J. G. *Chem. Commun.* **2004**, 1559.
193. Grunwaldt, J. D.; Caravati, M.; Baiker, A. *J. Phys. Chem. B* **2006**, *110*, 25586.
194. Wada, K.; Yano, K.; Kondo, T.; Mitsudo, T. *Catal. Today* **2006**, *117*, 242.
195. Stuchinskaya, T. L.; Kozhevnikov, I. V. *Catal. Commun.* **2003**, *4*, 417.
196. Uozumi, Y.; Nakao, R. *Angew. Chem. Int. Ed. Engl.* **2003**, *42*, 194.
197. Li, F.; Zhang, Q.; Wang, Y. *Appl. Catal. A: Gen.* **2008**, *334*, 217.
198. Kwon, M. S.; Kim, N.; Park, C. M.; Lee, J. S.; Kang, K. Y.; Park, J. *Org. Lett.* **2005**, *7*, 1077.
199. Pillai, U. R.; Sahle-Demessie, E. *Green Chem.* **2004**, *6*, 161.
200. Mori, K.; Hara, T.; Mizugaki, T.; Ebitani, K.; Kaneda, K. *J. Am. Chem. Soc.* **2004**, *126*, 10657.
201. Chen, J.; Zhang, Q.; Wang, Y.; Wan, H. *Adv. Synth. Catal.* **2008**, *350*, 453.
202. Ng, Y. H.; Ikeda, S.; Harada, T.; Morita, Y.; Matsumara, M. *Chem. Commun.* **2008**, *44*, 3181.
203. Miyamura, H.; Matsubara, R.; Kobayashi, S. *Chem. Commun.* **2008**, *44*, 2031.
204. Mallat, T.; Bodnar, Z.; Hug, P.; Baiker, A. *J. Catal.* **1995**, *153*, 131.
205. Jamwal, N.; Gupta, M.; Paul, S. *Green Chem.* **2008**, *10*, 999.
206. Yamada, Y. M. A.; Arakawa, T.; Hocke, H.; Uozumi, Y. *Angew. Chem. Int. Ed. Engl.* **2007**, *46*, 704.
207. Feng, B.; Hua, L.; Hou, Z.; Yang, H.; Hu, Y.; Li, H.; Zhao, X. *Catal. Commun.* **2009**, *10*, 1542.
208. Giachi, G.; Oberhauser, W.; Frediani, M.; Passaglia, E.; Capozzoli, L.; Rosi, L. *J. Polym. Sci., Part A: Polym. Chem.* **2013**, *51*, 2518.
209. Larock, R. C. *In: Comprehensive Organic Transformations*, Wiley-VCH **1999**.
210. Rappoport, Z. *In: The Cyano Group*, John Wiley & Sons. **1970**.
211. Ellis, G. P.; Romney-Alexander, T. M. *Chem. Rev.* **1987**, *87*, 779.
212. Schareina, T.; Zapf, A.; Beller, M. *Journal of Organometallic Chemistry* **2004**, *689*, 4576-4583.
213. Chattopadhyay, K.; Dey, R.; Ranu, B. C. *Tetrahedron Letters* **2009**, *50*, 3164-3167.

214. Polshettiwar, V.; Hesemann, P.; Moreau, J. J. E. *Tetrahedron* **2007**, *63*, 6784-6790.
215. Ren, Y.; Liu, Z.; He, S.; Zhao, S.; Wang, J.; Niu, R.; Yin, W. *Org. Proc. Res. Dev.* **2009**, *13*, 764.
216. Hajipour, A. R.; Karami, K.; Tavakoli, G.; Pirisedigh, A. *Journal of Organometallic Chemistry* **2011**, *696*, 819-824.
217. Schareina, T.; Zapf, A.; Beller, M. *Tetrahedron Letters* **2005**, *46*, 2585-2588.
218. Schareina, T.; Zapf, A.; Magerlein, W.; Muller, N.; Beller, M. *Chem. Eur. J.* **2007**, *13*, 6249-54.
219. Ren, Y.; Liu, Z.; Zhao, S.; Tian, X.; Wang, J.; Yin, W.; He, S. *Catalysis Communications* **2009**, *10*, 768-771.
220. Ren, Y.; Dong, C.; Zhao, S.; Sun, Y.; Wang, J.; Ma, J.; Hou, C. *Tetrahedron Letters* **2012**, *53*, 2825-2827.
221. Ren, Y.; Wang, W.; Zhao, S.; Tian, X.; Wang, J.; Yin, W.; Cheng, L. *Tetrahedron Letters* **2009**, *50*, 4595-4597.
222. DeBlase, C.; Leadbeater, N. E. *Tetrahedron* **2010**, *66*, 1098-1101.
223. Giachi, G.; Frediani, M.; Oberhauser, W.; Lamaty, F.; Martinez, J.; Colacino, E. *ChemSusChem*, submitted.
224. Mason, T. J. *Sonochemistry: The Uses of Ultrasound in Chemistry*; The Royal Society of Chemistry, 1990.
225. Suslick, K. S.; Hammerton, D. A.; Cline, R. E., Jr. *J. Am. Chem. Soc.* **1986**, *108*, 5641.
226. Flint, E. B.; Suslick, K. S. *Science* **1991**, *253*, 1397.
227. Tuulmets, A.; Cravotto, G.; Salmar, S.; Järv, J. *Mini-rev. Org. Chem.* **2010**, *7*, 204.
228. Ando, T.; Sumi, S.; Kawate, T.; Ichihara, J.; Hanafusa, T. *J. Chem. Soc. Chem. Commun.* **1984**, 439.
229. Hickenboth, C. R.; Moore, J. S.; White, S. R.; Sottos, N. R.; Baudry, J.; Wilson, S. R. *Nature* **2007**, *446*, 423.
230. Wiggins, K. M.; Syrett, J. A.; Haddleton, D. M.; Bielawski, C. W. *J. Am. Chem. Soc.* **2011**, *133*, 7180.
231. Tennyson, A. G.; Wiggins, K. M.; Bielawski, C. W. *J. Am. Chem. Soc.* **2010**, *132*, 16631.
232. Piermattei, A.; Karthikeyan, S.; Sijbesma, R. P. *Nat. Chem.* **2009**, *1*, 133.
233. Brantley, J. N.; Wiggins, K. M.; Bielawski, C. W. *Science* **2011**, *333*, 1606.
234. Cravotto, G.; Demetri, A.; Nano, Gian M.; Palmisano, G.; Penoni, A.; Tagliapietra, S. *Eur. J. Org. Chem.* **2003**, 4438.
235. Jin, T. S.; Xiao, J. C.; Wang, S. J.; Li, T. S. *Ultrason. Sonochem.* **2004**, *11*, 393.
236. Arcadi, A.; Alfonsi, M.; Marinelli, F. *Tetrahedron Lett.* **2009**, *50*, 2060.
237. An, G.; Ji, X.; Han, J.; Pan, Y. *Synth. Commun.* **2011**, *41*, 1464.
238. Zou, Y.; Wu, H.; Hu, Y.; Liu, H.; Zhao, X.; Ji, H.; Shi, D. *Ultrason. Sonochem.* **2011**, *18*, 708.
239. Zang, H.; Zhang, Y.; Zang, Y.; Cheng, B. W. *Ultrason. Sonochem.* **2010**, *17*, 495.
240. Rostamizadeh, S.; Amani, A. M.; Mahdavinia, G. H.; Amiri, G.; Sepehrian, H. *Ultrason. Sonochem.* **2010**, *17*, 306.
241. Biggs, S.; Grieser, F. *Macromolecules* **1995**, *28*, 4877.
242. Fujiwara, H.; Ishida, T.; Taniguchi, N.; Wada, S. *Polymer Bulletin* **1999**, *42*, 197.
243. Xia, H.; Wang, Q.; Liao, Y.; Xu, X.; Baxter, S. M.; Slone, R. V.; Wu, S.; Swift, G.; Westmoreland, D. G. *Ultrason. Sonochem.* **2002**, *9*, 151.
244. Yin, N.; Chen, K.; Kang, W. *Ultrason. Sonochem.* **2006**, *13*, 345.
245. Vijaya Kumar, R.; Mastai, Y.; Diamant, Y.; Gedanken, A. *J. Mater. Chem.* **2001**, *11*, 1209.

246. Prasad, K.; Sonawane, S.; Zhou, M.; Ashokkumar, M. *Chem. Eng. J.* **2013**, *219*, 254.
247. Chowdhury, P.; Saha, S. K.; Guha, A.; Saha, S. K. *Appl. Surf. Sci.* **2012**, *261*, 598.
248. Li, C.; Cai, W.; Kan, C.; Fu, G.; Zhang, L. *Mater. Lett.* **2003**, *58*, 196.
249. Cubillana-Aguilera, L. M.; Franco-Romano, M.; Gil, M. L.; Naranjo-Rodriguez, I.; de Cisneros, J. L.; Palacios-Santander, J. M. *Ultrason. Sonochem.* **2011**, *18*, 789.
250. Dang, F.; Enomoto, N.; Hojo, J.; Enpuku, K. *Ultrason. Sonochem.* **2009**, *16*, 649.
251. Morel, A.-L.; Nikitenko, S. I.; Gionnet, K.; Wattiaux, A.; Lai-Kee-Him, J.; Labrugere, C.; Chevalier, B.; Deleris, G.; Petibois, C.; Brisson, A.; Simonoff, M. *ACS Nano* **2008**, *2*, 847.
252. Kianpour, G.; Salavati-Niasari, M.; Emadi, H. *Ultrason. Sonochem.* **2013**, *20*, 418.
253. Mohandes, F.; Salavati-Niasari, M. *Ultrason. Sonochem.* **2013**, *20*, 354.
254. Lin, H.-t.; Li, H.-l.; Chen, X.-y.; Yang, M.; Qi, Y.-x. *Fenzi Cuihua* **2010**, *24*, 99.
255. Sanoop, P. K.; Mahesh, K. V.; Nampoothiri, K. M.; Mangalaraja, R. V.; Ananthakumar, S. *J. Appl. Polym. Sci.* **2012**, *126*, E232.
256. Kowsari, E. *J. Nanopart. Res.* **2011**, *13*, 3363.
257. Yadav, R. S.; Mishra, P.; Pandey, A. C. *Ultrason. Sonochem.* **2008**, *15*, 863.
258. Li, X.; Li, Y.; Li, S.; Zhou, W.; Chu, H.; Chen, W.; Li, I. L.; Tang, Z. *Cryst. Growth Des.* **2005**, *5*, 911.
259. Zhang, H.; Yang, D.; Ma, X. *Mater. Lett.* **2008**, *63*, 1.
260. Oxley, J. D.; Prozorov, T.; Suslick, K. S. *J. Am. Chem. Soc.* **2003**, *125*, 11138.
261. Dupont, J.; Spencer, J. *Angew. Chem. Int. Ed.* **2004**, *43*, 5296.
262. Swatloski, R. P.; Holbrey, J. D.; Rogers, R. D. *Green Chem.* **2003**, *5*, 361.
263. Gholap, A. R.; Venkatesan, K.; Daniel, T.; Lahoti, R. J.; Srinivasan, K. V. *Green Chem.* **2003**, *5*, 693.
264. Noei, J.; Khosropour, A. R. *Ultrason. Sonochem.* **2009**, *16*, 711.
265. Heravi, M. R. *Ultrason. Sonochem.* **2009**, *16*, 361.
266. Deshmukh, R. R.; Rajagopal, R.; Srinivasan, K. V. *Chem. Commun.* **2001**, 1544.
267. Rajagopal, R.; Jarikote, D. V.; Srinivasan, K. V. *Chem. Commun.* **2002**, 616.
268. Harjani, J. R.; Abraham, T. J.; Gomez, A. T.; Garcia, M. T.; Singer, R. D.; Scammells, P. J. *Green Chem.* **2010**, *12*, 650.
269. Lee, S. H.; Nguyen, H. M.; Koo, Y.-M.; Ha, S. H. *Proc. Biochem.* **2008**, *43*, 1009.
270. Jin, Y.; Wang, P.; Yin, D.; Liu, J.; Qin, L.; Yu, N.; Xie, G.; Li, B. *Colloids Surf. A: Physicochem. Eng. Asp.* **2007**, *302*, 366.
271. Zhang, S.; Zhang, Y.; Wang, Y.; Liu, S.; Deng, Y. *Phys. Chem. Chem. Phys.* **2012**, *14*, 5132.
272. Goharshadi, E. K.; Ding, Y.; Jorabchi, M. N.; Nancarrow, P. *Ultrason. Sonochem.* **2009**, *16*, 120.
273. Jacob, D. S.; Kahlenberg, V.; Wurst, K.; Solovyov, L. A.; Felner, I.; Shimon, L.; Gottlieb, H. E.; Gedanken, A. *Eur. J. Inorg. Chem.* **2005**, *2005*, 522.
274. Jacob, D. S.; Makhluif, S.; Brukental, I.; Lavi, R.; Solovyov, L. A.; Felner, I.; Nowik, I.; Persky, R.; Gottlieb, H. E.; Gedanken, A. *Eur. J. Inorg. Chem.* **2005**, *2005*, 2669-2677.
275. Silva, A. d. C.; de Souza, A. L. F.; Antunes, O. A. C. *J. Organomet. Chem.* **2007**, *692*, 3104.
276. Mesquita, P. R. R.; Almeida, J. S.; Teixeira, L. S. G.; da, S. A. F.; Silva, L. A. J. *Braz. Chem. Soc.* **2013**, *24*, 280.

277. Abu-Much, R.; Gedanken, A. *Chem. Eur. J.* **2008**, *14*, 10115.
278. Kuijpers, M. W. A.; van Eck, D.; Kemmere, M. F.; Keurentjes, J. T. F. *Science* **2002**, *298*, 1969.
279. Koltypin, Y.; Perkas, N.; Gedanken, A. *J. Mater. Chem.* **2004**, *14*, 2975.
280. Lopez-Pestana, J. M.; Avila-Rey, M. J.; Martin-Aranda, R. M. *Green Chem.* **2002**, *4*, 628.
281. Liu, Q.; Ai, H.; Li, Z. *Ultrason. Sonochem.* **2011**, *18*, 477.
282. Xia, M.; Lu, Y. D. *Ultrason. Sonochem.* **2007**, *14*, 235.
283. Cui, C.; Zhu, C.; Du, X.-J.; Wang, Z.-P.; Li, Z.-M.; Zhao, W.-G. *Green Chem.* **2012**, *14*, 3157.
284. Mojtahedi, M. M.; Javadpour, M.; Abaee, M. S. *Ultrason. Sonochem.* **2008**, *15*, 828.
285. Shukla, G.; Verma, R. K.; Verma, G. K.; Singh, M. S. *Tetrahedron Lett.* **2011**, *52*, 7195.
286. Nasr-Esfahani, M.; Montazerzohori, M.; Filvan, N. *J. Serb. Chem. Soc.* **2012**, *77*, 415.
287. Kruus, P.; Patraboy, T. J. *J. Phys. Chem.* **1985**, *89*, 3379.
288. Price, G. J.; Daw, M. R.; Newcombe, N. J.; Smith, P. F. *Brit. Polym. J.* **1990**, *23*, 63.
289. Koda, S.; Suzuki, A.; Nomura, H. *Polym. J.* **1995**, *27*, 1144.
290. Kojima, Y.; Koda, S.; Hiroyasu, N. *Ultrason. Sonochem.* **2001**, *8*, 75.
291. Kim, S. T.; Choi, H. J.; Hong, S. M. *Colloid Polym. Sci.* **2007**, *285*, 593.
292. Choi, H. J.; Zhang, K.; Lim, J. Y. *J. Nanosci. Nanotechnol.* **2007**, *7*, 3400.
293. Price, G. J.; Lenz, E. J.; Ansell, C. W. G. *Eur. Polym. J.* **2002**, *38*, 1753.
294. Tatsuno, Y.; Yoshida, T.; Otsuka, S. *Inorg. Synth.* **1990**, *28*, 342.
295. Bianchini, C.; Lenoble, G.; Oberhauser, W.; Parisel, S.; Zanobini, F. *Eur. J. Inorg. Chem.* **2005**, 4794.
296. Brookhart, M.; Grant, B.; Volpe Jr., A. F. *Organometallics* **1992**, *11*, 3920.
297. Mai, W.; Gao, L. *Synlett* **2006**, *16*, 2553.
298. Parkin, S.; Moezzi, B.; Hope, H. *J. Appl. Crystallogr.* **1995**, *28*, 53.
299. Sheldrick, G. M. *SHELX-97; University of Göttingen, Germany* **1997**.
300. Farrugia, L. J. *J. Appl. Crystallogr.* **1999**, *32*, 837.
301. Espartero, J. L.; Rashkov, I.; Li, S. M.; Manolova, N.; Vert, M. *Macromolecules* **1996**, *29*, 3535.
302. Malecki, J. G.; Maron, A. *Transition Met. Chem.* **2011**, *36*, 297.
303. Bianchini, C.; Meli, A.; Oberhauser, W. *Organometallics* **2003**, *22*, 4281.
304. Barth, H. G.; Carlin Jr, F. J. *J. Liq. Chromatogr.* **1984**, *7*, 1717.
305. Thoumazet, C.; Grutzmacher, H.; Deschamps, B.; Ricard, L.; le Floch, P. *Eur. J. Inorg. Chem.* **2006**, 3911.
306. Oilunkaniemi, R.; Laitinen, R. S.; Hannu-Kuure, M. S.; Ahlgren, M. J. *J. Organomet. Chem.* **2003**, *678*, 95.
307. Fambri, L.; Migliaresi, C. In: *Poly(lactic acid): Synthesis, Structure, Properties, Processing, and Application; Eds Wiley - New York* **2010**, Chapter 9, 113.
308. Choi, Y. K.; Bae, Y. H.; Kim, S. W. *Macromolecules* **1998**, *31*, 8766.
309. Pan, P.; Liang, Z.; Zhu, B.; Dong, T.; Inoue, Y. *Macromolecules* **2009**, *42*, 3374.
310. Tsuji, H. In: *Poly(lactic acid): Synthesis, Structure, Properties, Processing, and Application; Eds Wiley - New York* **2010**, Chapter 21, 345.
311. Cam, D.; Marucci, M. *Polymer* **1997**, *38*, 1879.
312. Nishida, H. In: *Poly(lactic acid): Synthesis, Structure, Properties, Processing, and Application; Eds Wiley - New York* **2010**, 401.
313. Lee, S. H.; Kim, S. H.; Han, Y. K.; Kim, Y. H. *J. Polym. Sci., Part A: Polym. Chem.* **2001**, *39*, 973.

314. Shin, K. M.; Dong, T.; He, Y.; Inoue, Y. *J. Polym. Sci., Part B: Polym. Phys.* **2005**, *43*, 1433.
315. Anthenius, H.; van der Meer, J. C.; de Geus, M.; Kingma, W.; Koning, C. E. *Macromolecules* **2009**, *42*, 2462.
316. *XRPD data were extracted from PDF-2 containing ICDD (international Centre for Diffraction Data) experimental powder data collection: <http://www.icdd.com>.*
317. Dust, J. M.; Fang, Z. H.; Harris, J. M. *Macromolecules* **1990**, *23*.
318. Angiolini, L.; Benelli, L.; Giorgini, L.; Salatelli, G. E. *Polymer* **2005**, *46*, 2424.
319. Creighton, J. A.; Eadon, D. G. *J. Chem. Soc. Faraday Trans.* **1991**, *87*, 3881.
320. Hall, B. D.; Zanchet, D.; Ugarte, D. *J. Appl. Crystallogr.* **2000**, *33*, 1335.
321. Han, S.; Kim, C.; Kwon, D. *Polymer* **1997**, *38*, 317.
322. Ten Brink, G. J.; Arends, I. W. C. E.; Hoogenraad, M.; Verspui, G.; Sheldon, R. A. *Adv. Synth. Catal.* **2003**, *345*, 1341.
323. Mallat, T.; Baiker, A. *Chem. Rev.* **2004**, *104*, 3037.
324. Keressegi, C.; Burgi, T.; Mallat, T.; Baiker, A. *J. Catal.* **2002**, *211*, 244.
325. Azua, A.; Mata, J. A.; Heymes, P.; Peris, E.; Lamaty, F.; Martinez, J.; Colacino, E. *Adv. Synth. Catal.* **2013**, 1107.
326. Kessler, L. W.; O'Brien, W. D.; Dunn, F. J. *Phys. Chem.* **1970**, *74*, 4096.
327. Chen, G.; Weng, J.; Zheng, Z.; Zhu, X.; Cai, Y.; Cai, J.; Wan, Y. *Eur. J. Org. Chem.* **2008**, *2008*, 3524.
328. Colacino, E.; Villebrun, L.; Martinez, J.; Lamaty, F. *Tetrahedron* **2010**, *66*, 3730-3735.
329. Declerck, V.; Martinez, J.; Lamaty, F. *Synlett* **2006**, 3029-3032.
330. *Institute of Medicine, Food and Nutrition Board, Dietary Reference Intakes – National Academy Press, Washington* **2001**, 1-28.
331. Santhanalakshmi, J.; Parimala, L. *J. Nanopart. Res.* **2012**, *14*, 1090-1114.
332. Bantreil, X.; Sidi-Ykhlef, M.; Aringhieri, L.; Colacino, E.; Martinez, J.; Lamaty, F. *J. Catal.* **2012**, *294*, 113.
333. Luo, S.; Zhang, S.; Wang, Y.; Xia, A.; Zhang, G.; Du, X.; Xu, D. *J. Org. Chem.* **2010**, *75*, 1888.

Aknowledgements

I would like to thank my PhD tutor Marco Frediani and any member of the research group of industrial chemistry at the Department of Chemistry – University of Florence as well as Werner Oberhauser and ICCOM-CNR of Florence for great support and scientific contribution to this thesis.

I am very grateful to Evelina Colacino and the group of green chemistry and enabling technologies at the IBMM – University of Montpellier-2 for hosting me during a fruitful period of scientific collaboration focused on sonochemical cyanation reactions.

Many thanks also to Elisa Passaglia and Marco Carlo Mascherpa of ICCOM-CNR of Pisa for DSC, TGA and ICP analyses; Laura Capozzoli at CEME-CNR of Florence and Franck Godiard at the University of Montpellier-2 for TEM analyses and Valerie Flaud at the University of Montpellier-2 for XPS analyses.

This work is dedicated to my friends and family and, especially, to my beloved Francesca ‘Bincesca’ Bianchi.